



**HAL**  
open science

## Porous and hybrid silica from biocompatible systems : application to drug release

Claudia Violeta Cervantes-Martinez

► **To cite this version:**

Claudia Violeta Cervantes-Martinez. Porous and hybrid silica from biocompatible systems : application to drug release. Chemical Sciences. Université de Lorraine, 2019. English. NNT : 2019LORR0295 . tel-02559524

**HAL Id: tel-02559524**

**<https://hal.univ-lorraine.fr/tel-02559524>**

Submitted on 11 Jan 2022

**HAL** is a multi-disciplinary open access archive for the deposit and dissemination of scientific research documents, whether they are published or not. The documents may come from teaching and research institutions in France or abroad, or from public or private research centers.

L'archive ouverte pluridisciplinaire **HAL**, est destinée au dépôt et à la diffusion de documents scientifiques de niveau recherche, publiés ou non, émanant des établissements d'enseignement et de recherche français ou étrangers, des laboratoires publics ou privés.



## AVERTISSEMENT

Ce document est le fruit d'un long travail approuvé par le jury de soutenance et mis à disposition de l'ensemble de la communauté universitaire élargie.

Il est soumis à la propriété intellectuelle de l'auteur. Ceci implique une obligation de citation et de référencement lors de l'utilisation de ce document.

D'autre part, toute contrefaçon, plagiat, reproduction illicite encourt une poursuite pénale.

Contact : [ddoc-theses-contact@univ-lorraine.fr](mailto:ddoc-theses-contact@univ-lorraine.fr)

## LIENS

Code de la Propriété Intellectuelle. articles L 122. 4

Code de la Propriété Intellectuelle. articles L 335.2- L 335.10

[http://www.cfcopies.com/V2/leg/leg\\_droi.php](http://www.cfcopies.com/V2/leg/leg_droi.php)

<http://www.culture.gouv.fr/culture/infos-pratiques/droits/protection.htm>



Collégium SCIENCES ET TECHNOLOGIES

Pôle Scientifique Chimie et Physique Moléculaires  
Ecole Doctorale Lorraine de Chimie et Physique Moléculaires

Thèse présentée pour l'obtention du titre de Docteur de l'Université de Lorraine en  
Chimie et Physico-chimie Moléculaires par :

**Claudia Violeta Cervantes Martínez**

Porous and hybrid silica from biocompatible systems: application to  
drug release

**Date de soutenance : 12 Décembre 2019**

Membres du Jury :

**Rapporteurs:**

Mme Viorica PARVULESCU

Professeur chercheur  
Département Chimie de Surface et Catalyse  
"Ilie Murgulescu" Institut de Chimie Physique de  
l'Académie Roumaine

M Carlos RODRIGUEZ ABREU

Chercheur  
Conseil Supérieur de la Recherche Scientifique  
CSIC  
Institut de Chimie Avancée de Catalogne IQAC

**Examineurs:**

Mme Marie-José Stèbè

Directrice de Recherches Emérite  
Centre National de Recherche Scientifique CNRS

Mme María-José GARCIA CELMA

Professeur  
Département de Pharmacie et Technologie  
Pharmaceutique Université de Barcelone

Mme Isabelle CHEVALOT

Professeur INPL-ENSAIA  
Université de Lorraine

**Directeur de thèse:**

M Jean-Luc BLIN

Professeur  
Laboratoire Lorrain de Chimie Moléculaire  
Université de Lorraine

*Sweet are the fruits of adversity,  
which like an ugly and poisonous toad  
carry a precious jewel on the head.*

*William Shakespeare*

*-As you like it-*

*To Bimba and all of those who supported me  
unconditionally along this journey*

*My eternal love and gratitude.*

## *Acknowledgements*

*This work was developed in the NANO team of the Lorraine Laboratory of Molecular Chemistry mixed research unit 7053 of the University of Lorraine in Nancy France.*

*First, I want to thank my thesis director M Jean-Luc Blin Professor at the University of Lorraine for all his support and giving me the opportunity to develop my doctoral thesis work within his research team. Then, I would like to express my special gratitude to Mme Marie-José Stébé, Director Emeritus of Research at Centre National de la Recherche Scientifique (CNRS) for driving me with her advices, shared knowledge, dedication, patience, time and efforts invested in the successful completion of this work.*

*I would also like to thank Professor María José García-Celma of the University of Barcelona for her warm reception at the Pharmaceutical Technology Laboratory of the University of Barcelona, for her advices, humane treatment and unconditional support during my time in Spain. I would also like to express my gratitude to Professor Isabelle Chevalot, Professor at the École Nationale Supérieure d'Agronomie et des Industries Alimentaires (ENSAIA), to Professor Viorica Parvulescu, Researcher Professor in the Department of Surface Chemistry and Catalysis at the Institute of Physical Chemistry of Romania and to Professor Carlos Rodríguez Abreu, Researcher at the Superior Council for Scientific Research (CSIC) of the Institute of Advanced Chemistry of Catalonia, for having accepted to evaluate this work as a reporters.*

*I would also like to thank M Philippe Gros, Professor at the University of Lorraine and Director of the Lorraine Laboratory of Molecular Chemistry, for having received me in the laboratory under his direction. I want to thank to Mélanie Emo, ex - Studies Engineer in charge of SAXS, for the numerous analyses and modelings that were crucial for the achievement of this work. I want to thank that besides the professional collaboration, she was kind enough to offer me her friendship during the realization time of this work. I would also like to thank M François Dupire and M Pascal Lemièrre responsables of HPLC equipment, for their confidence, patience and support during the training and methods concerned to this technique. I would also like to thank Marta Monje for her support in carrying out the cellular tests and Susana Vilches for her support in carrying out the rheological tests.*

*I would like to express my eternal gratitude to my country for having given me one of my most valuable possessions: my professional formation, for having accompanied me here and continuing to contribute to my professional life project. But above all for continuing to support the production of knowledge and development of technology inside and outside the country, which they entrust it to the National Council for Science and Technology (CONACyT) through the granting of postgraduate scholarships, from which I was benefited. Thank you México, thank you CONACyT and ¡Viva México! My eternal gratitude to the members of the Committee of Foreign Scholars "Carlos Pellicer Cámara" for their hard work in the negotiations with CONACyT and the achievements obtained.*

*I especially want to thank my friends Jimena and César who were with me throughout this adventure and taught me another side of life, changing not only my present but also my future perspectives. I want to thank all the friends I had the privilege to find on the way, who were my accomplices in the good times and my support in those not so good ones: La chula, François Vibert, Mélanie, Philippe, Rajiv, Issam, Laura, Pilar, Juan, Florian, Ibrahim, Emre, Ricardo, Dorota, Tony, Ziad, Youseff, Abderzak, Amal, Mohammad, Giuseppe, Ézéchiél, Miguelito, Eva, Esteban, Patty, Alicia, Karen, Ana, Laura, Vivi, to the Convent of the religious sisters of Betania, especially to the sisters Mercedes, Esperanza and Amparo, thanks to all of them for their incredible affection. To the Masson family for their trust and affection. To the group of Latinos from LACANA for their love, trust and support throughout these years. To my friends from México: Sandra and Omar, who despite the distance have accompanied me for many years.*

*I also want to thank all the people I had the pleasure to meet and work: Lionel, Laurent, Dominique, Eric, Paul, Nathalie, Stephan, Fabien, Gregoire, Gabriela, Elvira and Rosa. My eternal gratitude to M Pierrick Gaudin, for his personal and professional support, for his joy and his particular way of communicating with me in spanish.*

*And beyond of the science, I want to thank my family, my mother: María Cristina, my brothers: Ninel and Luis Alonso for always being by my side, supporting me with their words of encouragement and love when I needed it the most. To my grandfather, Ramón Cervantes<sup>†</sup> for his teachings and unconditional love. To Bimba, for having always been with me and giving me her unconditional loyalty.*

*To all of you: Muchas gracias.*

## Index

	Page
Index of figures	6
Index of table	11
Abbreviations	12
Résumé	13
Summary	19
General Introduction	25
Thesis goals	27
<b>Chapter I. Generalities</b>	<b>29</b>
1.1 Surfactants and their organized molecular systems	30
1.1.1 Classification of surfactants	30
A. Alcohol ethoxylates	31
B. Alkyl phenol ethoxylates	31
C. Fatty acid ethoxylates	31
D. Sorbitan esters and their ethoxylated derivatives	31
E. Amine ethoxylates	32
F. Ethylene Oxide Propylene Oxide co-polymers (EO/PO)	32
G. Ethoxylated fats and oils	32
1.1.2 Biocompatible surfactants	32
A. Sugar based surfactants	33
A1. Alkyl -polyglucosides (APGs)	33
A2. Sugar fatty acid esters (SFAEs)	34
A3. Surfactants prepared via fermentation	35
A3.1 Acylpolyols	35
A3.2 Glycolipids	36
A3.3 Acylpeptides	37
B. Amino acid as polar head group	37
C. Surfactants based on natural hydrophobic tail	38
C1. Fatty acid as hydrophobic tail	38
C2. Sterol as hydrophobic tail	40

	Page
1.1.3 Hydrophobic-lipophilic balance (HLB)	40
1.2 Organized Molecular Systems (OMS)	41
1.3 Systems thermodynamically stables	43
1.3.1 Micelles	43
1.3.2 Microemulsions	44
1.3.3 Liquid crystals	44
A. Lamellar phase	44
B. Cubic phase	45
C. Hexagonal phase	45
1.4 Phase behavior of nonionic surfactants	46
1.5 Systems kinetically stables	46
1.5.1 Emulsions	46
1.5.2 Nano-emulsions	47
A. Nano-emulsions preparation methods	49
A1. High energy emulsification method	49
A2. Low energy emulsification method	49
1.5.3 Concentrated emulsions	50
1.6 Porous silica materials (PSM)	51
1.6.1 Mesoporous materials and their formation mechanisms	52
A. Cooperative Templating Mechanism (CTM)	52
B. Liquid Crystal/emulsion Templating Mechanism	52
1.6.2 Meso-macro porous silica material	53
1.6.3 Hybrid materials	54
1.6.4 Applications of mesoporous silica materials	55
A. Chemical industry	55
B. Bio-application	55
C. Functional materials	55
1.7 Application of porous materials in Drug Delivery Field	56
1.7.1 Generalities on Drug Delivery Systems (DDS)	56
1.7.2 Porous silica material on drug loading and drug release	58
1.7.3 Kinetics models for the evaluation of DDS from mesoporous materials	58

	Page
<b>Chapter II. Materials and Methods</b>	61
2.1 Materials	62
2.1.1 Surfactants	62
2.1.2 Oils	63
A. Mygliol 812N	63
B. Isopropyl Myristate	64
2.1.3 Inorganic sources: Tetramethyl-ortho silicates (TMOS) as silica precursor	64
2.1.4 Ketoprofen as encapsulated model drug	65
2.1.5 Phosphate buffer solutions (PBS) in neutral and acidic conditions	66
2.1.6 Protocol for dialysis bag preparation	66
2.1.7 HeLa culture cells	67
2.2 Methods	67
2.2.1 Phase diagram determination	67
A. Polarized light microscope	68
B. Small Angle X-ray scattering	69
2.2.2 Emulsification process by Phase Inversion Composition (PIC)	69
A. Dynamic Light Scattering (DLS)	70
B. Rheological experiments	71
2.2.3 Mesostructured porous materials preparation	72
A. Bare silica materials preparation	72
B. Mesoporous materials prepared from partnership KEL/P123	73
2.2.4 Doped mesostructured hybrid materials preparation	74
A. Loaded mesostructured hybrid materials from KEL doped micelles	74
B. Loaded mesostructured hybrid materials from KEL fine emulsions	76
2.2.5 Materials characterization techniques	76
A. Nitrogen adsorption and desorption analysis	76
B. Scanning electron microscopy (SEM)	79
C. Transmission electron microscopy (TEM)	79
2.2.6 Dissolution test for the drug release evaluation	79
2.2.6.1 Methods for ketoprofen release quantification	80
A. High Performance Liquid Chromatography (HPLC)	80

	Page
2.2.7 In vitro cytotoxicity assay	81
<b>Chapter III. Investigation of the system Kolliphor EL/water for the preparation of mesoporous materials. Addition effect of biocompatible oils and active principles</b>	<b>84</b>
3.1 System Kolliphor EL/Water	85
3.1.1 Phase diagram of Kolliphor EL in water and the study of the observed phases	85
3.1.2 Mesoporous materials prepared from micellar solutions based in Kolliphor EL	89
3.2 Addition effect of the biocompatible oils into the Kolliphor EL/Water system	96
3.2.1 Solubilization effect of Isopropyl Myristate	96
A. Ternary phase diagram Kolliphor (KEL)/Isopropyl myristate (IM)/Water (W)	96
B. Structural parameters of the liquid crystal phases	97
C. Characterization structure of swollen micelles	99
D. Characterization structure of concentrated emulsions	101
E. Mesoporous materials characterization prepared from Kolliphor EL/Water/Isopropyl Myristate	102
3.2.2 Solubilization effect of Miglyol	104
A. Ternary phase diagram Kolliphor (KEL)/Miglyol (Mig)/Water (W)	104
B. Structural parameters of the lamellar and hexagonal phase	105
C. Characterization of the structure of the swollen micelles	106
D. Characterization structure of concentrated emulsions	107
E. Mesoporous materials characterization prepared from Kolliphor EL/Water/Isopropyl Myristate	109
<b>Chapter IV. Porous silica templated by the combination of fine emulsions (Em) and P123 micelles</b>	<b>111</b>
4.1 System Kolliphor EL (KEL) /P123/water	112
4.1.1 Phase diagram of KEL in water and structure of the observed phases	112
4.1.2 Micellar structure and determination of the structural parameters	113
4.2 Silica porous material synthesis	120

	Page
<b>Chapter V. Drug release and <i>in vitro</i> toxicity test</b>	127
5.1 Doped hybrid mesoporous materials characterization prepared from micellar solutions	128
5.2 Drug release of hybrid materials prepared from doped micelles	131
5.3 Doped hybrid mesoporous materials characterization prepared from fine emulsions (Em)	138
5.4 Drug release from loaded hybrid materials prepared with fine emulsions (Em)	141
5.5 Rheological characterization of the doped concentrated emulsions from the system KEL/Mig/Water	143
5.6 Drug release from loaded concentrated emulsions	150
5.7 Biological toxicity of hybrid materials towards HeLa cells	152
General Conclusions	155
Perspectives	158
Bibliography	160
Annexes	172

<b>Index of figures</b>	<b>Page</b>
<b>Figure 1-1.</b> Span structural formula	31
<b>Figure 1-2.</b> Amine ethoxylated structural formula	32
<b>Figure 1-3.</b> Examples of the structural formula of polyol surfactants	33
<b>Figure 1-4.</b> Sucrose molecule	35
<b>Figure 1-5.</b> A trehalose ester structural formula	35
<b>Figure 1-6.</b> Sophorolipids structure	36
<b>Figure 1-7.</b> Rhamnolipids structure	36
<b>Figure 1-8.</b> Lichenysin A and Surfactin structure	37
<b>Figure 1-9.</b> Different types of single chain amino acid-based surfactants (1) O-alkyl esters, (2) N-alkyl amides, and (3) N-acyl amino acids	38
<b>Figure 1-10.</b> Most common fatty acid derivates	39
<b>Figure 1-11.</b> Structure of protein hydrolysate fatty acid	40
<b>Figure 1-12.</b> B-Sitosterol ethoxylated	40
<b>Figure 1-13.</b> Schematic representation of OMS formation according to the surfactant concentration in oil and water	42
<b>Figure 1-14.</b> Schematic representation of the different type of micelles. A) Direct micelles ( $L_1$ ) B) Reverse micelles ( $L_2$ ) C) Bicontinuous phase ( $L_3$ )	43
<b>Figure 1-15.</b> Schematic representation of lamellar phase	44
<b>Figure 1-16.</b> Schematic representation of a bicontinuous cubic liquid crystal (right) and a micellar liquid crystal (left)	45
<b>Figure 1-17.</b> Schematic representation of a hexagonal phase. A) Schema model B) Usual aspect under Polarized Microscopy C) Usual aspect under polarized light	45
<b>Figure 1-18.</b> Ideal phase behavior of a surfactant in water in function of its HLB number and temperature	46
<b>Figure 1-19.</b> Schematic representation of an emulsion <i>Left:</i> O/W emulsion <i>Right:</i> W/O emulsion	47
<b>Figure 1-20.</b> Schematic representation of the free energy of microemulsion and nano-emulsion compared to the phase separated state	48
<b>Figure 1-21.</b> Schematic representation of PIT method	50
<b>Figure 1-22.</b> Typical compressed aspect of a concentrated emulsion under microscope Image from the system Kolliphor EL/Water(R')0.15+90wt% Mig	51
<b>Figure 1-23.</b> Schematic representation of the formation mechanisms. (1) Liquid Crystal Templating Mechanism (LCT), (2) Cooperative Templating Mechanism (CTM)	53
<b>Figure 1-24.</b> Typical drug release profiles from porous carriers	59

	Page
<b>Figure 2-1.</b> Kolliphor EL molecular structure ( $x+y+z = 35$ )	62
<b>Figure 2-2.</b> Poly(ethylene glycol)- <i>block</i> -poly (propylene glycol)- <i>block</i> poly(ethylene glycol) structure ( $x = 20, y = 70, z = 20$ )	63
<b>Figure 2-3.</b> Miglyol molecular structure	64
<b>Figure 2-4.</b> Isopropyl Myristate molecular structure	64
<b>Figure 2-5.</b> Ketoprofen molecular structure	65
<b>Figure 2-6.</b> Polarized light microscope configuration	68
<b>Figure 2-7.</b> Example of textures under polarized microscope	68
<b>Figure 2-8.</b> Preparation of the doped direct micelles of Kolliphor EL	74
<b>Figure 2-9.</b> Hybrid mesophase synthesis from the doped micelles (process A) and $C_{KTP}^{mat}$ determination (process B)	75
<b>Figure 2-10.</b> Type II and Type IV adsorption/desorption isotherms	77
<b>Figure 2-11.</b> Dissolution equipment for the release experiments	80
<b>Figure 2-12.</b> Process of the toxicity test for fresh samples (A), Process for the pre-treated samples before conducting toxicity test (B)	82
<b>Figure 3-1</b> Concentration-temperature phase diagram of the KEL/W binary system	85
<b>Figure 3-2.</b> SAXS spectra of the micellar solutions with 2.5, 5 and 10 wt% of KEL at 25 °C	87
<b>Figure 3-3.</b> Data analyzed by GIFT for the micellar structure determination	88
<b>Figure 3-4.</b> Excess-electron density profiles	89
<b>Figure 3-5.</b> SAXS patterns of the materials synthesized with a surfactant/TMOS molar ratio ( $R'$ ) equal to: 0.017, 0.024, 0.031, 0.049, 0.051, 0.066.	90
<b>Figure 3-6.</b> Nitrogen adsorption-desorption isotherms with the corresponding pore size distribution (insert) of the materials synthesized with a surfactant/TMOS molar ratio ( $R'$ ): 0.017, 0.024, 0.031, 0.049, 0.051, 0.066.	91
<b>Figure 3-7.</b> TEM images of the materials synthesized with a surfactant/TMOS molar ratio ( $R'$ ): 0.017, 0.024, 0.031, 0.049. The micellar concentration is equal to 2.5 wt%.	92
<b>Figure 3-8.</b> SAXS patterns (A) and Nitrogen adsorption-desorption isotherms (B) with the corresponding pore size distribution of the samples synthesized with a KEL concentration of 2.5, 5, 10, 20, 30, 40. The KEL/TMOS molar ratio ( $R'$ ) is fixed to 0.024.	93

<b>Figure 3-9.</b> TEM images of the samples synthesized with a KEL concentration (wt.%) of 2.5, 5,10, 20, 30. The KEL/TMOS molar ratio is fixed to 0.024	95
<b>Figure 3-10.</b> Ternary phase diagram for the system Kolliphor/water/isopropyl myristate at 25 °C	97
<b>Figure 3-11:</b> SAXS spectra of the samples in function of the addition of Isopropyl Myristate for the lamellar phase $L_{\alpha}$ ( $R = 0.25$ ) (a) and for the hexagonal phase $H_1$ ( $R = 0.43$ ) (b) at 25°C. Evolution of the structural parameters in function of $\beta$ for $L_{\alpha}$ (c) and for $H_1$ (d) at 25 °C. $\beta$ is the number of molecules of oil per molecule of surfactant.	98
<b>Figure 3-12.</b> (a) SAXS spectra of the micelles, (b) Corresponding experimental and approximated (GIFT) SAXS spectra in arbitrary units of the micelles, (c) Pair-distance distribution functions (PDDFs); (d) Corresponding excess-electron density profiles	100
<b>Figure 3-13.</b> (a) SAXS spectra of the concentrated emulsions at $R = 5.7$ in function of the weight percent of IM, (b) SAXS spectra of the concentrated emulsions at $R = 5.7$ for the various quantities of IM and of the swollen micelles.	101
<b>Figure 3-14.</b> (a) SAXS spectra of the silica material in function of % Isopropyl Myristate concentration. (b) Nitrogen adsorption-desorption analysis (c) Evolution of the pore volume.	103
<b>Figure 3-15.</b> Ternary phase diagram for the system Kolliphor EL/water/Miglyol at 25 °C.	104
<b>Figure 3-16.</b> SAXS spectra of the samples with the addition of oil at 25 °C for $R = 0.25$ (a) and for $R = 0.43$ (b); Evolution of the structural parameters in function of $\beta$ at 25 °C for $R = 0.25$ (c) and for $R = 0.43$ (d).	105
<b>Figure 3-17.</b> (a) Experimental and approximated (GIFT) SAXS spectra of the samples at $R = 19$ without Miglyol and with 1wt.% of Miglyol at 25 °C (b) Corresponding pair-distance distribution functions (c) Corresponding excess-electron density profiles.	107
<b>Figure 3-18.</b> (a) SAXS spectra of the concentrated emulsions at $R = 5.7$ in log-log representation in absolute units; (b) SAXS spectra of the concentrated emulsions and the micelles at $R = 5.7$ and of pure Miglyol.	107
<b>Figure 3-19.</b> (a) SAXS spectra of the silica material in function of % Miglyol concentration. (b) Nitrogen adsorption-desorption analysis (c) Evolution of the pore volume.	110
<b>Figure 4-1</b> Composition phase diagram (wt.%) at 25°C of the Kolliphor/P123/water system	112

<b>Figure 4-2</b> (A) Experimental and approximated (GIFT) SAXS spectra of mixed micellar solutions of Kolliphor and P123 with a total concentration of surfactant in water equal to 5 wt% at 25 °C. (B) Corresponding pair-distance distribution functions (PDDFs), (C) Corresponding excess-electron density profiles	113
<b>Figure 4-3.</b> Cubic liquid crystal phase. (A) Evolution of the SAXS pattern of the cubic with the Kolliphor (KEL) content in the surfactants mixture; (B) structural parameter of $l_1$ as a function of $x_{KEL}$ and (C) $\square\square$ The total surfactant concentration is 40 wt.%. $\blacksquare$ : $d$ , $\circ$ : $R_H$ and $\blacktriangle$ : S.	116
<b>Figure 4-4.</b> Hexagonal liquid crystal phase: (A) Evolution of the SAXS pattern of the hexagonal conformation with the Kolliphor (KEL) content in the surfactants mixture, (B) structural parameter of $H_1$ as a function of $x_{KEL}$ , (C) $\alpha$ $\blacksquare$ : $d_{100}$ , $\circ$ : $R_H$ and $\blacktriangle$ : S. The total surfactant concentration is 70 wt.%.	117
<b>Figure 4-5.</b> Lamellar liquid crystal phase. (A) Evolution of the SAXS pattern of the hexagonal with the Kolliphor (KEL) content in the surfactants mixture; (B) structural parameter of $L_{\square\square}$ as a function of $x_{KEL}$ and (C) $\square$ The total surfactant concentration is 85 wt.%. $\blacksquare$ : $d_{100}$ , $\circ$ : $d_B$ , $\star$ : $d_A$ and $\blacktriangle$ : S	118
<b>Figure 4-6.</b> Porous materials: Variation of the SAXS pattern as a function of the fine emulsion/P123 micellar solution weight ratio.	120
<b>Figure 4-7.</b> Porous materials: Nitrogen adsorption-desorption isotherms with the corresponding pore size distribution (insert) as a function of the fine emulsion/P123 micellar solution weight ratio.	122
<b>Figure 4-8.</b> Porous materials: Variation of the specific surface area and of the pore volume as a function of the proportion (%) of Em in the starting solution used to prepare the silica materials; $\blacksquare$ : specific surface area $\circ$ : pore volume.	123
<b>Figure 4-9.</b> Porous materials: SEM images of the samples prepared with different Em/P123 weight ratios.	126
<b>Figure 5-1.</b> SAXS spectra from hybrid materials in three different KEL/W (wt%) ratios: A. 0.026 B. 0.053 C. 0.11	129
<b>Figure 5-2.</b> Nitrogen sorption isotherms (A) and pore size distribution (B) for Drug Free materials in three different KEL/W (wt%) ratios: 0.026,0.053,	130
<b>Figure 5-3.</b> Nitrogen sorption isotherms (A) and pore size distribution (B) for calcined materials in three different KEL/W (wt%) ratios: 0.026,0.053, 0.11	130
<b>Figure 5-4.</b> Release profile of KTP to evaluate the retention of the dialysis bag	132
<b>Figure 5-5.</b> A) Effect of the hybrid matrix on the KTP release under the same conditions B) Effect of the addition of P123 micelles in KTP release from loaded hybrid materials KEL/W=0.053	134
<b>Figure 5-6.</b> Experimental KTP release curves from hybrid materials prepared with micellar solutions KEL/W=0.053 under the effect of the addition of P123 in the receptor solution and their corresponding mathematical model adjustment.	135
<b>Figure 5-7.</b> Effect of the pH in KTP release from hybrid materials K/W=0.053 and adjustment of their mathematical models	136
<b>Figure 5-8.</b> SAXS spectra of the materials from fine emulsions (Em) in different Mig/KEL ratios and 80 wt% water in all cases	139
<b>Figure 5-9.</b> Nitrogen sorption isotherms (A) and pore size distribution (B) of the calcined materials prepared from fine emulsions (Em) in three Mig/KEL ratios and 80 wt% water in all cases	140

<b>Figure 5-10.</b> Experimental curves of KTP release from hybrid materials prepared with doped fine emulsions (Mig/ KEL = 0.43) in function of the P123 amount into the receptor solution and the fitted mathematical models of the release.	141
<b>Figure 5-11.</b> Experimental curves of KTP release from hybrid materials prepared with doped fine emulsions (Mig/ KEL = 0.43) in function of the pH of the receptor solution and the fitted mathematical models of the release	142
<b>Figure 5-12.</b> A) Comparison of experimental data for viscoelastic behavior between drug free and loaded after-making concentrated emulsion with 70 wt% of Mig B, C Microscope Optical image for the samples CE70 and CE70_KTP, respectively	145
<b>Figure 5-13</b> Effect of the drug addition in the structural properties for drug free and loaded after-making emulsions with 70 wt% of Miglyol	145
<b>Figure 5-14.</b> Effect of the drug addition in the viscoelastic profile for CE70 in function of time	147
<b>Figure 5-15</b> Aging effect for CE90	148
<b>Figure 5-16</b> Aging effect for drug free CE90 over its structural properties	149
<b>Figure 5-17</b> Aging effect for CE90_KTP over its structural properties	149
<b>Figure 5-18.</b> Experimental curves of KTP release from CE: KEL/W= 0.17+ ● 70wt% Mig and ◆ 90wt% Mig in PbS as receptor solution at pH 7.4	150
<b>Figure 5-19.</b> Experimental curves of KTP release from concentrated emulsions KEL/W= 0.17+ ● 70wt% Mig and ◆ 90wt% Mig in PbS with fitted models	151
<b>Figure 5-20.</b> Graphical results of viability from the studied samples	152

## Index of table

		Page
<b>Table 2-1</b>	Composition of the PBS acetic/acetate buffer solution at pH = 4.6	66
<b>Table 2-2</b>	Compositions of systems used in HeLa experiments	82
<b>Table 3-1</b>	Lattice parameter (a), hydrophobic radius (R <sub>H</sub> ) and cross-sectional area (S) for the cubic and hexagonal phases at different surfactant/water ratios at 25°C	87
<b>Table 3-2</b>	Mesoporous materials characterization parameters	94
<b>Table 3-3</b>	Specific area (S <sub>V</sub> ) and radii of oil droplets (r) estimated from SAXS measurements for the direct concentrated emulsions at R = 5.7 at 25°C	102
<b>Table 3-4</b>	Calculated specific surface (S <sub>V</sub> ) and corresponding calculated radius of droplets (r) for the concentrated emulsions at R = 5.7 at 25°C	109
<b>Table 4-1</b>	Micelles diameter and hydrophobic radius of Kolliphor/P123 mixed micelles. The total concentration of surfactant in water is equal to 5 wt%	114
<b>Table 5-1</b>	Hydrodynamic diameter (nm) for free drug and doped micelles of KEL	128
<b>Table 5-2</b>	KTP rate into the micelles and hybrid materials	128
<b>Table 5-3</b>	Surface and pore volume of free drug and calcined materials	131
<b>Table 5-4</b>	Peppas Sahlin parameters for KTP release under the effect of P123 micelles from hybrid materials based on KEL/W micellar solutions	135
<b>Table 5-5</b>	Parameters of the fitted models for KTP release under pH effect	137
<b>Table 5-6</b>	Hydrodynamic diameter (nm) for drug free and doped fine emulsions (Em) at 25 °C	138
<b>Table 5-7</b>	KTP rate into the fine emulsions (Em) and hybrid materials	139
<b>Table 5-8</b>	Characteristics of calcined materials prepared from fine emulsions (Em) in different Mig/KEL ratios and 80 wt% of water	141
<b>Table 5-9</b>	Parameters of fitted models	142
<b>Table 5-10</b>	Composition of concentrated emulsions for rheology experiments KEL/water = 0.18 (w/w)	143
<b>Table 5-11</b>	Strength of colloidal forces for drug free and loaded after-making concentrated emulsions	144
<b>Table 5-12</b>	Droplet size (μm) of the concentrated emulsion in the aging	146
<b>Table 5-13</b>	Values of %strain for the elastic modulus in the aging	146
<b>Table 5-14</b>	Resultados de los modelos con emulsiones concentradas	150
<b>Table 5-15</b>	Viability results of the studied samples	153

## Abbreviations

**SMO:** Organized Molecular Systems

Direct (1) and inverse (2) phases:

L1, L2, L3: micellar solutions

I1, I2 : cubic micellar phases

H1, H2 : hexagonal phases

L $\alpha$ : lamellar phase

**LCT:** Liquid Crystal Templating

**CTM:** Cooperative Templating Mechanism

**DDS:** Drug Delivery System

**TMOS:** Tetramethyl orthosilicate

**PIC:** Phase Inversion Composition

**MCT:** Medium Chain Triglyceride

**Mig:** Miglyol 812N (oil)

**IM:** Isopropyl Myristate (oil)

**KTP:** Ketoprofen (active principle)

**KEL:** Kolliphor EI (surfactant)

**Em:** Fine emulsions

**CE:** Concentrated Emulsions

**CE90\_KTP:** Concentrated emulsion with 90wt% of doped oil

**MS5:** Micellar solution prepared with 5wt% of KEL

**SM:** Solution of micelles

**HSM:** Hybrid Material from micellar solution

**HSM-KTP:** Doped hybrid material from micellar solution

**CV:** Coefficient of Variability

**S<sub>BET</sub>:** specific surface area

**Ø:** pore diameter

**VP:** porous volume

## Résumé

Les matériaux poreux silicatés sont des composés attrayants en raison de leurs caractéristiques et de leurs propriétés, qui peuvent s'adapter à diverses conditions, selon l'application souhaitée. Puisqu'ils sont biocompatibles et chimiquement inertes, leurs applications sont très diverses, allant des produits pharmaceutiques et cosmétiques jusqu'à la catalyse. L'objectif de ce travail de thèse se concentre sur la préparation de matériaux poreux silicatés hybrides et dopés avec un principe actif, à base de composants biocompatibles pour des applications pharmaceutiques, en tant que systèmes d'administration de médicaments. Les méthodes d'encapsulation et les tests in vitro des matériaux hybrides ont été étudiés en fonction des conditions de synthèse et des caractéristiques physico-chimiques des composés. La motivation de cette étude est liée à la nécessité de répondre à la demande croissante de médicaments plus efficaces, qui peut être satisfaite par la mise au point de systèmes pour transporter des drogues de façon ciblée.

Une alternative pour augmenter la biodisponibilité des médicaments et pour améliorer leur efficacité thérapeutique est focalisée sur l'utilisation de matériaux mésoporeux. Selon la nomenclature et la classification IUPAC, les matériaux mésoporeux ont des tailles de pores comprises entre 2 et 50 nm, une grande surface spécifique et un grand volume poreux. Grâce à ces propriétés, ils peuvent par simple adsorption ou chimisorption encapsuler des principes actifs, dont la libération est soit soutenue, soit déclenchée par un paramètre comme le pH ou la température. Les effets secondaires de ce type de traitement sont atténués, ce qui est un avantage notable. Concernant les matériaux mésoporeux organisés, deux mécanismes de synthèse sont disponibles. La première fait référence à un mécanisme transcriptif appelé Liquid Crystal Templating (LCT), pour lequel le précurseur silicaté se condense directement dans le milieu aqueux d'une phase cristal liquide formée par des molécules de tensioactifs. Ce mécanisme a été appliqué à d'autres template, comme les émulsions. Le second, nommé Cooperative Templating Mechanism (CTM), est basé sur un phénomène coopératif et se produit en présence de micelles. L'ajout du précurseur de silice conduit, par interaction avec les micelles, à la formation d'une phase organisée hybride organique/inorganique analogue aux phases cristal liquide. Ce mécanisme est fondé sur un auto-assemblage, entre les micelles et le précurseur inorganique (tetraméthyl orthosilicate TMOS), soit par des liaisons hydrogène, soit par des interactions de type ionique, selon la nature du tensioactif. La littérature abondante sur le sujet révèle que le réseau poreux peut adopter différentes caractéristiques en fonction du tensioactif et du système moléculaire organisé choisis. De la même façon la taille des pores est modulable.

On peut donc dire que les caractéristiques finales des matériaux poreux sont fortement liées à la structure moléculaire du tensioactif. La plus souvent rencontré est un allongement des canaux poreux selon une symétrie hexagonale, mais il est possible d'obtenir une symétrie cubique ou lamellaire. Par ailleurs, selon la taille de la chaîne hydrophobe il est possible de moduler la taille des pores laquelle permet d'encapsuler et de libérer des quantités différents des principes actifs. Tout fois, la libération n'est pas réellement contrôlée, c'est pourquoi nous proposons d'utiliser des matériaux silicatés hybrides. La formulation est simple puisqu'au lieu d'enlever la partie organique utilisée pour synthétiser les matériaux, elle est maintenue à l'intérieur de la structure silicatée. La phase organique joue donc un double rôle: elle sert de modèle pour la formation de la mésostructure et permet d'augmenter la quantité de principes actifs dans le système par rapport à celle que peut encapsuler un matériau poreux. Ainsi il est probable que le contrôle de la dose libérée soit meilleur et surtout soi prévisible. De plus, la présence de stimuli externes et internes pour déclencher la libération au bon endroit est toujours possible. Ces matériaux sont compatibles avec le secteur pharmaceutique en raison de leur importante stabilité chimique et mécanique. On peut ajouter que, leur faible densité leur permet de s'adapter à la taille du tractus gastro-intestinal et de prolonger la rétention gastrique, si le médicament est pris sous forme orale.

Le premier point d'intérêt de cette étude concerne les composés utilisés qui doivent être biocompatibles, peu coûteux, et être de bons candidats pour la formation de matériaux mésostructurés. Nous avons choisi comme tensioactif le Kolliphor EL (KEL), obtenu à partir de la synthèse de graines de Ricinus communis et d'oxyde d'éthylène dans un rapport molaire de 1:35. Les huiles retenues sont le Miglyol 812N (Mig), un triglycéride à chaîne moyenne (TCM) composé principalement d'acides gras caprylique et caprique ainsi que le Myristate d'Isopropyl (IM) qui est une huile émolliente constituée d'alcool isopropylique et d'acide myristique. Pour le principe actif le Kétoprofène (KTP) a été choisi comme molécule modèle. C'est un composé hydrophobe de type non stéroïdien utilisé pour le traitement de la douleur et de l'inflammation Enfin, les cellules HeLa, qui sont un type particulier de cellules cancéreuses, ont été utilisées pour évaluer la toxicité des matériaux hybrides synthétisés.

Le premier chapitre est consacré à l'état de l'art des structures moléculaires des tensioactifs non-ioniques que s'intéressant en particulier aux composés biocompatibles. Il se termine par la description des propriétés du KEL, qui est un bon solubilisant des composés liposolubles, tels que les vitamines. Ensuite, les principales publications relatives aux matériaux poreux et hybrides en tant que vecteurs de drogues sont résumées. A la fin de ce chapitre, les modèles permettant

de décrire les cinétiques de libération de principes actifs ainsi que les équations correspondantes sont présentées.

Le second chapitre rassemble les modes opératoires ainsi que les techniques de caractérisation utilisés.

Le troisième chapitre est divisé en deux parties. Tout d'abord, le comportement de phase du système binaire KEL/eau est décrit. Les différents domaines à 1 et 2 phases ont été déterminés et caractérisés par inspection visuelle et à l'aide du microscopie optique à lumière polarisée. Afin de confirmer les structures des cristaux liquides, des expériences de diffusion des Rayons X petits angles (SAXS) ont été réalisées.

Les résultats montrent que le KEL forme des micelles sphériques ( $L_1$ ) jusqu'à 35 % en poids, dont la taille est environ 12-13 nm. Lorsque la concentration de KEL augmente, un domaine de cristal liquide apparaît. Tout d'abord une phase très visqueuse et isotrope, identifiée comme cubique ( $I_1$ ) du groupe spatial  $Pm\bar{3}n$  est mise en évidence, puis c'est une phase hexagonale directe ( $H_1$ ) qui fond à 45°C. Les paramètres structuraux de ces 2 phases ont été déterminés par SAXS. Puisqu'une phase micellaire est formée, la synthèse de matériaux mésoporeux a pu être réalisée en utilisant le mécanisme CTM. Ils ont été caractérisés par SAXS et adsorption-désorption d'azote. Les résultats révèlent que la structure du matériau est affectée par la variation du rapport molaire KEL/TMOS (précurseur de silice).

Dans la deuxième partie, l'influence de l'addition d'huile dans le système KEL/eau a été étudiée à 25 °. Les diagrammes de phase ternaires ont été établis avec le Miglyol (Mig) et l'Isopropyl Myristate (IM). Avec le Miglyol, une phase lamellaire apparaît lorsque la concentration en Miglyol est comprise entre 5 et 55 % en poids. Les phases hexagonales et cubiques sont toujours présentes et peuvent solubiliser respectivement 20% et 5% de Miglyol. Par ailleurs des émulsions huile-dans-eau, dites *finés*, avec ces 2 huiles ont pu être formées. Les gouttelettes d'huile des émulsions conventionnelles ont un diamètre de 500 nm à plusieurs microns, tandis que la taille des gouttelettes de ces émulsions fines est inférieure à 100 nm et sont ainsi particulièrement stables. Avec le Miglyol, les émulsions ont été préparées par la méthode PIC, qui consiste à ajouter progressivement l'eau, au mélange huile/KEL. La taille moyenne des gouttelettes d'huile est entre 20-40 nm. D'autre part, dans le domaine riche en huile des émulsions O/W ont été formulées avec une teneur en huile comprise entre 75% et 95%, ces émulsions concentrées sont stables sur plusieurs mois. Dans le cas du IM, les mêmes systèmes ont été mis en évidence. La phase lamellaire est particulièrement stable puisqu'elle peut solubiliser de 2% à 70% d'huile. Les phases hexagonale et cubique sont plus réduites puisque la solubilité d'IM est présentes jusqu'à 15% et 5%, respectivement. De émulsions fines

et émulsions concentrées O/W ont été formulés dans les régions similaires au système contenant du Miglyol.

A partir de des émulsions fines à base de Mig et IM, des matériaux mésoporeux ont été préparés. Avec des conditions de synthèse optimisées, on a réussi à structurer dans les deux cas le réseau mésoporeux. Les matériaux synthétisés à partir des émulsions fines à base de IM ont un diamètre de pores légèrement plus grand (43,2 nm) que ceux préparés avec les émulsions fines à base de Miglyol (35,4 nm). Dans les deux cas, la surface spécifique est d'environ 700 m<sup>2</sup>/g et le volume poreux est proche de 2 cm<sup>3</sup>/g.

Le quatrième chapitre est également divisé en deux sections. Tout d'abord, l'influence de l'addition d'un copolymère block, le P123, dans le système KEL/eau est reportée. Le diagramme de phase est tout d'abord présenté. Il a permis de montrer la compatibilité des deux tensioactifs puisque des micelles et des cristaux liquides ont formés. La phase micellaire existe jusqu'à une concentration totale en tensioactif de 25%, quelle que soit le rapport KEL/P123. Les phases cubique et hexagonale sont présentes. La capacité de ces deux tensioactifs est en relation avec leurs structure moléculaire en présence d'unités oxéthyléniques et de chaînes alkyles dans les deux cas. Dans la deuxième partie du chapitre l'effet de l'addition de micelles de P123 dans les émulsions fines à base d'Isopropyl Myristate, sur les caractéristiques des matériaux poreux ainsi préparés est reporté, ou il est possible de faire varier le degré de porosité des matériaux. Faisant varier la proportion de émulsions (Em) et de micelles de P123 pour des valeurs inférieures à 50/50, on obtient des silices mésoporeuses avec deux tailles de meso-pores. Car le méthanol libéré lors de l'hydrolyse TMOS et la présence des micelles de P123 déstabilisent les émulsions fines qui ne jouent pas le rôle de template et seuls des mesoporous sont présents dans le matériau. Lorsque le rapport Em/P123 augmente, et les émulsions fines restent stables. La quantité de micelles diminue et du coup la quantité de méthanol libéré lors de l'hydrolyse est aussi diminuée et dans ce cas ce sont les gouttes d'huile de l'émulsion fine qui contrôlent la porosité du matériau.

Le cinquième chapitre concerne l'étude de l'encapsulation du KTP dans différents systèmes et de sa libération dans des solutions tampon. Des émulsions concentrées ainsi que des matériaux hybrides préparés à partir de solutions micellaires et d'émulsions fines ont été ainsi sélectionnés. La quantité de KTP qui peut être encapsulée augmente avec la concentration d'huile nécessaire à la préparation du système. Ainsi, les émulsions concentrées sont les meilleurs réservoirs ce point de vue les plus appropriées.

On montre que la structure des matériaux hybride est conservée lorsqu'ils sont dopés avec le KTP. En effet, ces matériaux dopés ont été calcinés pour éliminer la phase organique, et leurs caractéristiques sont identiques à ceux qui n'ont pas été

dopés. La structure de la charpente silicatée est hexagonale, l'isotherme d'adsorption et désorption est de type IV.

Les études de libération du KTP ont été effectuées avec une solution réceptrice tampon de PBS à différents pH : 7,4 ; 1, 2 et 4,6. Ces conditions ont été choisies pour simuler les conditions gastro-intestinales. Les résultats ont montré que, dans des conditions neutres, le pourcentage de KTP libéré par les matériaux préparés à partir de solutions micellaires atteint 38% au bout de 24h. L'effet du pH permet d'augmenter la quantité de KTP libéré.

La libération de KTP a ensuite été étudiée avec une solution réceptrice contenant différentes concentrations en micelles de P123. Dans ce cas la quantité de KTP libéré augmente notablement en présence de 5% de P123, pour atteindre 65% au bout de 24h. La présence de micelles dans la solution réceptrice agit comme un accélérateur de libération. Le KTP étant hydrophobe et très peu soluble dans l'eau, il se dissout dans le cœur hydrophobe des micelles et favorise le phénomène de libération.

Dans la dernière partie de ce travail, l'évaluation de la toxicité des matériaux hybrides dopés en KTP ainsi que systèmes à base de tensioactif utilisés pour leur préparation, à savoir les micelles et les émulsions fines a été réalisée en examinant le comportement de cellules HeLa qui sont un type spécial des cellules cancéreuses. Les résultats montrent que la viabilité cellulaire est augmentée, de 64 à presque 80% avec les matériaux hybrides, car la matrice de silice protège les cellules.

Le tableau suivant résume les résultats obtenus au cours de ces travaux :

Système Moléculaire Organisé	Taille de gouttelettes (Ø)	Materiaux poreux		Libération de KTP à partir des matériaux hybrides	
		Organisation	Taille des pores	% KTP max libérée	Modèle cinétique
Micelles KEL/eau	12-13 nm	Hexagonale	4-6 nm	38 à 64 <sup>(1)</sup>	Peppas Sahlin
Micelles gonflées KEL/eau +IM	18 nm	Vermiforme		--	--
Micelles gonflées KEL/eau +Mig	19-20 nm	Vermiforme		--	--
Fine émulsions KEL/eau/IM	30-46 nm	Hexagonale	10-12 nm	--	--
Fine émulsions KEL/eau/Mig	20-40 nm	Hexagonale	8-10 nm	41 à 57 <sup>(1)</sup>	1er ordre et Higuchi
Fine émulsions KEL/IM/ P123		Double reseau		--	--
		Vermiforme		--	--
Système Moléculaire Organisé	Taille de gouttelettes (Ø)			% KTP max libérée	Modèle cinétique
Émulsions concentrées KEL/eau/IM	4-7 µm			--	--
Émulsions concentrées KEL/eau/Mig	7-10 µm			60 à 97 <sup>(1)</sup>	Peppas Sahlin

(1) Quantité de KTP libérée en fonction des conditions de la solution réceptrice : pH et %wt de P123

## Summary

Silicate porous materials are attractive compounds because of their characteristics and properties, which can be adapted to various conditions, depending on the desired application. Since they are biocompatible and chemically inert, their applications are very diverse, ranging from pharmaceuticals and cosmetics to catalysis. The objective of this thesis work focuses on the preparation of porous hybrid silicate materials doped with an active ingredient, based on biocompatible components for pharmaceutical applications, as drug delivery systems.

Encapsulation methods and *in vitro* tests of hybrid materials were studied according to the synthesis conditions and physico-chemical characteristics of the compounds. The motivation for this study is related to the need to meet the growing demand for more effective drugs, which can be met by developing systems to transport drugs in a targeted manner.

An alternative to increase the bioavailability of drugs and improve their therapeutic effectiveness is focused on the use of mesoporous materials. According to the IUPAC nomenclature and classification, mesoporous materials have pore sizes between 2 and 50 nm, a large specific surface area and a large pore volume. Thanks to these properties, they can simply adsorb or chemisorb active ingredients by encapsulating them, the release of which is either sustained or triggered by a parameter such as pH or temperature. The side effects of this type of treatment are reduced, which is a significant advantage.

For organized mesoporous materials, two synthesis mechanisms are available. The first refers to a transcription mechanism called Liquid Crystal Templating (LCT), for which the silicate precursor condenses directly in the aqueous medium of a liquid crystal phase formed by surfactant molecules. This mechanism has been applied to other templates, such as emulsions. The second, called Cooperative Templating Mechanism (CTM), is based on a cooperative phenomenon and occurs in the presence of micelles. The addition of the silica precursor leads, through interaction with the micelles, to the formation of an organized organic/inorganic hybrid phase similar to liquid crystal phases. This mechanism is

based on self-assembly, between the micelles and the inorganic precursor (tetramethyl orthosilicate TMOS), either by hydrogen bonding or by ionic interactions, depending on the nature of the surfactant. The abundant literature on the subject reveals that the porous network can adopt different characteristics depending on the surfactant and the organized molecular system chosen. In the same way, the pore size can be adjusted.

It can therefore be said that the final characteristics of porous materials are strongly linked to the molecular structure of the surfactant. The most common is an elongation of the porous channels according to hexagonal symmetry, but it is possible to obtain cubic or lamellar symmetry. In addition, depending on the size of the hydrophobic chain, it is possible to modulate the pore size, which allows the encapsulation and release of different quantities of the active ingredients. However, the release is not really controlled, which is why we propose to use hybrid silicate materials. The formulation is simple since instead of removing the organic part used to synthesize the materials, it is maintained inside the silicate structure. The organic phase therefore plays a dual role: it serves as a model for the formation of the mesostructure and makes it possible to increase the quantity of active ingredients in the system compared to the quantity that can be encapsulated by a porous material. Thus, it is likely that the control of the released dose will be better and above all predictable. In addition, the presence of external and internal stimuli to trigger release in the right place is always possible. These materials are compatible with the pharmaceutical sector due to their high chemical and mechanical stability. It can be added that, because of their low density, they can adapt to the size of the gastrointestinal tract and prolong gastric retention, if the drug is taken orally.

The first point of interest of this study concerns the compounds used, which must be biocompatible, inexpensive and good candidates for the formation of mesostructured materials. We have chosen Kolliphor EL (KEL), obtained from the synthesis of *Ricinus communis* seeds and ethylene oxide in a molar ratio of 1:35, as the surfactant. The oils selected are Miglyol 812N (Mig), a medium chain triglyceride (MCT) composed mainly of caprylic and capric fatty acids, and Isopropyl Myristate (IM), an emollient oil composed of isopropyl alcohol and myristic acid. For the active

ingredient, Ketoprofen (KTP) was chosen as the model molecule. It is a hydrophobic non-steroidal compound used for the treatment of pain and inflammation. Finally, HeLa cells, which are a particular type of cancer cells, have been used to evaluate the toxicity of synthesized hybrid materials

The first chapter is devoted to the state of the art of molecular structures of non-ionic surfactants, with a particular focus on biocompatible compounds. It ends with a description of the properties of KEL, which is a good solubilizer of fat-soluble compounds, such as vitamins. Then, the main publications relating to porous and hybrid materials as drug carriers are summarized. At the end of this chapter, the models describing the kinetics of active ingredient release and the corresponding equations are presented.

The second chapter brings together the operating methods and characterization techniques used.

The third chapter is divided into two parts. First of all, the phase behavior of the KEL/water binary system is described. The different 1- and 2-phase domains were determined and characterized by visual inspection and polarized light optical microscopy. In order to confirm the structures of the liquid crystals, small angle X-ray (SAXS) scattering experiments were performed.

The results show that KEL forms spherical micelles (L1) up to 35% by weight, whose size is about 12-13 nm. When the concentration of KEL increases, a liquid crystal domain appears. First of all, a highly viscous and isotropic phase, identified as cubic (I1) of the space group  $Pm\bar{3}n$  is highlighted, then a direct hexagonal phase (H1) melts at 45°C. The structural parameters of these 2 phases were determined by SAXS. Since a micellar phase is formed, the synthesis of mesoporous materials could be achieved using the CTM mechanism. They were characterized by SAXS and nitrogen adsorption-desorption.

The results show that the structure of the material is affected by the variation in the molar ratio KEL/TMOS (silica precursor). In the second part, the influence of oil addition in the KEL/water system was studied at 25°. Ternary phase diagrams were established with Miglyol (Mig) and Isopropyl Myristate (IM). With Miglyol, a lamellar phase occurs when the concentration of Miglyol is between 5 and 55% by weight.

The hexagonal and cubic phases are always present and can solubilize 20% and 5% of Miglyol respectively. In addition, oil-in-water emulsions, called fine, with these 2 oils could be formed. The oil droplets of conventional emulsions have a diameter of 500 nm to several microns, while the droplet size of these fine emulsions is less than 100 nm and are therefore particularly stable.

With Miglyol, the emulsions were prepared by the PIC method, which consists of gradually adding water to the oil/KEL mixture. The average oil droplet size is between 20-40 nm. On the other hand, in the oil-rich area, O/W emulsions have been formulated with an oil content between 75% and 95%, these concentrated emulsions are stable over several months. In the case of IM, the same systems were identified. The lamellar phase is particularly stable since it can solubilize from 2% to 70% of oil. The hexagonal and cubic phases are smaller since the solubility of IM is present up to 15% and 5%, respectively. Fine and concentrated O/W emulsions have been formulated in areas similar to the Miglyol system.

From fine emulsions based on Mig and IM, mesoporous materials were prepared. With optimized synthesis conditions, it was possible to structure the mesoporous network in both cases. Materials synthesized from IM-based fine emulsions have a slightly larger pore diameter (43.2 nm) than those prepared with Miglyol-based fine emulsions (35.4 nm). In both cases, the specific surface area is about 700 m<sup>2</sup>/g and the pore volume is close to 2 cm<sup>3</sup>/g.

The fourth chapter is also divided into two sections. First, the influence of the addition of a block copolymer, P123, in the KEL/water system is reported. The phase diagram is first presented. It showed the compatibility of the two surfactants since micelles and liquid crystals formed. The micellar phase exists up to a total surfactant concentration of 25%, regardless of the KEL/P123 ratio. The cubic and hexagonal phases are present. The capacity of these two surfactants is related to their molecular structure in the presence of oxyethylene units and alkyl chains in both cases. In the second part of the chapter the effect of the addition of P123 micelles in Isopropyl Myristate based fine emulsions on the characteristics of the porous materials thus prepared is reported, or it is possible to vary the degree of porosity of the materials. By varying the proportion of emulsions ( $E_m$ ) and micelles of P123 for

values below 50/50, mesoporous silicas are obtained with two sizes of mesopores. Because the methanol released during the TMOS hydrolysis and the presence of P123 micelles destabilize the fine emulsions that do not act as templates and only mesoporous are present in the material. When the Em/P123 ratio increases, and the fine emulsions remain stable.

The quantity of micelles decreases and as a result the quantity of methanol released during hydrolysis is also reduced and in this case it is the oil drops of the fine emulsion that control the porosity of the material. The fifth chapter concerns the study of the encapsulation of KTP in different systems and its release in buffer solutions. Concentrated emulsions as well as hybrid materials prepared from micellar solutions and fine emulsions have been selected. The amount of KTP that can be encapsulated increases with the oil concentration required to prepare the system. Thus, concentrated emulsions are the best reservoirs from this point of view most appropriate.

It is shown that the structure of hybrid materials is preserved when they are doped with KTP. Indeed, these doped materials have been calcined to eliminate the organic phase, and their characteristics are identical to those that have not been doped. The structure of the silicate structure is hexagonal, the adsorption and desorption isotherm is of type IV. KTP release studies were performed with a PbS buffer receptor solution at different pH levels: 7.4; 1, 2 and 4.6. These conditions were chosen to simulate gastrointestinal conditions. The results showed that, under neutral conditions, the percentage of KTP released by materials prepared from micellar solutions reaches 38% after 24 hours. The effect of pH increases the amount of KTP released.

The release of KTP was then studied with a receptor solution containing different concentrations of P123 micelles. In this case, the quantity of KTP released increases significantly in the presence of 5% P123, to reach 65% after 24 hours. The presence of micelles in the receptor solution acts as a release accelerator. As KTP is hydrophobic and very poorly soluble in water, it dissolves in the hydrophobic core of the micelles and promotes the release phenomenon.

In the last part of this work, the toxicity assessment of hybrid KTP-doped materials and surfactant-based systems used in their preparation, namely micelles and fine emulsions, was carried out by examining the behaviour of HeLa cells which are a special type of cancer cells. The results show that cell viability is increased, from 64 to almost 80% with hybrid materials, because the silica matrix protects the cells. The following table summarizes the results obtained during this work:

<b>Organized Molecular System</b>	<b>Droplet size (Ø)</b>	<b>Porous material</b>		<b>KTP release from hybrid materials</b>	
		<b>Organization</b>	<b>Pore sizes</b>	<b>% KTP max released</b>	<b>Kinetic model</b>
Micelles KEL/water	12-13 nm	Hexagonal	4-6 nm	38 à 64 <sup>(1)</sup>	Peppas Sahlin
Swollen micelles KEL/water +IM	18 nm	Vermiform		--	--
Swollen micelles KEL/water +Mig	19-20 nm	Vermiform		--	--
Fine emulsions KEL/water/IM	30-46 nm	Hexagonal	10-12 nm	--	--
Fine emulsions KEL/water/Mig	20-40 nm	Hexagonal	8-10 nm	41 à 57 <sup>(1)</sup>	1st order and Higuchi
Fine emulsions KEL/IM/ P123		Double network		--	--
		Vermiform		--	--
<b>Organized Molecular System</b>	<b>Droplet size (Ø)</b>			<b>% KTP max released</b>	<b>Kinetic model</b>
Concentrated emulsions KEL/water/IM	4-7 µm			--	--
Concentrated emulsions KEL/water/Mig	7-10 µm			60 à 97 <sup>(1)</sup>	Peppas Sahlin

(1) Amount of KTP released with the conditions of the receptor solution: pH and %wt of P123

## Introduction

Over the past few years the silicated porous materials have been attractive due to their properties which confers an adaptability to several conditions according to the desired application. As biocompatibles and chemically inert, they can be considered for several applications as pharmacy, cosmetics or catalysis, among others. These materials are obtained by polycondensation of an silica precursor: TMOS in presence of surfactants where the molecular assemblies that they form in water are acting as a template. Multiple structures have been obtained with the use of different surfactants that allows to form several molecular arrays to modulate the size of the porous. Then, the resulting characteristics of meso- or macro-mesoporous materials are highly related to the type of surfactant.

The interest of this work is focused in the pharmaceutical domain. Drug Delivery Systems (DDS) is an important component of drug development and therapeutic. It is defined as a formulation or device that enables to introduce a therapeutic substance in the body and improving the efficacy and safety by controlling the rate, time, and place of release of drugs. This process includes also the administration of therapeutic products, the release of active ingredients and the subsequent transport until the active site. If a device is introduced into the human body for other purposes than drug administration, such as therapeutic effect, the drug may be incorporated into a device for preventing complications resulting from the device.

Normally as a criterion of regulation the device has to include certain characteristics as: increasing the bioavailability of the drug, provide for controlled drug delivery, transport the drug into the site of action avoiding the non-diseased host tissues, the product should be stable, to have a high degree of drug dispersion, should be easy to administer to the patients, among others. The formulation should be according to the purpose into the body and the drug specifications. Into this application, structured porous inorganic materials have been used due to their match with the regulation criterions for a DDS vector formulation as their important chemical and mechanical stability under an-array of physiological conditions. In the case of mesoporous materials, the matrix of pores can be organized, such property has been used to achieve a sustained, controlled or pulsed release in DDS. Their large surface area together with their large pore volume have been used to improve the solubility of poorly soluble drugs. Their low density allows them to flat into the gastrointestinal tract and prolong the gastric retention of oral drugs. Finally, the diffusion-controlling porous membranes or coatings of those materials can be tailored with specific pore sizes to control drug release in eluting devices.

To achieve a good carrier, the hybrid materials and/or the hierarchical porous silica materials can offer good solutions due to their capacity to encapsulate an important amount of active principle and their ability to control the drug release thanks to the external or internal stimuli. Into this research silica hybrid mesostructures, were prepared from organized molecular assemblies based in biocompatible compounds, using Kolliphor EL (KEL) as surfactant and Miglyol (Mig) or Isopropyl Myristate (IM) as oil. The literature reports the advantages of Kolliphor EL (KEL) as solubilizer of fat-soluble compounds, as for example vitamins and hydrophobic drugs, showing good compatibility with other biocompatibles products. This assertion motivates the use of silica materials prepared from the KEL systems that will act as template to their further application as drug nanocarrier. The synthesis of hybrid materials combines the sol-gel chemistry and the use of surfactant molecules assemblies as framework templates.

Into this investigation, the first work concerns the study of the KEL/water system and the preparation of silicated hybrid materials in presence of micelles using the Cooperative Templating Mechanism (CTM). Then the influence of the addition of Miglyol 812N or Isopropyl Myristate, as oil, was studied and the corresponding ternary phase diagrams were established. Then, the mineralization of fine emulsions allowed to obtain hybrid materials using the Liquid Crystal Template Mechanism (LCT). In the fourth chapter the hierarchical porous silica was prepared by combining the Pluronic P123 micellar solution and the fine emulsions formulated from the system KEL/ water / IM. Previously, to have information about the compatibility degree between the two surfactants, the system KEL/P123/water was studied in detail.

Finally, the fifth chapter is focused in the study of the encapsulation of a hydrophobic active principle, the Ketoprofen (KTP), chosen as a model drug into the hybrid materials developed, and its release under different conditions. Various systems as micelles, fine emulsions and concentrated emulsion into which the drug was solubilized were used for the hybrid materials synthesis. The release is carried out in a PbS buffered receptor solution at pH 7.4. In addition, these profiles are compared with those obtained in acidic conditions, which try to simulate the acidic conditions in the stomach. Eventually the study of the influence of addition of micelles of Pluronic block copolymer (P123) into the receptor solution is also followed. In the last part the evaluation of the toxicity degree for the hybrid materials and the non-silicate systems is carried out through cells test, in the HeLa cells cultures which are a special type of cancer cells.

## Aim of the thesis

The proposed subject falls under the general scope adopted by the research group several years ago. This scope aims to elaborate and understand the function of structured porous materials in relation with organized molecular assemblies used for the preparation of porous silica. Emulsions are used in order to control the size of the macropores in the hierarchically porous materials; moreover, they present advantages over other templates such as the capacity to dissolve large amounts of hydrophobic molecules. The general application of interest in this research is the drug delivery from hybrid materials: which are the silicated materials that preserve the inner organic phase which contain the active ingredient entrapped.

The first proposition is to characterize the systems as micelles, liquid crystals, fine and concentrated emulsions formed from biocompatible components as Kolliphor EL, Mygliol 812N, Isopropyl Myristate and P123. So as first step is proposed to describe the behaviour of Kolliphor EL in water, characterizing the phases obtained, then, the second goal correspond to the study of the addition effect of a third component as Miglyol or Isopropyl Myristate into the Kolliphor/water system, determining the best conditions for the formation of fine and concentrated emulsions as well as an in depth characterization of their physicochemical properties throughout their aging . The mineralization of the systems will be then considered. Once knowing the behaviour of the Kolliphor in water and its interaction with the biocompatibles oils, is proposed to study the synergy with a triblock copolymer in order to prepare the porous silica templated by the combination of fine emulsions and P123 micelles to obtain hierarchically porous silica materials. Once the synthesis conditions of materials can be optimized, and the resulting materials deeply characterized, it is possible to get to the heart of this research: to design a new drug delivery system from hybrid materials based in biocompatible components.

The drug delivery system will be achieved by encapsulating a model drug molecule “Ketoprofen” and *in vitro* study of the release profile will be engaged. Ketoprofen ( $C_{16}H_{14}O_3$ ), is a potent non-steroidal anti-inflammatory drug (NSAID) possesses also analgesic and antipyretic properties which has a very low water solubility ( $0.0213 \text{ mg}\cdot\text{ml}^{-1}$ ) with a pKa value of 4.2 – 4.4. Prescription ketoprofen is used to relieve tenderness, swelling, and stiffness caused by osteoarthritis (arthritis caused by a breakdown of the lining of the joints) and rheumatoid arthritis (arthritis caused by swelling of the lining of the joints). Ketoprofen capsules are also used to relieve pain, including menstrual pain (pain that occurs before or during a menstrual period). It works by stopping the body's production of prostaglandin a substance that causes pain, fever, and inflammation (Coaccioli, 2011).

The release mechanism of this hydrophobic component will be investigated in detail in order to propose the pharmacokinetic models that can explain the phenomena of drug dissolution into different conditions of pH: 1.2, 4.6 and 7.4 trying to simulate the conditions of the gastrointestinal tract, this goal will be reached in collaboration with the pharmaceutics group of Professor Maria José García-Celma at the University of Barcelona.

In the last part of this study the toxicity of these synthesized hybrid carriers will be determined by performing *in vitro* tests over HeLa cells. HeLa cells are a special type of cancer cells. HeLa cells have error-filled genomes, with one or more copies of many chromosomes: a normal cell contains 46 chromosomes, whereas HeLa cells contains 76 to 80, some of which are mutated. This is due to the Human Papillomavirus (HPV), the cause of nearly all cervical cancers (Landry, 2013). HeLa was the first human cell line established, that grows unusually fast, doubling cellular count in only 24 hours, making them ideal for large scale testing. This cell culture is characterized to be highly resistant to apoptosis, meaning they will divide several times. This performance can be explained by the expression of an overactive telomerase that rebuilds the telomeres after each division, allowing the perpetual proliferation (Bidon 2018). With all these characteristics, HeLa cells were selected as a potentially more sensitive bioassay organism because of the absence of a protective tissue. The toxicity of different carriers prepared will be evaluated with response of the bioavailability in this culture.

# Chapter I. Generalities

This chapter briefly explains some notions necessary for the understanding of the development of this thesis.

The first part focuses on the description of the different types of surfactants that are currently known and emphasizes those of a non-ionic nature of the biocompatible type.

Then, the second part mentioned the self-assembling characteristics of surfactant molecules, known as Organized Molecular Systems (OMS).

The third part present the porous materials prepared from OMS prepared with nonionic surfactants as structuring agent, the involvement of surfactant in the formation of these materials, their properties and a brief compilation of their applications.

In the fourth and last part, the application of these porous materials as carriers for the release of drugs is highlighted. It also explains the type of response obtained in the release of the active principle according to the material configuration as well as the applicable kinetic models that are used to describe the behaviour.

## 1.1 Surfactants and their Organized Molecular Systems

Surface active agents, usually known as surfactants, are amphiphilic molecules divided in two parts: a moiety that have an affinity towards polar compounds, hydrophilic part known as “head group”, that normally contains heteroatoms such as O, S, P or N, included in functional groups such as alcohol, ether, ester, acid, sulfate, sulfonate, phosphate, amine, amide, etc. (Salager, et al., 2002) and a moiety that have an affinity towards non-polar compounds (hydrophobic part known as: “tail group”) composed generally by one or several alkyl or alkyl-aryl chain, sometimes with halogen atoms and even a few non ionized oxygen atoms. (Porter, 1993). The hydrophobic chain can be a single, double, straight or branched hydrogenated part, but it may be also a fluorocarbon or siloxane chain. (Tadros, 2004)

### 1.1.1 Classification of surfactants

From the commercial point of view, the surfactants are classified according to their use, however, from the technical and scientific aspect the classification is given according to their hydrophilic identity (Salager, 2002). The surfactants have three types of hydrophilic groups: anionic, cationic or zwitterionic (*amphoteric*) (Zana, R. 2005).

The *cationic surfactants* are positively charged. A very large proportion of the cationic part correspond to nitrogen compounds such as fatty amine salts and quaternary ammoniums, with one or several long chains of the alkyl type, often coming from natural fatty acids (Salager, 2002).

The *anionic surfactants* are dissociated in water in an amphiphilic anion, and a cation which is general an alkaline metal ( $\text{Na}^+$ ,  $\text{K}^+$ ) or a quaternary ammonium. They include alkylbenzene sulfonates (detergents), (fatty acids), soaps, lauryl sulfate (foaming agent), di-alkyl sulfosuccinate (wetting agent), lignosulfonates (dispersants), etc. Anionic surfactants account about 50% of the world production (Salager, 2002).

Into this work the interest will be focused in the *nonionic surfactants*, which are close about 45% of the world production. The most common nonionic surfactant are those based on ethylene oxide, referred as ethoxylated surfactants. This type of surfactants do not ionize in aqueous solution, because their hydrophilic group is non-dissociable, such: alcohol, phenol, ester or amide (Tadros, 2005).

. As a particularity, the nonionic surfactants have their critical micellar concentration (CMC) about two orders of magnitude lower than the corresponding anionics with the same alkyl chain length. (Salager, 2002). According to the literature

these surfactants are classified into eight main groups: (Schick M. J., 1966, 1987 and 1970)

A. Alcohol ethoxylates. Produced by ethoxylation of a fatty chain alcohol such a dodecanol. A typical example is dodecyl hexaoxyethylene-glycol monoether (C<sub>12</sub>E<sub>6</sub>). The solubility of this type of surfactant depends both on the alkyl chain length and the number of ethylene oxide units in the molecule.

B. Alkyl phenol ethoxylates. These surfactants are prepared by reaction of ethylene oxide with appropriate alkyl phenol. The most common are those based on nonylphenol having a good disperssion properties, they are potentially toxics, therefore have been removed partially from the market.

C. Fatty acid ethoxylates. They are produced by reaction of ethylene oxide with a fatty acid or a polyglycol and have the general formula RCOO-(CH<sub>2</sub>CH<sub>2</sub>O)<sub>n</sub>H. These surfactants are generally soluble in water if they are enough EO units and the alkyl chain lenght of the acid is not too long.

D. Sorbitan esters and their ethoxylated derivatives

Fatty acid esters of sorbitan (Span) and their ethoxylated derivatives (Tweens) are the most used nonionics surfactants in food additives, cosmetics and pharmaceutical preparations. The Spans are produced by reacting sorbitol with a fatty acid at a high temperature (>200°C). After the reaction with a fatty acid, the sorbitan monoester has the next structural formula of the Figure 1-1:

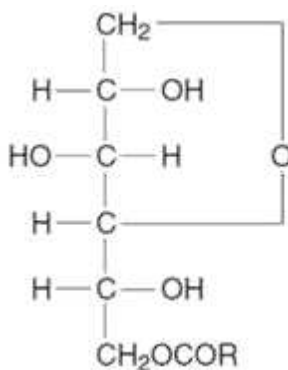


**Figure 1-1.** Span chemical structure  
From: PubChem website

## E. Amine ethoxylates

These surfactants are prepared by addition of ethylene oxide to primary or secondary fatty amines. With primary amines, both hydrogen atoms on the amine group react with ethylene oxide, then the surfactant results as the Figure 1-2:

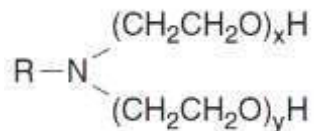


**Figure 1-2.** Amine ethoxylated chemical structure  
From: PubChem website

## F. Ethylene Oxide Propylene Oxide co-polymers (EO/PO)

These surfactants may be regarded as polymeric surfactants, their trade name is mostly known as *Pluronic*. Two types may be distinguished. Those prepared by reaction of poly(oxypropylene glycol) with EO or mixed EO/PO giving block copolymers:  $(\text{EO})_n(\text{PO})_m(\text{EO})_n$ . The second type is prepared by the reaction of poly(ethylene glycol) with a PO or mixed PO/EO giving the structure:  $(\text{PO})_n(\text{EO})_m(\text{PO})_n$ , where  $n$  and  $m$  are varied systematically.

## G. Ethoxylated fats and oils

Recently, the natural fatty acids have been used as intermediate materials in several industries replacing the harmful and expensive petrochemicals. Most fatty acids are obtained by hydrolysis of oils from various oleochemical sources and their composition is determined by the origin and production method. Ethoxylated fatty acids are well known as ether-ester-type nonionic surfactants with wide applications in pharmaceutical, oral and cosmetic fields (Shattory, 2012).

Another important class of surfactants are those classified as biosurfactants, which are generally biocompatible and have been introduced into the industry thanks to their low toxicity. This type of surfactants are classified according to their synthesis method and chemical characteristics: surfactants prepared by fermentation, surfactants based on a natural polar headgroup and surfactant based on a natural hydrophobic tail (Holmberg, 2001).

### 1.1.2 Biocompatible surfactants

Society is increasingly concerned with safety issues, while looking for a sustainable future. In response, the sustainable chemistry aspires to raise the bet on less dangerous chemicals as well as production of environmentally friendly high-quality products from renewable resources, which result in the development of surfactants based on carbohydrates and vegetable oils.

The challenge is to find renewable surfactants with biocompatible and multifunctional capabilities. The use of hydrophilic renewable raw materials, such as amino acids, sugar fatty acids and vegetable oil derivatives to prepare biocompatible surfactants that grant the mild reaction conditions, is an attractive activity to prepare “natural” surfactants.

The term “natural surfactant” is not unambiguous. The source may be of either plant or animal origin and the product should be obtained by separation process as extraction, precipitation or distillation (Holmberg, 2001). However, the surfactants obtained by microorganisms are also becoming important biotechnology products for industrial and medical applications due to their specific modes of action, low toxicity, relative ease of preparation and widespread applicability (Singh, 2007).

The biocompatible surfactants are better known as natural ones. These types of surfactants have the hydrophobic and hydrophilic part from a natural source. The sub-classification of the natural surfactants into this part is done according to these characteristics.

#### A. Sugar-based surfactants

##### A1. Alkyl-polyglucosides (APGs)

The most common surfactants of this type have been sorbitane alkanooates and ethoxylated sorbitane alkanooates known with the trade name of Span® and Tween®, respectively. Three classes of surfactants with sugar or polyol as polar head has been studied: alkyl polyglucosides (APGs), alkyl glucamides and sugar esters (Figure 1-3).

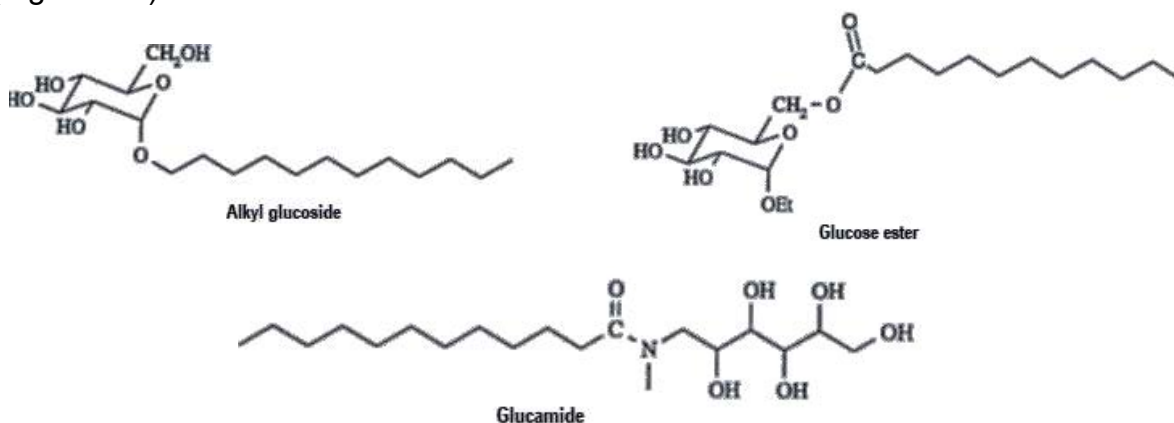


**Figure 1-3.** Examples of the chemical structure of polyol surfactants  
From: PubChem website

AGPs are synthesized by direct reaction of glucose with fatty alcohol, using a large excess of alcohol in order to minimize sugar oligomerization. Alternatively, they are made by transacetalization of a short chain alkyl glucoside, such as ethyl or butyl glucoside. Alkyl glucoside are stable at high pH because in low pH they hydrolyze to sugar and fatty alcohol. AGPs and other polyol-based surfactants are more lipophobic than their polyethylene-based counterparts (Holmberg, 2001).

The main attractiveness of APGs lies in their favorable environmental profile: the biodegradability index is high, and the water toxicity is low. AGPs also exhibit favorable dermatological properties, being very mild to skin and eye. This property makes this surfactant class attractive for personal care products, but also for technical applications.

## A2. Sugar fatty acid esters (SFAEs)

Sugar fatty acid esters has been receiving attention due to their natural and single characteristics. Condensation of one of the reactive sugar hydroxyl functionalities with a fatty acid yields a biosurfactant that has potential application in food, cosmetic and pharmaceuticals (Holmberg, 2003). SFAEs contain one or more saccharide rings, linked to one or multiple hydrophobic fatty acid chains.

The most common fatty acids observed in sugar esters are: lauric (C12:0), myristic (C14:0), palmitic (C16:0), stearic (C18:0), oleic (C18:1), behenic (C22:0) and erucic acid (C22:1). (Pérez, 2017) SFAEs can be synthetically tailored for a specific application and present a variety of hydrophilic-lipophilic balance (HLB) values ranging from 1-16. Depending on this value the physicochemical properties for specific uses are determined. Due to their tasteless, odorless, nontoxic and biodegradability are excellent for food emulsifiers (Ducret, 1996). Then, thanks to their antimicrobial and antitumor properties, they have demonstrated their importance for pharmaceutical applications. (Ferrer 2005a).

Sugar esters may be produced by either chemical or enzymatic pathways, they were commercialized first by Mitsubishi-Kasei Co. in the late 1960s. The chemical method is based on transesterification with alkalyne catalyst in dimethyl sulfoxide using the fatty acid methyl ester as acilating agent and operating the system at high temperature (Holmberg, 2003). As an alternative synthesis method, the enzymatic approach provides good control in the stereoselectivity and regioselectivity under milder conditions. In contrast with the chemical process, enzymatic reactions are environmentally friendly, afford sugar esters with a high degree of selectivity and control over substitution without caramelization risk produced often in the transesterification step. (Van Der Plank and Rozendaal, 1991)

One of the most common sugar fatty acid esters due to their low cost and availability is the sucrose (Figure 1-4). Sucrose is abundantly in the world at very high purity, its being synthesised as a by-product of photosynthesis.

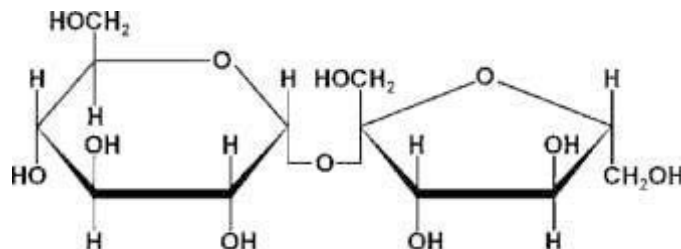


**Figure 1-4.** Sucrose chemical structure  
From: PubChem website

### A3. Surfactants prepared *via* fermentation

#### A.3.1. Acylpolyols

This type of surfactants are usually fatty acids connected to disaccharides by ester bonds. They are an extracellular compound produced by actinomycetes such as *Mycobacterium*, *Corynebacterium* and *Brevibacterium* (Haferburg,1986). A common example is the *trehalose ester* (Figure1-5), highly used in the pharmaceutical industry, tested into the microparticles synthesis for the release mechanism of insulin via inhaled. (Davidson, 2003)

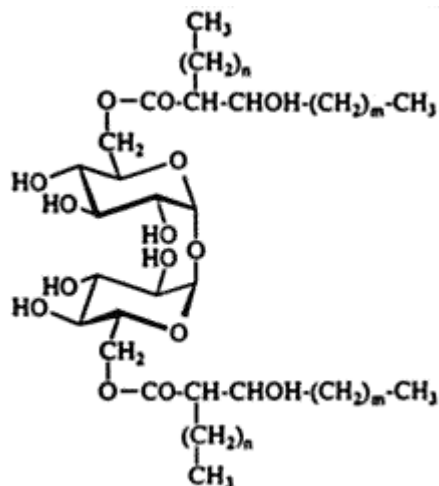


**Figure 1-5.** A trehalose ester chemical structure  
From: PubChem website

### A.3.2 Glycolipids

This type of surfactants are usually hydroxy fatty acids attached to a sugar via glycosidic bond. Sophorolipids (Figure 1-6) and rhamnolipids (schema 1-7) are good examples, produced by *Candida bombicola* and by *Pseudomonas aeruginosa* as exoproducts respectively (Guerra-Santos, 1986).

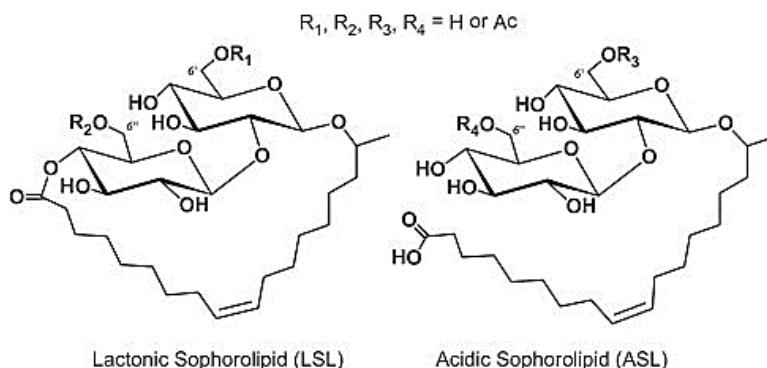


**Figure 1-6.** Sophorolipids chemical structure  
From: PubChem website

Sophorolipids are scalable biosurfactants with promising surface activity. By tuning the surfactant structure, adsorption and emulsification can be optimized, but also those structures modified can cause depletion flocculation in the oil/water surface (Koh,2016).

Rhamnolipids are surface-active glycolipids (Figure 7), that normally are produced by *Pseudomonas aeruginosa*, but recently has been found that other bacteria species can produce them as well (Mohammad A. *et al.*, 2010). The rhamnolipids represent one of the most important classes of microbial surfactants, differing in fatty acid chain composition (C8, C10, C12), showing even unsaturated forms (C12:1), as well as rhamnose moieties (Costa, 2010).

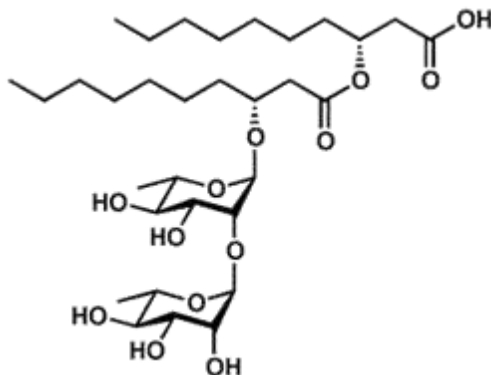


**Figure 1-7.** Rhamnolipids chemical structure  
From: PubChem website

Therhamnolipid properties depend on their relative composition which is determined by the bacterial strain, culture conditions, and medium composition. Rhamnolipids have been used in various processes such as in bioremediation of hydrocarbons from contaminated soil and water, heavy metal removal, soil washing and oil spills. Due to their physicochemical characteristics, rhamnolipids are expected to be more effective than synthetic surfactants and can be blended with other (bio and/or synthetic) surfactants to offer the desired performance characteristics (Costa, *et al.*, 2010).

### A.3.3 Acylpeptides

Knowns also as lipopeptides, they are usually cyclic compounds based on hydroxy acid and a short peptide chain. The most common are produced by *Bacillus subtilis* and *Bacillus licheniformis* and are commercially trades as Surfactin® and Lychenysin® respectively (Figure 1-8). Surfactin is well recognized due to its antibiotic, antibacterial, antiviral, anty-mycoplasma and hemolytic activities. In contrast, Lychenysin® is widely used for enhancement of oil recovery and Bioremediation (Eruke, 2015).

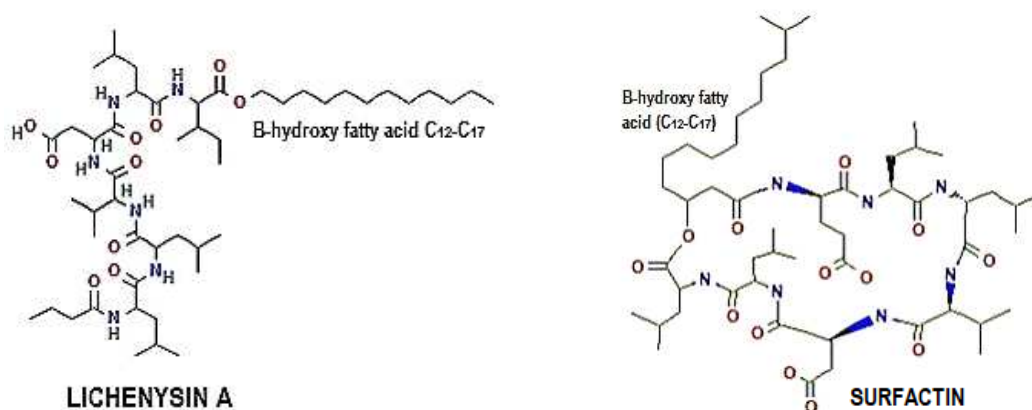


**Figure 1-8.** Lichenysin A and Surfactin chemical structure  
From: PubChem website

### B. Amino acid as polar head group

Aminoacids and short peptides constitute an alternative to sugars as natural polar headgroup surfactants (Figure 1-9). This type of surfactants constitute an important class of natural surface-active bio-molecules and are derived from acidic, basic or neutral aminoacids. Aminoacids such as glutamic acid, glycine, alanine, arginine, aspartic acid, leucine serine, among others has been used to synthesize biosurfactants that are commercialized into human use products as: toothpaste, wound cleaners, shampoo, etc (Pinazo 2011).

More recently has been demonstrated that the amino acid esters and amides have an excellent emulsifying and strong antimicrobial properties, which make them an attractive alternative as a food additive. The amino acid-based surfactants are possible candidates for pharmaceutical applications and the hemolytic action of some lysine-based anionic surfactants has been investigated (Holmberg, 2001).

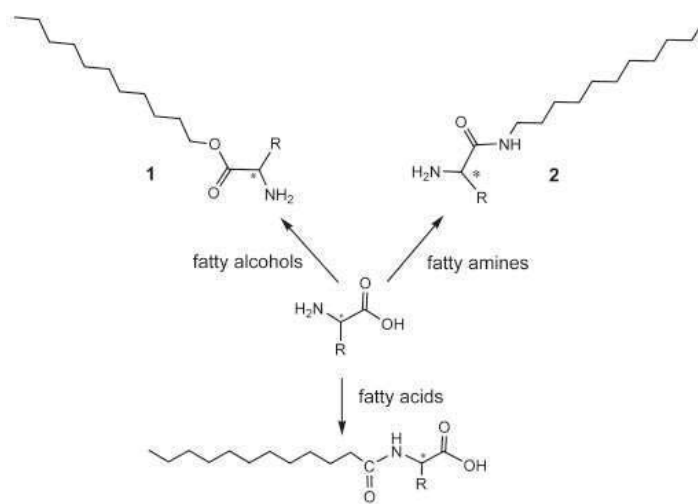


**Figure 1-9.** Different types of single chain amino acid-based surfactants:  
 (1) O-alkyl esters, (2) N-alkyl amides, and (3) N-acyl amino acids.  
 From: PubChem website

Using a combination of organic and bio-organic synthesis arginine-based gemini surfactants have been synthesized by the group of Infante and their properties were investigated. These gemini surfactants consisted of two N-acylarginine moieties connected via arginine carboxyl groups by a diamino spacer molecule. The gemini surfactants synthesized from cystine and arginine have applications into the textile industry and as antibacterial agent respectively (Pinazo, 2011).

## C. Surfactants based on a natural hydrophobic tail

### C1. Fatty acid as hydrophobic tail

Most fatty acids are obtained by hydrolysis of oils from various oleochemical sources: animal, marine and plant. And the composition is determined by the origin and production method. Animal sources, as lard and tallow are characterized by high concentrations of saturated fatty acids, while marine sources (fish oils) are characterized by long-chain and unsaturated acids (Svensson, 2010).

The fatty acid composition of oils from plant sources varies greatly according to plant origin and cultivar. Commercially exploited seeds such soya, rape, sunflower and linseed have been the subject of many years breeding programmes to obtain oils with a particular fatty acid patterns (Johansson, 2001). The number of possible

derivatives of fatty acids is overwhelming, the figure 1-10 shows the most common compounds, which are also divided in anionic and nonionic.

Due to the low hard water stability and high skin irritation, traditional fatty acid soaps cause problems in many practical applications. To overcome this, surfactants as  $\alpha$ -sulfo fatty acid methylesters ( $\alpha$ SME) and sulfates like cocomonoglyceride sulfates has been synthesised and investigated. The  $\alpha$ -sulfo alkyl fatty acid esters are versatile products with many structural variation possibilities.

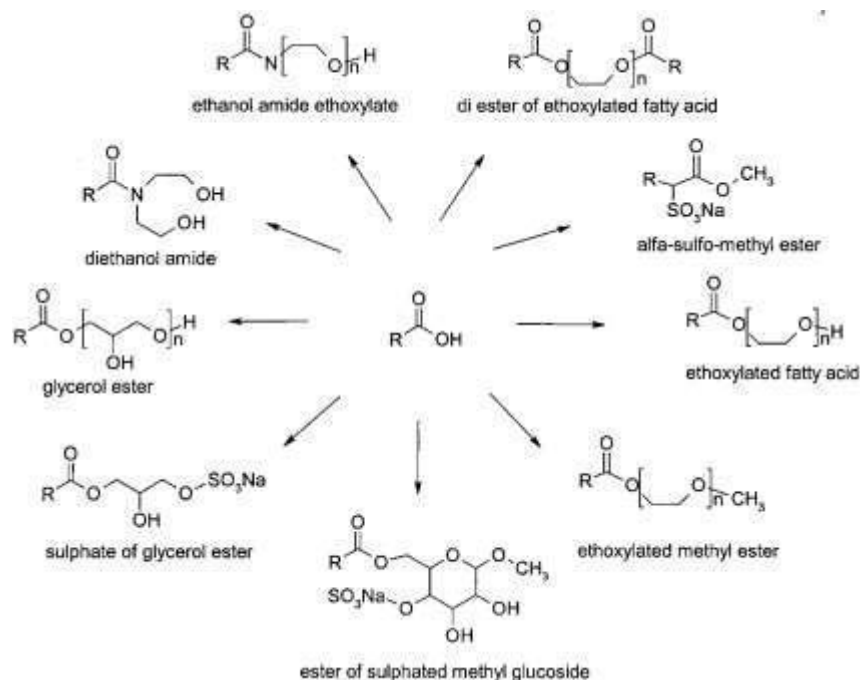


**Figure 1-10** Most common fatty acid derivatives  
Johansson and Svensson, 2001

The use of proteins as raw material for personal and home care products has been known about more than 60 years. Typically, the natural proteins are degraded by hydrolysis (either chemically or enzymatically) and the respective protein hydrolysates are obtained. Subsequent acylation of the protein hydrolysates with fatty acids results in protein surfactants, the so-called *protein fatty acid condensates*. These products are based completely on natural raw materials, namely fatty acids (from vegetable oil) and the protein or protein hydrolysate as the hydrophilic part in the surfactant molecule (Figure 1-11) and are widely used in the skin care.

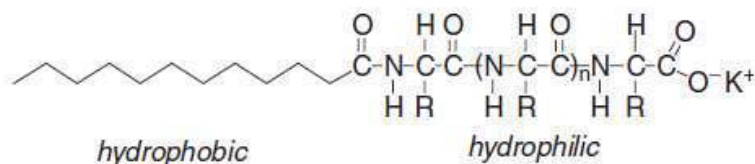


**Figure 1-11.** Chemical structure of protein hydrolysate fatty acid condensates  
 EI-Shattory, 2012

Appart of the excellent skin compatibility with an excellent performance in the cleaning, in combination with other surfactants, lead to an increase the synergy. For instance, even small additions of the acylated protein hydrolysate improve the skin compatibility of other surfactants (EI-Shattory, 2012).

## C2. Sterol as hydrophobic tail

Sterol-based surfactants are of interest because of the large hydrophobic group of fully natural origin. Phytosterols are sterols of plant origin and their structure is like that of colessterol. The sterols contain a secondary hydroxyl group that can be ethoxylated. The alcohol is sterically blocked, and the reaction with ethylene oxide is not straightforward (Folmer, 1999). The structure of a representative sterol ethoxylate is shown in the Figure 1-12.

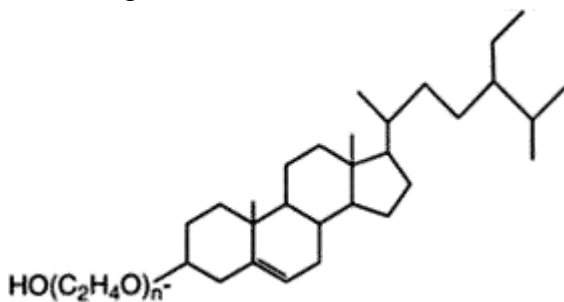


**Figure 1-12.** B-Sitosterol ethoxylated chemical structure  
 From: PubChem website

### 1.1.3 Hydrophilic-lipophilic balance (HLB)

Many attempts have been made to correlate surfactant structures with their efectiveness as emulsifiers, the most successful and still used is the HLB scale proposed by Griffin in 1949 (Griffin, 1949). For the alkoxyated non-ionic surfactants  $C_x(EO)_y$ . (Tadros, 2005). This size is calculated according to the following equation:

$$HLB = 20 * \left( \frac{M_{hydrophile}}{M_{tensioactif}} \right)$$

were  $M_{\text{surfactant}}$  = molecular weight of the surfactant and  $M_{\text{hydrophilic}}$  = molecular weight of the hydrophilic part of the surfactant.

The HLB number for a given data of amphiphilic compounds allows to have an idea about the sequence of the structures that can be obtained. For example, a surfactant that shows an HLB <10, can be classified as hydrophilic, forming reverse structures and eventually lamellar phases. For an HLB value >12 the surfactant is considered as hydrophobic and form direct structures, in the last if the HLB value between 10-12 the surfactant can be considered as equilibrated and its possible to obtain direct and reverse structures in the same time (Sjöblom, J. 2001).

## 1.2 Organized Molecular Systems (OMS)

The interaction media are among others the most important factor to be considered into the aggregation surfactant phenomena. This interaction is given thanks to self-association phenomena, which is cooperative mechanism and starts at a certain concentration, the so-called *Critical Micellization Concentration (CMC)* for water-soluble surfactants or low HLB value, the Critical Agregation Concentration (CAC) for the surfactants with hydrophobic character.

The CMC and HLB are the most important characteristics of surfactants. From the CMC or CAC, the surfactant molecules can self-organizing to give rise different types of aggregates as independent entities. These arrays depend of the surfactant molecular structure, when the concentration is low the micelles appears, or different types of arrangements with big distance appears, being known as liquid crystals. (Zana, R. 2005).

In the case of the water-soluble surfactants, with non-ionic compounds, the molecular self-assemblies correspond to the following evolution, according with the surfactant concentration:  $L_1$ - $I_1$ - $H_1$ - $V_1$ - $L_\alpha$ - $V_2$ - $H_2$ - $I_2$ - $L_2$ . This sequence describes the passage of direct phases (where the amphiphilic film courvature turns into the apolaire medium) through the inverse phases (courvature turned into the water), passing for a lamellar phase where the courvature is nulle or zero. (Figure 1-13) (Bize, 2010).

In addition to the surfactant concentration, the temperature is an important factor for the variation in the curvature of the interface between the hydrophilic and hydrophobic domains. For a water-soluble surfactant with weak concentrations of water correspond to a continuous medium, the aggregates formed are referred to as direct (hydrophobic part at core of the structure and hydrophilic part in contact with water) whose curvature is defined as positive.

OMS are very useful when efforts are being made to replace organic solvents, to carry out reactions in water and to work with low-energy conditions. The OMS

posses a big number of advantages: solubilization of substances that are not normally soluble in the continuous phase, localization of reactants and products, among others. (Gibson, 2000).

OMS are very efficient for the applications of some green chemistry principles and are considered as a double beneficial if are based in biocompatible compounds. A variety of synthetic reactions have been performed in OMS formed by aggregations of individual molecules. Organized structures are employed to facilitate chemical processes and are prepared dissolving amphiphilic molecules in water or organic solvents. These organized systems may be split into two levels of interest: 1) study of molecular aggregates and 2) host-guest interactions.

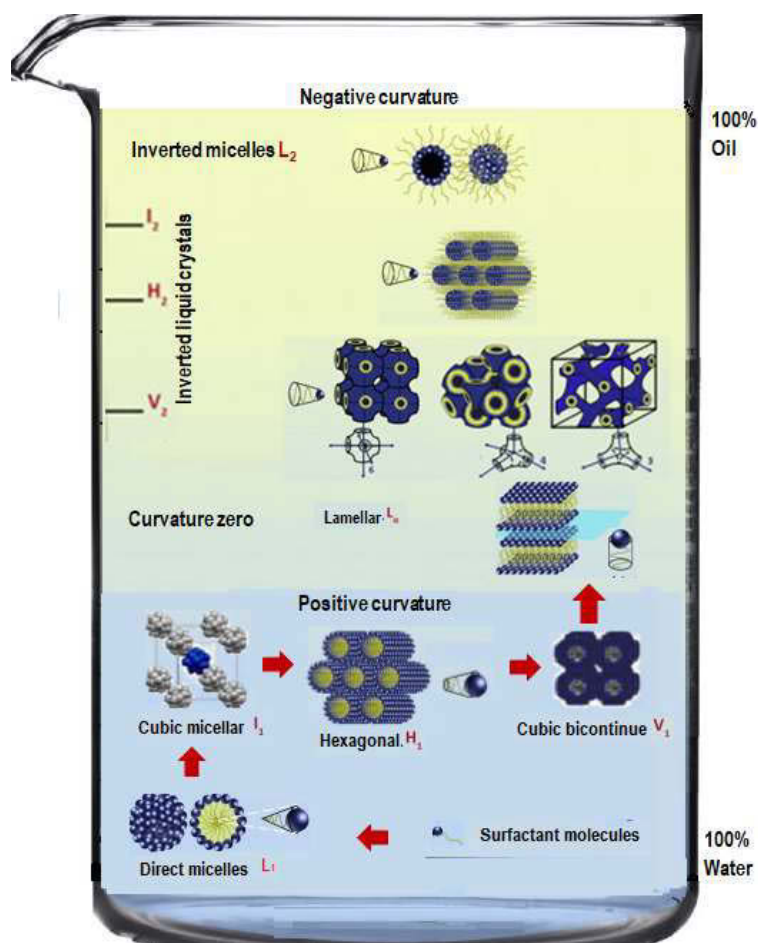


**Figure 1-13.** Schematic representation of OMS formation according to the surfactant concentration in oil and water

### 1.3 Systems thermodynamically stable

When the concentration is low the water-soluble surfactants are located at the air-water interface or the monomers are solubilized in the water depending on the structure of the molecule. When the concentration reaches a certain value known as Critical Micellar Concentration (CMC) they form micelles. The CMC value depends on the hydrophilic/hydrophobic character of the surfactant, the more hydrophobic it is the smaller the value of the CMC. When the surfactant is not soluble in the water form aggregates from certain concentrations, and this point is known as Critical Aggregation Concentration (CAC).

#### 1.3.1 Micelles

This systems are formed when the surfactant concentration is low, however they may also exist from concentration of 50%. Micelles formed in water are direct micelles ( $L_1$ ), and those formed in oil phase, are reverse micelles ( $L_2$ ). The moiety on the surface, whether it is hydrophilic or hydrophobic, forms a screen, to prevent the interaction between the medium and the core that is not compatible. Both the direct and reverse micellar solutions are transparent and optically isotropic.

There is a third type of micellar phase, known as bicontinuous system (designated as  $L_3$ ) or sponge phase. In this phase the medium forms two interlinked continuous networks separated by a bilayer of surfactant molecules (Anderson, 1989). This phase is fluid and usually shows shear birefringence when examined by polarized light. (Figure 1-14).

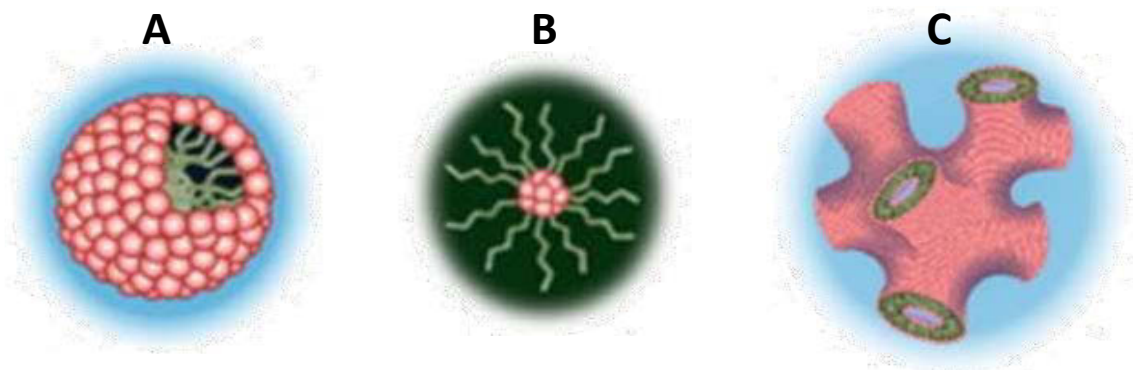


**Figure 1-14.** Schematic representation of the different type of micelles.  
A) Direct micelles ( $L_1$ ) B) Reverse micelles ( $L_2$ ) C) Bicontinuous phase ( $L_3$ )  
Anderson, 1989

### 1.3.2 Microemulsions

When oil is added into the direct micellar solution, or water is added into a reverse micellar solution, the oil or water are solubilised into the core of the micelles and the direct or reverse microemulsions appears respectively. (Anton, 2011). Microemulsions may be considered as swollen micelles if the quantity of oil or water solubilized is slow. The O/W microemulsions can contain a larger capacity for solubilize lipophilic molecules, and the W/O microemulsions can contain big quantities of aqueous compounds.

Several physical methods may be applied to characterize these systems for determine the aggregate structures: conductivity, Small Angle Neutron and X-ray light Scattering (SANS or SAXS), viscosity and Nuclear Magnetic Resonance (NMR) are the most used.

### 1.3.3 Liquid crystals

The formation of liquid crystals is taking place when the surfactant concentration increased, those liquid crystals have long range patterns and the structure of mesophases can be mono-, di- and tri-dimensional.

#### A. Lamellar phase

The lamellar phase (designated as  $L_{\alpha}$ , Figure 1-15) consists of surfactant bilayers alternated by water layers. This phase is translucent and optically anisotropic. This phase appear usually at higher concentration than those for hexagonal phase. Through a polarized light microscope can be identified from its typical Maltese cross or oily streaks (Laughlin, 1994)

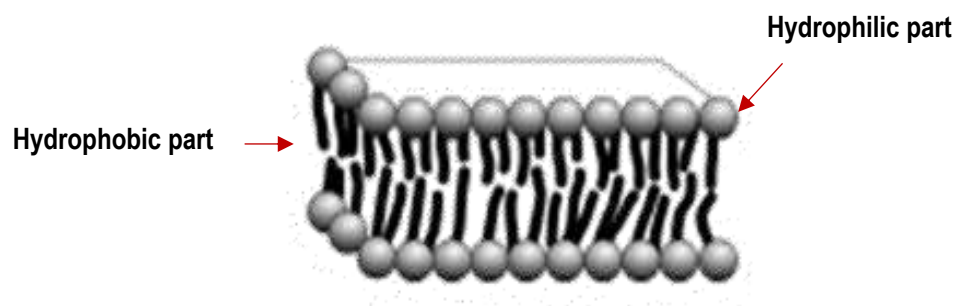


**Figure 1-15.** Schematic representation of lamellar phase  
Laughlin, 1994

## B. Cubic phase

There are two types of cubic micellar phase: micellar and bicontinuous and are characterized by their isotropy. The cubic liquid micellar phase are three-dimensional structures (Figure 1-16) formed by spherical or cylindrical aggregates. According to the continuous phase: aqueous or oily can be named as  $I_1$  or  $I_2$  respectively. And they can be organized along a primary, face-centered or bodycentered symmetry ( $Pm3m$ ,  $Fd3m$ ,  $Im3m$ ). Otherwise, the bicontinuous cubic phases ( $V1$ ,  $V2$ ) are, as their name suggests, two interlinked continuous networks separated by a bilayer of surfactant (Tiddy, 1980).

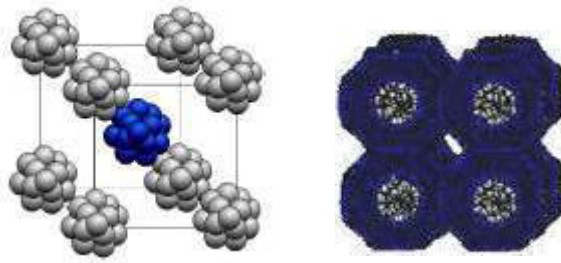


**Figure 1-16.** Schematic representation of a bicontinuous cubic phase (right) and a micellar cubic phase (left)  
Du, 2010

## C. Hexagonal phase

A hexagonal liquid crystal consists of cylindrical micelles on a two-dimensional hexagonal ordering. If the surfactant molecules in the structure have their heads towards the continuous medium is a direct hexagonal phase ( $H_1$ ), if the tails are towards the continuous medium is a reverse hexagonal phase ( $H_2$ ). Those phases are optically anisotropic. They have a mosaic structure when observed through a polarized light microscope (Tiddy, 1980). (Figure 1-17).

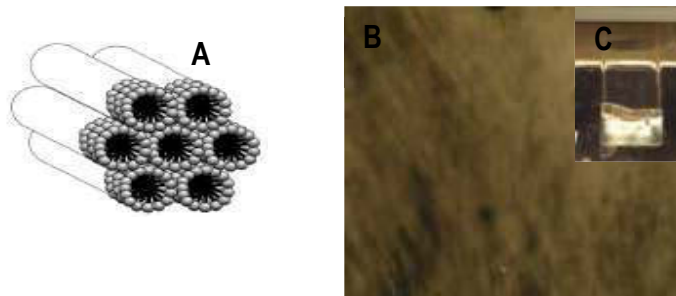


**Figure 1-17.** Schematic representation of a hexagonal phase.  
A) Schema model B) Usual aspect under Polarized Microscopy C) Usual aspect under polarized light

## 1.4 Phase behaviour of nonionic surfactants

The importance of HLB number for the surfactants behaviour in solution was mentioned before. For low HLB values, lamellar and inverse phases are often found. In contrast, when the HLB increase the sequency is  $L_1$ - $I_1$ - $H_1$ - $V_1$ - $L_\alpha$ - $L_2$  in function of the surfactant concentration (Ravey, 1994). According to the HLB number of the studied surfactant, just a part of the diagram, presented in the figure 1-18, can be obtained into the experimental temperature (0-100 °C). (Michaux F., 2009).

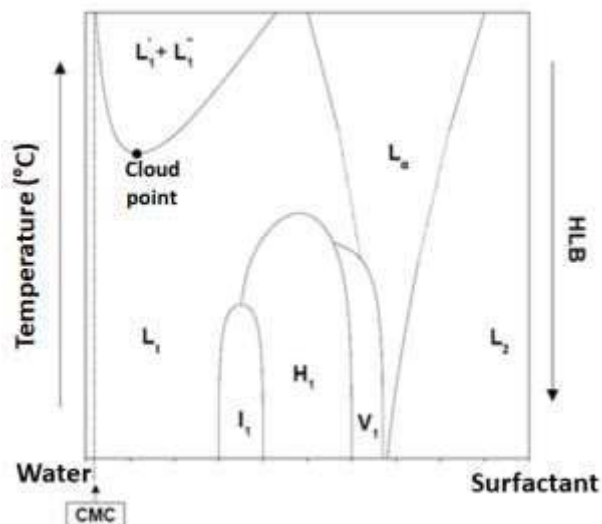


**Figure 1-18.** Ideal phase behaviour of a surfactant in water in function of its HLB number and temperature  
Michaux, 2009

## 1.5 Systems kinetically stables

### 1.5.1 Emulsions

Emulsions are a mixture of two immiscible liquids, typically oil and water, homogeneous at macroscopic scale, but heterogeneous at microscopic scale. Since the mixtures of oil and water are not stable, the surfactant is added to stabilize the mixture. The surfactant role is to lower the surface tension between the dispersed and the continuous phase, favoring the formation droplets.

There are two types of emulsions: the oil in water (O/W) emulsions which is formed by oil droplets in a water continuous medium and water in oil (W/O) emulsions which are formed by water droplets in an oil continuous medium

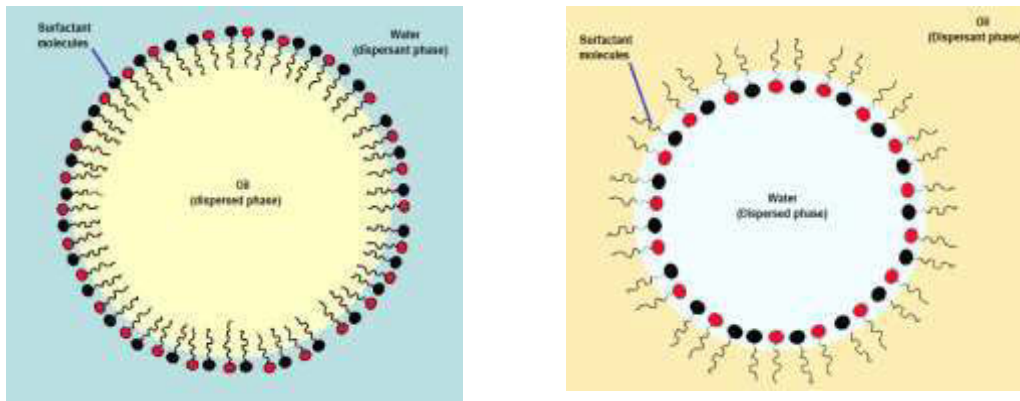


**Figure 1-19.** Schematic representation of an emulsion  
*Left: O/W emulsion    Right: W/O emulsion*

As emulsions are kinetically stable, changes of the properties will occur in time. Due to the Brownian motion, gravity or mechanical movement of the droplets, the collision phenomenon occurs constantly, and the result is the emulsion destabilization under different mechanisms.

There are four types of important mechanisms: creaming, sedimentation, flocculation and coalescence. The difference in density between the dispersed and dispersing phases is at the origin of creaming and sedimentation. Creaming is the migration of droplets from the dispersed phase upwards while sedimentation is the migration of droplets downwards. The force driving these droplets depends on their size, the difference in density between the two phases and gravity.

If the density is higher than that of the dispersant phase, there is a creaming. Otherwise, there is sedimentation. Flocculation is the aggregation of droplets without altering their physical properties (size, shape) and can be reversible, while coalescence is the aggregation of droplets that merge to form larger droplets, this process is irreversible. In the case that one of the liquids is slightly soluble in the other, a third aging process might take place, the Ostwald ripening. It is the process of gradual growth of the larger droplets at the expense of smaller ones due to mass transport of soluble dispersed phase into the continuous phase, this process is accelerated when the droplets are initially polydisperse.

### 1.5.2 Nano-emulsions

Nano-emulsions known also as mini-emulsions, ultrafine emulsions, submicron emulsions are a specific kind emulsion that have sub-micrometer droplet size that can be relatively monodisperses. Generally, the droplets of a nano-emulsion have a size smaller than 200 nm. Due to their characteristic size, nano-

emulsions have a transparent or bluish aspect and are stable against sedimentation or creaming because it is prevented by the brownian motion of their droplets.

Colloidal delivery systems based on microemulsions or nano-emulsions are increasingly being utilized in the food and pharmaceutical industries to encapsulate, protect, and delivering lipophilic bioactive components in the case of direct systems. The small size of the droplets in these kinds of delivery systems means that they have a number of potential benefits for certain applications: enhanced long-term stability; high optical clarity; and, increased bioavailability.

Microemulsions and nano-emulsions are distinctly different types of colloidal dispersions: a microemulsion is thermodynamically stable because the free energy of the colloidal dispersion (droplets in water) is lower than the free energy of the separate phases (oil and water), whereas a nano-emulsion is a system kinetically stable due to the free energy of the colloidal dispersion (droplets in water) is higher than the free energy of the separate phases (oil and water).

Nano-emulsions may be of the oil-in-water (O/W) or water-in-oil (W/O) types depending on whether the oil is dispersed as droplets in water, or *viceversa* (Anton, 2010). Sometimes a combination of surfactants rather than a single surfactant is used to form and stabilize nano-emulsions. (Figure 1-20).

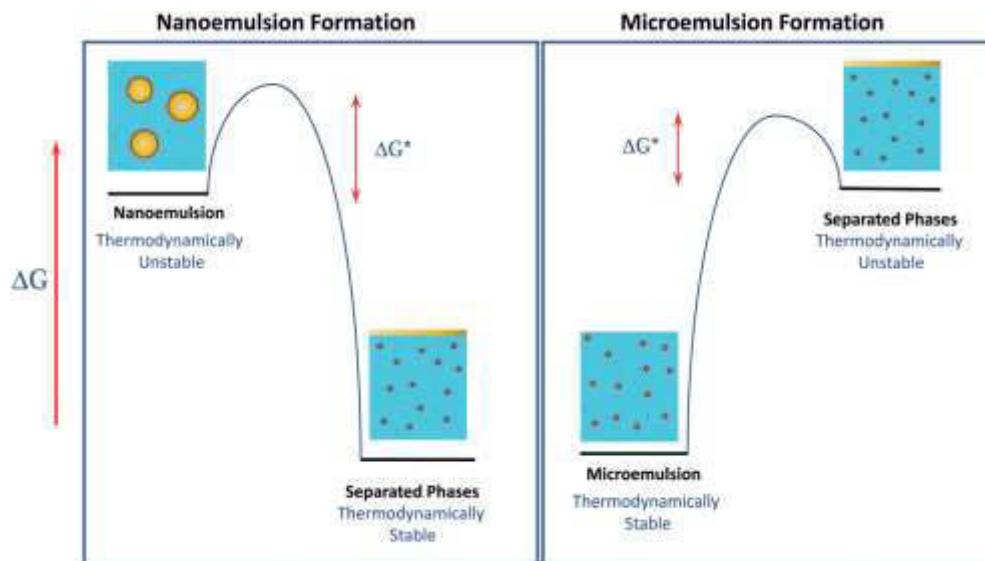


**Figure 1-20.** Schematic representation of the free energy of microemulsion and nano-emulsion compared to the phase separated state  
McClements, 2012

## A. Nano-emulsions preparation methods

### A1. High-energy emulsification method

Into this emulsification method, the mechanical energy is needed. The droplets are generated by high-shear mixing or by sonication. Those systems are obtained with a large array of surfactants, and for a large water/oil/surfactant composition range. The droplet size can be tuned by varying the amount of energy input (rotation speed, frequency) and can be scaled to an industrial level. On the other side this energy can generate heat which is unfavorable in the presence of volatile oils or thermally fragile components (Fryd, 2012).

### A2. Low energy emulsification method

In the case of this emulsification method, the chemical energy is the main factor. This method form nano-emulsions with a low energy input, taking advantage of the intrinsic properties of the components in the system, and particularly the surfactant properties. There are two classes: self-emulsification and phase inversión, which consist in the transformation of macroemulsion into a nano-emulsion by reducing the surfactant concentration and the hability of the surfactant to change its curvature during the emulsification process respectively (Solans, 2012).

The hydration grade can be controlled by modifying the temperature or the composition. The approach in the phase inversion to form direct nano-emulsions consists of the progressive addition of water to an oil/surfactant mixture and is known as Phase Inversion Composition (PIC). The whole process takes place at constant temperature. In the other hand, the Phase Inversión Temperature (PIT) approach, consists of the changing of the curvature of the surfactant by changing the temperature (Figure 1-21) (Shinoda, 1967). The nonionic surfactants change their curvature with temperature, at low temperature their curvature is positive and at high temperature their curvature is negative. The temperature at which the curvature is zero is called the phase inversion temperature.

PIT method takes advantage of the low interfacial tensions achieved at the phase inversion temperature, where small diameter droplets can be formed. But at such a temperature the surfactant's curvature is close to zero which increases the coalescence rates. Consequently, the cooling process must be fast in order to form small droplets while avoiding any coalescence.

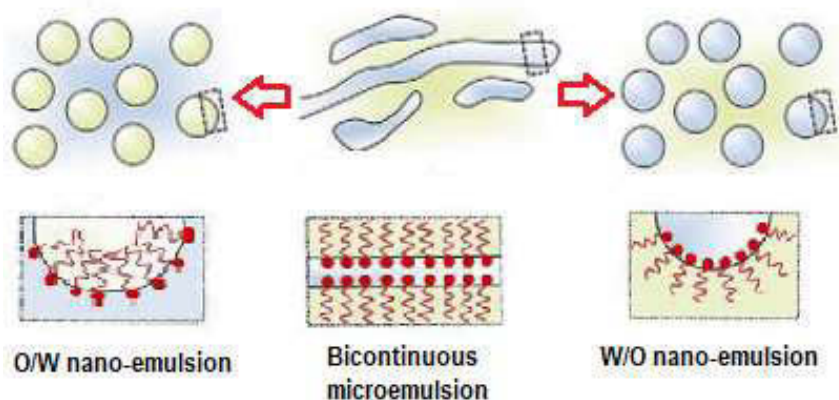


**Figure 1-21.** Schematic representation of PIT method  
Solans, 2012

Depending on the composition of the system, a bicontinuous microemulsion is present around the phase inversion temperature, a transition through one or more of these phases is necessary in order to form the nano-emulsions. For both phase inversion approaches, the amount of surfactant presents in the system influence the size of the droplets formed, the more surfactant presents the smaller the size. It should be noted that a nano-emulsion requires much less surfactant than a microemulsion.

### 1.5.3 Concentrated emulsions

The term “concentrated emulsion” covers a wide concentration domain. Its boundaries are: from one side, the limit of dilute emulsion and from the other the concentration of closely packed spherical drops (drops remain spherical but is impossible to add a single drop without deformation of the others). (Svetlana, 2009).

Highly concentrated emulsions are an important class of emulsions, due to their very high-volume fraction in dispersed phase (up to 99%), their high stability and low surfactant concentration (about 0.50%). These emulsions contain a volume fraction above the maximum closest packing fraction if the droplets are monodispersed,  $\phi_v = 0.74$ , and this fraction correspond to the compact stacking of spherique drops into the emulsion separated by liquid films between them.

The formation of highly concentrated oil-in-water emulsions is strongly linked to the HLB of the surfactant. The Bancroft rule predicts that a surfactant hydrophobic gives inverse W/O system and conversely, direct W/O emulsions are obtained from hydrophilic surfactants. The most studied highly concentrated emulsions and used to date are direct O/W emulsions. Their preparation consists in solubilizing the surfactant in the continuous phase (aqueous phase) followed by the progressive addition of the phase dispersed (oil), the mixture being maintained under continuous agitation (Bleta, 2007)

Concentrated emulsions are made up of two phases: a micellar phase forming the continuous phase and a dispersed phase: water or oil depending on the emulsion type W/O or O/W respectively. (Ravey, 1994 bis) The continuous phase of water-in-oil concentrated emulsions are obtained from reverse micellar solution ( $L_2$ ), while the continuous phase for oil-in-water concentrated emulsions is a direct micellar phase ( $L_1$ ). This type of emulsions has a widely applications, from where is important to highlight the pharmaceutical field.

A typical compressed nature of a high concentrated emulsion is shown in the figure 1-22. As it can be seen, in the dense admixtures, the touching droplets from a flattened interdroplet layer where the disjoining pressure and the contact force are equilibrated and resist to the coalescence.

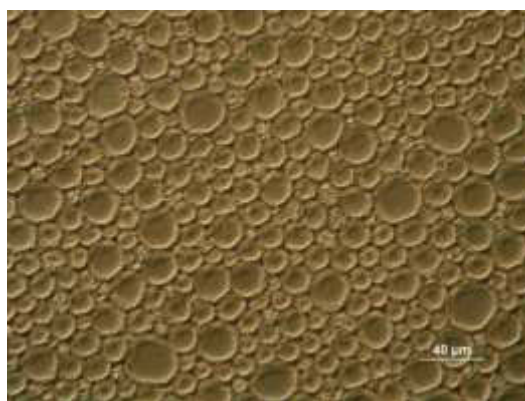


**Figure 1-22.** Typical compressed aspect of a concentrated emulsion under microscope  
*Image belonging to the system Kolliphor EL/Water ( $R'$ ) = 0.15 and 90 wt% Mygliol*

### 1.6 Porous silica materials (PSM)

Porous silica materials are classified according to their pore size into microporous ( $< 2$  nm), mesoporous (2–50 nm) and macroporous ( $> 50$  nm) materials. Porous materials widely exist around the world play a role in many aspects of the daily lives; among the fields they can be found in are energy management, vibration suppression, heat insulation, sound absorption, and fluid filtration.

These porous materials can be more functionally for integrative applications because the porous size is thought as a functional phase that optimize the performance of the material (Schueth, 2002). For example, there has been rapid growth in emerging areas such as nanotechnology, photonics and bioengineering, which require porous structures with well-defined structural, interfacial, compositional and morphological properties, where the mesoporous materials are good candidates due to their structural characteristics that make them affordables for many applications as: adsorbents, catalysts, drug delivery, among others. (Blin, 2013).

### 1.6.1 Mesoporous organised silica materials and their formation mechanisms

Mesoporous materials were first discovered by the Kuroda group and Mobil Company in the early 1990 (Yanagisawa, 1990, Gao 2006). Since then this kind of materials have attracted wide interest of researchers because the pore size of these materials is beyond the limit of conventional zeolites, and thus can be used in a much more broad field, for example, heterogeneous catalysis with large molecules involved, biologic molecule manipulations, etc.

The characteristics of these materials include: (1) highly ordered mesostructures, (2) uniformly distributed pore size, (3) large surface area ( $\sim 1000 \text{ m}^2/\text{g}$ ) and pore volume ( $\sim 1 \text{ cm}^3/\text{g}$ ), (4) designable chemical composition and functionalizable surface and (5) controllable size and morphology (Gao 2006, Blin 2013). Surfactant micelles or liquid crystals are commonly used for the preparation of mesoporous materials. Many families of mesoporous materials have been developed so far, including M41S (Kresge, 1992, Zhao, 1998), SBA (Zhao 1998, Huo 1994, Huo 1994). These materials were synthesized by using different organized molecular systems with various surfactants, co-surfactants, synthesis conditions and methods.

#### A. Cooperative Templating Mechanism (CTM)

This mechanism requires the presence of a micellar solution and a silica source. The first step consists of the polymerization of the inorganic precursor around the micelles, or intra-micellar polymerization, which is the result of the interaction between the polar heads of the surfactants and the inorganic precursor (Beck, 1992). The interactions are essentially hydrogen bonds with the non-ionic surfactant. The second step is the intermicellar condensation, in which the micelles self-assemble into a close-packed structure, usually hexagonal, and is designated as a hybrid mesophase (Schema 24., route 2) (Michaux, 2009, adapted from Beck 1992). In order to complete the process and to ensure the complete condensation of the inorganic matrix, a hydrothermal treatment is used. Finally, the final material is obtained after the removal of the surfactant via calcination or Soxhlet extraction using ethanol.

#### B. Liquid Crystal Templating Mechanism (LCT)

This mechanism transcribed requires the presence of an initial macromolecular structure which will serve as an organic template. Those templates can be liquid crystals, or emulsions or solid particles. The silica precursor is added to the template, which condenses and polymerizes directly around the template. Finally, after the elimination of the template, the silica material adopts the shape and

the structure correspond to the template arrangement. (Figure 1-23, route 1) (Beck, 1992).

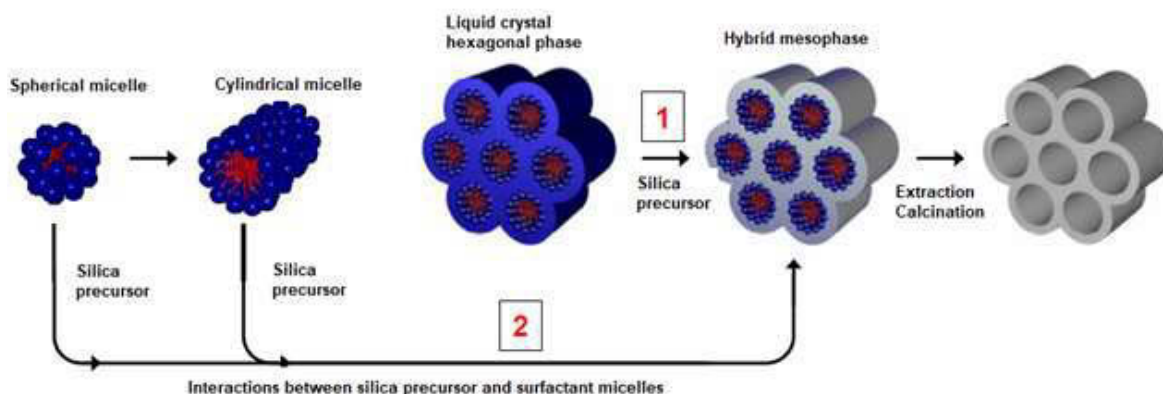


**Figure 1-23.** Schematic representation of the formation mechanisms. (1) Liquid Crystal Templating Mechanism (LCT) and (2) Cooperative Templating Mechanism (CTM). Michaux, 2009

### 1.6.2 Meso-macro porous silica materials

The increased demand for the encapsulation and release of large molecules with a big molecular weight such as proteins drove the researchers to develop porous silica materials with a large pore size (30 nm). For the encapsulation of molecules of interest: drugs, active principles, among others, the organized mesoporous materials are interesting due to their specific area, but the diffusion of the molecules is limited. These applications require porous materials with hierarchical pore structure at different scales in order to achieve highly organized functions and improve the diffusion of encapsulated molecules. The development of hierarchical porous materials at multiple scales was the subject of interest over the last few years (Fan, 2005)

The presence of mesopores in the walls of the macropores is interesting and useful for the catalysis and drug delivery systems. From an application viewpoint, drugs or catalysts can be loaded in the mesopores, while the macropores enhance the mass transfer and reduce the transport limitations. This is particularly beneficial in the case of large molecules or in viscous systems, where diffusion rates are low. For the sake of large performance improvement, such materials should possess adjustable and well-defined macropores and tunable mesopores in the macropore walls (Yuan, 2006).

On all length scales, the bigger pores should be connected via smaller pores. Thus, it remains a challenge to synthesize hierarchically bimodal mesoporous-macroporous materials with controlled individual pore sizes and pore structures, although several methods have been reported that combine dual templating of

surfactant systems and colloids. In the synthesis of hierarchical meso-macroporous inorganic silica materials, self-assembled molecular aggregates or supramolecular assemblies are generally employed as the structure directing systems of meso-structures. Meanwhile, a lot of techniques can be employed for the design of the macroporous network (Yang, 2009).

### 1.6.3 Hybrid materials

In recent years, research into organic-inorganic hybrid materials has become an important subject of study for materials and biomaterials sciences. The term *hybrid* is commonly used for any combination of materials that can be classified into the various chemical subdisciplines. The most investigated due to their importance have been: organic-inorganic hybrids, stretching into the fields of biomolecular-inorganic and polymeric-inorganic materials (Rurack, 2010).

In the scientific literature, the term organic-inorganic hybrid material was used by G.L. Wilke's group in the context of organically modified silica materials prepared by sol-gel route (Rurack, 2010). Hybrid materials are formed by two components, and generally their behavior depends of the nature, content and constitution of the components, but also of the experimental conditions. Combination of organic or biological moieties with inorganic materials helps to obtain well-structured material at the mesoscopic level through the assembly processes thanks to the inorganic materials can improve the stability in the resulting hybrid materials (Kickelbick, 2007).

The hybrid silica materials can be functionalized and thus can contain a very large array of guest molecules (ranging from hydrophilic to hydrophobic) and an adjuvant that facilitates their applications. The adjuvant is usually a organized molecular system used as template to construct the silica organized network, but is not eliminated after the synthesis of the material.

Among the different materials, silica has a peculiar interest. Indeed, for fields of bioimaging, diagnosis, controlled drug or DNA delivery and phototherapy or cancer therapies offering their multiple advantages as: biocompatibility, bioactivity, photonic media as result of their low optical losses. But also, good mechanical properties, thermal, chemical, and photochemical stability. One of the biggest impacts of the hybrid materials are their natural applications, for example, the hybrid silica nanoparticles developed in our group, have been demonstrated important influence into the therapeutic fields as nanocarriers of active principles (Blin, 2013).

#### 1.6.4 Applications of mesoporous silica materials

The industrial applications of mesoporous materials have been a growing interest of research in the recent years, and the focus is in the fields of chemical industry, bio-application and functional materials, etc. This section presents a brief overview on the most common application research of mesoporous materials.

##### A. Chemical industry

Catalysis Mesoporous materials have large surface area, defined pore structure and large pore size. For reactions with large molecules involved, mesoporous materials-based catalysts show better performance than traditional zeolitic. Therefore, it opens possibilities for many heterogeneous catalysis reactions. Kozhevnikov et al showed when loading the heteropoly acid (HPA) into mesoporous materials, the catalysis reactivity of the materials was significantly enhanced which became close to that of concentrated sulfuric acid. Mesoporous materials can be used as confined reactors, for many reactions e.g. polymerization. The lifetime of free radicals is elongated, and the distribution of molecular weight becomes narrower by using this nano-reactor.

##### B. Bio-application

The encapsulation of enzymes and other proteins into mesoporous materials has attracted considerable attention over the past few years. Biocatalysts and biosensors have been developed based on the absorbed proteins in the mesopores. Carrier for biomedicines mesoporous material was first used as a drug carrier by Vallet-Regí et al. They further demonstrated that the characteristics of mesoporous materials: pore size, surface area, pore volume, functionalities, affect dramatically the release kinetics of drugs. Based on the mesoporous materials, researchers also developed various kinds of “smart” devices, which can release the drug in response to external stimuli, such as pH, temperature, light irradiation and redox reagents, etc. which have potential applications in targeted and controlled drug delivery systems (Kewal,2008).

##### C. Functional materials

Functional materials are compounds specially designed for a determined function, enhancing the properties of each component, considering the types of interactions present, the surface energy, and taking advantage of the play role of the existence of labile bonds which make them useful for several applications: electrical, optical, mechanical, separation capacity, catalysis, sensing capability, pharmaceutical and chemical and thermal stability.

The functional materials can be categorized into two main families depending on the nature of the interface combining their components: *Class I* deals with hybrid systems where the organic and inorganic parts interact by weak bonds including Van der Waals, electrostatic or hydrogen bonds. *Class II* indicates materials in which its components are linked by covalent or ionic-covalent chemical bonds (Mir, 2018).

Indeed, various functional materials consist of both types of interfaces, strong and weak, that provides a strong chemical bond on the final material properties. One of the most common examples are mesoporous silica materials having a high surface area and large pore volume that make possible the energy storage. Due to the large porosities mesoporous materials have low dielectric constant ( $k$ ), which may find use in electronic industries e.g. integrated circuit. (Bruinsma, 2015)

## 1.7 Application of porous materials in Drug Delivery Field

Regarding to the importance to this thesis work is necessary to know the role of the porous silica materials into the pharmaceutical applications as Drug Delivery Systems (DDS), specially encapsulating hydrophobic drugs. The drugs administration routes, *methods of encapsulation*, and the use and importance of hybrid materials as drug carrier are then described.

One of the main targets of the current delivery systems in the pharmaceutical industry is to provide a sustained and controlled release over time in order to maintain its concentration within therapeutic values and below the toxicity threshold. From this point of view the mesoporous silica-based carrier matrices have attracted much attention during the last years, due to their intrinsic stability to the physical and chemical agents, excellent biocompatibility and multifunctionalization. (Botella 2010)

### 1.7.1 Drug Delivery Systems (DDS)

Drug delivery systems (DDS) is an important component of drug development and therapeutic advancement, and this has been attracted much attention during the last decades. A DDS, is defined as a formulation or device that enables the introduction of a therapeutic substances in the body and improving the efficacy and safety by controlling the rate, time, and place of drugs release (Kewal, 2008).

The administration of therapeutic products, the release of active ingredients and the subsequent transport until the active site are also part of the study into the DDS. Normally as a criterion of regulation the device has to include certain characteristics as: increasing the bioavailability of the drug, it should provide for controlled drug delivery, it should transport the drug into the site of action avoiding the healthy tissues, the active principle should be stable, to ensure high degree of

drug dispersión and it should be easy to administer to the patients, among the most important. All of criteria should be formulated according to the purpose into the body and the drug specifications.

Many systems have been developed as drug delivery trying to reach the most novel but safe method. The general goal is to reach high proficiency in the drug release playing with the parameters of time and accumulated concentration into the organism.

Depending of the needs, the DDS synthesis must be planned for fast track treatment: to accurate chronic disease or to prescribe monodose or multidose, increasing the the drug bioavailability, while decreasing its toxicity, because the drug efficiency is often altered by its non-controlled biodistribution (Roig, 2018). Other factors as low production cost, improved compliance, chronopharmacological benefits, life extension of the products, reduction of the risk of failure in the new product development, high distribution level and accesibility are also considered into the DDS development (Kewal, 2008).

In order to cover the majority needs into this field, systems as matrix and vesicular carriers has been developed, these systems have a large range of size and sructures, however the active principle is still exposed to some external perturbations (Dumitriu 1994). Due to many drugs have physicochemical characteristics that are not favorable to transit through the biological barriers that separate the administration site from the action site, vectorization is one of the major challenges in therapeutic research.

Around the mid-20th century, Eugene Rochow got the major approaches of the century, understanding the role of the silica on the healt and how it can be responsible for disease, silica molecule is capable of forming four bonds and is known for its ability to polymerize and form network covalent structures. It is inert, which implies less risk with the cells interactions and chemicals in the body, it sustains high temperature, which suggest facilities for the material synthesis and sterilization process. (Dumitriu 1994).

Amorphous or crystalline silica can be also obtained by synthetic thermal process, sol-gel route among others, to obtain mesoporous materials, with high surface area and pore volumes. This characteristics make them suitable for several applications, from wherre nanomedicine has a high interest. Drug delivery and bio-imaging are topics were the use of this type of materials is interesting due to their biocompatibility and capacity to transport poorly soluble drugs (Diab 2017).

### 1.7.2 Porous silica material on drug loading and drug release

Researches done into the fields for porous silica material shows that a controlled synthesis of these sieves has a great impact on their properties and applications, having high potential as: drug delivers, bioimaging, regenerative medicine, optical and electrochemical biosensing, enzyme immobilization, biomolecule sorption and separation, among others. Good results were showed into the pharmaceutical field for the porous materials was being the carrier for ibuprofen as a poorly water-soluble drug (Xu, 2009), then the pharmaceutical applications have been modified according to the needs.

The DDS based on porous silica materials can be divided into the systems of improved drug dissolution prolonged drug release, zero order kinetics drug release and stimuli- responsive, enzyme mediated light-controlled and biologically stimulated systems. According to the US Food and Drug Administration and the European Food Safety Authority, amorphous forms of silica and silicates are generally recognized to be safe as oral delivery ingredients in amounts up to 1500 mg per day in solid dosage forms. (Moritz 2015),

Several concepts have been created to express the drug loading results. One is the specific surface area (SSA) which consists of the total surface area per unit of the particle mass. The higher the number of pores the larger is the value of the SSA. A wider SSA increases the opportunities of drugs to interact with the surface of a carrier. On the other hand, the small volume of pores means the fact that only few drugs are capable to fit into the narrow internal space of the small nano-pores. (Limnell 2007). The amount of the loaded drug is generally expressed as loading degree using the dry weight of both the loaded drug and silica particles.

### 1.7.3 Kinetics models for the evaluation of DDS from mesoporous materials

Recently research into organic-inorganic chemistry materials science, porous materials has been more studied because these materials are capable to respond to external stimuli, and present improved drug dissolution profiles (schema 24 A-D). One of the challenges to which the hybrid material can constitute a solution is to add mesopores as reservoirs that can be opened and closed as a response to an external stimulus, giving rise to the so-called "*stimuli responsive drug delivery systems*". Drugs can be confined into the mesoporous cavities and then locally delivered when and where needed (Moritz,2015).

There are several factors that can activate the release of the guest molecules such as pH, temperature, magnetism, chemicals, light or ultrasound. The DDS of prolonged release facilitate the dosage and duration of the drug effect, minimizing the toxicity to the patients, since they reduce the dosage frequency. The systems with prolonged release are preferred for the water-soluble drugs.

The improvement of dissolution kinetics of poorly water-soluble drugs, the solid dispersion technique is the most effective method for improving the dissolution rate of poorly soluble drugs, however this is reliant to the suitable carrier and the solvent selected.

The schema 24B corresponds to diffusion process characteristic for first order kinetics. The application of the mathematical model to describe the first order kinetic, was proposed by (Gibaldi and Feldman 2006) and modified by Wagner (2013). This model can be used in the analysis of dissolution profile for poorly soluble drugs. (Ahuja, 2007). The following relation can express the model:

$$Q_t = Q_\infty [1 - e^{-k_d(t-t_0)}]$$

were  $Q_t$  is the amount of drug released in time  $t$ ,  $Q_\infty$  is the initial amount of drug in the solution,  $K_d$  is the first order constant. The data must be plotted as log cumulative percentage of drug remaining vs time which would yield a straight line with a slope of  $K/2.303$  (Mulye, 1995).

The schema 24C, represents the extended drug release with initial burst effect followed by the slow drug desorption (formation of microporous space). This behaviour is characteristic of a fickian model, where the release process is accelerated in short times, but the release ratio decelerates at longer periods.

The schema 24 D shows a zero-order kinetics of a drug evolution. In this kind of system, the same amount of drug by unit of time is released and is ideal method of drug release to achieve a pharmacological prolonged action. The following relation can explain in a simple way the model:

$$Q_t = Q_0 + K_0 t$$

where  $Q_t$  is the amount of drug dissolved in time  $t$ ,  $Q_0$  is the initial amount of drug in the receptor solution and  $K_0$  is the zero-order release constant (Ramteke 2014).

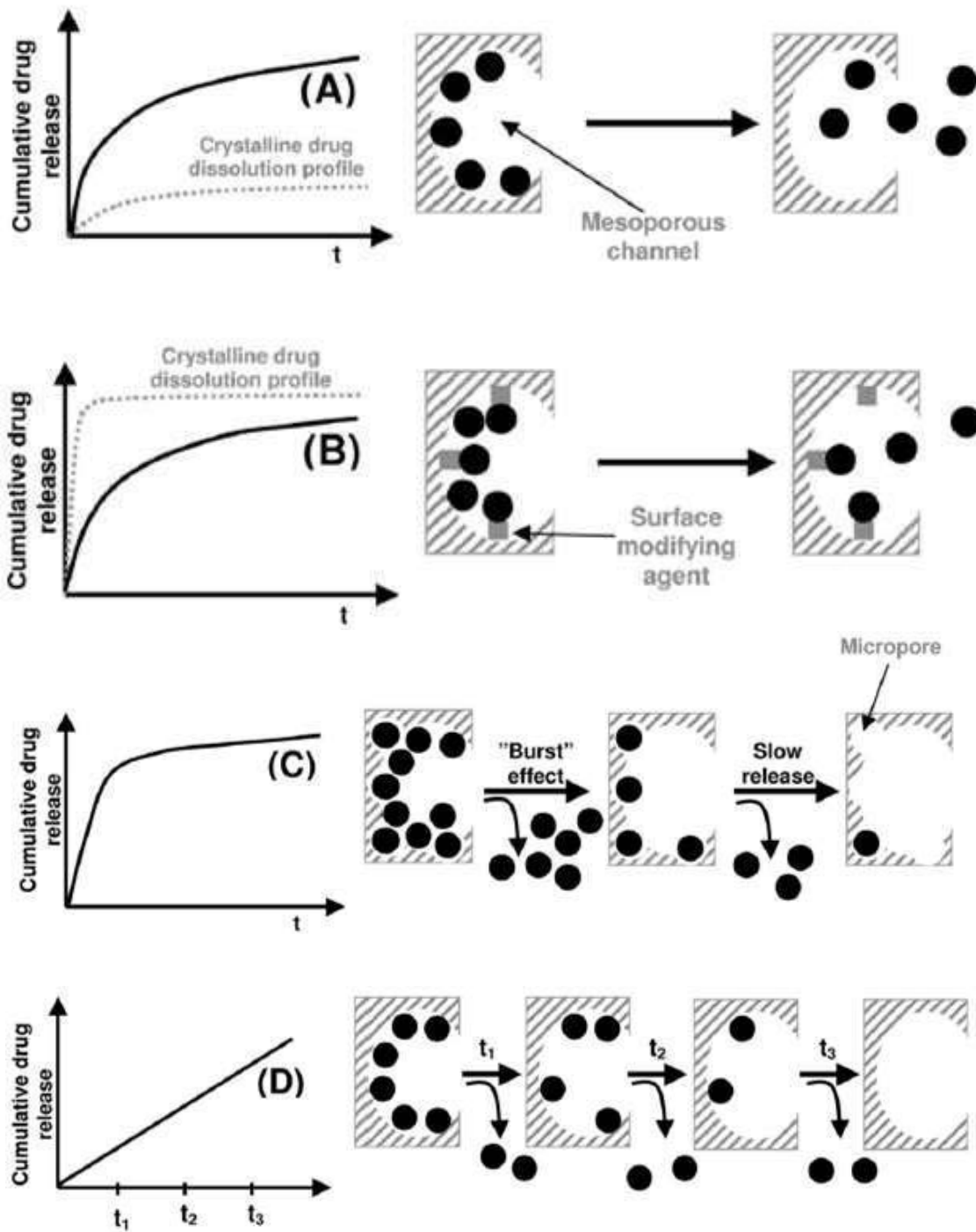


Figure 1-24. Typical drug release profiles from porous carriers  
Ramteke,2014

## **Chapter II. Materials and Methods**

The first part of the chapter indicates the products used and describe the techniques applied for the characterization of surfactant-based systems: phase diagrams, liquid crystal and micellar structure.

The second part describes the protocol for the synthesis of porous and hybrid silica materials synthesized from micellar solutions, fine and concentrated emulsions and their characterization techniques: structure, texture and morphology.

In the third part of this chapter, the techniques used for the evaluation of hybrid materials as drug carriers are given: dissolution tests, quantification of released active ingredient and mathematical models applied to the release kinetics.

The fourth and final part provides the techniques for the evaluation of toxicity on HeLa cell culture of surfactant-based systems and doped hybrid materials.



KEL is well known for the stability enhancement to the formulations, however in high concentrations may produce hypersensitivity reactions and neurological toxicity and depending on the dose and duration of infusion may alter the pharmacokinetics of many drugs as cyclosporin A, doxorubicin, among others, being the responsible of the non-linearity deposition (Gelderblom, 2001).

In the other hand we worked with Pluronic P123 poly(ethylene oxide)-poly(propylene oxide)-poly(ethylene oxide) (PEO-PPO-PEO) triblock copolymer which has the formula  $EO_{20}PO_{70}EO_{20}$ , with a molecular weight of 5750 g/mol. It was purchased from Sigma Aldrich and used as received (Sigma-Aldrich tech info). It is a triblock copolymer formed by three parts, two hydrophilic parts constituted by large -EO blocks linked to each other by a hydrophobic group formed by propylene-oxides chains. The toxicity of this surfactant is very low and is considered safe for use for cosmetic and pharmaceutical applications (Singh-joy 2008), (Figure 2-2).

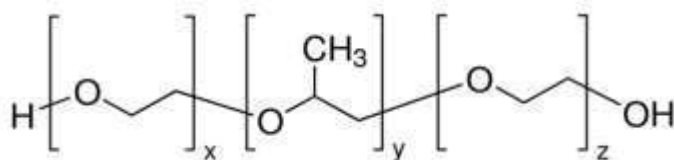


**Figure 2-2.** Poly(ethylene glycol)-*block*-poly (propylene glycol)-*block*-poly(ethylene glycol) chemical structure  
( $x = 20$ ,  $y = 70$ ,  $z = 20$ )  
From: PubChem website

## 2.1.2 Oils

### A. Miglyol ® 812N

Miglyol ® 812N is the trademark for a Caprylic/ Capric triglyceride mixture. It is a semisynthetic medium-chain triglyceride composed of 55% triglycerides of  $C_8$  and 45% of  $C_{10}$  fatty acids. Neutral and clear oil, slightly yellowish, odor and tasteless. Miglyol® 812N was obtained from IOI Oleo GmbH-IOI Oleochemical Company as a gift and used as received. Is a good carrier and solubilizer for oil soluble actives as lipid-soluble drugs, fat-soluble vitamins and steroids. (Figure 2-3).

This compound of short chains gives to Miglyol® 812N properties advantageous over long-chain fatty acids because it allows to diffuse passively and directly across the gastrointestinal tract making easier and quicker its absorption without undergoing the prolonged sequential molecular modifications that long-chain fatty acids must undertake.

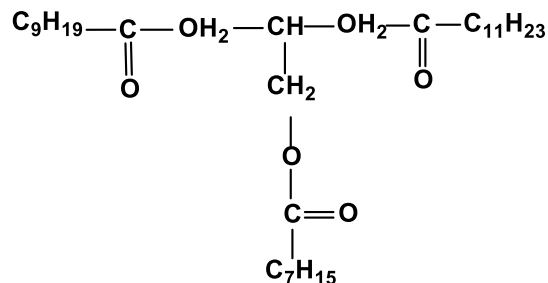


**Figure 2-3.** Miglyol molecular chemical structure

## B. Isopropyl Myristate

Isopropyl myristate is a fatty acid ester (myristic acid) combined with isopropyl alcohol (Figure 2-4). Is a polar emollient and is used in cosmetic and topical medicinal preparations, where good absorption into the skin is desired. Isopropyl myristate is being studied as a skin enhancer. It is used as a solvent in perfume materials. It is the non-aqueous component of the two-phase dentifrices, cosmetic and pharmaceutical products. The hydrolysis of the ester from isopropyl myristate can liberate the acid and the alcohol. The acid could be responsible for decreasing of the pH value of formulations. Isopropyl Myristate was obtained from Sigma Aldrich and used as received.

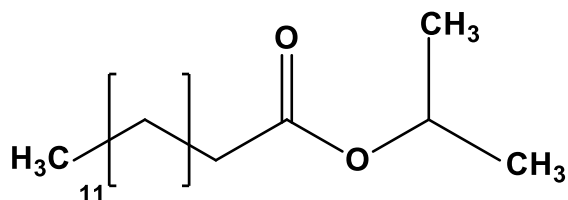


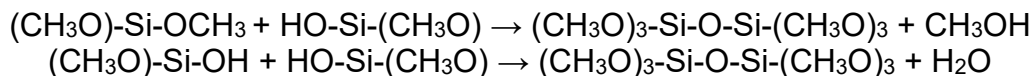
**Figure 2-4.** Isopropyl Myristate chemical structure

### 2.1.3 Inorganic sources: Tetramethyl-ortho silicates (TMOS) as silica precursor

The silica precursor used for this work is the tetramethoxysilane (TMOS). The polymerization mechanism involves two reactions. The first one is the initiation reaction or the hydrolysis which leads to the formation of hydroxyl groups (Si-OH).



Then, the condensation, leads to the formation of oxygen bridges between silicon atoms:



The polymerization can take up from a few hours to several weeks but can be accelerated by varying the pH. In particular, the condensation reactions are strongly pH dependent. The TMOS was obtained from Sigma Aldrich and used as received.

#### 2.1.4 Ketoprofen as encapsulated model drug

The racemic form of  $\alpha$ -(3benzoylphenyl) propionic acid ( $\pm$ ) or Ketoprofen ( $\text{C}_{16}\text{H}_{14}\text{O}_3$ ) (Figure 2-5), is a potent non-steroidal anti-inflammatory drug (NSAID) possesses also analgesic and antipyretic properties which has a very low water solubility ( $0.0213 \text{ mg}\cdot\text{ml}^{-1}$ ) with a pKa value of 4.2 – 4.4. This product was obtained from Sigma Aldrich and used as received, it is a product dry and an irritant to the breath, and it causes sneezing in extremely contact conditions. It is not sensitive to the temperature variations, but it may start to decompose above  $340^\circ\text{C}$ , is stable if its screened from the light (Espitalier, 1995).

Ketoprofen is considered as a model hydrophobic drug because of its simple metabolism and broad therapeutic window (Kantor, 1986). The main administration route of ketoprofen is orally, but it has been associated with systemic adverse events and gastrointestinal disorders (Coaccioli, 2011), so other routes has been developed such as topical, transdermal in order to avoid those events. Prescription ketoprofen is used to relieve tenderness, swelling, and stiffness caused by osteoarthritis (arthritis caused by a breakdown of the lining of the joints) and rheumatoid arthritis (arthritis caused by swelling of the lining of the joints).

Ketoprofen capsules are also used to relieve pain, including menstrual pain (pain that occurs before or during a menstrual period). It works by stopping the body's production of prostaglandin a substance that causes pain, fever, and inflammation.

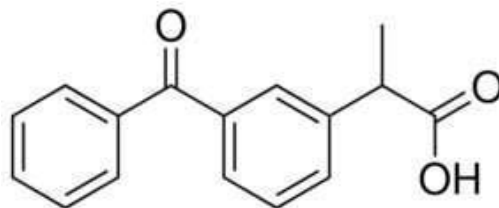


**Figure 2-5.** Ketoprofen chemical structure  
From: PubChem website

### 2.1.5 Phosphate buffer solutions (PBS) in neutral and acidic conditions

PBS is commonly used for biochemical procedures. Its osmolarity and concentration of ions ( $\text{Cl}^-$ ,  $\text{Na}^+$  and  $\text{K}^+$ ) is very similar to the extracellular liquid of mammals. The PBS is an isotonic and not toxic solution. The pH values can be modified according to the physiological conditions under that the drug loaded carrier want to be tested. For example, regarding to the digestive system, three important pHs were tested: 7.4, 1.2 and 4.6 in accordance with oral cavity (pH 6.8-7.5), stomach cavity (pH 1.0-2.0 up to 4-5), and small intestine (7.2 – 7.5). (Balamuralidhara, 2011)

The PBS solution in neutral conditions (pH=7.4) was directly prepared from the commercial powder purchased at SIGMA-ALDRICH and was used as received. The acid PBS buffer solutions were prepared according to the *USP pharmacopeia*. The hydrochloric acid buffer at pH= 1.2 was prepared dissolving 2g NaCl + 7.0 mL HCl concentrated in 1L of distilled water, whereas the PBS acetic/ acetate buffer solution at pH=4.6 was prepared as following:

Stock solution A: Acetic acid 2M: 11.55 ml glacial acetic acid in 1L of distilled water  
Stock solution B: Sodium acetate 2M: 27.2g Sodium acetate in 1L of distilled water

**Table 2-1** Composition of the PBS acetic/acetate buffer solution at pH = 4.6

Stock solution A (ml)	Stock solution B (ml)	Water (ml)	pH-value
255	245	500	4.6*

\* Adjust the pH if necessary

### 2.1.6 Protocol for dialysis bag preparation

The dialysis tube was purchased by SIGMA and pre-treated according their recommendations. It is a cellulose tubing No. D-9277 with average flat width of 10 mm, average diameter 6 mm, Molecular weight cut-off (MWCO) =12,400 Da and with a capacity of 10 ml/ft approximately. We followed the pre-treatment protocol that SIGMA suggested. Three solutions were prepared corresponding with the indications described below:

Solution A: 0.3% (w/v) NaS solution at 80 °C

Solution B: Filtered distilled water at 60 °C

Solution C: 0.2% (v/v)  $\text{H}_2\text{SO}_4$  acid solution

Then, different steps were realized:

1. The glycerin included as humectant was removed washing the tube in running water during 3-4h.
  2. The sulfur compounds were removed by treating the tube with the solution A for 1 minute
  3. The tube was washed with the solution B for 2 minutes
  4. The tube was acidified with the solution C washing the tube for 2 minutes.
  5. Then the rinse was done carefully to remove the acid with the solution B for 2-3 minutes.
  6. The dialysis bag were stored in a sealed flask filled with filtered distilled water in the fridge until the use. It is not recommended to keep the stock of pre-treated dialysis bag more than three months.
- After following the protocol, this tubing will retain most proteins of molecular weight 12,000 or greater.

### 2.1.7 HeLa culture cells

HeLa cells are a special type of cancer cells. HeLa cells have error-filled genomes, with one or more copies of many chromosomes: a normal cell contains 46 chromosomes, whereas HeLa cells contains 76 to 80, some of which are mutated. This is due to the Human Papillomavirus (HPV), the cause of nearly all cervical cancers (Landry, 2013). HeLa was the first human cell line established, that grows unusually fast, doubling cellular count in only 24 hours, making them ideal for large scale testing. This cell culture is characterized to be highly resistant to apoptosis, meaning they will divide several times. This performance can be explained by the expression of an overactive telomerase that rebuilds the telomeres after each division, allowing the perpetual proliferation (Bidon 2018). With all these characteristics, HeLa cells were selected as a potentially more sensitive bioassay organism because of the absence of a protective tissue. The toxicity of different carriers prepared were evaluated with response of the bioavailability in this culture.

## 2.2 Methods

### 2.2.1 Phase diagram determination

Samples were prepared, by weighting the needed amounts of surfactant and water in hermetically sealed glass tubes. The homogenization of the samples was done with a vortex stirrer. The phase diagrams were established by preparing samples over the whole range of surfactant/water concentrations and placing them in a water bath at the desired temperature until reaching equilibrium, for 1 week. For ternary systems, the third component was added cumulatively. Visual observations coupled with polarized light optical microscopy (Olympus BX 50) were used to identify the structure of the liquid crystal phases. Small angle X-ray scattering

(SAXS) measurements were performed to establish precisely the phase boundaries, to confirm the nature of the different phases and to determine the space group of the cubic phase.

### A. Polarized light microscopy

The polarized microscope is equipped with two perpendicular polarizing filters: polarizer and analyzer. The first allows the polarization of light in a direction. The light after passing through a polarized filter, it vibrates in a specific direction. The passage of this light polarized through an anisotropic crystal causes a doubling of the light beam into two rays of different polarizations which propagate at two different speeds.

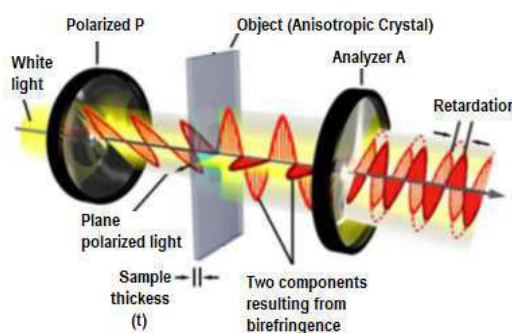


**Figure 2-6.** Polarized light microscope configuration  
Murphy, 2000

This phenomenon is called birefringence and is due to the difference in index of refraction anisotropic compounds whose optical properties are different depending on the direction of the propagation of the light ray. The analyzer placed after the sample is oriented perpendicular to the polarized, then allows the merger of the two light beams and the image obtained is the result of the interference between two rays having different speeds of propagation (Na Du, 2010).

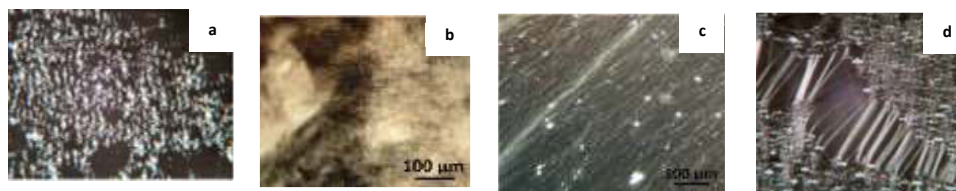


**Figure 2-7.** Example of textures under polarized microscope from a sample into a vial  
a) Texture of "Maltese Cross" in lamellar phase; b) The  $H_1$  hexagonal phase; c) The  $L_\alpha$  lamellar phase; d) The  $L_\alpha$  phase oily streaks

## B. Small Angle X-ray scattering - SAXS

Small angle X-Ray scattering (SAXS) measurements were carried out on a “SAXSess mc<sup>2</sup>” instrument (Anton Paar), using line-collimation system. This instrument is attached to an ID 3003 laboratory X-Ray generator (General Electric) equipped with a sealed X-Ray tube (PANalytical,  $\lambda_{\text{Cu, K}\alpha} = 0.1542 \text{ nm}$ ) operating at 40 kV and 50 mA. Each sample was introduced in a “Special Glass” capillary, with a diameter equal to 1.5 mm and 2.0 mm for micellar solutions and liquid crystals, respectively, or between two sheets of Kapton® for materials. Then placed inside an evacuated sample chamber and exposed to X-Ray beam. Scattering of X-Ray beam was recorded on a CCD detector (Princeton Instruments, 2084 x 2084 pixels array with  $24 \times 24 \mu\text{m}^2$  pixel size, sample-detector distance = 309 mm).

Using SAXS Quant software (Anton Paar), the two-dimensional image was integrated into one-dimensional scattering intensities  $I(q)$  as a function of the scattering vector  $q = (4\pi/\lambda) \sin(\theta)$ , where  $2\theta$  is the total scattering angle. Thanks to a translucent beam stop allowing the measurement of an attenuated primary beam at  $q = 0$ , all measured intensities can be calibrated by normalizing the attenuated primary intensity. All data were then corrected for the background scattering from the cell and for slit-smearing effects by a desmearing procedure from SAXS Quant software, using Lake method. For micellar solutions, after correction, obtained intensities are scaled into absolute units using water as a reference material.

### 2.2.2 Emulsification process by Phase Inversion Composition (PIC)

The *fine emulsions (Em)* were formed by Phase Inversion Composition (PIC) method, where the mixtures of the oil and surfactant with different oil / surfactant ratios were first prepared. Then, water was added dropwise by using an automatic peristaltic pump which injects the right amount of water in a constant settled rate of  $250 \mu\text{L}\cdot\text{s}^{-1}$ ; the mixture was constantly magnetically stirred at 1250 rpm at 25 °C.

The *concentrated emulsions (CE)* were prepared mixing water and surfactant in different water/surfactant ratios between 3.6 to 9. Then, the oil is manually added dropwise to the mixture under continuous stirring. The CE are obtained with oil weight contents between 70 and 95%. The droplet size of the CE was determined by Microscope Optical Polarized (MOP) and Small Angle X-ray Scattering (SAXS).

To prepare the doped CE or Em, an oily solution with KTP was previously prepared, dispersing a certain amount of this drug in Miglyol by calculating a concentration of 2% KTP in the final formulation. The corresponding doped oil concentration to add in each formulation was prepared by separate. Then the

procedure was followed as described in the corresponding section. In the case of CE the samples are ready to rheological characterization.

#### A. Dynamic Light Scattering (DLS)

The samples were prepared with demineralized water filtered using a surfactant free cellulose filter (pore size = 0.45  $\mu\text{m}$ ). Two or three drops of the sample are placed in a disposable polystyrene cells, then the cell must be totally filled with filtered water. Is necessary to do the measurement in diluted samples in order to eliminate the inter particular effect. To confirm the results the analysis must be carried out at constant temperature (25°C) and by triplicate. The measurements were carried out in a Malvern Setasizer 3000 HSa apparatus equipped with a He.Ne laser 633 nm, 5 mW, its detection range is from 2 nm to a few micrometers.

This technique is used to determine the size distribution profile of small particles in the sub-micron region dispersed in a liquid. It is based on the measurement of the Brownian movement. In order to detect this movement, an incident laser beam pass through a cell containing the dispersed particles. These particles scatter the laser beam and thus fluctuating its intensity. As the particles are in a perpetual movement the exiting beam's intensity fluctuates as a function of time. These fluctuations are detected and quantified using a detector, which send the signal to the correlator.

This correlator works as a signal comparator, that analyze the signal at given time (t) to the signal in the initial time ( $t_0$ ) and calculates the correlation between them. This correlation decays through time till it becomes null. The decaying time is a function of particle size, the smaller the particle the faster it is for the correlation to decay. The correlator used in a DLS instrument will construct the correlation function  $G(\tau)$  of the scattered intensity, when  $\tau$  is the sample time:

$$G(\tau) = \frac{I(t_0)I(t_0 + \tau_0)}{I(t_\infty)^2} \quad \text{Eq. 2 - 1}$$

For many monodisperse particles in Brownian motion, the correlation function is an exponential decaying function of the correlator time delay  $\tau$  :

$$G(\tau) = A[1 + B \exp(-2\Gamma\tau)] \quad \text{Eq. 2 - 2}$$

Where A is the base line of the correlation function, B is the intercept of the correlation function and  $\Gamma$  is the decay rate calculated as:

$$\Gamma = D_t q^2 \quad \text{Eq. 2 - 3}$$

Where the  $D_t$  is the translational diffusion coefficient and  $q$  is the wave vector:

$$q = \left( \frac{4\pi n}{\lambda_0} \sin \frac{\theta}{2} \right) \quad \text{Eq. 2 - 4}$$

with  $n$  is the refractive index of dispersant,  $\lambda_0$  is the wavelength of the laser (633 nm) and  $\theta$  is the scattering angle. Hydrodynamic diameter  $D_H$  is obtained from the correlation function using the Stokes-Einstein law:

$$D_H = \frac{kT}{6\pi\eta D_t} \quad \text{Eq. 2 - 5}$$

Where  $k$  is the Boltzmann constant,  $T$  the absolute temperature,  $\eta$  the viscosity of the continuous medium. There are two approaches that can be taken: if the curve corresponds to an exponential to the correlation function to obtain the mean size, and an estimate of the width of the distribution (polydispersity index) or multiple exponential to the correlation function to obtain the distribution of particle sizes.

In the experiments, there are two approaches that can be taken: if the curve corresponds to an exponential to the correlation function to obtain the mean size (z-average diameter) and an estimate of the width of the distribution (polydispersity index), this is called cumulants analysis, or multiple exponential to the correlation function to obtain the distribution of particle sizes such as non-negative least squares (NNLS) or CONTIN. The size distribution obtained is a plot of the relative intensity of light scattered by particles in various size classes and is therefore known as an intensity size distribution.

## B. Rheological experiments

Rheological experiments were carried out at 25°C with after making (AFM), 24h and one-week (1 wk) aging samples which were maintained at 25°C in a temperature-controlled bath and protected from the natural light into their amber tubes. The results of the experiments were performed to highlight the viscoelastic and structural properties of the samples in function of the oil content and the influence of ketoprofen addition through the aging time.

All the rheological experiments were carried out at least by duplicate in a controlled stress rheometer (AR-G2, TA Instruments) using a cone-plate geometry with a diameter of 40 mm and 2° cone angle. The deformation experiment was performed at 1 Hz frequency to determine the linear viscoelasticity zone. The

temperature was kept at  $25 \pm 0.1$  °C using a water bath circulation (Cole-Parmer Polystat, U.S. and Peltier ARG2).

All these experiments have been performed in the Nanostructured Liquid Characterization Unit, located at the Institute of Advanced Chemistry of Catalonia (IQAC), belonging to the Spanish National Research Council (CSIC) and affiliated to the NANOBIOISIS ICTS of the Biomedical Networking Center (CIBER-BBN).

### 2.2.3 Mesostructured porous materials preparation

#### A. Bare silica materials preparation

Micelles were prepared with aqueous solutions at pH = 7.0 and at 25°C. Six concentrations of surfactant in water were investigated, 2.5, 5, 10, 20, 30 and 40 wt. %. For the mineralization of the samples, TMOS was dropwise added to the solutions and the mixtures were stirred at 300 rpm for 1 h. The surfactant / silica molar ratio was varied from 0.017 to 0.066, The mixtures were placed into sealed Teflon autoclaves at 40°C during 24 h, then at 100°C for 24 h. Next, the materials were transferred into cellulose extraction cartridges to remove the template by Soxhlet ethanol extraction for 48 h. After drying at room temperature during 24 h, samples were thermally treated under synthetic air as follow. A first temperature increase was applied at 2 °C/min until 150 °C with a 1 h plateau, followed by a second temperature ramp at 2 °C/min to reach 350 °C where the temperature was held for 1 h, then, a final temperature ramp at 2 °C/min was imposed to reach 550 °C with a 1 h plateau. The cooling process was uncontrolled and directed by the oven inertia.

Finally, the materials were dried at room temperature during 24h. For the *fine emulsion (Em)*, first the oil and the surfactant were mixed at 1250 rpm at 25°C, then water was added at a fixed rate of  $250 \mu\text{L}\cdot\text{s}^{-1}$ . For each investigated surfactant concentration in water: 2.5, 5 and 10 wt. %, samples containing 1, 3, 5, 7, 10 and 15 wt. % of oil were studied.

For the *CE* the water and surfactant were mixed with the help of a vortex, later, the oil was manually added, while the continuous mixing, then the TMOS silica precursor was dropwise added and mixed at 300 rpm. The composition of the samples is given in the chapter V in the table.

## B. Mesoporous materials prepared from the partnership KEL/P123

Emulsions of small size or fine emulsions (Em) (20-50 nm) were prepared from the system: KEL/Isopropyl Myristate/Water. Having an oil/surfactant mass ratio of 0,43 and 0.66 with three water contents: 70, 80 and 90 wt%. The stability study of the samples was determined according to the variation of the droplet size, which was measured by DLS and visual aspect. The study was carried out considering the emulsion size after-making (AFM), 24 h and 1week after preparation. The samples were kept protected from the light and heat sources during all the study. Those which resulted more stable according to the minimum variation of the droplet size and visual aspect, were selected to prepare the mesoporous materials with the help of a 5wt% solution of P123 in different ratios between Em/P123 under two pH conditions: 7 and 0.3.

The emulsions were prepared with the PIC method, mixing first the Kolliphor EL and Isopropyl Myristate at 300 rpm and 25 °C, then the water was dropwise added with the help of a CRIMSON pump in a flow of 500 $\mu$ l s<sup>-1</sup> until obtain a bluish solution free of any bubble. Futhermore, the solution of P123 was prepared at pH=7 and the mixtures with the fine emulsion were done in the following P123/Em mass proportions: 100-0, 90-10, 80-20, 70-30...0-100, always having a total mass of 10g. The speed of mixing was always kept at 300 rpm, then the silica precursor was dropwise added while the speed of mixing was decreased to 150 rpm during 40 min, then the final mix was placed into a sealed Teflon autoclaves to carry out the hydrothermal treatment 24 h at 40 °C and 48 h at 100 °C.

After that, the materials were transferred into cellulose extraction cartridges to remove the template by Soxhlet ethanol extraction for 48 h. At the end the samples were dried at room temperature. Finally, the samples were characterized by SAXS and adsorption-desorption nitrogen. To make sure that any residue of the organic phase could remain into the silica structure, samples were thermally treated under synthetic air as follow: first temperature increase was applied at 2 °C/min until 150 °C with a 1 h plateau, followed by a second temperature ramp at 2 °C/min to reach 350 °C.

Temperature was held for 1 h, then, a final temperature ramp at 2 °C/min was imposed to reach 550 °C with a 1 h plateau. The cooling process was uncontrolled and directed by the oven inertia. At the end of all the process, the sample were characterized again by SAXS and adsorption-desorption nitrogen. The same process was repeated with the samples prepared from the mixture of the fine emulsion and P123 solution at pH=0.3, the acidic solution was prepared using HCl.

## 2.2.4 Doped mesostructured hybrid materials preparation

In order to entrap the KTP into the hybrid materials which must be able to perform the release under controlled conditions, the synthesis was done with doped Micelles of KEL in water and fine emulsions (*Em*) with the system KEL/water/Miglyol. For all preparations a drug free hybrid system was prepared to contrast the results with that drug loaded.

### A. Loaded mesostructured hybrid materials from KEL doped micelles.

The O/W micelles prepared with Kolliphor EL (KEL) are nanostructures varying in size around 15-20 nm, where drugs can be encapsulated. For this study, Ketoprofen (KTP) was chosen as active principle model. This drug is located inside of the micelle core and entrapped into the hydrophobic part. The drug is just physically associated into the micelles, therefore does not need chemical reaction to be released. (Figure 2-8)

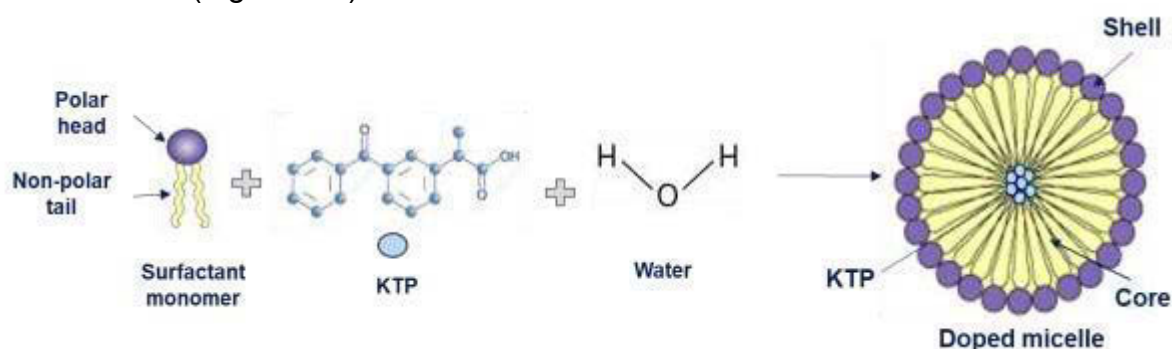


**Figure 2-8.** Preparation of the doped direct micelles of Kolliphor EL

For the hybrid materials prepared from doped micelles of KEL, the KTP was solubilized into the surfactant and mixed at 300 rpm and 25 °C until the complete dissolution. Then the water was dropwise added to form three different KEL/water ratios (wt%): 0.026, 0.053 and 0.11. While the water was being added the mixture was constantly magnetically stirred at 1250 rpm at 25°C. The KTP/KEL ratio was took at 0.075, expecting to have 2% of the drug into the final material. This concentration is based in the commercial content of the prescribed medicaments. The micelles were doped according to the following equation:

$$2\% \text{ KTP} = \frac{\text{drug (g)}}{\text{drug (g)} + \text{TMOS (g)} + \text{KEL (g)}} \times 100 \quad \text{Eq. 2 - 6}$$

Is crucial to protect the doped preparations from the sunlight during all the synthesis process. The doped micellar solutions and along with those drug free

ones, must be stored at 4°C in order to eliminate the remaining bubbles after the preparation. The KEL concentrations used to synthesize the hybrid materials were: 2.5, 5 and 10 wt% in water. After that, the mineralization was carried out adding slowly the TMOS while stirring at 500 rpm during 40 min. The KEL/TMOS molar ratio was fixed at 0.024. The final mixture was placed into sealed Teflon autoclaves at 40 °C during 24 h, then at 70 °C during 48 h. After these optimized conditions for the hydrothermal treatment, the hybrid materials were dried at room temperature (RT) during 24 h (Fig. 2-9 process A) for their subsequent characterization. A reference material from non-doped micellar solutions must be prepared under the same conditions.

At the end of synthesis, the amount of drug trapped inside the hybrid materials was determined by HPLC and this value was named as  $C_{KTP}^{mat}$ , for which 5 ml of methanol were placed into a tube with 0.01 g of doped hybrid material in order to extract the KTP from the organic phase. The tube was centrifugated at 4500 rpm for 5 minutes. Later, the silica settled in the bottom and the supernatant was recovered. Then, the doped methanol was recovered with a pipette and injected in the HPLC to be analyzed under the same conditions as the aliquots from the release tryouts (Fig. 2-9 process B). The proportions obey the sink conditions used for the release experiments. The value of  $C_{KTP}^{mat}$  was employed for the further calculations of KTP profile released.



**Figure 2-9.** Hybrid mesophase synthesis from the doped micelles (process A) and  $C_{KTP}^{mat}$  determination (process B)

Subsequently, in order to determine the materials structuration, SAXS experiments were carried out with the hybrid mesoporous silica materials, which were later calcined according with the process description in the page XX and then characterized. Finally, the resulting SAXS spectra were contrasted with those materials obtained in the synthesis without KTP (identified as drug free) during mineralization.

#### B. Loaded mesostructured hybrid materials from KEL fine emulsions.

For the doped hybrid materials prepared from fine Emulsions (*Em*) the KTP was solubilized in the Miglyol at 300 rpm at 25 °C until the complete dissolution expecting to have 2% in the final formulation also. The Mig/KEL ratios considered for the formulations were 0.25, 0.43 and 0.66 with 80 wt% of water in all cases, while the KEL/TMOS molar ratio was always considered as 0.024. The KEL is stirred with the doped oil at 300 rpm at 25 °C. When the preparation is completely transparent and bubbles free the water is dropwise added while is constantly magnetically stirred at 1250 rpm at 25°C. Once the fine emulsions were ready, they were characterized by DLS.

Our strategy to develop this nanocarriers consists in to involve the KTP addition in the material synthesis, this method will allow also to entrap a higher amount of drug. For this purpose, the doped fine emulsions *Em* were used as a template and the source of silica polymerize around the Miglyol drops and interact with the KTP. The mineralization conditions were followed as in the point 2.2.4. When the final hybrid doped materials were obtained, the SAXS and adsorption/desorption nitrogen characterizations were carried out. At the end, in order to know the KTP amount trapped into the materials the  $C_{KTP}^{mat}$  method was followed as in the Figure 2-9 process B and the result was used for the quantification of KTP released during the kinetic experiments.

### 2.2.5 Materials characterization techniques

#### A. Nitrogen adsorption and desorption analysis

The textural properties of the organized porous materials are measured by nitrogen adsorption and desorption test. These materials have alongside their structure a high specific area and a small pore size distribution.

The adsorption corresponds to the adsorption of the molecules in a solid surface, there are two types of adsorption: physisorption and chemisorption. The

characterization of porous material is done by physical adsorption and desorption of nitrogen at its liquefaction temperature:  $-196\text{ }^{\circ}\text{C}$  ( $77\text{ K}$ ) at the surface of the material.

The equilibrium established between the gaseous state and adsorbed of the absorbable compound, can be compared at equilibrium existing between a liquid and its vapor. At a given temperature, the quantity of the adsorbed species is plotted as a function of the equilibrium pressure ( $P/P_0$ ) of the gas on the pressure domain between 0 and the saturating vapor pressure, forms the adsorption isotherm.

The shape of the adsorption isotherm allows the qualitative determination of the textural properties of the studied material. The different isotherms are classified according to six distinct types, however, just those founded in this work will be explained (Figure 8).

A1. Isotherm type II. This is obtained with a wide distribution of pore sizes, which allow unrestricted monolayer-multilayer adsorption to occur at high  $P/P_0$ .

A2. Isotherm type IV. This isotherm indicates the presence of the mesopores in the given system. This type of isotherm is known by the fast increase of the adsorbed nitrogen quantity for relatively small pressures that correspond to the adsorption of a monolayer. For higher pressures, the progressive increase of the adsorbed volume is translated by a capillary condensation phenomenon characteristic of the presence of mesopores (pores with a diameter between 2 and 5 nm), which is followed by the appearance of a plateau.

A hysteresis loop appears when the nitrogen starts the desorption process, and this loop is due to the irreversible nature of the capillary condensation inside the mesopores.

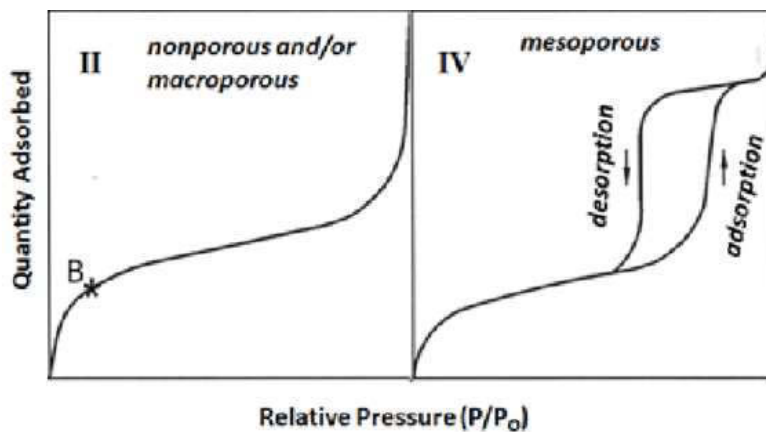


**Figure 2-10.** Type II and Type IV adsorption/desorption isotherms

The analysis of this type of isotherms uses mathematical algorithms, that allow the calculation of the surface area, the pore volume and the pore diameter of the studied material. The surface area is calculated from the adsorbed volume of the monolayer (for lower pressure values) and the molecular cross-sectional area:

$$S_{BET} = \frac{V_m}{V_{mol}} N \sigma$$

Eq. 2 – 7

$\sigma$  = molecular area per an adsorbed molecular  
( $\sigma = 16.2 \text{ \AA}^2$  for  $N_2$  at  $-196 \text{ }^\circ\text{C}$ )

$V_{mol}$  = molar volume of gas

$N$  = Avogadro number

The volume of the monolayer  $V_m$  is calculated using the Brunauer, Emmett, Teller (BET) equation:

$$\frac{P}{V(P_0 - P)} = \frac{1}{V_m C} + \frac{(C - 1)P}{V_m C P_0}$$

Eq. 2 – 8

$V$  = adsorbed volume at pressure  $P$

$V_m$  = monolayer volume

$P_0$  = saturating vapor pressure of the adsorbent

$C$  = constant

The pore size distribution is calculated using the Barret, Jayne and Halenda (BJH) equation:

$$\ln \frac{P}{P_0} = \frac{\gamma V_m}{(r_p - t)RT}$$

Eq. 2 – 9

$\gamma$  = Surface tension at temperature  $T$

$r_p$  = pore radius

$t$  = tickness of an adsorbed layer

This theory is based on the phenomenon of capillary condensation which appears in the mesopores, and by applying the Kelvin law, which links the pressure  $P$  at which the condensation happens to the curvature radius of the meniscus of the formed liquid. Based on an iterative calculation, it allows the calculation of the quantity adsorbed in a defined pressure span.

From the pore radius as a function of the relative pressure, it is possible to calculate the cumulated volume of all the pressure spans as a function of pore radius, which gives by derivation the pore size distribution. The apparatus used is a Micromeritic Tristar 3000. The samples were degassed at least 12 hours before the analysis in order to eliminate water and  $\text{CO}_2$  physisorbed inside the pores of the material.

## B. Scanning Electron Microscopy (SEM)

The electronic microscopy methods are direct techniques that allows the visualization of the silica materials in real time, unlike the previous techniques that require further calculations in order to exploit the results. Scanning Electron Microscopy (SEM) consists of the scanning of the surface of the sample using a high energy electron beam. The interaction between the electrons and the sample's surface leads to the generation of backscattered electrons, X-rays and Auger electrons, UV/visible/IR cathodoluminescence and secondary electrons. The latter have low energy and are generated from the most superficial atoms of the sample, this makes them responsive to the sample's surface topography. Those electrons are collected point by point on the scanned area, and the resulting signals are normalized and converted to an image of the scanned surface.

The SEM used for this experience is a HITACHI S-2500. The samples were dispersed in ethanol using ultrasound, then spread on an aluminum sample holder and dried at room temperature.

## C. Transmission Electron Microscopy (TEM)

In this technique, the image obtained is the result of the interactions between the sample and the passing through electron beam. The intensity of the electron beam is controlled by the density and the thickness of the sample producing a fluctuation of the contrast analogous to the sample's texture. This technique was used to observe the organization and the general morphology of the mesopores. The images of TEM were recorded on a JEOL ARM200-CFEG microscope operating at 200KV. For TEM observations, samples were previously dispersed in chloroform with ultrasounds and few drops of the suspension was spread on Au grid covered by Formvar/amorphous carbon film.

### 2.2.6 Dissolution test and KTP release conditions from synthesized carriers.

The release experiments were conducted in 3 replicas. 0.3 g of the material was introduced in the pre-treated dialysis bag and immersed into 150 ml of a receptor solution inside amber glasses, then sink conditions, where the volume of the medium should be at least 10 times the drug saturation volume, were respected. The amber glasses are immersed into a bath-controlled temperature (30°C), and the receptor solution was stirred with a mechanical palette (Figure 2-11). The dissolution test was followed for 24 hours.

The measurements were done each 15 minutes during the first five hours, then every 30 minutes until complete 10 hours and after that every hour until the end. The cumulative releases profiles of ketoprofen from the divers synthesized

carriers, were also evaluated under three different pH values: 1.2, 4.6 and 7.4 of the receptor solutions that was prepared according to the *USP pharmacopeia* and under 3 different content of P123: 1,3,5 wt%.

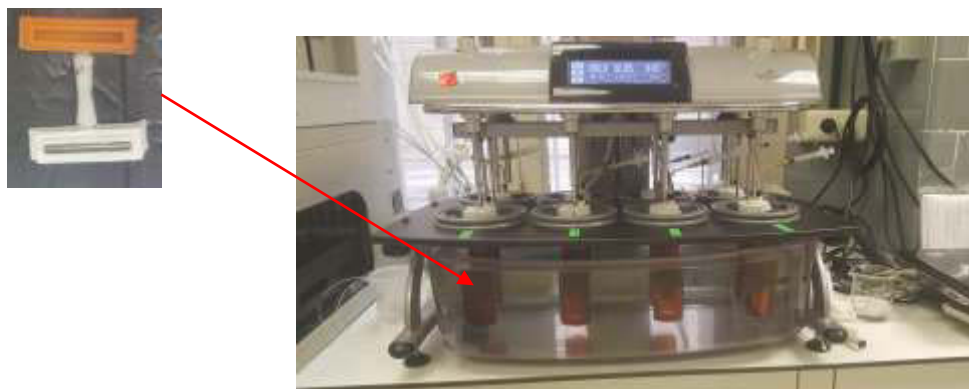


**Figure 2-11.** Dissolution equipment for the release experiments

During the realization of whole experiment, the samples were stirred using a magnetic stirrer at 100 rpm at room temperature. Samples of 1 ml of the receptor solution were extracted in a fixed height inside of the container at the described intervals. The volume taken was replaced with 1 ml of fresh medium solution so that the volume of the receptor solution keeps constant.

This added volumes that dilute the release medium are counted into the calculations. The aliquots are then analyzed using HPLC at 260 nm and the obtained curves were modeled with a Drug Solver software (Yong Zhang, 2010).

#### 2.2.6.1 Methods for Ketoprofen release quantification

##### A. High Performance Liquid Chromatography

High efficiency liquid chromatography (HPLC) is a technique used for the separation of components of a mixture, based on different types of chemical and physical interactions between the analytes, the mobile phase and the chromatographic column. The separation was done in a C18 column based on the partition coefficient, that is defined as the ratio of the concentration of a solute (analyte) in the organic phase ( $C_1$ ) and its concentration in the water phase ( $C_2$ ), when the two concentrations are at equilibrium.

The sample to be analyzed passes through a chromatographic column by pumping liquid at constant flow, that leads the high pressure in the initial conditions (125 bar) through the column. The time required for a component to elute from the column is called retention time ( $T_R$ ) and is considered a characteristic property of

identification of a component in each mobile and stationary phase. The retention time of the components depends on their nature, the mobile phase and the stationary phase.

The calibration curve has been determined from a minimum of six solutions at different concentrations of the active principle to be quantified. The graphical representation of the areas under the chromatographic peaks obtained for each concentration allows to obtain calibration curve with the form:

$$y = A + Bx \quad \text{Eq. 2 - 10}$$

Where  $y$  is the value of the chromatographic area,  $A$  is the ordinate at the origin,  $B$  is the slope of the line and  $x$  is the concentration. The concentration of the active principle in the test solution is determined by interpolation of the chromatographic area obtained from the calibration line. The chromatographic system used to analyze ketoprofen has been a Shimadzu equipped with an Interchim VKR5C18-250mm/4.6 mm reverse phase column and a UV detector diode array at a wavelength of 260 nm. The elution of ketoprofen was carried out in the column placed into an oven at 35°C using a mobile phase composed of a mixture of 65% acetonitrile acidified with 2% (v/v) of formic acid as organic phase (phase B) and 35% acidic aqueous phase at pH 3.0 (phase A). The flow rate was 1 mL / min and the injection volume were 50  $\mu$ L. The retention time for ketoprofen was 4.5 minutes. The gradient elution for the method developed in our lab was carried out with the phase B, and set as: 0 min at 65%, 4 min 65%; 6 min 100%, 10 min 100%; 11 min 65% and 15 min 65%.

### 2.2.7 In vitro cytotoxicity assay

To carry out the toxicity assays, first the cells must be prepared to receive the samples, then the method is divided in two. First,  $1 \times 10^4$  cells were plated in 96-well plates (Thermo Fisher Scientific S.L.) and incubated for 24h at 37°C and 5% CO<sub>2</sub>. HeLa cells were cultured in Dulbecco's modified Eagle's medium (DMEM high glucose) supplemented with 10% fetal bovine serum (FBS) and 1 wt% of antibiotics: penicillin and streptomycin. (Mosmann, 1983). All the culture medium components were purchased from Life Technologies (Paisley, Scotland, UK). The assays were carried out in ten replicates. After 18h of incubation at 37°C the medium was withdrawn, and cells were seeded with fresh medium and MTT reagent solution (Sigma Aldrich) was added in each well to a final concentration of 0.5 mg/mL and cells were incubated for two additional hours at 37°C. Then, the solution was aspirated and 100  $\mu$ L of dimethyl sulfoxide (DMSO) were added to each well to dissolve the formazan crystals. The plate was gently shaken for 15 min at room

temperature. Then the samples were prepared to test their toxicity. The Table 2-2 regroup the composition of the three types of systems for the experiments and the Figure 2-12 A, B explains the followed process. In the preliminary trials (Figure 2.12 A), the after making (AFM) samples were applied directly on the cell culture: 0.0022 g of each one in  $10^4$  cfu/ml<sub>cm</sub> each borehole (cfu: culture formation units, cm: fetal bovine serum as culture medium). However according to the results observed, a second protocol was proposed (Figure 2.12B).

**Table2-2.** Compositions of systems used in HeLa experiments

Sample	KEL (wt%)	Mig (wt%)	KTP (wt%)	KEL/TMOS (molar ratio)
MS5	5	0	0	0
HMS5	5	0	0	0.024
SM5-KTP	5	0	2.5	0
HMS5-KTP	5	0	2.75	0.024
FE40	60	40	0	0
FE40-KTP	60	40	2.4	0
CE90	15	90	0	0
CE90-KTP	15	90	2	0

*MS5: Micellar solution with 5wt% KEL, HMS5: Hybrid material from micellar solution, FE40: Fine Emulsion with 40 wt% Miglyol, CE90: Concentrated Emulsion with 90wt% Miglyol. The "-KTP" means KTP added.*

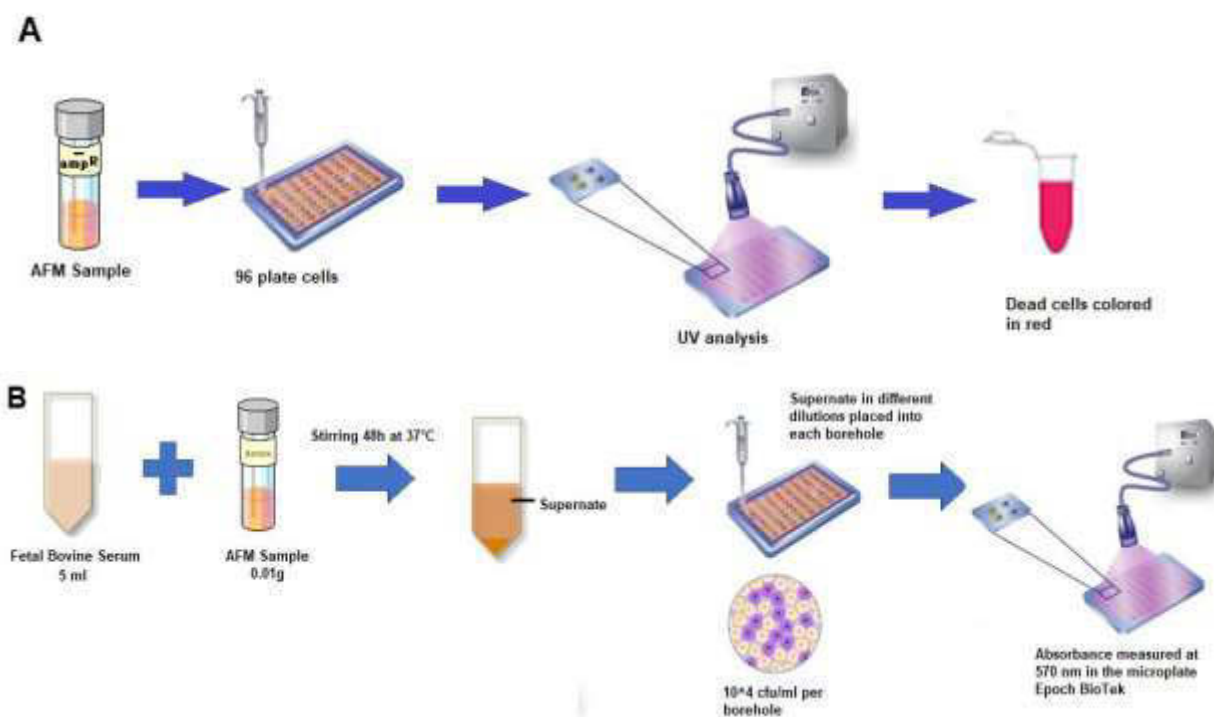


**Figure 2-12.** Process of the toxicity test for AFM samples (A), Process for the pre-treated samples before conducting toxicity test (B).

Following the process B was proposed to test only the supernatant (SN) resulting from the mixture of the culture medium and certain amount of each sample. For that purpose, 0.01g of each sample was dissolved in 5 ml of culture medium by stirring for 48 hours at 37°C. All the quantities correspond proportionally to the amounts used for the release experiments respecting the sink conditions.

The supernate was considered as the initial concentration, then from this, the following dilutions: 1/2, 1/5, 1/10, 1/50, and 1/100 (v/v), were prepared to know the viability of the cells in function of the concentration. Just in the case of solid materials, the mixture was made, but the tubes were mixed at 1500 rpm during 15 min at 37°C, then the supernatant free of solids was recovered and the dilutions were done to continue with the analysis. The plates were analysed in the Epoch™BioTek reader with an absorbance at  $\lambda=570$  nm. Results were expressed as a relative percentage to the control cells.

# **Chapter III. Investigation of the system Kolliphor EL/water for the preparation of mesoporous materials. Addition effect of biocompatible oils.**

This chapter explain how the mesostructured silica materials have been prepared through the Cooperative Templating Mechanism (CTM) from micelles of Kolliphor EL (KEL) which is a biocompatible surfactant.

The first part concerns the study of phase diagram of the system Kolliphor EL / water and the structural determination of various Organized Molecular Systems (OMS) as micelles and liquid crystals. The structures are studied by Small Angle X-ray Scattering (SAXS). Furthermore, the synthesis and structure of mesoporous silica materials obtained from Kolliphor EL micelles are described. The conditions to obtain the organized materials are explained.

The second part of this chapter concerns the influence addition of the Isopropyl Myristate (IM) and Miglyol 812K (Myg812N) used as oils into the KEL/water system. The ternary phase diagram is first determined for each oil. Then the preparation of mesostructured materials from the systems based in Kolliphor EL containing Miglyol are considered.

### 3.1 System Kolliphor EL/Water

#### 3.1.1 Phase diagram of Kolliphor EL in water and structure of the observed phases

The surfactant behavior in water was studied by establishing its phase diagram, for which several samples were prepared according to the method explained in Chapter 2. For concentrations below to 45 wt% of surfactant, stable micellar solutions with temperature are obtained. For higher concentrations of KEL, liquid crystals phase domain appears. From 46 wt% to 58 wt% of surfactant, a very stiff and isotropic phase which melts at 30°C is observed; it can be attributed to a cubic phase. The identification of the space group of this cubic phase was determined by SAXS. The figure 3-1 show the phase diagram obtained. The relative positions of the reflection lines are  $1:\sqrt{3/2}:\sqrt{2}:\sqrt{5/2}:\sqrt{3}:\sqrt{29/4}$ , which can be assigned to the Pm3n direct micellar cubic phase. From 58 wt% to 68 wt% of surfactant and up to almost 50 °C a hexagonal phase is observed. Indeed, the pictures observed by polarized light optical microscopy show a characteristic texture and the relative positions of the reflection lines on the SAXS patterns are:  $1:\sqrt{3}:2$ .

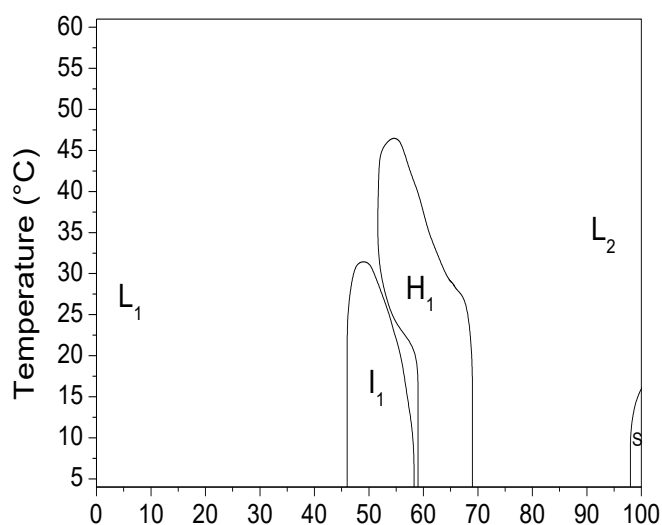


**Figure 3-1.** Concentration-temperature phase diagram of the KEL/W binary system.  $L_1$  and  $L_2$  correspond to direct and reverse micellar phase respectively,  $I_1$  corresponds to a direct micellar cubic phase and  $H_1$  corresponds to a direct hexagonal phase. S denotes solid.

The structural parameters of these liquid crystal phases were determined at several temperatures (10, 20, 25 and 30 °C). For the cubic phase, the ratio W/KEL ( $R'$ ) equal to 1 was investigated and for the hexagonal phase the studied ratios were 0.67 and 0.54. The structural parameters were determined in accordance with the equations reported in literature (ref).

The lattice parameters  $a$  were obtained from the following equations:

$$\frac{q_{hkl}}{2\pi} = \frac{1}{a} \cdot \sqrt{h^2 + k^2 + l^2} \text{ (cubic phase) Eq. 3 - 1}$$

and,

$$a = \frac{4\pi}{q_0\sqrt{3}} \text{ (hexagonal phase) Eq. 3 - 2}$$

where:  $q_0$  is the position of the first reflection and  $q_{hkl}$  is the peak for the reflection line  $hkl$ .

For the hexagonal phase, the hydrophobic radius  $R_H$  is related to the distance  $d$  associated to the first reflection by the following equations:

$$\frac{V_B}{V_S + \alpha V_W} = \frac{\sqrt{3}\pi R_H^2}{2d^2} \text{ Eq. 3 - 3}$$

where  $\alpha$  stands for the number of water molecules per molecule of surfactant,  $V_B$ ,  $V_S$ ,  $V_W$  respectively stand for the molar volumes of the hydrophobic part of the surfactant, the surfactant, the surfactant and water. Having as  $V_W = 18 \text{ cm}^3/\text{mol}$ ,  $V_B = 834 \text{ cm}^3/\text{mol}$  and  $V_S = 2354 \text{ cm}^3/\text{mol}$ , the cross-sectional area  $S$  can be deduced as:

$$S = \frac{3V_B}{N_A R_H} \text{ Eq. 3 - 4}$$

The results are shown in Table 1. For the hexagonal phase, the lattice parameter  $a$  slightly increases with the content of water from 10.4 to 10.7 nm, while the hydrophobic radius ( $R_H$ ) and the cross sectional ( $S$ ) area remain constant, equal to 2.6 nm and  $1.1 \text{ nm}^2$ , respectively.

For the cubic phase, the hydrophobic radius is determined by the following equation:

$$R_H = d\sqrt{h^2 + k^2 + l^2} * \left(\frac{3}{4n_m\pi} \phi_L\right)^{\frac{1}{3}} \text{ Eq. 3 - 5}$$

where  $h, k, l$  are the Miller indices corresponding to the diffracting planes.

The value of the  $R_H$  is given in Table 3-1. The first radius is higher for the cubic phase (3.5 nm) than for the hexagonal phase, while the cross-sectional area is in the same range ( $1.2 \text{ nm}^2$ ) for the two liquid crystal phases.

**Table 3-1.** Lattice parameter ( $a$ ), hydrophobic radius ( $R_H$ ) and cross-sectional area ( $S$ ) for the cubic and hexagonal phases at different surfactant/water ratios at 25°C

KEL/W (wt/wt)	Phase	$a$ (nm)	$R_H$ (nm)	$S$ $nm^2$
1.0	Pm3n	20.0	3.5	1.2
0.67	H1	10.7	2.6	1.1
0.54	H1	10.4	2.6	1.1

In the hexagonal phase, no significant change of the structural parameters in function of the temperature was observed. Given that, from the length of the bonds, the extended alkyl chains have a dimension of about 2.5 nm and looking at the determined values of the hydrophobic radius, so it is possible to deduce that the alkyl chains are completely extended in this phase. For the cubic phase, the hydrophobic radius is bigger than the estimated value. This result can be due to the deviation from the perfect spherical micelles to slightly rods in the Pm3n cubic phase, as suggested by Fontell 1985, or to disks as proposed in the Charvolin and Sadoc model. Concerning to the micellar phase, the structure of the micelles of Kolliphor in water were determined by SAXS with the samples at 2.5, 5 and 10 wt % of surfactant in water. The SAXS spectra are given on figure 3-2 in absolute units.

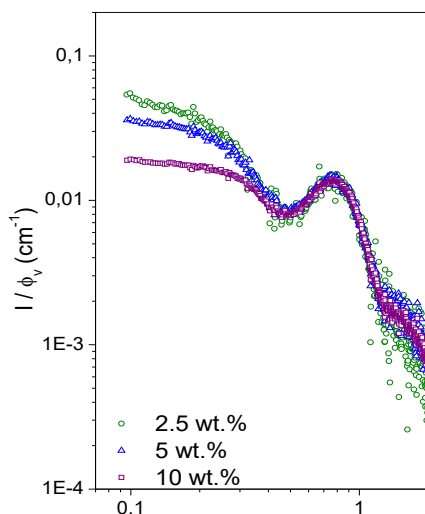


**Figure 3-2.** SAXS spectra of the micellar solutions with 2.5 wt % (green  $\circ$ ), 5 wt % (blue  $\Delta$ ) and 10 wt % (purple  $\square$ ) of Kolliphor at 25 °C in log-log representation in absolute units and normalized regarding to the surfactant volume fraction.

For all the studied concentrations, the spectra present the same profile. All the curves are overlapped for  $q > 0.45 \text{ nm}^{-1}$  and they exhibit a maximum at  $0.78 \text{ nm}^{-1}$ . For low  $q$  values ( $q < 0.45 \text{ nm}^{-1}$ ), the intensity decreases with the

concentration. This feature is characteristic of the existence of interparticle interactions.

To determine the micellar structure, the data were analyzed by using the Generalized Indirect Fourier Transform (GIFT) method Glatter 1982, Fritz 2006, taking into consideration the interparticle interactions as it is observed in the figure 3-3a. The obtained pair-distance distribution functions (PDDFs) were represented on Fig. 3b. The curves exhibit a pronounced dip, which even goes to negative values for the concentrated solution (10 wt %), indicating that the micelles can be considered as inhomogeneous and so called “core-shell” type particles.

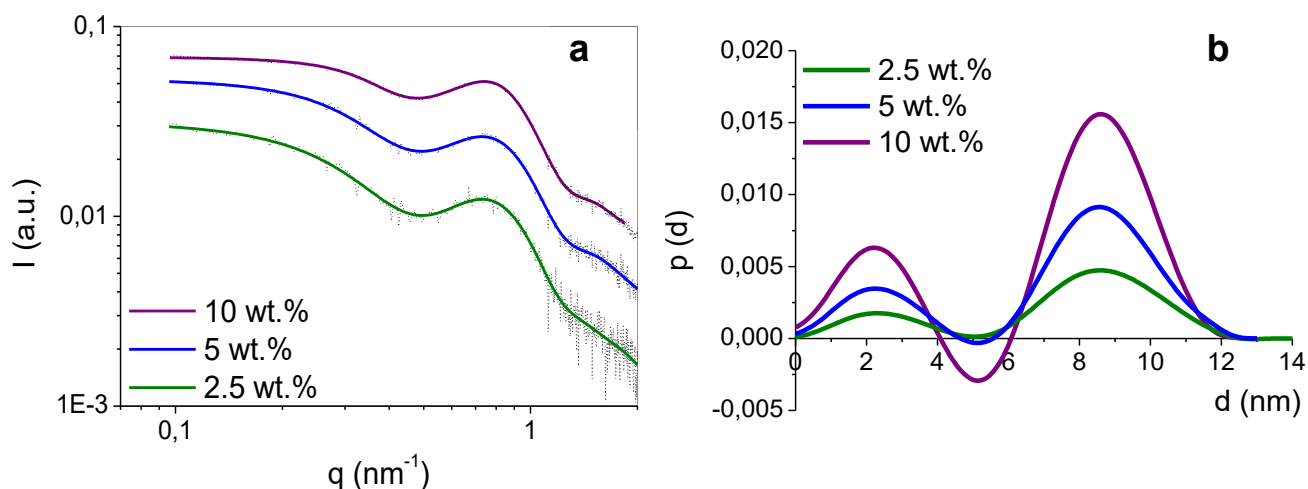


**Figure 3-3.** Data analyzed by GIFT for the micellar structure determination. (a) Experimental (black dotted line) and approximated (GIFT) (solid line) SAXS spectra at 2.5 wt % (green), 5 wt % (blue) and 10 wt % (purple) of Kolliphor at 25 °C; (b) Corresponding pair-distance distribution functions (PDDFs).

All the curves present also a bell-like shape, characteristic of spherical micelles, with a maximum dimension of about 12.5–13 nm, regardless of the surfactant concentration. These results are in good agreement with the hydrodynamic diameter determined at 25 °C by Dynamic Light Scattering (DLS) (14 nm with diluted micellar solutions, <2 wt% of surfactant). Additionally, the excess-electron density profiles have been determined by deconvolution of the pair-distance distribution functions for the three micellar solutions. ( $\rho_{\text{philic}} = 369 \text{ e/nm}^3$ ). The hydrophobic radius corresponds to the  $r$ -value when the sign of  $\Delta\rho(r)$  changes. It can be estimated at 3.1 nm for the 2.5 wt% of surfactant and 3.3 nm for the 5 and 10 wt% of surfactant. Then, the micelles radii can be evaluated at 6.2 for 2.5 wt% of surfactant and 6.5 nm for 10 wt % of surfactant. These values are in accordance with the maximum dimension found on the PDDFs. The excess electron density profile are show in the Fig. 4. The part corresponding to the lowest values of  $\Delta\rho(r)$ , having

a dimension of about 1.9–2.0 nm can be attributed to the hydrophobic chains since their dimension is estimated at 2.5 nm, considering the length of the links. So, it is possible then to deduce that the alkyl chains are slightly folded. For the hydrophilic chains, considering that one EO group has a dimension of 0.35 nm, their total dimension can be evaluated at 4.5 nm. From Figure 3-4, the hydrophilic part has a length of 4–4.5 nm. Thus, these chains have a rather extended conformation.

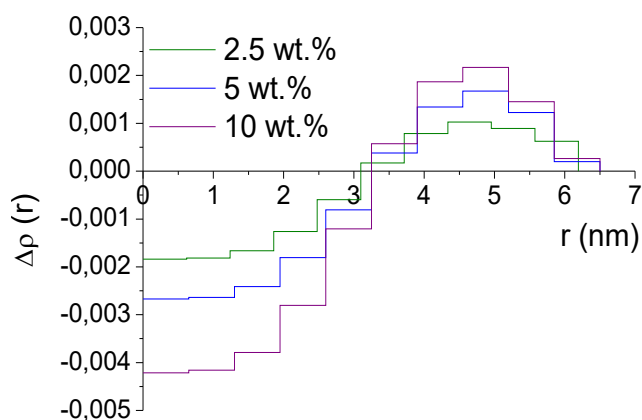


**Figure 3-4.** Excess-electron density profiles

### 3.1.2 Mesoporous materials prepared from micellar solutions based in Kolliphor EL

To synthesize the mesostructured materials, micellar solutions were first prepared with aqueous solutions at pH = 7.0 and at 25 °C. Six concentrations of surfactant in water were investigated: 2.5, 5, 10, 20, 30 and 40 wt % and the synthesis protocol was followed as is described in Chapter 2. The extracted and calcined material obtained at the end of the synthesis was characterized by SAXS, SEM and adsorption-desorption nitrogen analysis.

When the cooperative mechanism is used to prepare the mesostructured silica, the surfactant must form micelles in solution, but this is not a sufficient condition. Indeed, the other partner, the silica precursor, also plays a crucial role in the formation of the materials. In particular, the surfactant/silica molar ratio is an important parameter that should be optimized.

For two Kolliphor concentrations belonging to the micellar domain (2.5 and 10 wt%), the Kolliphor/TMOS molar ratio ( $R'$ ) has been varied from 0.017 to 0.066. By this way, from the surfactant point of view, the conditions are gathered for the CTM to occur. The observed variations will thus be due to the effect of the inorganic precursor. Whatever the Kolliphor concentration, mesostructured silica materials are recovered until a Kolliphor/TMOS ratio of 0.031 (Figure 3-5).

If the value of  $R'$  is increased the main peak becomes less intense and no secondary reflections are detected any longer. This means that the mesopores arrangement evolves towards a wormhole-like structure. In that case, the quantity of the added TMOS is not enough to cover all the micelles and the interactions between micelles and hydrolyzed precursor are disturbed. Consequently, the inter-micellar condensation leads to a less ordered hybrid mesophase and wormhole-like mesostructures are obtained.

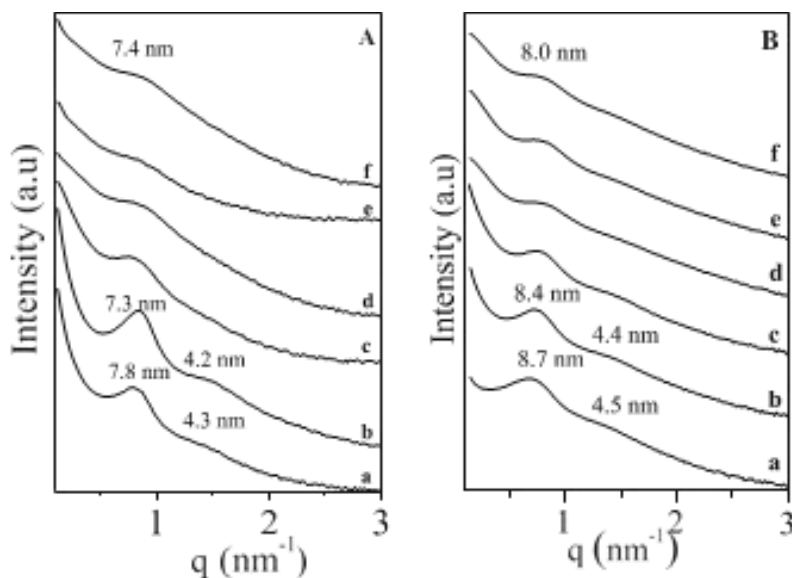


**Figure 3-5.** SAXS patterns of the materials synthesized with a surfactant/TMOS molar ratio ( $R'$ ) equal to a: 0.017; b: 0.024; c: 0.031; d: 0.049; e: 0.051 and f:0.066. The micellar concentration is equal to 2.5 (A) and 10 wt% (B).

Concerning the nitrogen adsorption-isotherm, regardless the synthesis conditions, all the materials present a type IV isotherm (Figure 3-5), characteristic of mesoporous materials. For  $R'$  ratios in the range 0.017–0.031, the mesopore size distribution is quite narrow and the pore diameter remains almost constant for a given Kolliphor concentration (insert of Figure 3-5). An increase of the mesopore size is noted when the KEL concentration is varied from 2.5 to 10 wt%, for example, for  $R' = 0.017$  the pore diameter increases from 4.7 to 5.7 nm

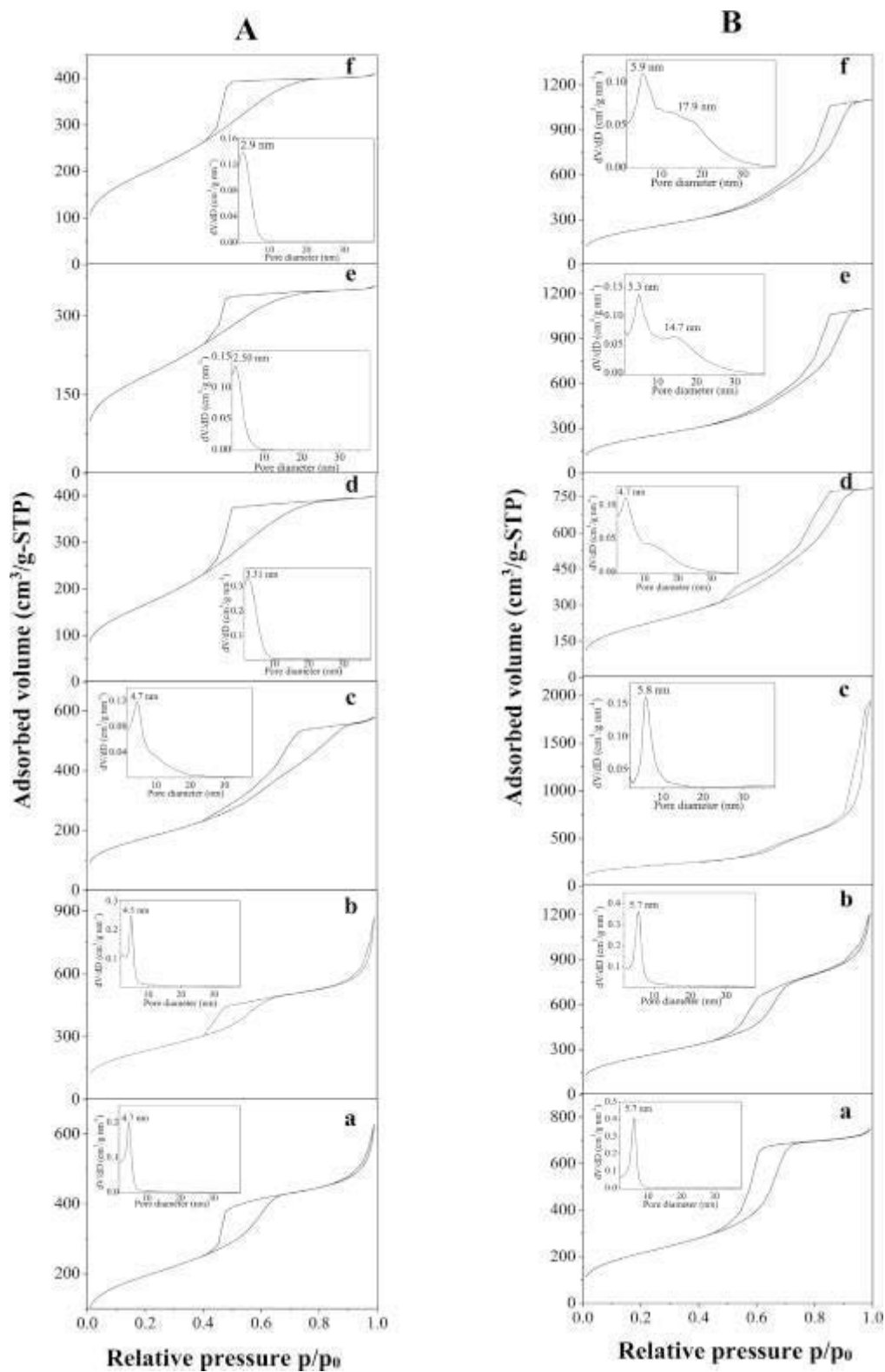


**Figure 3-6.** Nitrogen adsorption-desorption isotherms with the corresponding pore size distribution (insert) of the materials synthesized with a surfactant/TMOS molar ratio ( $R'$ ) equal to a: 0.017; b: 0.024; c: 0.031; d: 0.049; e: 0.051 and f: 0.066. The micellar concentration is equal to 2.5 (A) and 10 wt% (B).

At high relative pressure it is possible to confirm the increasing of the adsorbed volume instead of reaching a plateau as usually observed for type IV isotherms. This behavior has already been reported in literature (Stébé, 2013) and can be related to the pH conditions which favor the appearance of an inter-particle porosity, which is responsible of the ascent of the adsorbed volume at high  $p/p_0$  values. For  $R'$  beyond 0.031, the disorganization of the mesopores network is accompanied by a decrease of the pore diameter (insert of Figure 3-6A) or by the appearance of a broad second component in the mesopore size distribution (insert of Figure 3-6B), consequence of the hybrid mesophase reorganization due to the insufficiency of the amount of the inorganic precursor.

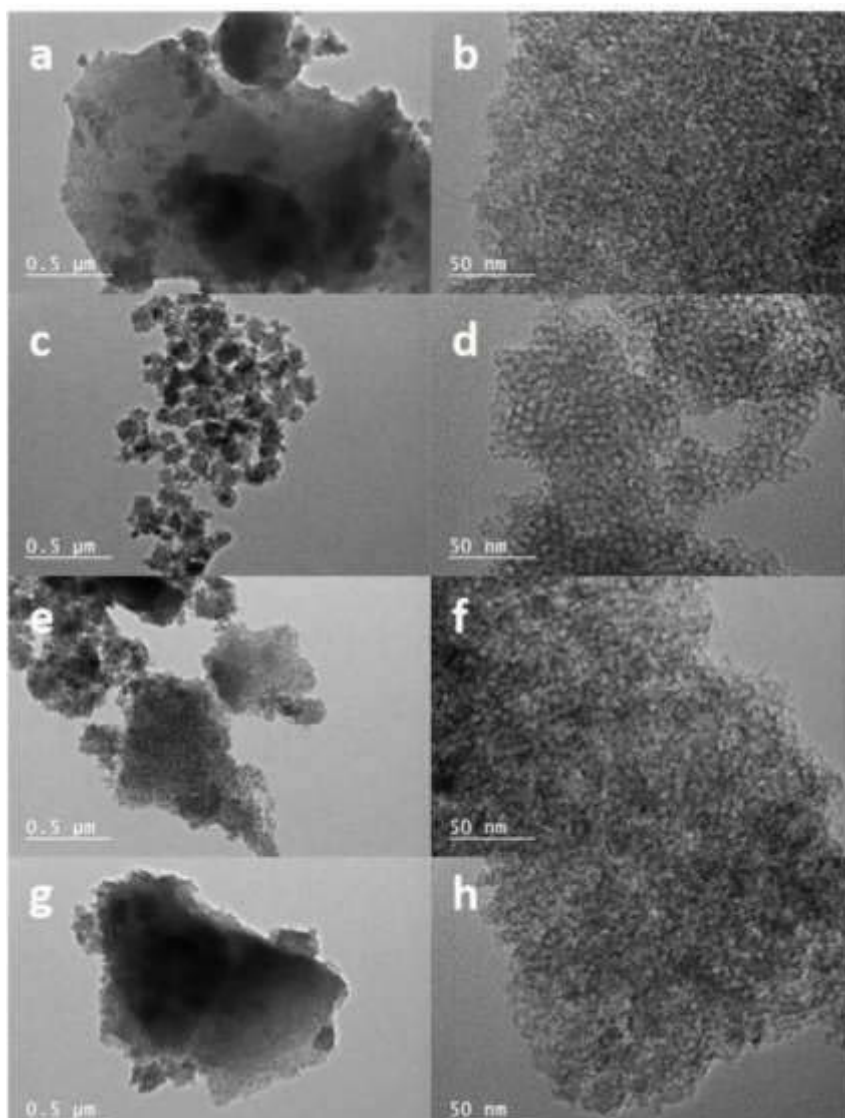


**Figure 3-7.** TEM images of the materials synthesized with a surfactant/TMOS molar ratio ( $R'$ ) equal to a,b: 0.017; c,d: 0.024; e,f: 0.031; g,h: 0.049. The micellar concentration is equal to 2.5 wt%.

According to TEM observations at high magnification (Figure 3-7) materials with KEL concentration of 2.5% are mesoporous. Mesopores appear larger and more regular in size for  $R' = 0.024$ , that is consistent with SAXS and nitrogen adsorption/desorption data. It can be clearly observed that pore size increases from  $R' = 0.017$  to 0.024 and then decreases from  $R' = 0.024$  to 0.044. It is interesting to note that particles at  $R' = 0,024$  are smaller and regular in size compared to the others.

From the above results, obtained for 2.5 wt% and 10wt% of surfactant concentration, it appears that to recover a mesostructured silica with a well-defined pore size distribution the  $R'$  value should be in the range between 0.017 and 0.031. Thus, for the next studies, the KEL/ TMOS ratio has been fixed to 0.024. Since it also appears that the pore size varies as a function of the Kolliphor concentration, the surfactant amount has been varied from 2.5 to 40 wt% to explore the overall micellar domain. The SAXS patterns depicted on Figure 3-8A show that mesostructured silica materials are recovered until 20 wt% of Kolliphor in water (Figure 3-8A, a-d).

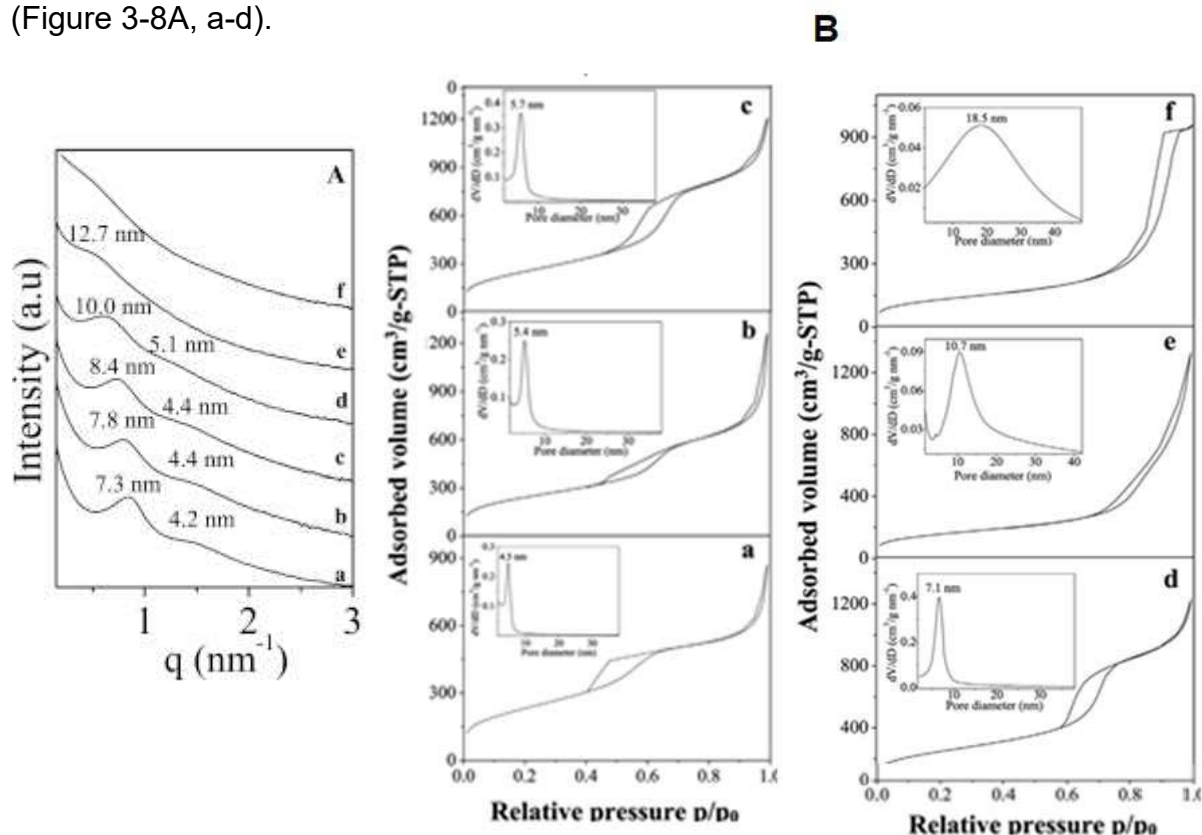


**Figure 3-8.** SAXS patterns (A) and Nitrogen adsorption-desorption isotherms (B) with the corresponding pore size distribution (insert) of the samples synthesized with a KEL concentration (wt.%) of a: 2.5, b: 5, c: 10, d: 20, e: 30 and f: 40. The KEL/TMOS molar ratio ( $R'$ ) is fixed to 0.024.

Increasing the concentration of the micellar solution from 2.5 to 20 wt%, the first peak  $d_{100}$  is shifted from 7.3 to 10 nm, the cell parameter  $a_0$  thus varies from 8.4 to 11.5 nm. Since the cell parameter is the sum of mesopore diameter and the silica wall thickness ( $e$ ) this suggests that either the mesoporous diameter or both decrease as a function of the KEL concentration. In this range of KEL concentration, the mesostructured silica presents a type IV isotherm (Figure 3-8B, a-d) characteristic of mesoporous materials, according to the IUPAC classification. The relative pressure at which the capillary condensation occurs is progressively shifted to higher  $p/p_0$  values when the surfactant concentration used to prepare the materials is increased. Since this value is related to the mesopore diameter according to the Kelvin equation this means that bigger mesopores are formed.

This is confirmed by the pore size distribution, whose maximum is shifted from 4.5 to 7.1 nm as a function of the KEL concentration. By contrast it can be seen from Table 3-2 that the mesopore wall thickness ( $e$ ) remains almost constant to 4.0 nm. It is also interesting to note that the mesopore diameter is in good accordance with the hydrophobic core size of the micelles determined by SAXS. This observation confirms the templating effect of the KEL micelles. The specific surface area and the pore volume slowly increase from respectively 702 to around 900  $m^2/g$  and from 0.7 to 1.5  $cm^3 g^{-1}$ , when the KEL concentration varies from 2.5 to 20 wt%

**Table 3-2.** Mesoporous materials characterization parameters

KEL (wt%)	$a_0$ (nm)	$S_{BET}$ ( $m^2/g$ )	$V_p$ ( $cm^3/g - STP$ )	Mesoporous diameter (nm)	$e$ (nm)
2.5	8.4	702	0.7	4.5	3.9
5	9.0	872	0.6	5.4	6.6
10	9.7	928	1.4	5.7	4.0
20	11.5	885	1.5	7.1	4.4
30	-	560	1.4	10.7	-
40	-	466	1.4	18.5	-

The SAXS spectrum of the material synthesized with 30 wt% of Kolliphor is characteristic of a wormhole-like structure since it exhibits only a broad peak at 12.7 nm (Figure 3-8A,e). If the KEL concentration is raised to 40 wt% no peak is detected any longer (Figure 3-8A,f), meaning that the channel arrangement is completely random. The shape of the isotherm of the samples prepared with a KEL concentration higher than 20 wt% is modified and it becomes intermediate between type IV and type II (Figure 3-8 B,ef). Meanwhile the pore size is broader, its maximum is shifted towards higher mesopore diameter and the  $dV/dD$  values decrease.

Meantime the specific surface area drops to around 460 m<sup>2</sup>/g, reflecting disorganization of the channel array even if all the conditions are gathered to get an ordered mesostructured silica material. TEM observations confirm the presence of regular mesopores for all samples with  $R' = 0.024$  when KEL concentration increased from 2.5 to 30 wt% (Figure 3-9).

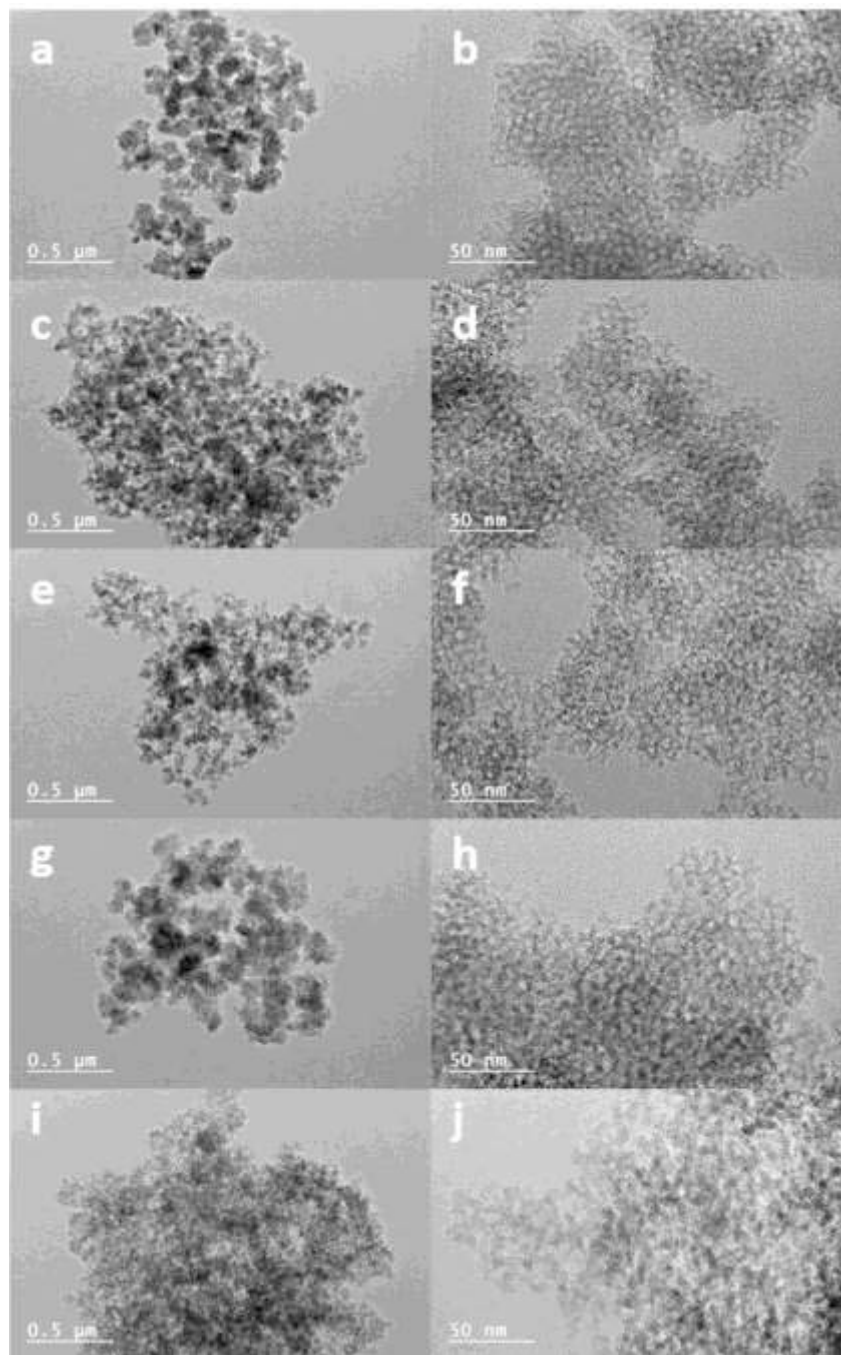


**Figure 3-9.** TEM images of the samples synthesized with a KEL concentration (wt.%) of a,b: 2.5, c,d: 5, e,f: 10, g,h: 20 and i,j: 30. The KEL/TMOS molar ratio is fixed to 0.024

On the TEM images at high magnification (Figure 3-9 b,d,f,h,j) the gradual loss of pore ordering is clearly observed when KEL concentration increased from 10 to 30 wt%. The origin of the loss of the mesopore ordering with the increase of the surfactant concentration can be due to a change of the micelles shape for example from spherical to rods, which disturbs the Cooperative Templating Mechanism. Indeed, when micelles are closed together, due to the limitations on the conformation of oxyethylene groups arising from steric hindrance, repulsive forces occur. This leads to a micelle shape transition like sphere-to-rod (Mitchel, 1983). We can also assume that with the increase of the concentration of the micellar solution more and more micelles are formed and the interactions between micelles predominate in the detriment of the ones with the hydrolyzed precursor.

Finally, is not possible to exclude a shift of the domain of the phase diagram because of the release of the methanol produced during the hydrolysis of the TMOS. Indeed, it is well known that the presence of additives such as salt or alcohol strongly modify the surfactant behavior in water (Schott 1997, Shinoda, 1978) and therefore affect the formation of the mesostructured silica materials (Blin, 2012, Zimny, 2009).

## 3.2 Addition effect of the biocompatible oils into the Kolliphor EL/Water system

### 3.2.1 Solubilization effect of Isopropyl Myristate

#### A. Ternary phase diagram Kolliphor (KEL) / Isopropyl myristate (IM) / Water (W)

The phase diagram of Kolliphor / water / isopropyl myristate (IM) is shown on figure 3-13. The solubilization of IM in micellar solutions which exists until 45 wt.% is limited to 1wt.%. However, the cubic phase whose space group remains Pm3n can incorporate some amounts of IM, up to around 8 wt. %, and in the hexagonal phase, it is possible to solubilize until 15 wt. %.

If the concentration of Kolliphor in water is increased (from 75wt% to 90wt%), a lamellar phase appears (figure 3-13), but only after the addition of few quantities of oil (4 wt. %). This phase is very stable, since it can incorporate until 70 wt.% of IM. On the other hand, two types of emulsions have been highlighted. In the water-rich domain, emulsions which can contain until 16% of oil, stable from few hours to few days, were identified. In the oil-rich domain, highly concentrated emulsions (CE) (between 70 and 95 wt. % of oil) were prepared (Figure 3-13) for  $1.9 < R < 9$ .

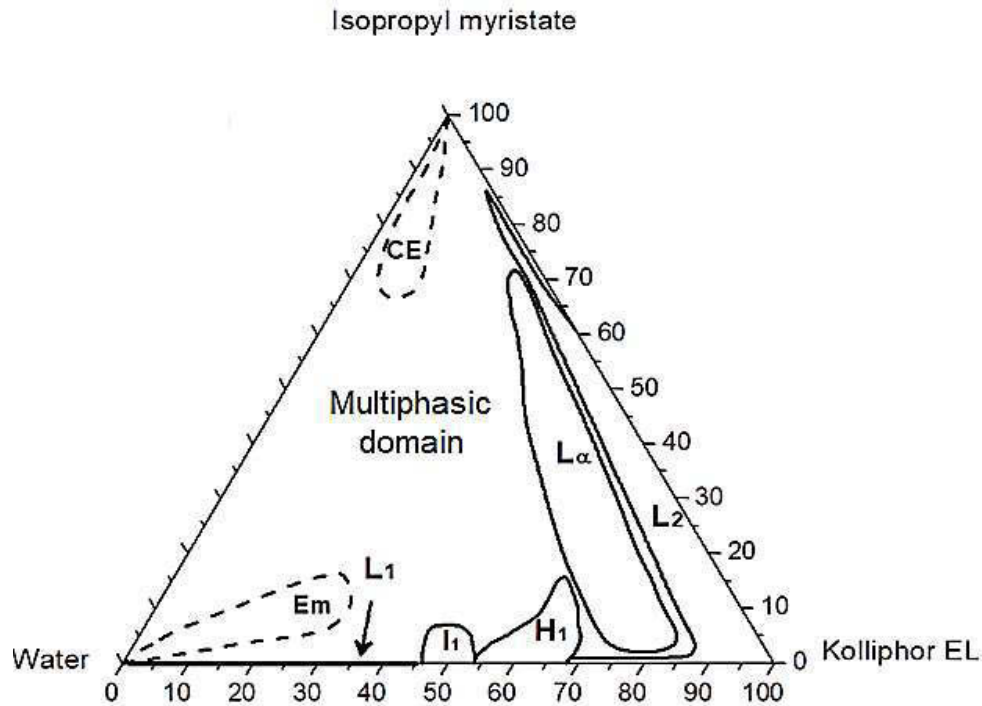


**Figure 3-10.** Ternary phase diagram for the system Kolliphor/water/isopropyl myristate at 25 °C.  $L_1$  and  $L_2$  correspond to direct and reverse micellar phase, respectively.  $I_1$ ,  $H_1$  and  $L_\alpha$  denote direct micellar cubic phase, direct hexagonal phase and lamellar phase, respectively.  $Em$  and  $CE$  correspond to fine emulsion and direct concentrated emulsion, respectively.

### B. Structural parameters of the liquid crystal phases

SAXS measurements were performed to determine the evolution of the structural parameters of the liquid crystals in function of the addition of Isopropyl Myristate in the Kolliphor EL/water system. The SAXS spectra are presented on Figure 3-14a for the lamellar phase of KEL/water  $R' = 0.25$  and on Figure 3-14b for the hexagonal phase of KEL/water  $R' = 0.43$ . The structural parameters were determined in accordance with the equations reported in the literature. For the hexagonal phase, the hydrophobic radius  $R_H$  is related to the distance  $d$  associated to the first peak by the following relation :

$$\frac{V_B + \beta V_O}{V_S + \alpha V_W + \beta V_O} = \frac{\sqrt{3}\pi R_H^2}{2d^2} \quad \text{Eq. 3 - 6}$$

where  $\alpha$  stands for the number of molecules of water per molecule of surfactant,  $\beta$  stands for the number of molecules of oil per molecule of surfactant, and  $V_B$ ,  $V_S$ ,  $V_W$ ,  $V_O$  respectively stand for the molar volumes of the hydrophobic part of the surfactant, the surfactant, water and Isopropyl Myristate. The cross sectional area  $S$  can be deduced as:

$$S = \frac{2(V_B + \beta V_O)}{N_A R_H} \text{ Eq. 3 - 7}$$

For the lamellar phase, the cross sectional area  $S$  can be obtained from the the following equation :

$$S = \frac{2(V_S + \alpha V_W + \beta V_O)}{N_A d} \text{ Eq. 3 - 8}$$

The hydrophobic thickness  $d_B$  and the hydrophilic thickness  $d_A$  can be deduced from the following equations :

$$d_B = \frac{2(V_B + \beta V_O)}{N_A S} \text{ (A)} \quad \text{and} \quad d = d_A + d_B \text{ (B) Eq. 3 - 9}$$

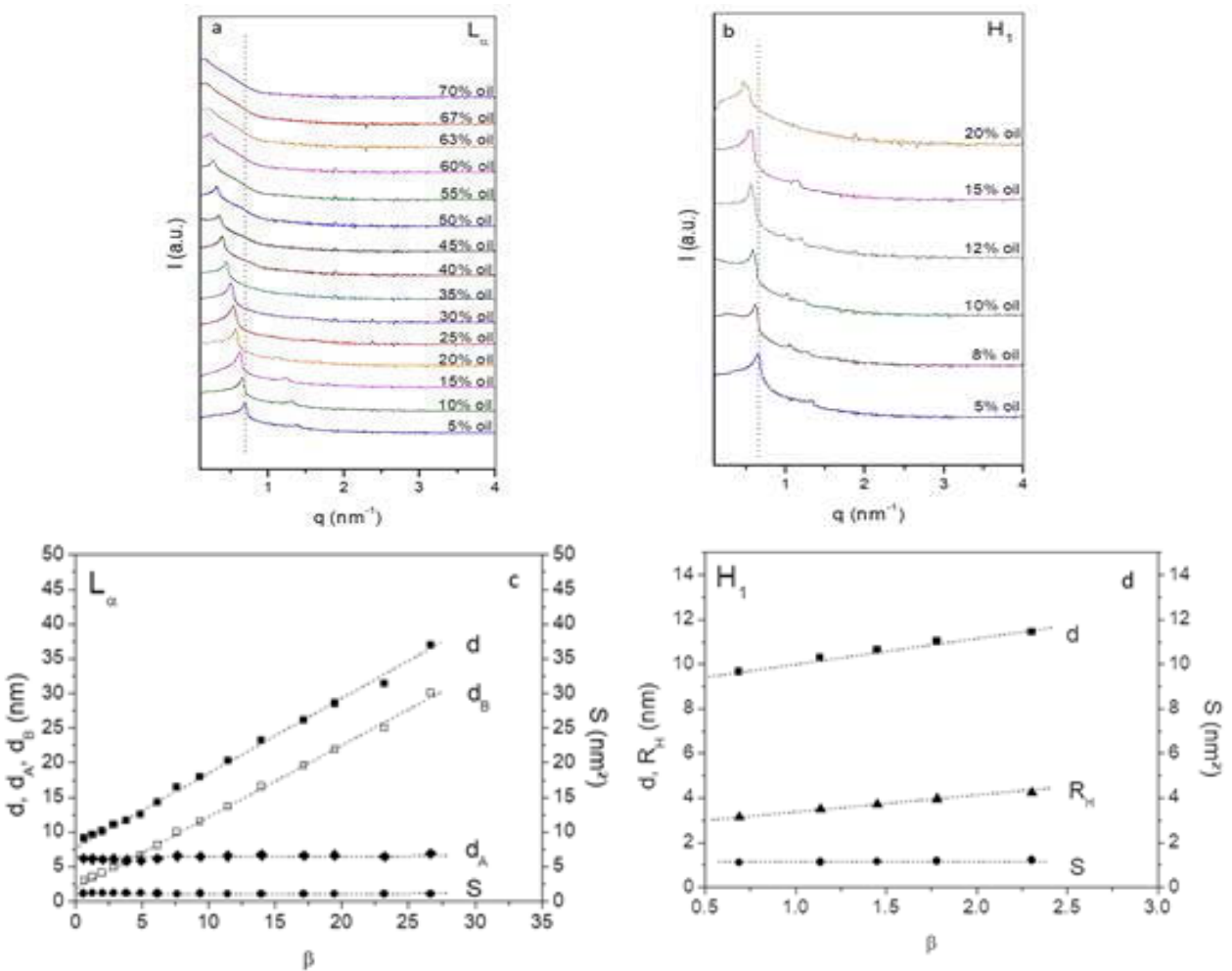


**Figure 3-11:** SAXS spectra of the samples in function of the addition of Isopropyl Myristate for the lamellar phase  $L_\alpha$  ( $R = 0.25$ ) (a) and for the hexagonal phase  $H_1$  ( $R = 0.43$ ) (b) at 25°C. Evolution of the structural parameters in function of  $\beta$  for  $L_\alpha$  (c) and for  $H_1$  (d) at 25 °C.  $\beta$  is the number of molecules of oil per molecule of surfactant.

For KEL/water  $R' = 0.25$ , the SAXS patterns give reflection lines obeying to the 1 :2 :3 relationship and which become less pronounced and broader when increasing the content of oil (until 70 wt.%), characteristic of a swollen lamellar phase. For  $R' = 0.43$ , the relative positions of the reflection lines are 1:  $\sqrt{3}$  : 2. Beyond 15 wt. % of oil, two intensive peaks are detected, indicating the coexistence of two phases in the system. Additionally, the swelling of the structures with the incorporation of oil is shown by a shift of the reflection lines to smaller  $q$  values.

The evolution of the structural parameters with the addition of oil are represented on the Figure3-14c shows the results for  $R' = 0.25$  of the lamellar phase and Figure 3-14d,  $R' = 0.43$  of the hexagonal phase. For the lamellar phase, the spacing parameter  $d$  and the hydrophobic thickness  $d_B$  increase proportionally with  $\beta$ , from 9 to 37 nm for  $d$  and from 3 to 30 nm for  $d_B$ , while the hydrophilic thickness  $d_A$  and the area of the polar head  $S$  are constant and equal to 6.4 nm and 1.1 nm<sup>2</sup>, respectively.

By extrapolating the value for  $\beta = 0$ , the hydrophobic thickness of the lamellar phase is equal to 2.0 nm. Given that the mean dimension of an alkyl chain of Kolliphor can be estimated at 2.5 nm, it suggests that these chains are completely folded in the lamellar phase. Thus, it is possible that the oil penetrates lightly in the hydrophobic chains of Kolliphor, which would then be more extended, but the essential part of the oil seems to form an interstitial film, which becomes thicker with the incorporation of oil.

For the hexagonal phase ( $R = 0.43$ ), the spacing parameter  $d$  and the hydrophobic radius  $R_H$  increase with the incorporation of oil, from 9.5 to 11.5 nm for  $d$  and from 3.1 to 4 nm for  $R_H$ , whereas the area of the polar head  $S$  is constant and equal to 1.2 nm<sup>2</sup>. By extrapolating the value for  $\beta = 0$ , the hydrophobic radius is 2.7 nm. This dimension corresponds to completely extended chains. This suggests that the oil is mainly located in the hydrophobic core of the cylinders.

### C. Characterization structure of swollen micelles

The influence of the addition of small quantities of isopropyl myristate on the structure of the micelles was evaluated by comparing the SAXS spectra of solutions of Kolliphor in water ( $R = 19$ ), without oil and with 1 wt.% of IM. The results are shown below on Figure 3-15a in absolute units. The appearance of the spectra is different. While the micellar solution presents a weak interaction peak at  $q = 0.78 \text{ nm}^{-1}$ , the spectrum of the micelles swollen with IM presents a broad peak at  $q = 0.53 \text{ nm}^{-1}$ .

The data were then analyzed by using the Generalized Indirect Fourier Transform (GIFT) method (Figure 3-15b, the intensities are in arbitrary units) and we can see that the theoretical spectra are in good accordance with the experimental spectra. The obtained pair-distance distribution functions (PDDFs) are depicted on Figure 3-15c. For both samples, the curves exhibit a pronounced dip which goes to negative values, indicating that the micelles are inhomogeneous and so called “core-shell” type particles. The PDDFs present a bell-like shape, characteristic of spherical particles, with a maximum dimension of about 12.5 - 13 nm for the micelles and 17.5-18 nm for the swollen micelles. These results are in the same range than the hydrodynamic diameter found by Dynamic Light Scattering (DLS) measurements. Additionally, looking at the excess-electron profile presented on Figure 3-15d, the hydrophobic radius  $R_H$  can be determined when  $\Delta\rho(r) = 0$ . It is equal to 3.3 nm for the micelles and 5.2 nm for the micelles swollen with the oil.

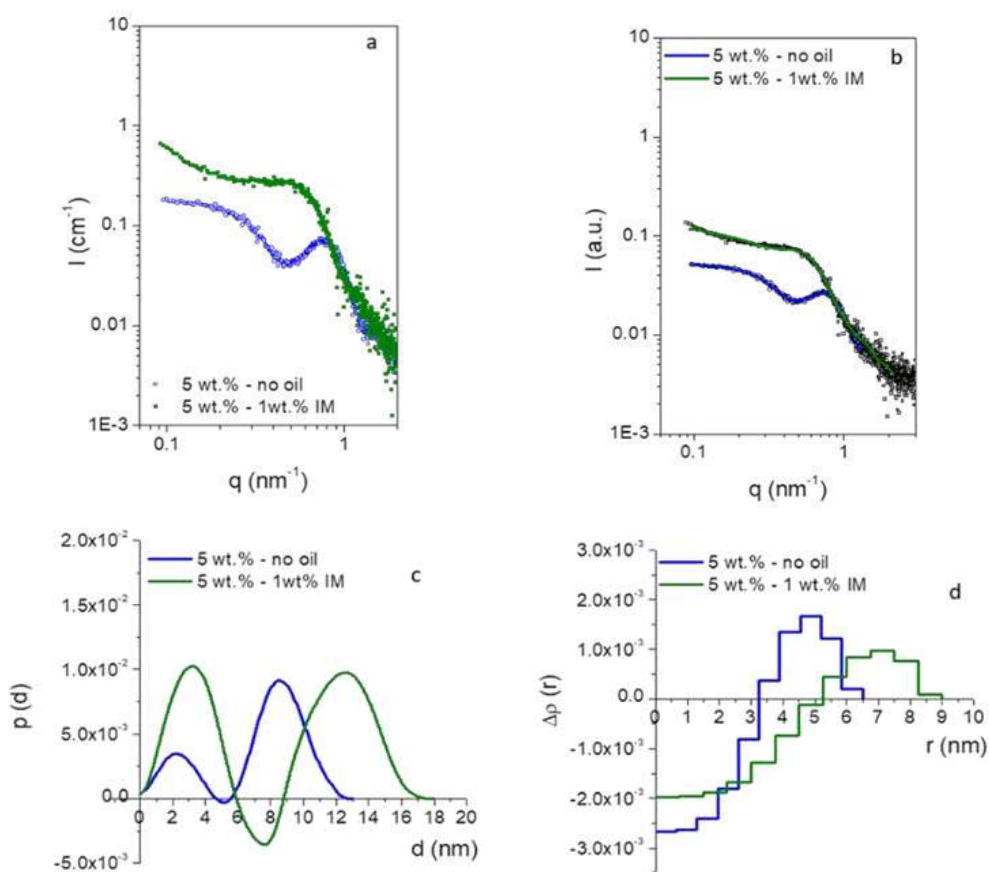


**Figure 3-12.** (a) SAXS spectra of the micelles ( $R = 19$ ) (blue  $\circ$ ) and with 1 wt. % of IM (green  $\bullet$ ) at 25 °C in log-log representation and in absolute units; (b) Corresponding experimental (scatter) and approximated (GIFT) (solid line) SAXS spectra in arbitrary units of the micelles (blue) and with 1 wt. % of IM (green); (c) Pair-distance distribution functions (PDDFs); (d) Corresponding excess-electron density profiles.

The micelle diameter increases of 2.5 nm when adding oil. This indicates that with the addition of few quantities of IM, the micelles become bigger. Moreover, the dimension of the alkyl chains in the swollen micelles, corresponding to the lowest value of  $\Delta\rho(r)$ , can be estimated at about 2.3 nm, slightly increasing from the value found for the sample without oil (1.9-2.0 nm). Given that the dimension of the alkyl chains in Kolliphor is 2.5 nm, the hydrophobic chains are completely extended in the micelles.

#### D. SAXS characterization of concentrated emulsions of the system IM/KEL/W

Highly direct concentrated emulsions were prepared with a ratio  $R = 5.7$  and for oil concentrations between 70 and 95 wt. %. These systems are stable for several weeks. Their observation by optical microscopy shows that the Isopropyl Myristate droplets are polydisperse. SAXS experiments were carried out on these samples and the results are given below (Figure 3-16).

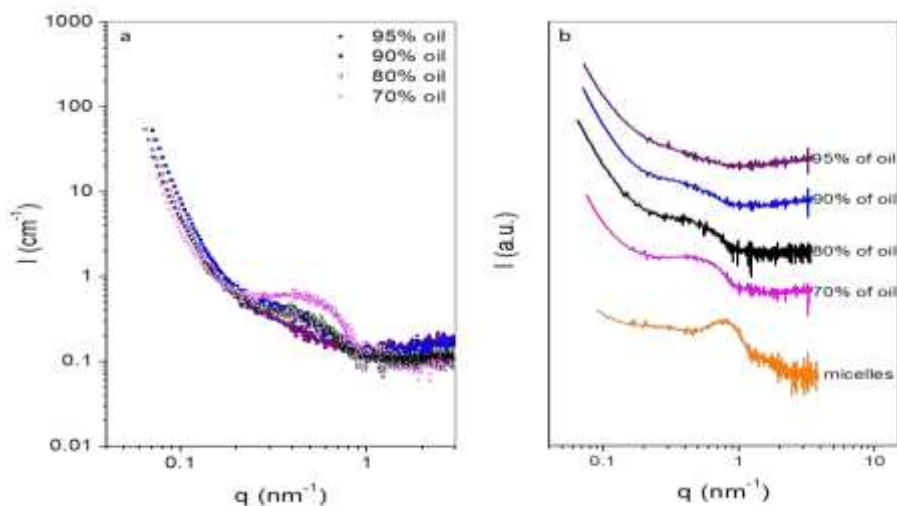


**Figure 3-13.** (a) SAXS spectra of the concentrated emulsions at  $R = 5.7$  in function of the weight percent of IM, in absolute units and in log-log representation. (b) SAXS spectra of the concentrated emulsions at  $R = 5.7$  for the various quantities of IM and of the swollen micelles. For clarity reasons, the spectra are shifted towards y-axis.

For all the studied oil concentrations, SAXS spectra present the same behavior. The intensity is proportional to  $q^{-4}$  at low  $q$  values and features the existence of big droplets. At higher  $q$ -values, a broad peak ( $q \approx 0.5 \text{ nm}^{-1}$ ), which is attenuated with the increase of oil content, is present. The position of this peak corresponds to the presence of micelles in the system (Figure 3-16b).

Looking at the ternary phase diagram, we can deduce that the prepared concentrated emulsions are two phases systems, which are constituted of big

Isopropyl Myristate droplets stabilized by some molecules of Kolliphor and of a continuous medium composed of swollen micelles of Kolliphor in water. The scattered intensity is thus the sum of the scattering of the big oil droplets and of the swollen micelles in water.

The size of the IM droplets was determined by SAXS and the results are given in Table 3-6 for 90 and 95 wt.% of isopropyl myristate. It must be precised that, given that the number of points is limited on the portion of the curve, where the scattered intensity is proportional to  $q^{-4}$ , some errors on the calculation of the radius of the big droplets can therefore be done. Therefore, these results must be considered only as an estimation.

**Table 3-3:** Specific area ( $S_v$ ) and radii of oil droplets ( $r$ ) estimated from SAXS measurements for the direct concentrated emulsions at  $R = 5.7$  at  $25^\circ\text{C}$

wt. % oil	$S_v$ ( $10^3 \text{ cm}^{-1}$ )	$r$ ( $\mu\text{m}$ )
90	6.3	4.4
95	4.3	6.7

#### E. Mesoporous materials characterization prepared from Kolliphor EL/Water/Isopropyl Myristate

The materials from Kolliphor EL/Water/Isopropyl Myristate were prepared by solubilizing small amounts of oil in the micellar solution, the swollen micelles were obtained with the addition of 1% of IM, when the amount of IM increased a stable small size emulsions were obtained, the materials synthesis was carried out following the process described in the Chapter 2.

The synthesized materials were characterized by SAXS (Figure 3-17a) and adsorption-desorption nitrogen. The results show that the silicated materials prepared with small amounts of IM (until 3%) have a mesopores network was clearly obtained and the formation mechanism is characteristic of CTM since the swollen micelles are present.

Under the same conditions the Figure 3-17b shows an isotherm type IV characteristic of mesoporous. The pore size distribution Figure 3-17c indicates the presence of pores having a centered size around 10nm. Moreover, this material shows a surface area of  $650 \text{ m}^2/\text{g}$  and a pore volume of  $1.2 \text{ cm}^3/\text{g}$ .

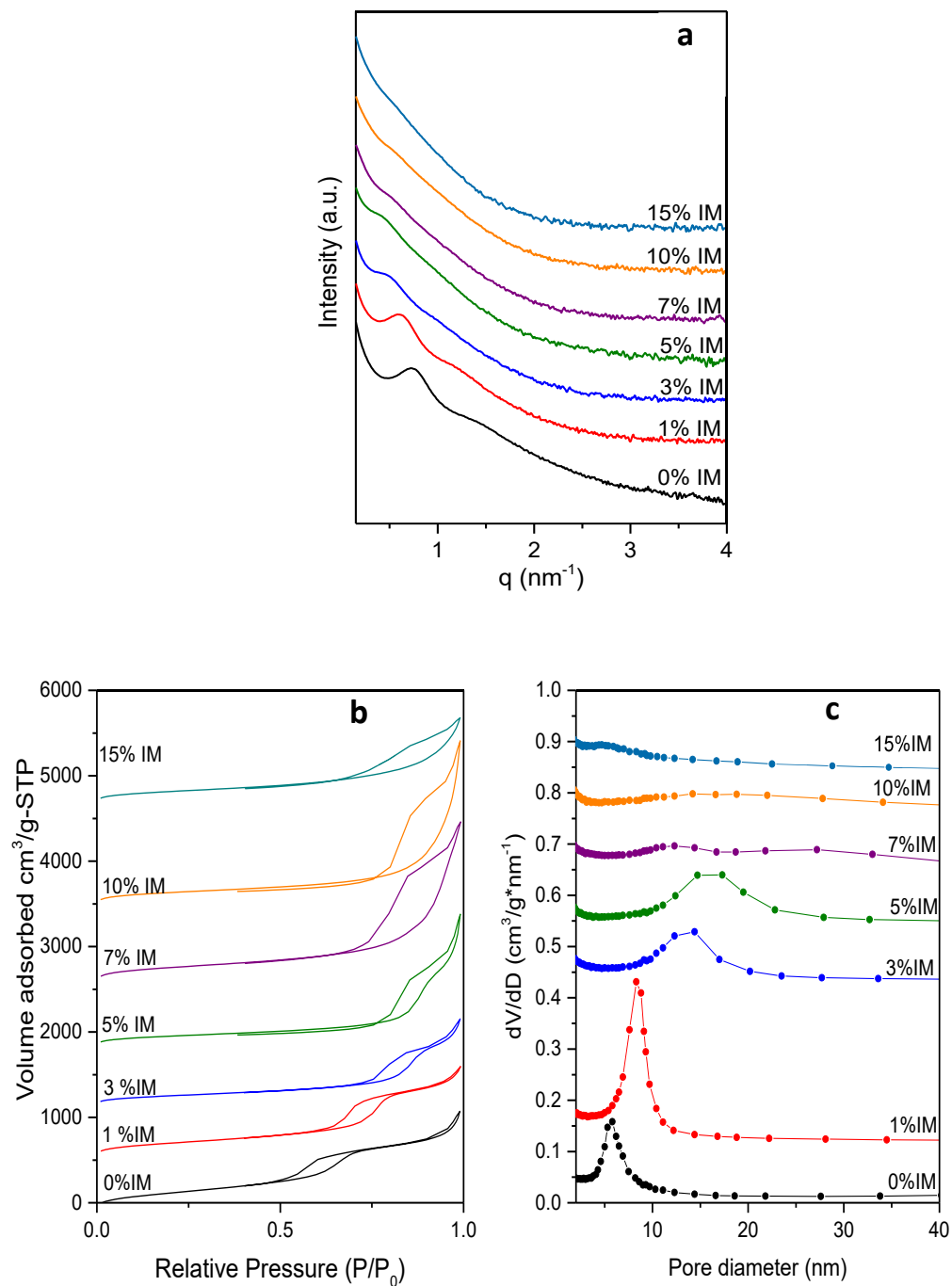


**Figure 3-14.** (a) SAXS spectra of the silica material in function of % Isopropyl Myristate concentration. (b) Nitrogen adsorption-desorption analysis (c) Evolution of the pore volume.

### 3.2.2 Solubilization effect of Miglyol

#### A. Ternary phase diagram Kolliphor (KEL) / Miglyol (Myg) / Water (W)

The phase diagram of Kolliphor/water/Miglyol at 25°C is reported on Figure 3-18. A micellar solution is observed for surfactant concentrations until 45 wt. %. Only a few quantity (1wt. %) of Miglyol can be solubilized in the micelles of Kolliphor. On the other side, the liquid crystal phases can incorporate significant quantities of Miglyol, up to 5 wt. % in the cubic phase for which the space group remains  $Pm3n$ , and up to 20 wt. % for the hexagonal phase.

For smaller ratios R (between 0.18 and 0.33), a lamellar phase appears, but only after the addition of 5 wt. % of oil. This lamellar phase is highly stable, because it can incorporate until 55 wt. % of Miglyol. Two types of direct emulsions can be prepared. On the one hand, by the PIC method, emulsions stable for few days were formed in the water-rich domain and can incorporated until 15 wt. % of Miglyol. On the other hand, in the oil-rich domain, high concentrated emulsions (between 70 and 95 wt. % of Miglyol) were highlighted.

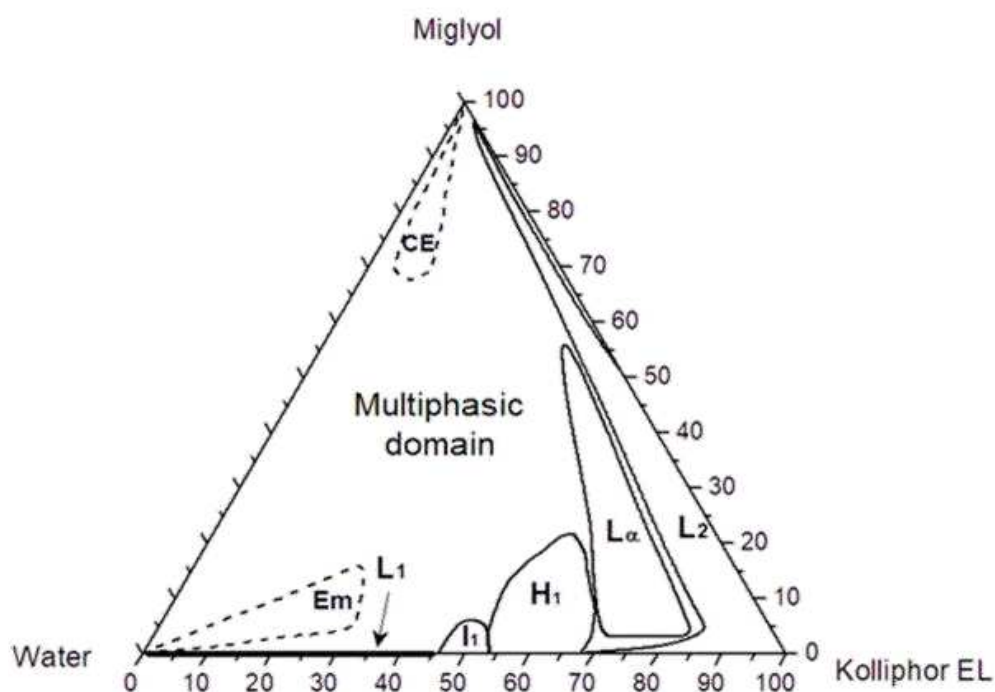


**Figure 3-15.** Ternary phase diagram for the system Kolliphor EL/water/Miglyol at 25 °C.  $L_1$  and  $L_2$  denote direct and reverse micellar phase respectively.  $I_1$ ,  $H_1$  and  $L_\alpha$  correspond to direct micellar cubic phase, direct hexagonal phase and lamellar phase, respectively. Em and CE correspond to emulsion and concentrated emulsion, respectively.

## B. Structural parameters of the lamellar and hexagonal phase

SAXS experiments were carried out to investigate the effect of the addition of Miglyol on the structural parameters of the lamellar and the hexagonal phase. The SAXS patterns of the samples in function of the incorporation of Miglyol are represented on Figure 3-19a for the ratio  $R$  equal to 0.25 for the lamellar phase and on Figure 3-19b for  $R = 0.43$  for the hexagonal phase. For  $R = 0.25$ , the reflection lines follow the relationship 1:2 and the oily streaked texture observed by polarized light microscopy confirms the presence of a lamellar phase. For  $R = 0.43$ , the observed reflection lines are  $1:\sqrt{3}:2$  and the characteristic texture observed by polarized-light microscopy confirms the presence of a hexagonal phase. Looking at the SAXS patterns, the reflection lines are shifted to smaller  $q$  values with the incorporation of oil, suggesting the swelling of the structure. For the ratio  $R = 0.25$ , the peaks become less pronounced and broader with the increasing content of oil. The structural parameters were determined in the same manner as were determined for Isopropyl Myristate in accordance with the equations reported before.

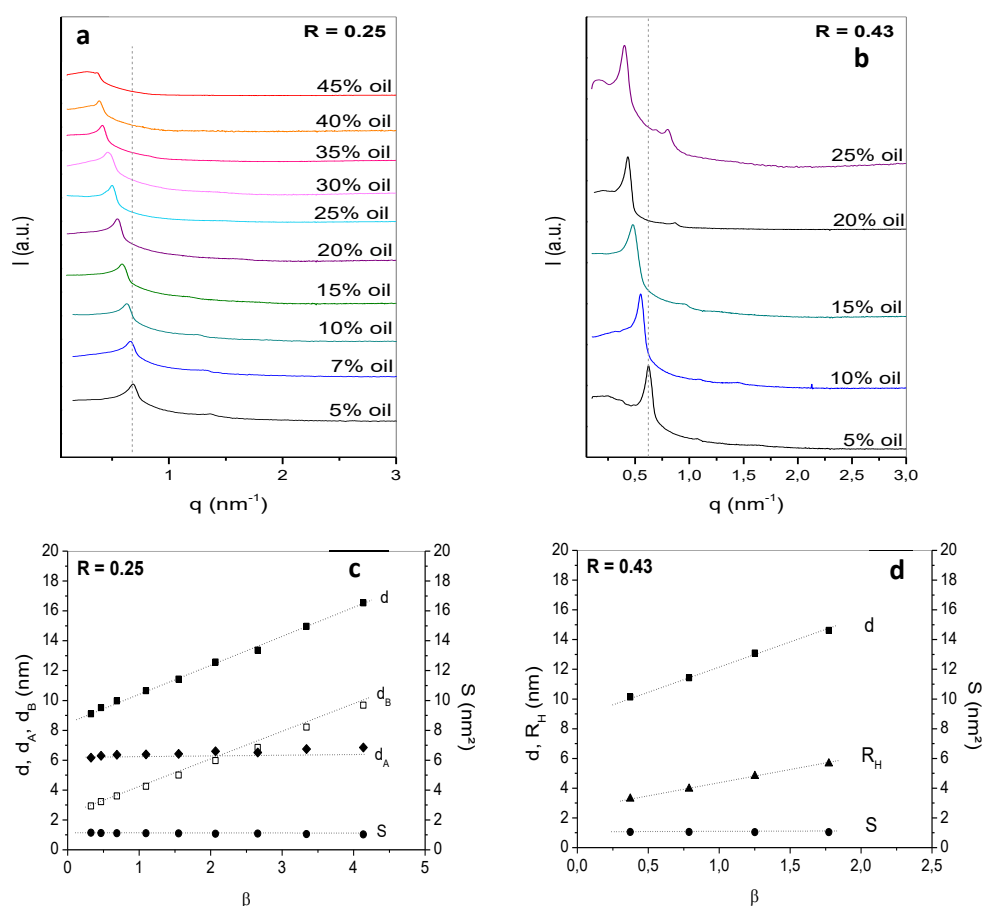


**Figure 3-16.** SAXS spectra of the samples with the addition of oil at 25 °C for  $R = 0.25$  (a) and for  $R = 0.43$  (b); Evolution of the structural parameters in function of  $\beta$  at 25 °C for  $R = 0.25$  (c) and for  $R = 0.43$  (d).  $\beta$  is the number of molecules of oil per molecule of surfactant.

The structural parameters in function of the quantity of incorporated oil are represented on Figure 3-19c and 3-19d for the lamellar and hexagonal phases, respectively. Concerning the lamellar phase (Figure 3-19-c), the spacing parameter  $d$  and the hydrophobic thickness  $d_B$  increase with the addition of oil in the system, while the area of the polar head  $S$  and the hydrophilic thickness  $d_A$  are constant and equal to  $1.1 \text{ nm}^2$  and  $6.5 \text{ nm}$ , respectively.

This means that the oil probably does not penetrate between the hydrophobic chains, but rather forms an oily film which becomes thicker with the addition of Miglyol. For the hexagonal phase (Figure 3-19d), the spacing parameter  $d$  and the hydrophobic radius  $R_H$  increase with the addition of oil in the system, whereas the area of the polar head  $S$  remains constant and equal at  $1.1 \text{ nm}^2$ . This indicates that the oil is located essentially in the hydrophobic core of the cylinders.

Interestingly, by extrapolating the value for  $\beta = 0$ , the hydrophobic thickness for the lamellar phase at the ratio  $R = 0.25$  is equal to  $2.5 \text{ nm}$ . Given that the dimension of a hydrophobic chain is estimated at  $2.5 \text{ nm}$ , we can deduce that the alkyl chains in the lamellar phase are completely folded.

### C. Characterization of the structure of the swollen micelles

The effect of the addition of Miglyol on the structure of the micelles was examined by comparing the SAXS spectrum of the micelles containing 5 wt. % of Kolliphor in water ( $R = 19$ ) with the one of the swollen micelles with 1 wt. % of Miglyol. The two spectra exhibit a broad peak, but its position depends of the presence of Miglyol ( $q = 0.78 \text{ nm}^{-1}$  for the micelles and  $q = 0.50 \text{ nm}^{-1}$  for the swollen micelles). (Figure 3-20a).

The data were analyzed by using the Generalized Indirect Fourier Transform (GIFT) method. The obtained pair-distance distribution functions (PDDFs) were represented on Figure 3-20b. For both samples, the PDDFs exhibit a pronounced dip which goes to negative values, suggesting that the micelles are inhomogeneous ("core-shell" type particles).

The curve presents also a bell-like shape, characteristic of spherical micelles, with a maximum dimension of about  $12.5 - 13 \text{ nm}$  for the micelles, while it presents a slightly elongated tail with the maximum dimension at about  $19-20 \text{ nm}$ , for the swollen micelles. This result is in good agreement with the hydrodynamic diameter found by DLS measurements. Moreover, looking at the excess-electron profile on Figure 3-20c, the core-shell type is confirmed for both samples. The hydrophobic radius  $R_H$  increases of  $2 \text{ nm}$  when the micelles are swollen, and the micelle diameter increases of  $2.4 \text{ nm}$  at the same time. This suggests that with the incorporation of small quantities of Miglyol, the micelles become bigger and slightly elongated.

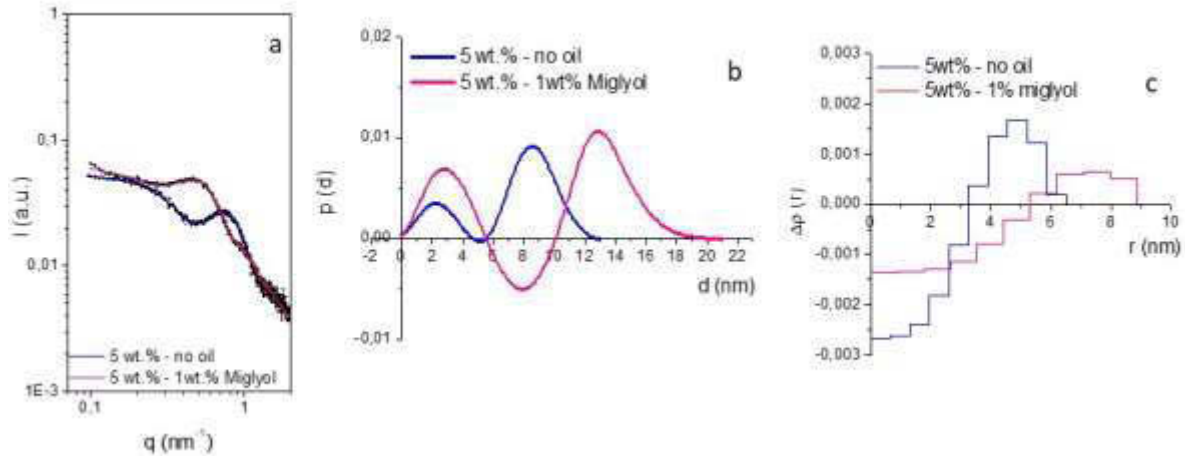


**Figure 3-17.** (a) Experimental (dotted line) and approximated (GIFT) (solid line) SAXS spectra of the samples at  $R = 19$  without Miglyol (blue) and with 1wt. % of Miglyol (pink) at 25 °C ; (b) Corresponding pair-distance distribution functions : (c) Corresponding excess-electron density profiles.

#### D. SAXS characterization of concentrated emulsions of the system Mig/KEL/W

Highly direct concentrated emulsions were prepared for a ratio  $R = 5.7$  and quantities of oil varying from 70 to 95 wt. %. The systems are stable for several weeks. These emulsions were observed by optical microscopy and the oil droplets are polydisperse. SAXS experiments were performed and for all the samples, the SAXS spectra present the same behavior. (Figure 3-21a).

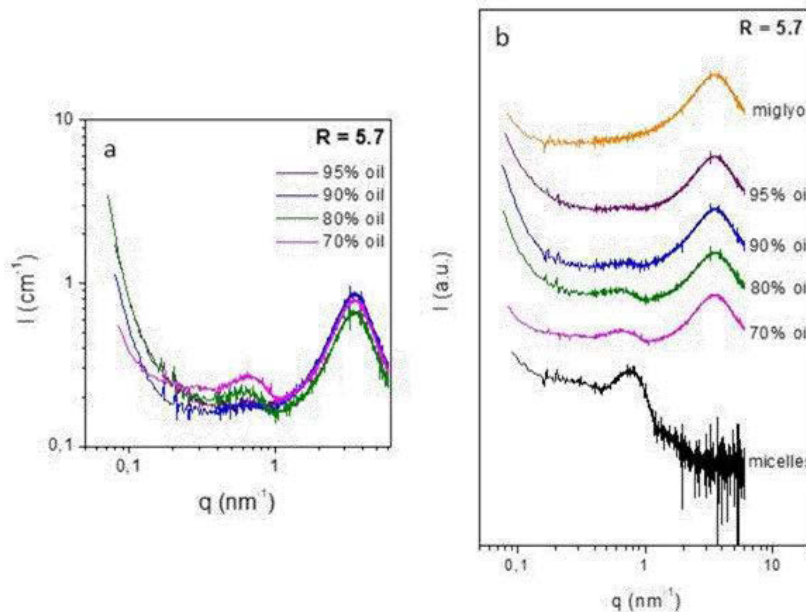


**Figure 3-18.** (a) SAXS spectra of the concentrated emulsions at  $R = 5.7$  in log-log representation in absolute units ; (b) SAXS spectra of the concentrated emulsions and the micelles at  $R = 5.7$  and of pure Miglyol. For clarity reasons, the spectra are shifted towards y-axis.

At low  $q$ -values, the intensity is proportional to  $q^{-4}$  and characterizes the presence of big oil droplets. At higher  $q$ -values, a broad peak ( $q \approx 0.7\text{nm}^{-1}$ ) which becomes less visible for higher concentrations of oil is observed. The position of this broad peak corresponds to the micelles. Finally, at  $3.5\text{ nm}^{-1}$ , a very broad peak is observed.

This peak, which is associated to a repeated distance of 1.8 nm, has the same appearance and the same position than the one on the SAXS spectrum of pure Miglyol. Given that Miglyol is mostly a mixture of triglycerides of capric (C10 :0) and caprylic acids (C8 :0), the dimension of the backbone of the triglycerides can be estimated around 1.7-1.8 nm, which fits to the position of this peak.

Papadimitriou *et al* observed the same phenomenon with veiled virgin olive oils, showing a broad peak on SAXS spectra corresponding to the structural organization of triglycerides in the oils. Thus, the SAXS spectra of the concentrated emulsions correspond to the sum of the scattering of the big droplets of Miglyol and the scattering of the swollen micelles, completed by the diffraction peak of Miglyol due to the molecular structure of the triglycerides.

To summarize, looking at the ternary diagram (Figure 3-18), the structure of the concentrated emulsions are thus big droplets of Miglyol stabilized by molecules of Kolliphor and the continuous phase is constituted of swollen micelles of Kolliphor in water. The scattered intensity  $I(q)$  of such concentrated emulsions has already been studied before and can be expressed by the following equation:

$$I(q) = \frac{2\pi \cdot S_v \cdot I_s(q)}{q^4} + (1 - \Phi_v) I_m(q) \quad \text{Eq. 3 - 10}$$

where the first term represents the diffusion due to large droplets and is approximated by Porod-Auvray's law. The specific area  $S_v$  can be calculated from the portion of the curve with a scattering proportional to  $q^{-4}$ . The second term  $I_m$  can be defined as the contribution of the continuous phase. Then, the corresponding radius of oil droplets  $r$  can be estimated as:

$$r = \frac{3 \Phi_v}{S_v} \quad \text{Eq. 3 - 11}$$

where  $\phi_v$  is the volume fraction of Miglyol.

With  $S_v$  the specific surface and  $I_s$  is a function of the scattering length density  $Q$  profile at the water /oil interface and can be noted as:

$$I_s(q) = (Q_{ext} - Q_{int})^2 \quad \text{Eq. 3 - 12}$$

Where  $Q_{\text{ext}}$  and  $Q_{\text{int}}$  represent the scattering length densities of the external and internal phase of the emulsion respectively.

The results are given in Table 3-7 for the two higher concentrations of Miglyol. Given that the number of points in the portion of the curve with a scattering proportional to  $q^{-4}$  is limited, the error on the calculation of the radius of the droplets can be important. Consequently, the calculated values given in Table 3-7 must be taken as an estimation.

**Table 3-4.** Calculated specific surface ( $S_v$ ) and corresponding calculated radius of droplets ( $r$ ) for the concentrated emulsions at  $R = 5.7$  at  $25^\circ\text{C}$

Wt % oil	$S_v$ ( $\text{cm}^{-1}$ )	$r$ ( $\mu\text{m}$ )
90	2605	10
95	3985	7

#### E. Mesoporous materials characterization prepared from Kolliphor EL/Water/ Miglyol

The materials from Kolliphor EL/Water/ Miglyol were prepared in the same manner than those prepared with Isopropyl Myristate. The swollen micelles were obtained with the addition of 1% of IM, when the amount of Miglyol increased a stable small size emulsion were obtained, the materials synthesis was carried out following the process described in the Chapter 2.

The synthesized materials were characterized by SAXS (Figure 3-28a) and adsorption-desorption nitrogen (Figure 3-28 b, c). The results show that the silicated materials prepared with small amounts of Myg (until 5%) have a mesopores network was obtained and the formation mechanism is characteristic of CTM since the swollen micelles are present.

The Figure 3-28b shows an isotherm type IV characteristic of mesoporous in concentrations of oil lower than 3 wt%, then the ordering of the material is decreasing while the amount of oil is increased, this can be supported with the SAXS results where the organization of the materials from 5 wt% of Miglyol can be considered the worm-like. The pore size distribution Figure 3-28c indicates the presence of pores having a centered size around 10nm. Moreover, this material shows a surface area of  $750 \text{ m}^2/\text{g}$  and a pore volume of  $1.3 \text{ cm}^3/\text{g}$ .

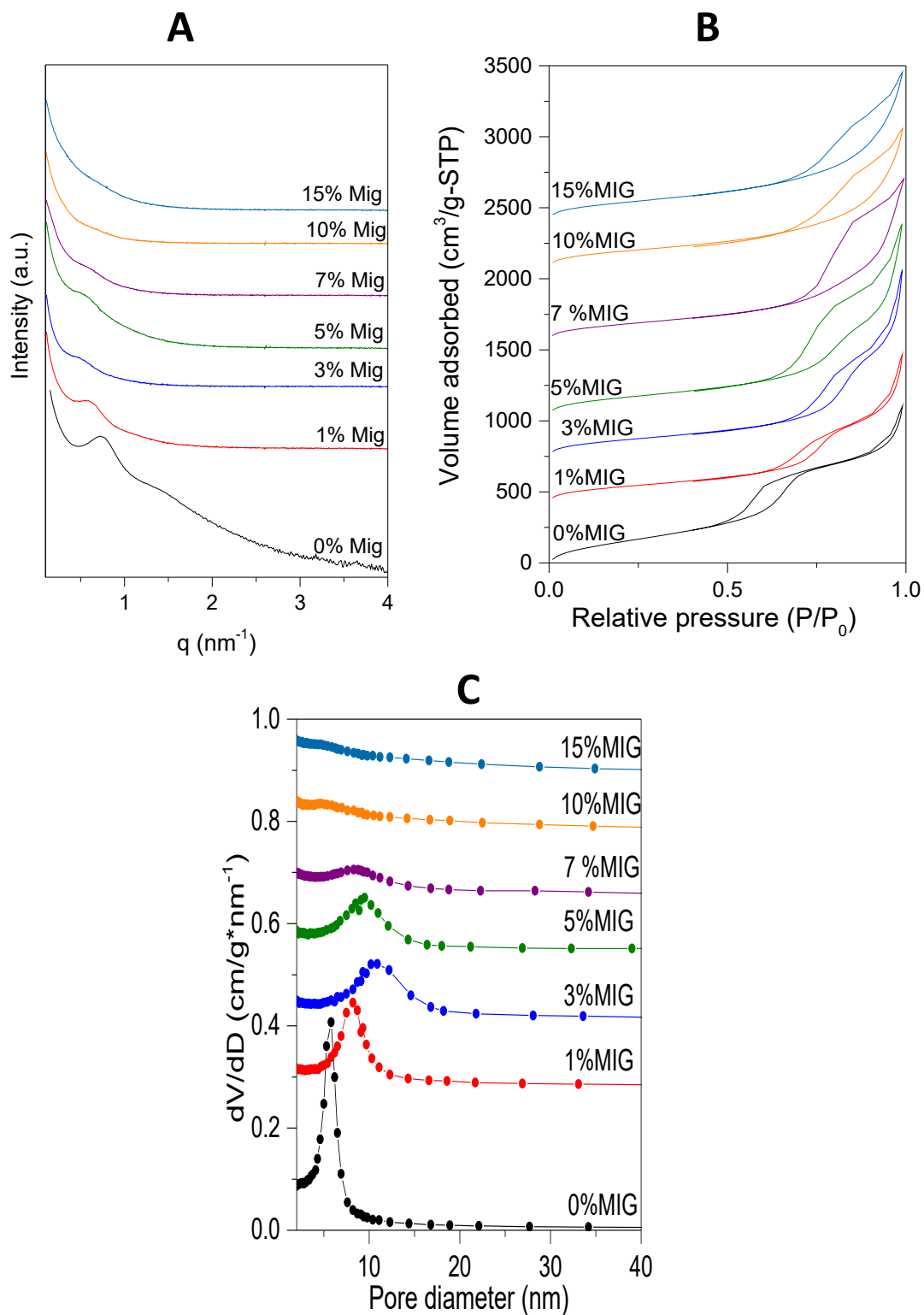


**Figure 3-19.** (a) SAXS spectra of the silica material in function of % Miglyol concentration. (b) Nitrogen adsorption-desorption analysis (c) Evolution of the pore volume.

# **Chapter IV. Porous silica templated by the combination of fine emulsions (Em) and P123 micelles**

This chapter explain the characteristics of porous silica material obtained by combination from the fine emulsions formulated with: Kolliphor EL (KEL)/Isopropil Myristate/ Water and P123 micellar solution.

The first part concerns the study about the compatibility between the partnership of surfactants: KEL and P123, for that, the ternary phase diagram KEL/P123/water is described first and the structural determination of different Organized Molecular Systems (OMS) as micelles and liquid crystals are studied by Small Angle X-ray Scattering (SAXS).

As mentioned throughout this work, the type of surfactant or its synergy with other compounds can influence the characteristics of the final porosity in the material, therefore based on the results obtained in the chapter III concerning to the stability of the small size emulsions (Em) prepared with Isopropyl Myristate/KEL/water the second part of this chapter consider the relationship between the fine emulsions and the P123 micellar solution which will serve as template for the materials.

## 4.1 System Kolliphor EL (KEL)/ P123/water

### 4.1.1 Phase diagram of KEL in water and structure of the observed phases

To get information concerning the degree of compatibility between the two surfactants, which can affect the formation of the porous materials, the Kolliphor/P123/water system has been first investigated in detail. The surfactant behavior in water was studied by establishing its phase diagram which shows that in the water rich part of the diagram (Figure 4-1)

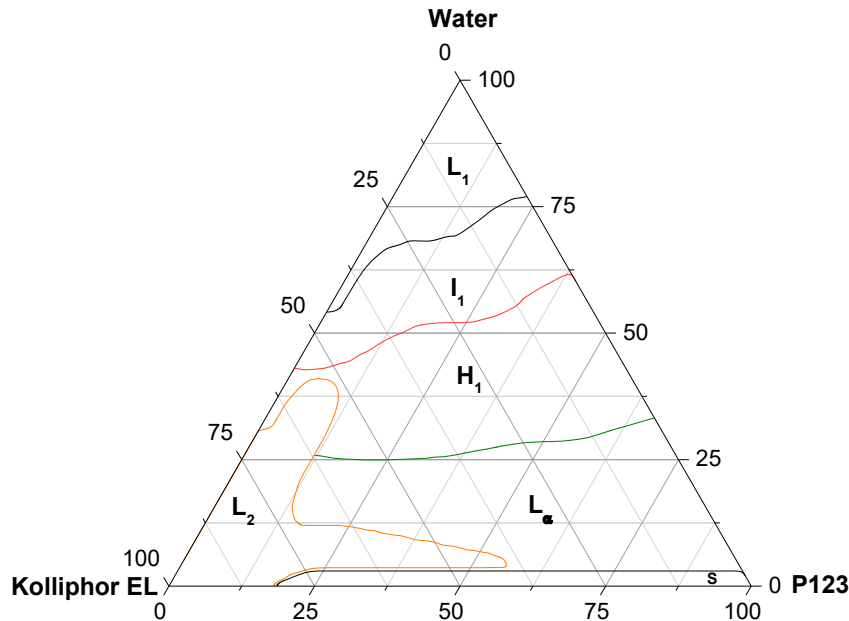


**Figure 4-1.** Composition phase diagram (wt.%) at 25°C of the Kolliphor/P123/water system

A micellar solution ( $L_1$ ) is obtained up to a total surfactant concentration equal to 25 wt.%, whatever is the ratio between Kolliphor and P123. The  $L_1$  domain is extended up to 46 wt.% of surfactant for solutions rich in Kolliphor. The cubic ( $I_1$ ), the hexagonal ( $H_1$ ) and the lamellar ( $L_\alpha$ ) liquid crystal domains appear as the total surfactant concentration increases.

The limits of  $I_1$  are unbroken and almost continuous between the pure cubic phase of Kolliphor and that of P123 from 46 to 58 wt. % of KEL and from 22 to 37 wt.% of P123. In the same way, except for the Kolliphor-rich domain, which gives way to a reverse micellar phase, a hexagonal phase whose water quantity corresponds approximately to the one present in the pure liquid crystals of Kolliphor and P123 appears. This observation suggests the existence of mixed liquid crystals.

For the pure KEL system this phase is detected between 58 and 68 wt.% of Kolliphor in water, whereas it is located between 40 and 65 wt.% of Pluronic in the P123/water system. If the total surfactant concentration is further increased the lamellar phase ( $L_\alpha$ ), which is not detected in the Kolliphor/water binary system appears. However,  $L_\alpha$  can incorporate up to 71.5% of Kolliphor.

For the Kolliphor rich part, a reverse micellar phase ( $L_2$ ) can be formed for total surfactant concentrations higher than 87%. This  $L_2$  phase extends into a tongue shape when it is enriched in P123. Finally, a solid phase is observed for total surfactant concentrations higher than 97 wt.% if the P123 loading in the mixture is higher than 21%. Any the organized molecular system, the compatibility between the head groups, composed of oxyethylene units and of the alkyl chains of Kolliphor and P123 allows the formation of mixed entities in all proportion. Any gap of miscibility was observed.

#### 4.1.2 Micellar structure and determination of the structural parameters

The micelle characterization was done by SAXS experiments (chapter II, page XX). The Figure 4-2 presents the experimental SAXS spectra of mixed solutions with total surfactant concentration of 5wt% in water for several ratios between KEL and P123.

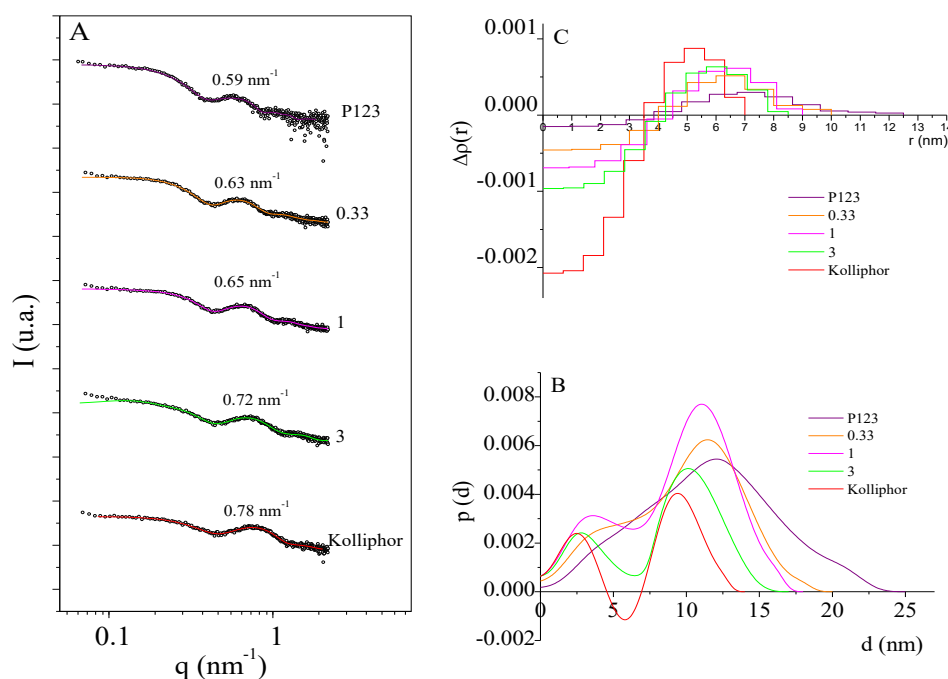


**Figure 4-2.** (A) Experimental (dotted line) and approximated (GIFT) (solid line) SAXS spectra of mixed micellar solutions of Kolliphor and P123 with a total concentration of surfactant in water equal to 5 wt% at 25 °C. (B) Corresponding pair-distance distribution functions (PDDFs), (C) Corresponding excess-electron density profiles

All the spectra present only one broad peak which is shifted from 0.78 to 0.59 nm<sup>-1</sup> when the quantity of P123 in the surfactants mixture varies from 0 to 100%. To determine the micellar structure, the data were analyzed by using the Generalized Indirect Fourier Transform (GIFT) method, taking into consideration the interparticle interactions (Figure 4-2 solid line). The obtained pair-distance distribution functions (PDDFs) are depicted in Figure 4-2B. All the curves present a bell-like shape, characteristic of spherical micelles, with a dimension which depends on the P123 content in the surfactants mixture.

It is noted that like for the P123 micelles, the PDDF of the curve corresponding to the solution prepared with a Kolliphor/P123 ratio of 0.33 presents a shoulder on the left side of the maximum of the  $\rho(r)$  functions at around 4 nm, featuring a lower inhomogeneity of the particles compared with the ones of the pure Kolliphor solution and with the other mixed solutions.

The excess-electron density profiles have been determined by the deconvolution of the pair-distance distribution functions (PDDFs) (Fig. 4-2C). The profiles confirm the core-shell type particles for the different micellar solutions. Indeed, the negative density difference corresponds to the hydrophobic part, whereas the positive density difference can be attributed to the hydrophilic shell.

In the table 4-1 the size of micelles diameters are show, where it is noted that the size increase from 14.0 to 25.0 nm when the amount of P123 in the surfactants mixtures is changed from 0 to 100%.

**Table 4-1:** Micelles diameter and hydrophobic radius of Kolliphor/P123 mixed micelles. The total concentration of surfactant in water is equal to 5 wt%

Sample	Micelles diameter (nm)*	Micelles diameter (nm)**	Hydrophobic radius R <sub>H</sub> (nm)
Kolliphor	13.9	14.0	3.5
Kolliphor/P123 = 3	16.6	17.0	4.3
Kolliphor/P123 = 1	17.8	18.0	4.5
Kolliphor/P123 = 0.33	19.6	20.0	4.0
P123	24.3	25.0	3.9

\* Values obtained from GIFT analysis

\*\* Values obtained from the excess electron density profiles

These values are in accordance with the micelle size found on the PDDFs. When the P123/Kolliphor ratio is increased more and more P123 molecules are accommodated in the micelles leading to micelles with bigger size. The hydrophobic

radius corresponds to the  $r$ -value when the sign of  $\Delta\rho(r)$  changes. It can be estimated at 3.5 and 3.9 nm for the Kolliphor and P123 micelles, respectively.

For the mixed systems its value varies between 4.0 and 4.5 nm, depending on the P123 content (Table 4-1). The dimension of the alkyl chains in the micelles, corresponding to the lowest value of  $\Delta\rho(r)$ , can be estimated at about 2.5 and 3.8 nm respectively for the Kolliphor and P123 micelles. From the length of the bonds, the extended alkyl chains of Kolliphor have a dimension of about 2.5 nm, this show that the alkyl chains, in the pure Kolliphor micelles, are rather extended.

In the same way, estimating that the length of the Polypropylene oxide (PPO) part of the P123 is equal to 24.5 nm (1 PPO unit = 0.35 nm), we can deduce that the PPO chain, in the pure P123 micelles, can only be self-folded and it rather adopts a meandering conformation as previously reported. Looking at the dimension of the hydrophobic moieties in the mixed-micelles, around 3 nm, we can assume that the alkyl chains of Kolliphor and PPO chain of P123 likely adopt the same conformation than in the pure micelles.

All the observations reported above support the existence of mixed micelles regardless the proportion between the two surfactants in the solutions. Assuming that the mixture of surfactant forms a mixed entity, the structural parameters of the liquid crystal phases have also been determined. The water amount has been kept constant and the weight fraction of Kolliphor in the surfactant mixture, noted  $x_{KEL}$ , has been varied from 0 to 1. For a given composition the average molar weight ( $M$ ) of the mixed entity is:

$$M = \frac{N^P M^P + n^{KEL} M^{KEL}}{N^P + n^{KEL}} \quad Eq. 4 - 1$$

Where:

$n^P$  and  $n^{KEL}$  respectively stand for the mole number of Pluronic and KEL surfactant  $M^P$  and  $M^{KEL}$  are the corresponding molar weight.

For the cubic phase, the hydrophobic radius  $R_H$  is related to the lattice parameter  $a$  by the following equation:

$$\frac{V_B}{V_s + \alpha V_w} = \frac{4 v \pi R_H^3}{3a^3} \quad Eq. 4 - 2$$

where  $v$  is the number of micelles per cubic lattice.  $v = 8$  and  $v = 4$  for the Pm3n and Fm3m space group, respectively. Where  $\alpha$  stands for the number of water molecules per surfactant molecule and  $V_s, V_B, V_w$  respectively stand for the molar volumes of the mixed surfactant, the hydrophobic part of the mixed surfactant and water ( $V_w =$

18 cm<sup>3</sup>/mol).  $V_s$  and  $V_B$  depend on the molar ratio between the two amphiphiles. For example, for a mixture containing 30 wt.% of Kolliphor, these values are  $V_s = 4016$  cm<sup>3</sup>/mol and  $V_B = 2656$ . The values of  $V_s$  and  $V_B$  for the pure surfactant were calculated from densities and are  $V_s = 2354$ ,  $V_B = 834$  cm<sup>3</sup>/mol for Kolliphor and  $V_s = 5577$  and  $V_B = 4030$  cm<sup>3</sup>/mol for P123. Then, the cross sectional area  $S$  can be deduced as:

$$S = \frac{3 V_B}{N R_H} \quad \text{Eq. 4 - 3}$$

$N$  is the number of Avogadro. Scattering spectra of samples belonging to the cubic domain are reported in Figure 3A. Until  $x_{KEL} = 0.8$ , The relative positions of the Bragg reflections are:  $\sqrt{4/3}, \sqrt{8/3}, \sqrt{11/3}, \sqrt{12/3}, \sqrt{16/3}, \sqrt{20/3}$ . According to results published by Tiddy et al. they can be indexed in the Fm3m space group. For  $x_{KEL} = 0.9$  the ratios between the reflection lines change and they become  $1: \sqrt{3/2}: \sqrt{2}: \sqrt{5/2}: \sqrt{3}: \sqrt{29/4}$  which can be assigned to the Pm3n direct micellar cubic phase. The cell parameter is related to the space spacing by the relations:  $a = d_{111} \sqrt{3}$  and  $a = 2d_{200}$  for the Fm3m and Pm3n space group, respectively.

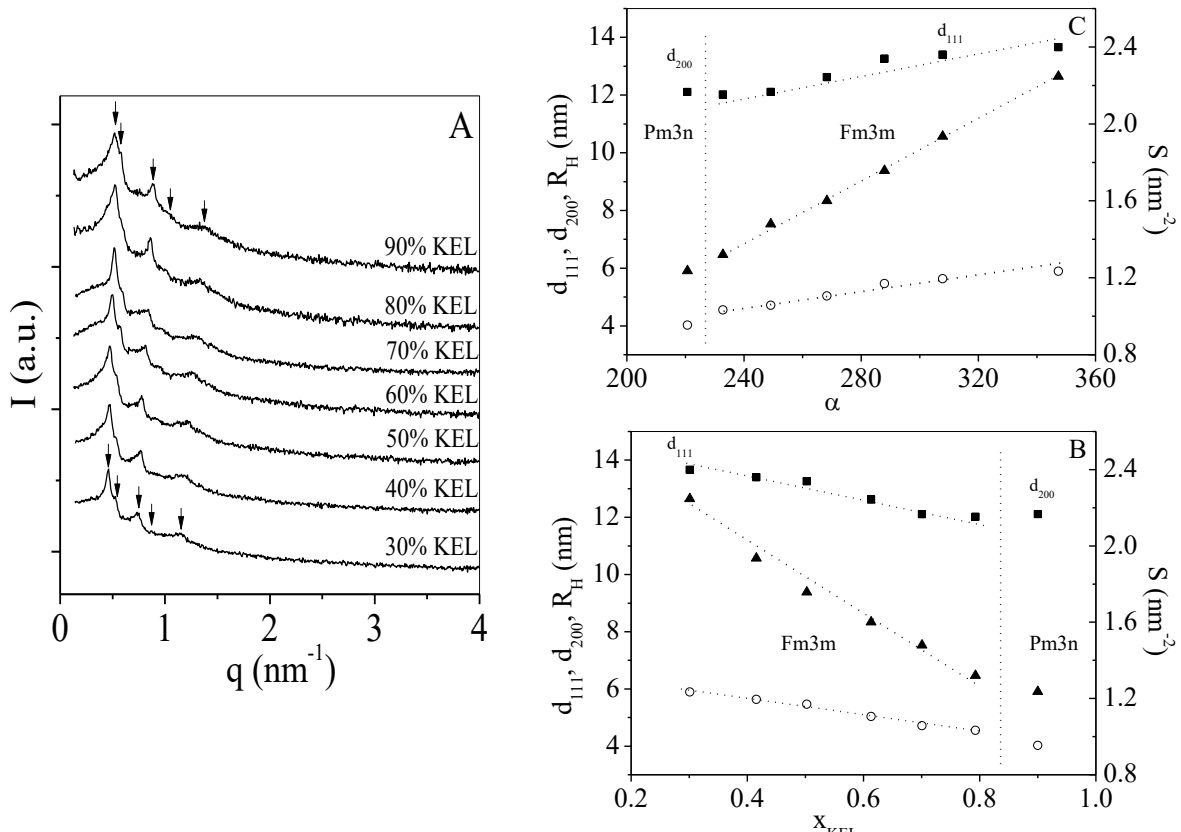


**Figure 4-3.** Cubic liquid crystal phase. (A) Evolution of the SAXS pattern of the cubic with the Kolliphor (KEL) content in the surfactants mixture; (B) structural parameter of  $I_1$  as a function of  $x_{KEL}$  and (C)  $\square\square$  The total surfactant concentration is 40 wt.%.  
**■** :  $d$ , **○** :  $R_H$  and **▲** :  $S$ .

The hexagonal phase is composed of infinite cylinders packed in a hexagonal array. In case of direct systems, cylinders are filled by the hydrophobic chains and are covered by both head groups and water. The Figure 4-3A, show the SAXS profile characterization of the hexagonal phase with the relative peak positions, 1,  $\sqrt{3}$ , 2. The distance  $d_{100}$  associated to the first peak is related to the hydrophobic core radius  $R_H$  by the relation:

$$\frac{V_B}{V_s + \alpha V_w} = \frac{\sqrt{3}\pi R_H^2}{2d_{100}^2} \quad Eq. 4 - 4$$

The cross-sectional area  $S$  can then be deduced from the following relation:

$$S = \frac{2 V_B}{N R_H} \quad Eq. 4 - 5$$

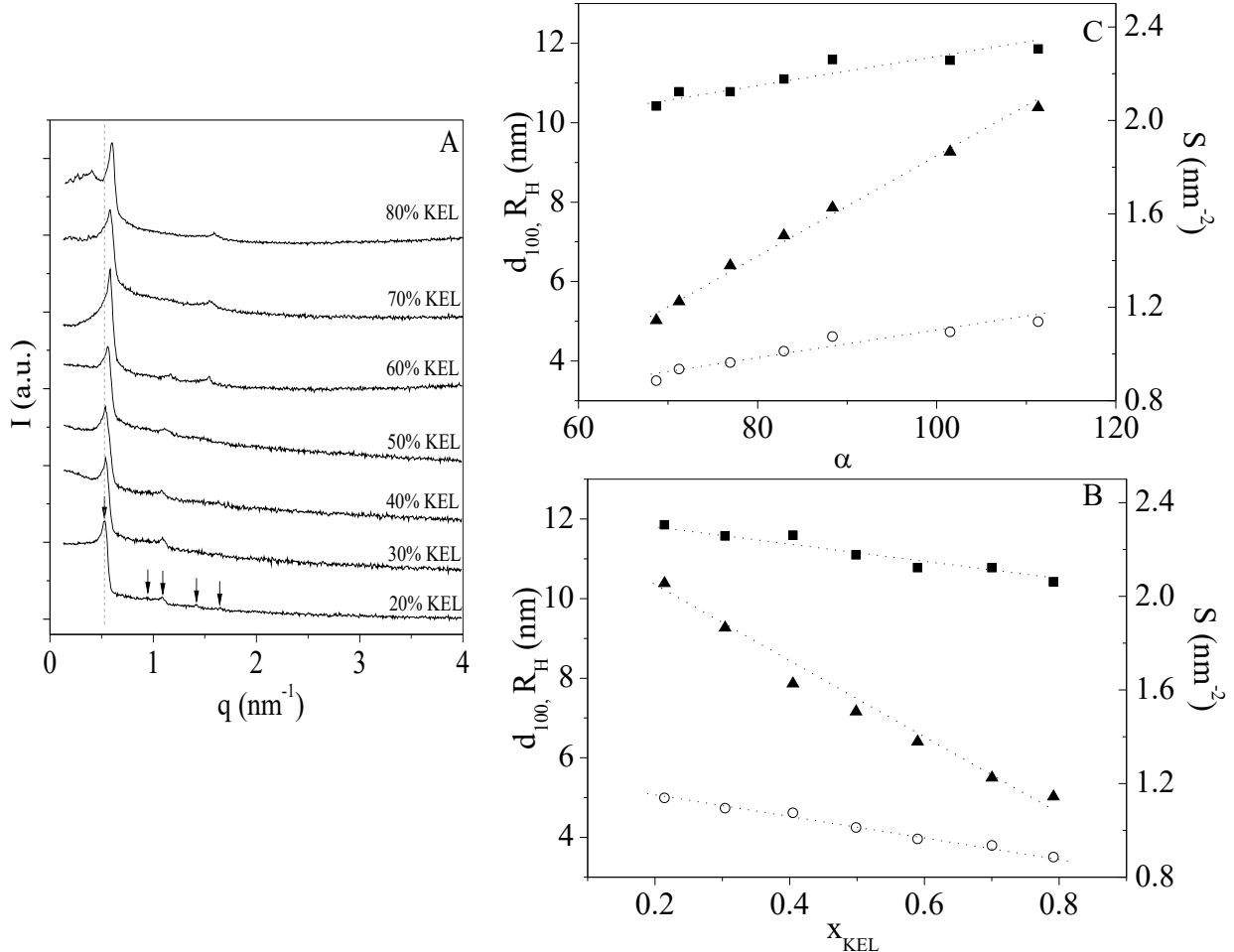


**Figure 4-4.** Hexagonal liquid crystal phase: (A) Evolution of the SAXS pattern of the hexagonal conformation with the Kolliphor (KEL) content in the surfactants mixture, (B) structural parameter of  $H_1$  as a function of  $x_{KEL}$ , (C)  $\alpha$  ■:  $d_{100}$ , ○:  $R_H$  and ▲:  $S$ . The total surfactant concentration is 70 wt.%.

The lamellar phase can be described as an infinite bilayer of surfactants stacked in a parallel manner. The diffraction pattern exhibits two reflections with the relative peak positions 1, 2 (Figure 4-5A). The repetition distance corresponds to the layer spacing, which comprises the water separated by the surfactant bilayer. The cross-sectional area can be calculated from the following formula:

$$S = \frac{2(V_s + \alpha V_w)}{N d_{001}} \quad \text{Eq. 4 - 6}$$

Where  $d_{001}$  stands for the repetition distance.

The hydrophobic thickness  $d_B$  and the hydrophilic thickness  $d_A$  can be deduced from the following equations:

$$d_B = \frac{2V_B}{S} \quad \text{and} \quad d_A = d_{001} - d_B \quad \text{Eq. 4 - 7}$$

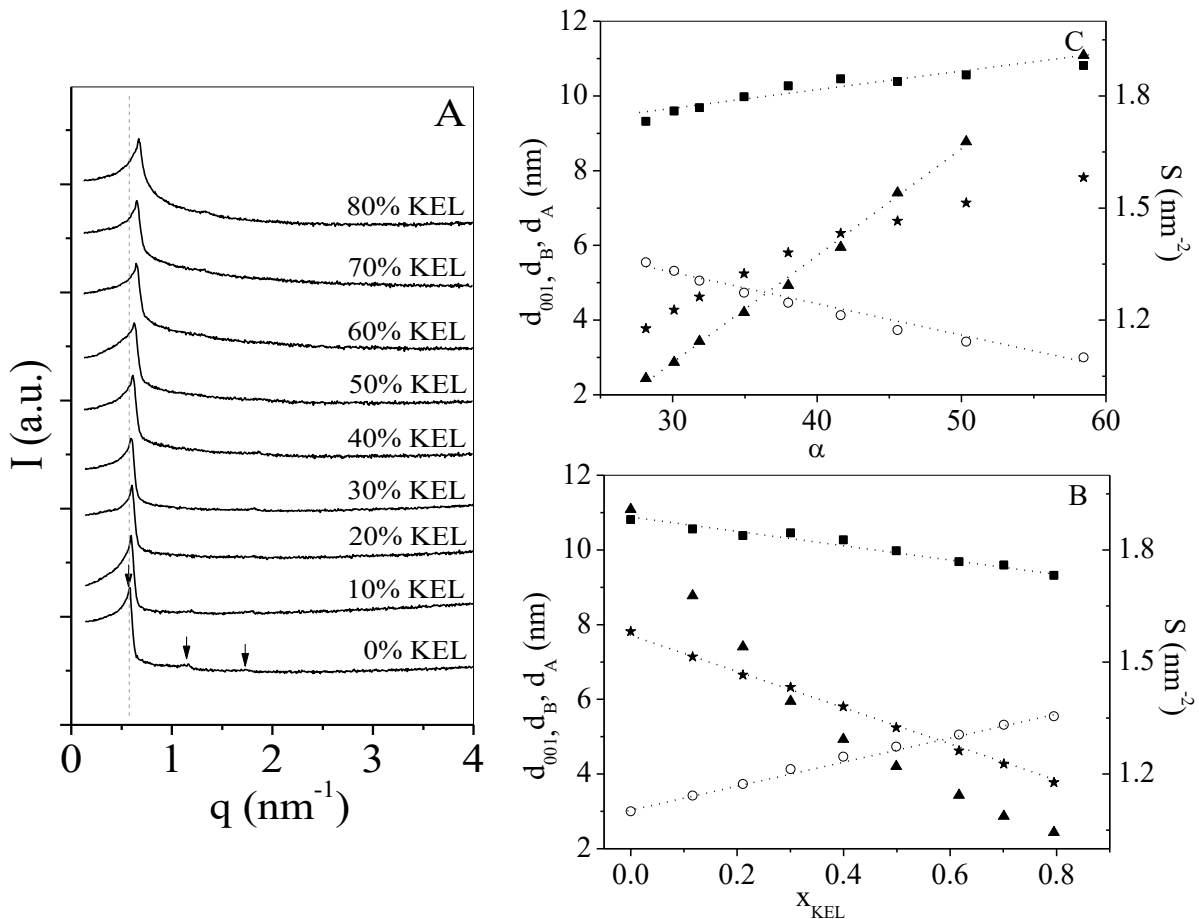


**Figure 4-5.** Lamellar liquid crystal phase. (A) Evolution of the SAXS pattern of the hexagonal with the Kolliphor (KEL) content in the surfactants mixture; (B) structural parameter of  $L_{\square}$  as a function of  $x_{\text{KEL}}$  and (C)  $\square$  The total surfactant concentration is 85 wt.%.  $\blacksquare$  :  $d_{100}$ ,  $\circ$  :  $d_B$ ,  $\star$  :  $d_A$  and  $\blacktriangle$  :  $S$

Figures 4-3B, 4-4B and 4-5B display the variation of structural parameter as a function of  $x_{KEL}$  for the cubic, the hexagonal and the lamellar liquid crystal phases, respectively. From these figures it can be noted that with the increase of  $x_{KEL}$ , whatever the liquid crystal, all the structural parameters vary in a linear manner between the values corresponding to the two binary systems. As an example, in the Fig. 4-3B for the cubic phase  $R_H$  and  $S$  decrease from 5.9 to 4.6 nm and from 2.3 to 1.3 nm<sup>2</sup> when  $x_{KEL}$  is changed from 0.30 to 0.80. The linear relationship between the structural parameters and the weight fraction of Kolliphor ( $x_{KEL}$ ) in the surfactants mixture is in a good agreement with the formation of a mixed liquid crystal phases in which both the Kolliphor and P123 molecules are present without segregation of the surfactants. The formation of mixed entities is possible thanks to the compatibility of the hydrophilic and the hydrophobic parts of the two surfactants.

Figure 4-3C, 4-4C and 4-5C describe the evolution of the structural parameters as a function of  $\alpha$ , the number of water molecules per surfactant molecule. We can note an increase in the d-spacing due to the hydration of the head group and the water surrounding the surfactant. As it could be expected for mixed liquid crystal phases, the variation of the structural parameters as a function of  $\alpha$  follows the same trend than as a function of  $x_{KEL}$ . Indeed, in that case, even if the water content and the total surfactant concentration are constant, since the proportion between Kolliphor and P123 varies in the surfactant mixture, the average molar weight ( $M$ ) of the mixed entity is changed for each content of Kolliphor present in the mixture. The number of surfactant molecules is thus modified and consequently,  $\alpha$  which is the number of water molecules per surfactant molecules also varies when  $x_{KEL}$  is increased from 0 to 1.

It has been reported that in the pure P123  $H_1$  and  $I_1$  domains, the values of  $R_H$  are around 4.8 and 4.5 nm, respectively. Considering the different bonds, the length of the extended PPO block is 24.5 nm and comparing this value to the hydrophobic radius, it was concluded that the hydrophobic chains of the P123 hexagonal and cubic phases are completely self-folded. In the pure Kolliphor/water system, from the length of the bonds the dimension of the extended alkyl chains it was concluded that in  $H_1$  and  $I_1$  the alkyl chains adopt an extended conformation. Looking at the  $R_H$  values reported in Figure 5-3 and 5-4, we can therefore assume that, in the mixed hexagonal and cubic phases, the alkyl chains are also completely extended, whereas the PPO blocks are self-folded.

In the Figure 4-5, the  $L\alpha$  phase,  $d_B$  varies from 7.8 to 3.8 nm when  $x_{KEL}$  is increases from 0 to 0.8, considering the dimensions of the alkyl chains and of the PPO units in an extended conformation the variation of  $d_B$  suggests that the hydrophobic parts in the mixed lamellar phase are rather extended.

## 4.2 Sílica porous material synthesis

In this section, the porous materials obtained from the system KEL/P123/eau were characterized. These materials were prepared by combining the fine emulsion and the P123 micelles. The Figure 4-6 presents the variation of the SAXS pattern as a function of Em/P123 weight ratio, it can be noted that under the synthetic conditions reported (see chapter II, point 2.2.3 A), no mesopore ordering is recovered when P123 micelles are used alone as templates.

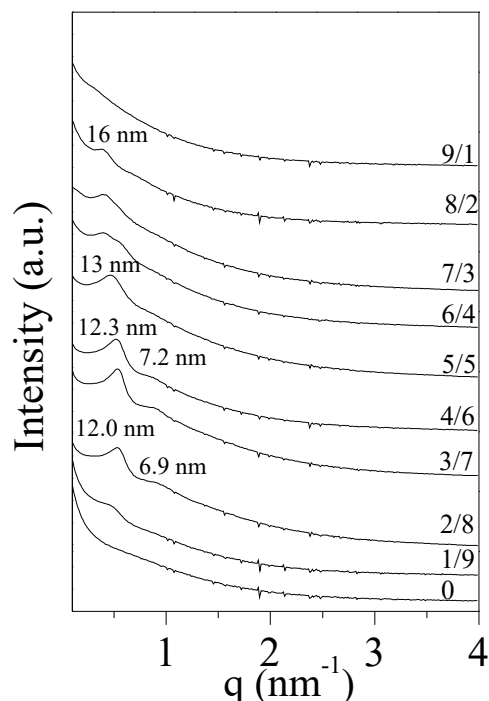


**Figure 4-6.** Porous materials: Variation of the SAXS pattern as a function of the fine emulsion/P123 micellar solution weight ratio.

Indeed, in that case no peak is detected on the SAXS pattern. For Em/P123 ratios comprised between 2/8 and 4/6, two peaks around 12 and 7 nm are observed on the SAXS patterns (Figure 4-6). Their relative position  $1, \sqrt{3}$  shows that in this range of Em/P123 ratios, ordered mesostructured silica materials are recovered.

The unit cell  $a_0$ , which is the sum of the pore diameter and of the thickness of the pore wall, can be deduced from the following relation:  $a_0 = 2d_{100} / (3)^{1/2}$ , and its value is found around to 13.9 nm. Increasing Em/P123 from 5/5 to 8/2, no secondary reflections are detected any longer. Only a broad peak characteristic of a wormhole-like mesostructured, is detected at 13.0 nm for Em/P123 = 5/5 (Figure 4-6). This peak gives an indication of the average pore-to-pore distance in the disordered wormhole framework, which presents a lack of long-range crystallographic order. It

is shifted toward smaller  $q$  values, when the Em/P123 ratio is raised until 8/2. Beyond Em/P123 = 8/2, no reflection is detected anymore on the SAXS pattern, meaning that the channel arrangement is completely random. The Figure 4-7 reports the results of the adsorption-desorption Nitrogen for the materials prepared.

The sample prepared from the pure P123 micellar solutions exhibits a type IV isotherm (Figure 4-7), characteristic of mesoporous materials according to the IUPAC classification. The pore size distribution presents a maximum at around 2.8 nm.

The values of the specific surface area and of the pore volume are 818 m<sup>2</sup>/g and 0.52 cm<sup>3</sup>/g, respectively. Preparing the silica materials from the P123 micelles and fine emulsion mixture, the isotherm remains type IV until an Em/P123 weight ratio of 5/5. It should be noted that with the addition of Em, the capillary condensation step is more pronounced and is shifted towards higher relative pressure for example it occurs at  $p/p_0 = 0.45$  for the material prepared from the pure P123 micelles and at  $p/p_0 = 0.75$  for the sample synthesized with a Em/P123 ratio higher from 1/9 to 5/5 (Figure 4-7).

Since the  $p/p_0$  position of the inflection point is related to the pore diameter according to the Kelvin's equation, it can be inferred that bigger mesopores appear when the porous silica are prepared from the Em/P123 mixture. Nevertheless, on the mesopore size distribution the component at 2.8 nm is observed until a Em/P123 weight ratio of 3/7. A second maximum at 9.3 and 8.7 nm is observed for materials prepared in the presence of 10 and 20% of Em, respectively.

The materials synthesized present at least a dual mesoporosity. Increasing the Em/P123 from 2/8 to 5/5, the component at 2.8 disappears in favor of a doubling of the one at 8.7 nm, which is split into two maxima one around 10.0 nm and the other one at around 8.5 nm.

The intensity of the two peaks gradually reversed when the Em/P123 ratio is increased. Beyond Em/P123 = 5/5, the mesopore size distribution becomes broader and only one large component with a maximum between 15.0 and 23 nm (insert Fig.7). It should be noted that whatever the Em/P123 ratio both the mesopore size distribution and the shape of the isotherms at very low relative pressure suggest also the presence of micropores.

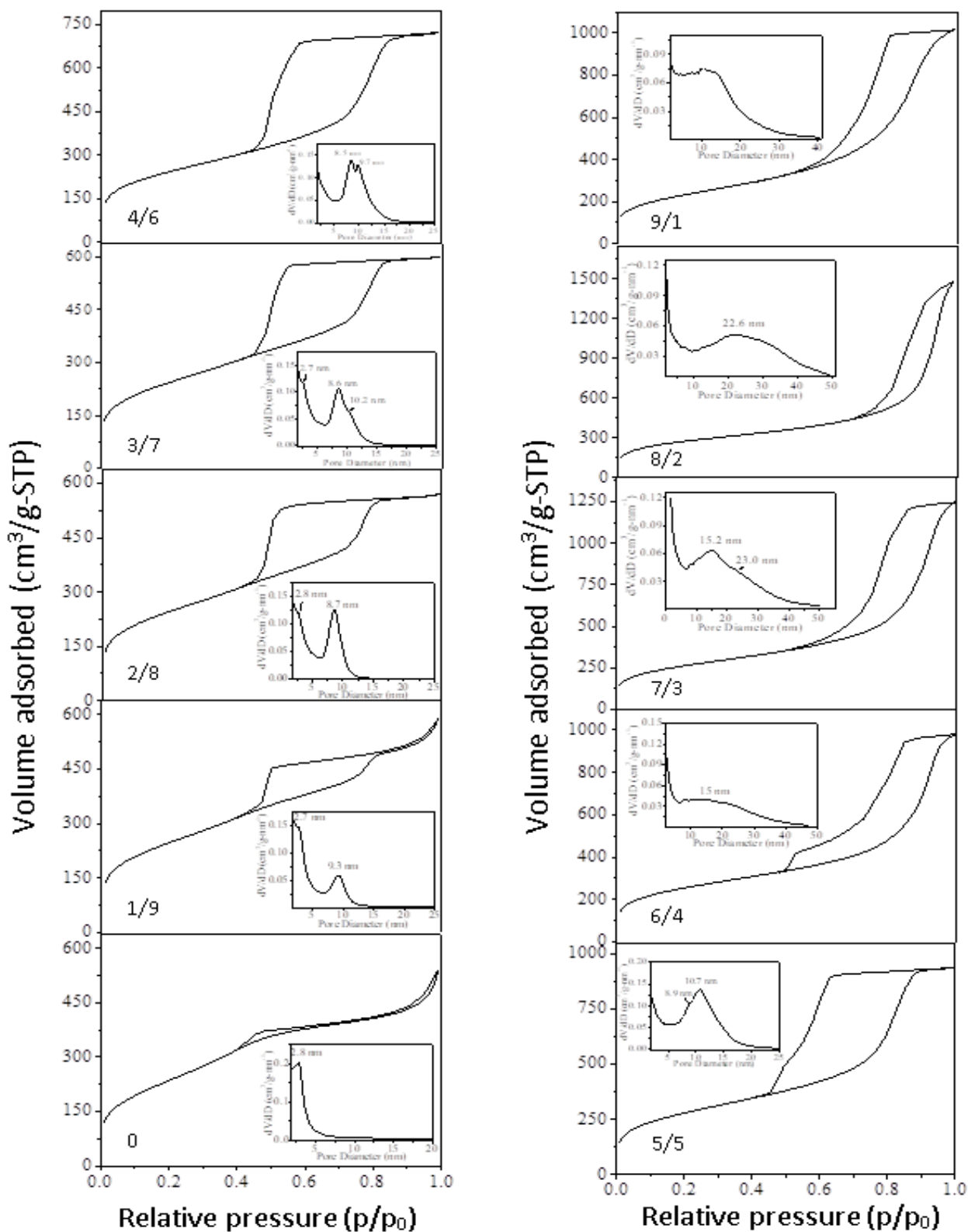


**Figure 4-7.** Porous materials: Nitrogen adsorption-desorption isotherms with the corresponding pore size distribution (insert) as a function of the fine emulsion/P123 micellar solution weight ratio.

The specific surface area is quite high (Figure 4-8) and it slightly increases when the proportion of Em is raised. For example, its value varies from 890 to 970 m<sup>2</sup>/g when the Em/P123 ratio is changed from 1/9 to 8/2. From Figure 8 it can also be seen that the pore volume gradually increases from 0.52 to 1.40 cm<sup>3</sup>/g as a function of the Em/P123 weight ratio.

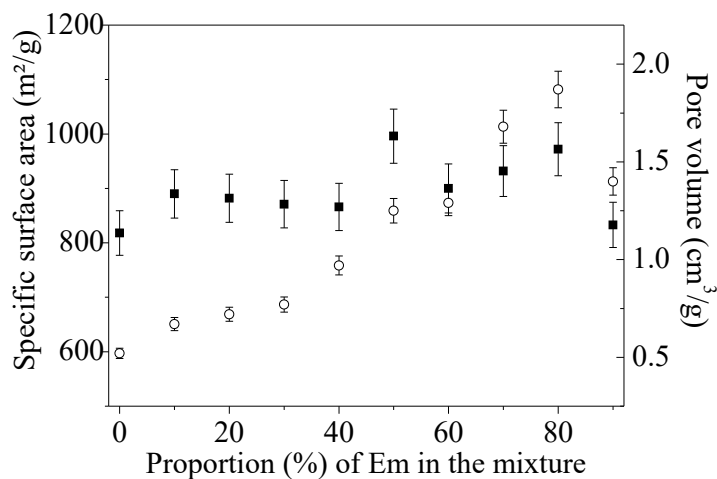


**Figure 4-8.** Porous materials: Variation of the specific surface area and of the pore volume as a function of the proportion (%) of Em in the starting solution used to prepare the silica materials; ■ : specific surface area ○ : pore volume.

When pure P123 micelles are used as template, the mesostructured silica is obtained through the Cooperative Templating Mechanism (CTM). In the initial step, when the silica is added to the micellar solution, hydrogen-bonding interactions between the oxygen atoms of the oxyethylene groups of the surfactant and OH groups of the hydrolyzed TMOS are formed. Then, the condensation of the inorganic precursor at the external surface of the micelles occurs. The mesophase is obtained after inter-micellar condensation.

Finally, the hydrothermal treatment at higher temperature completes the assembly of micelles and the polymerization of the silica source. The mesostructured material is recovered after surfactant removal by solvent extraction or/and by calcination. Under the conditions reported here, no mesopore ordering is obtained and the mesopore size distribution is centered at around 2.8 nm. Consequently, preparing the porous silica from the P123 micelles and fine emulsion mixtures, the component at 2.8 nm observed until an Em/P123 weight ratio of 3/7 can be attributed to mesopores templated by the pure P123 micelles.

To explain the evolution of the pore size distributions as a function of the Em/P123 ratio, we have also to consider the potential effect of methanol, released during the hydrolysis on both the micellar solution and the fine emulsion. In previous studies we have shown that while the methanol does not significantly disturb the CTM mechanism for the preparation of mesostructured silica, it has a negative effect on the stability of the fine emulsion.

Riachy et al, 2016, reported that in the case of nano-emulsions formulated from the Remcopal/decane/water system we have reported that the methanol addition leads to an increase of the oil drop and to a destabilization of the nano-emulsion. Moreover, the existence of the nano-emulsions is not favored in the presence of the Pluronic micelles since the system becomes more hydrophilic.

Here, up to a Em/P123 ratio of 5/5, since P123 micelles predominate and since high amounts of methanol is released, it is possible to assume that the negative effects of both methanol and P123 micelles involve a destabilization of the fine emulsion. With the low amount of Em, this can explain why no pore size due to the mineralization of the fine emulsion is observed until an Em/P123 ratio of 5/5. The Kolliphor molecules arising from the destabilization of the fine emulsion can associate with P123 to form mixed-micelles, which can eventually be swollen by Myristate.

Actually, the investigation of the Kolliphor/P123/water phase diagram has shown that the mixture of these two surfactants leads to the formation of mixed organized molecular systems and in particular mixed micelles. The formation of the mixed micelles is supported by the disappearance of the component at 2.7 nm in the mesopore size distribution when the quantity of P123 micelles decreases. This strongly suggests that the P123 micelles accommodate the Kolliphor molecules. The mixed micelles are likely responsible for the mesopore diameter at around 8.7 nm. As a matter of fact, this size at 8.7 nm is in accordance with the hydrophobic diameter (between 8.0 and 9.6 nm, depending on the Kolliphor/P123 ratio). The swollen mixed micelles by Myristate give the peak at around 10.0 nm. As observed by the SEM the oil droplets arising from the fine emulsion can also coalesce to lead to the formation of macropores having a size of few microns in diameter.

With the increase of the Em/P123 weight ratio beyond 5/5, the proportion of Pluronic micelles is lower. It should be reminded that the TMOS amount has been fixed to get a P123/TMOS molar ratio of 0.005. Due to the lower amount of methanol and P123 micelles, the fine emulsion is more stable and is possible to assume that the porosity mainly arises from the fine emulsion, which proportion increases with the Em/P123 ratio.

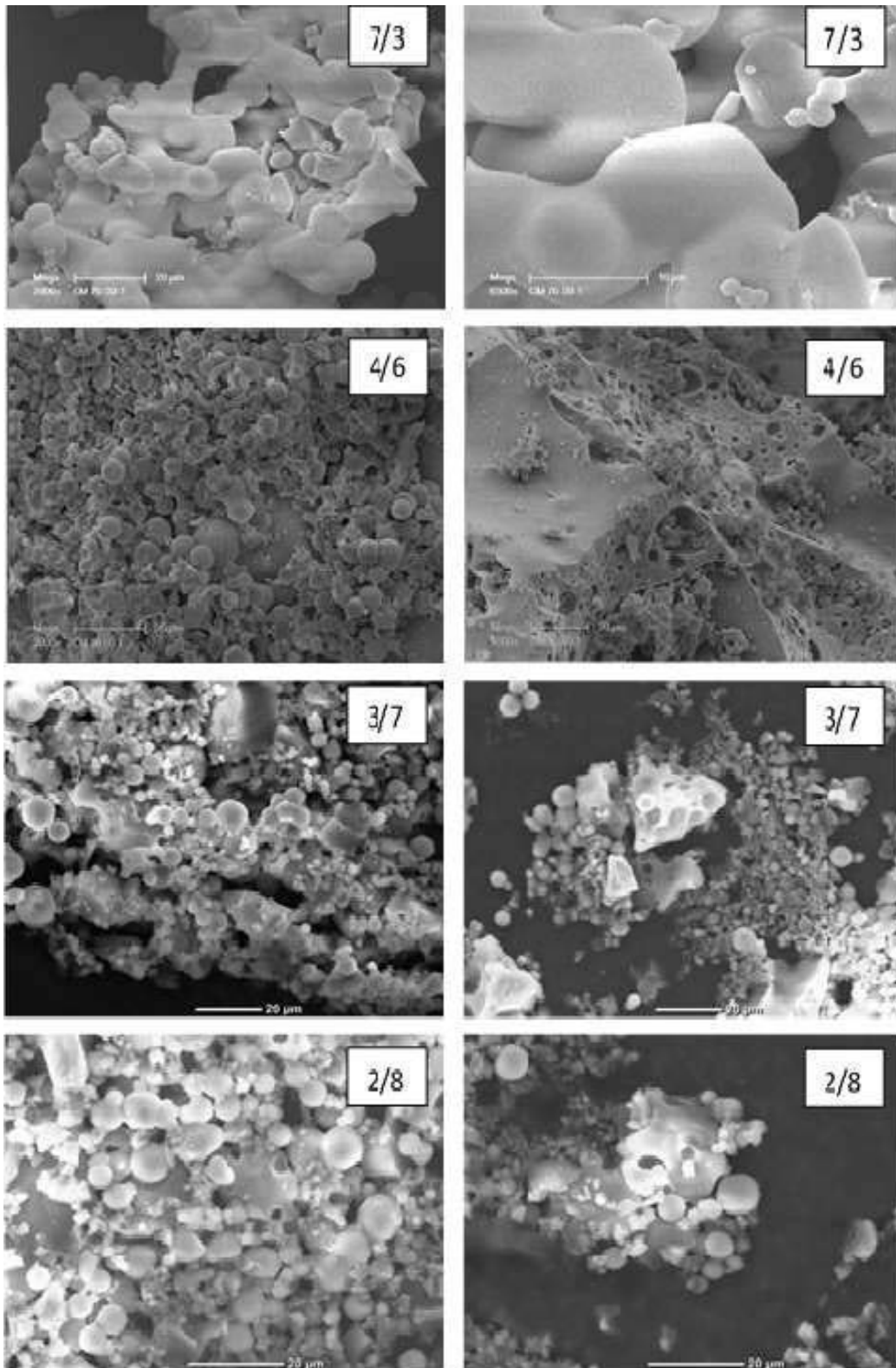
In that case the hydrolyzed TMOS interacts with the Kolliphor molecules at the surface of the Myristate droplets. Finally, for all samples the microporosity can arise from the penetration of the oxyethylene units in the silica framework. After surfactant removal this leads to the formation of micropores. This phenomenon is well reported in the literature for the synthesis of SBA-15.

Figure 4-9 shows SEM pictures of the samples synthesized at different Em/P123 weight ratios. The morphology of the materials can be mainly described as an agglomerate of small spheres having a diameter less than 10  $\mu\text{m}$ . Higher the Em/P123 ratio is, more agglomerated the spheres become. Besides the spheres, macropores of a few microns looking like the imprints of droplets can also be detected, in particular for silica prepared with a Em/P123 ratio of 3/7 and 4/6.

As a conclusion we can note Using a mixture of fine emulsion (Em) and Pluronic P123 micelles, hierarchical porous silica materials can be prepared. The porosity features of the materials are strongly depend on the Em/P123 weight ratio. Indeed, if this ratio is lower than 5/5 dual mesoporous silica are obtained. In that case, methanol released during the hydrolysis of TMOS and the presence of P123 micelles have a negative effect on the fine emulsion, which is destabilized.

The Kolliphor molecules likely associate with the P123 micelles to form mixed micelles. Indeed, the investigation of the Kolliphor/P123/water systems have shown that when both surfactants are mixed, they formed mixed micelles and liquid crystal phases (cubic, hexagonal and lamellar). A part of Myristate released by the fine emulsion can swell the mixed micelles and the oil droplets of the fine emulsion can also give macropores.

Increasing the Em/P123 weight ratio both the proportion of P123 micelles and methanol decrease and the fine emulsion is not completely destabilized any longer. The porosity is then controlled by the fine emulsion. Whatever the Em/P123 ratio micropores are also formed likely by the penetration of the EO groups in the silica framework



**Figure 4-9.** Porous materials: SEM images of the samples prepared with different Em/P123 weight ratios.

## **Chapter V. Drug release and *in vitro* toxicity test**

The increasing need for drug delivery systems that improve specificity and activity has led to the development of a great variety of drug vectors. At the same time, these administration systems must ensure the maximum treatment safety through the toxicity reduction. Especially the vectors based on biocompatible surfactants are highly valued as they expand the bioavailability of the drug.

The first part of this chapter reports a potent carrier for drug entrapment and release where ketoprofen was used as a model drug. More precisely are silicate hybrid materials prepared from systems of non-ionic surfactant as Kolliphor EL and Miglyol 812N as oil. Micelles or emulsions and the silica represent the organic and mineral part, respectively. In the second part of the chapter, the toxicity of these hybrid systems is described, which were obtained from the response of a HeLa cells culture.

## 5.1 Doped hybrid mesoporous materials characterization prepared from micellar solutions

This section explains the characterization of doped hybrid materials elaborated from micellar solutions and used in KTP release experiments. For this, the first step to realize is to determine the solubility of KTP in different solutions, in order to know if the systems proposed will entrap the required KTP quantity for the mentioned purposes, to see the results consult the annex IV. Then, O/W doped micelles were prepared and the DLS experiments were carried out (according to the method described in chapter II) in three surfactant/water ratios to know their size. The non-doped micellar solutions were also prepared, and their sizes were contrasted with those containing KTP. The results sizes of the micelles are presented in the Table 5-1. Regarding to the size of doped micelles, the swelling effect produced by the KTP addition is notable.

**Table 5-1.** Hydrodynamic diameter (nm) for free drug and doped micelles of KEL

KEL/W (wt %)	Non-doped	Doped with KTP
0.026	15.1	17.2
0.053	14.2	16.4
0.11	12.8	15.2

After the micellar solutions were prepared, the hybrid material synthesis from doped micelles was carried out following the method described in the chapter II. To set the basis of the release experiments, the determination of the trapped amount into the hybrid materials is fundamental ( $C_{KTP}^{mat}$ ), and as a criterion of control is important to contrast this quantity with the total drug added in the micellar solution at the beginning of the process. The method to  $C_{KTP}^{mat}$  determination is described in the chapter II. The results are given in Table 5-2. Consult the annex V for the composition of each sample

**Table 5-2.** KTP rate into the micelles and hybrid materials

KEL/W (wt %)	KTP in micellar solution (%wt)	$C_{KTP}^{mat}$ (wt%)
0.026	3.6	2.3
0.053	3.8	2.5
0.11	3.6	2.8

Subsequently, in order to determine the materials structuration, SAXS experiments were carried out with the hybrid mesoporous silica materials (noted as HM), which were later calcined (noted as CM) and characterized. Finally, the resulting SAXS spectra were contrasted with those from the materials obtained in the synthesis without KTP (noted as DF) during mineralization (Figure 5-1 A, B, C).

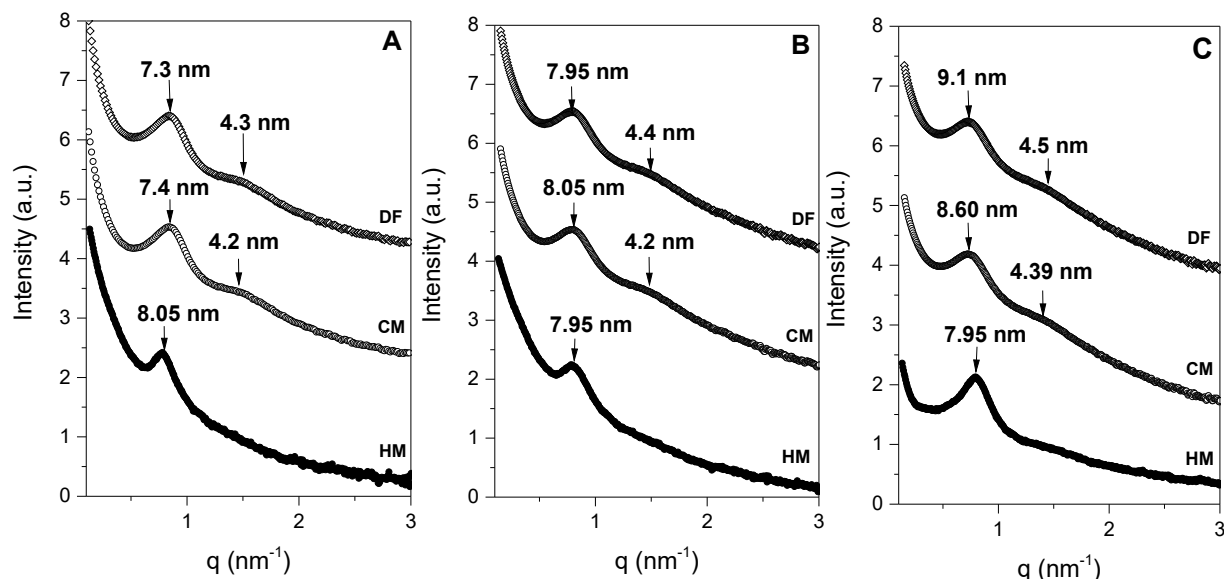


**Figure 5-1.** SAXS spectra from hybrid materials in three different KEL/W (wt%) ratios: A. 0.026 B. 0.053 C. 0.11

◇ DF Drug Free Material ● HM = Hybrid Material ○ CM = Calcined Material

The SAXS spectra showed in the Fig. 5-1 presents the organization for Drug Free material (DF), Calcined Material (CM) and Hybrid Material (HM). For the drug free materials two peaks that are characteristic of a hexagonal organization of the channels are presents, which are still appearing in the spectra for Calcined Materials and approximately in the same sizes. Concerning to the materials loaded with KTP, the second peak disappears showing a wormhole-like structure, since it exhibits only a wide peak around 8 nm. This may be attributed to the presence of the drug that probably disrupt the CTM mechanism changing the micellar structure. A shape modification from spherical to elongated objects probably result of a random channel arrangement. When micelles are too close, repulsion forces can occur causing the detriment of the hydrolyzed precursor.

In the other hand, the figure 5-2A, B shows the characterization by adsorption-desorption nitrogen of the Drug Free materials, these results note that the mesostructured silica presents a type IV isotherm, characteristic of mesoporous material. This is confirmed by the pore size distribution in a range from 4 to 6 nm. After that, the evaluation of the KTP influence over the mesostructuration was evaluated, for that the hybrid materials were calcined in order to remove the organic

phase, the further adsorption/desorption characterization was also conducted. The values of the surface area, pore volume and pore distribution for the calcined and drug free materials are given in Table 5-3.

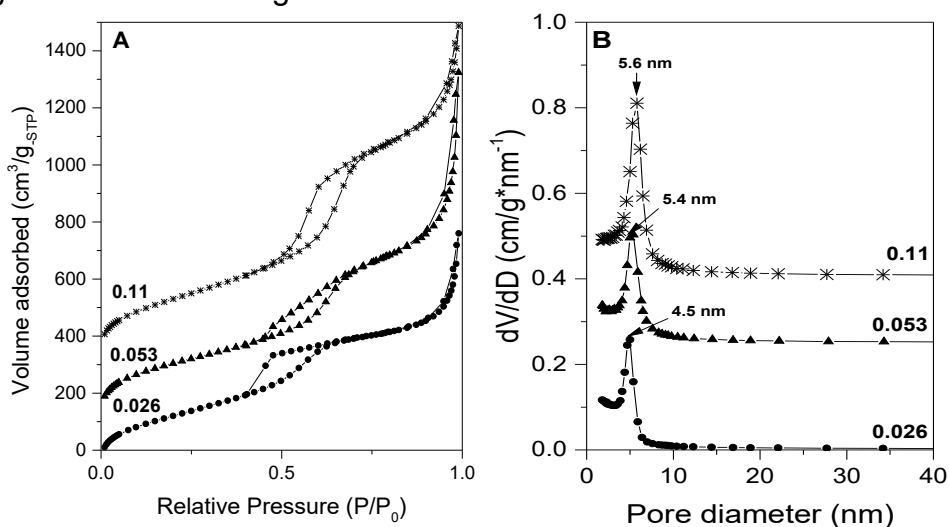


**Figure 5-2.** Nitrogen sorption isotherms (A) and pore size distribution (B) for Drug Free materials in three different KEL/W (wt%) ratios: 0.026,0.053, 0.11

The isotherms obtained from the calcined materials are shown in the Figure 3-12A. The results show a shape of the isotherm type IV with no evidence of mesoporous disruption. Previous studies as Salonen 2005, showed that the KTP loading and further eliminations didn't destructured the mesoporosity. In addition, the sharpness of the adsorption branches (located at a relative pressure around 0.5-0.6) indicates a narrow mesopore sizes distribution, characteristic of a good quality material. (Abd-Elrahmad, 2016).

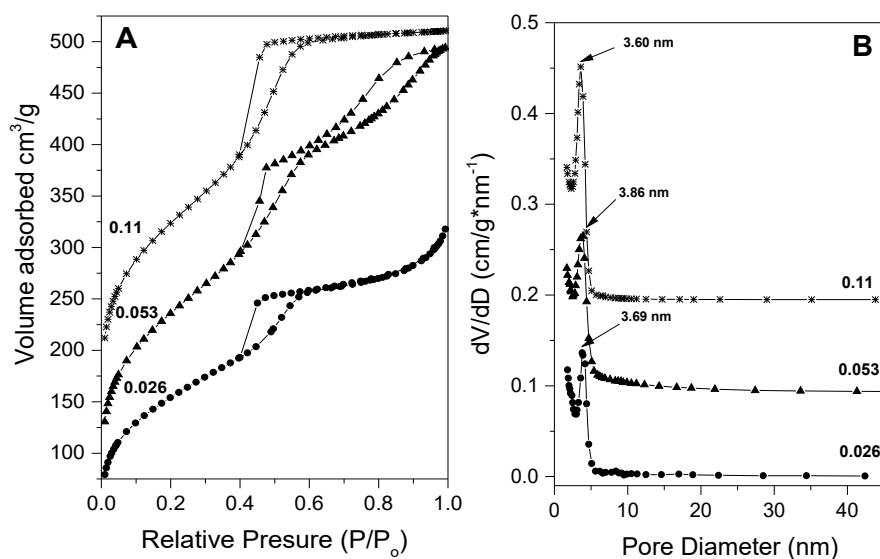


**Figure 5-3.** Nitrogen sorption isotherms (A) and pore size distribution (B) for calcined materials in three different KEL/W (wt%) ratios: 0.026,0.053, 0.11 • KEL/W = 0.026, ▲ KEL/W = 0.053, \* KEL/W = 0.11

**Table 5-3.** Surface and pore volume of free drug and calcined materials

KEL/W (wt %)	Surface area(m <sup>2</sup> /g)		Pore volume (cm <sup>3</sup> /g)		Pore distribution (nm)	
	CM	DF	CM	DF	CM	DF
0.026	615	844	0.32	1.3	3.7	4.5
0.053	823	872	0.55	0.7	3.9	5.4
0.11	868	928	0.43	1.4	3.7	5.6

## 5.2 Drug release of hybrid materials prepared from doped micelles.

In this section the KTP release from hybrid materials fabricated from micellar solutions will be explained, as well as kinetic models that can explain their behavior. Drug loading efficiency varies widely between different active principles, surfactants and reaction conditions. According to the molecule to be transported, the use of micelles has the advantage of playing a dual role, first they allow the solubilization of the active ingredient, then act as template for the formation of organized silica network. This kind of materials have the advantage of releasing their active principle at specific sites if the structure is prepared to be sensitive in the environment where it is located. It means, the active principles can be released thanks to the destabilization of the micelle under specific conditions.

In order to know the behavior of the KTP dissolution and to ensure that the active ingredient was not retained in the dialysis bag used for the release experiments, the diffusion of a solution of KTP in PBS to a PBS receptor solution was studied. The KTP concentration chosen was 0.5 mg/ml, which is lower than the maximum solubility value of this active ingredient in PBS (4.2 mg/ml). The figure 5-4 presents the effect of the dialysis bag in the release profile of the KTP. The observed tendency shows a rapid release in the first hour followed by a gradual and continuous release up to 6h, then almost the total amount of the active principle was achieved after 8 hours.

The kinetic models are based on different mathematical functions, in order to choose the model that adjust better to the release profile, one of the parameters to follow is the Akaike criterion (AIC). This criterion is an estimator of the relative quality of statistical models for a given data and provide a tool for the model selection. When a statistical model is used to represent the process that generated the data, the representation will almost never exact, so some information will be lost by using the model to represent the process. AIC estimates the relative amount of information lost by a given model and deals with the trade-off between the goodness of fit and the simplicity of the model. (Akaike, 1974). Into the model comparison the smallest AIC value must be selected to determine the model that will describe the dissolution rate.

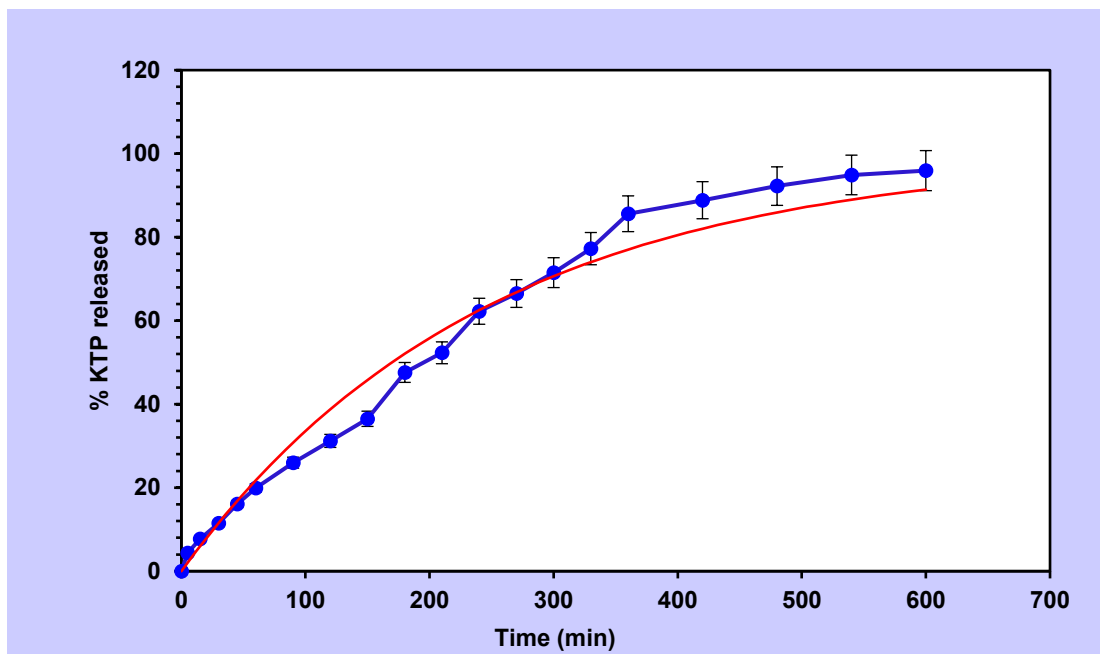


**Figure 5-4.** Release profile of KTP to evaluate the retention effect of the dialysis bag  
 • Data points      — First order model data fitting

According to the adjustment of the data ( $R^2 = 0.98$ ), the Akaike criterion (AIC) of this results (AIC = 43.04) adjust the release profile into a first order array, this was chosen over Order 0, Arrhenius, Higuchi or Weibull models which presented an AIC of 47.4, 43.4, 44.8 and 49.5 respectively. The first order model describes the release of drug from a system where the release rate is concentration dependent:

$$Q_t = Q_0 e^{-k_1 t} \quad \text{Eq. 5 - 1}$$

Where:

$Q_t$  is the amount of the drug released in time  $t$

$Q_0$  is the initial amount of the drug in the solution

$k_1 = 0.004$  is the first order release constant for this case

Despite that the application of this model is commonly used to describe the drug dissolution in pharmaceutical dosage forms such as those containing water soluble drugs in porous matrices, Ahuja, 2007 studied dissolution enhancement and this mathematical modelling for drug release in hydrophobic drugs and they demonstrated that first order model fitted well at early time periods.

This model explains that during the kinetic at early periods, the amount of the drug released is proportional to the amount remaining in the matrix, this the amount tends to decrease in function of time.

Numerous studies have been carried with the potential applications for micelles as a carrier, however when the micelles are placed in the receptor solution can act as

a solubility enhancer for the hydrophobic drugs as KTP entrapped into the silica material. Based in the hypothesis that the hydrophobic molecules can be diffused and solubilized in the core of the Pluronic micelles acting as aid release, many authors recognize the P123 as a stabilizer cage (Soussan 2009, Riachy 2016, among others).

In our study in order to explore the influence of the addition of P123 micelles in the receptor solution and to evaluate their effectiveness supporting the release of KTP, three concentrations of P123 solution were studied: 1, 3 and 5 wt% and the results were compared with the solution free of P123 micelles.

In the figure 5-5A, the results contrast the KTP release profile from the dialysis bag with the behavior of the drug trapped into the hybrid material. The amount of the drug trapped into the carrier synthesized was around 3.8%, giving a KTP/KEL wt% ratio equal to 0.075, the experiment was carried out at 25°C. To avoid any precipitation due to the acidic conditions the pH of the receptor solution was kept 7.4 and to avoid the degradation of the medicament the experiment was carried out in amber glass.

This release profiles can show that the KTP migrate into the receptor solution slowly from the material matrix. During the release experiments the receptor solution penetrate the carrier and since the micelles are embedded in the silica, the release of KTP is more difficult. Silica behaves as a barrier of the diffusion of the drug molecules, this can explain why under the same conditions a lower amount of drug is released.

In the Figure 5-5B, in all cases the results displayed a slow rate release, having less than 20% of KTP released in the first 3 hours. In the first 2h the drug release is slow, the profile increase reaching a value of 15%, then taking a stepped profile until the end of the experiment, having a final KTP release value of 38%. The effect of the addition of micelles of P123 in the PbS solution shows that the increasing concentration of P123 promotes the increasing the Ketoprofen dissolution into the receptor solution, reaching until 64% of release with 5 wt% P123 in the receptor medium. The presence of KTP in amorphous state, foresees a retained dissolution in release experiments and due to the small confined space full of active principle this can presumes a pumping effect.

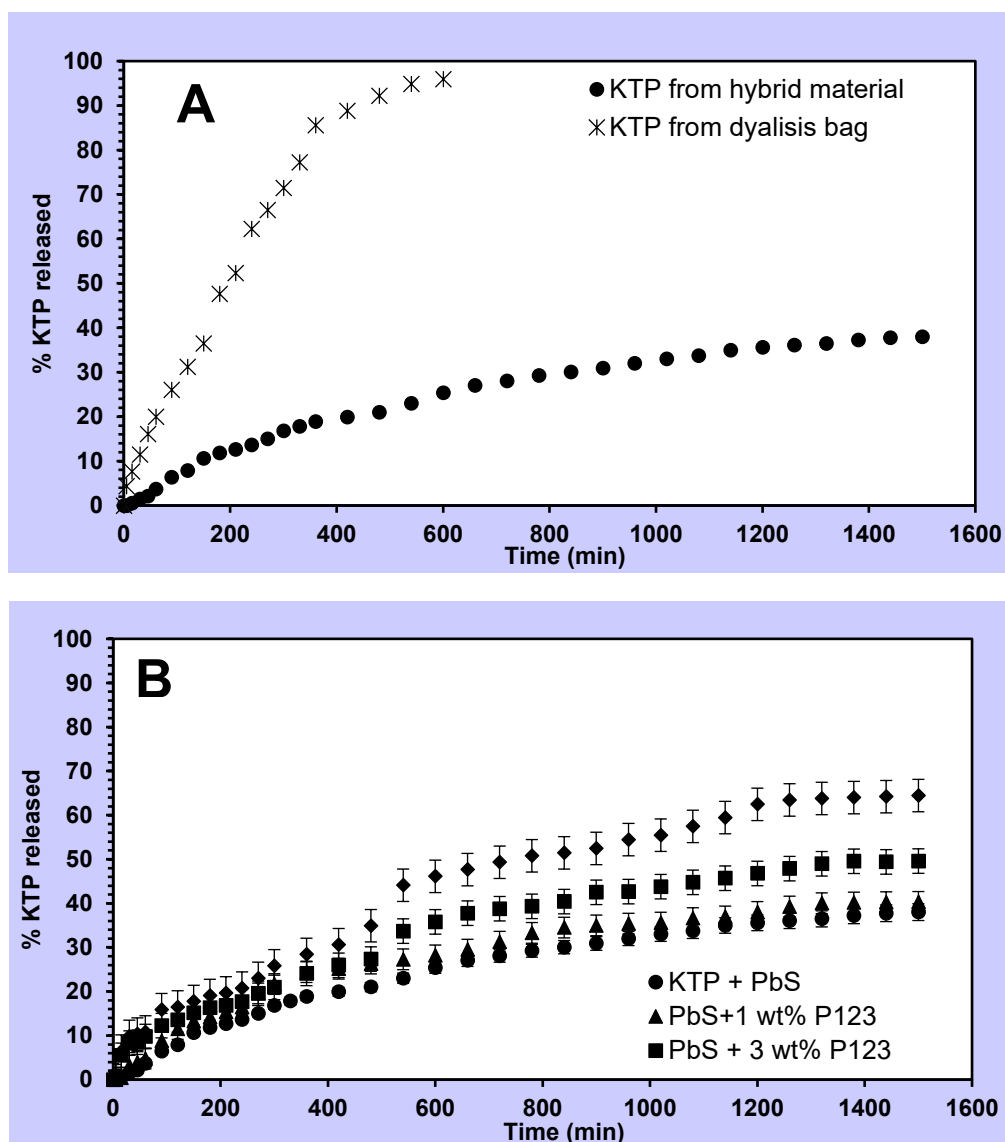


**Figure 5-5.** A) Effect of the hybrid matrix on the KTP release under the same conditions B) Effect of the addition of P123 micelles in KTP release from loaded hybrid materials KEL/W=0.053

The dissolution profile with 3 and 5 wt% of P123 shows a jump step around  $t = 540$  min, that can be related with to an experimental error. In almost all the cases, the concentration of ketoprofen continue increasing over 12h, which can presume KTP retention in the material giving rise to extended releases. The Figure 5-3 shows the mathematical model fitted for the different dissolution profiles of KTP under the influence of P123 micelles. And the Table 5-4 gives the parameters of each experiment.

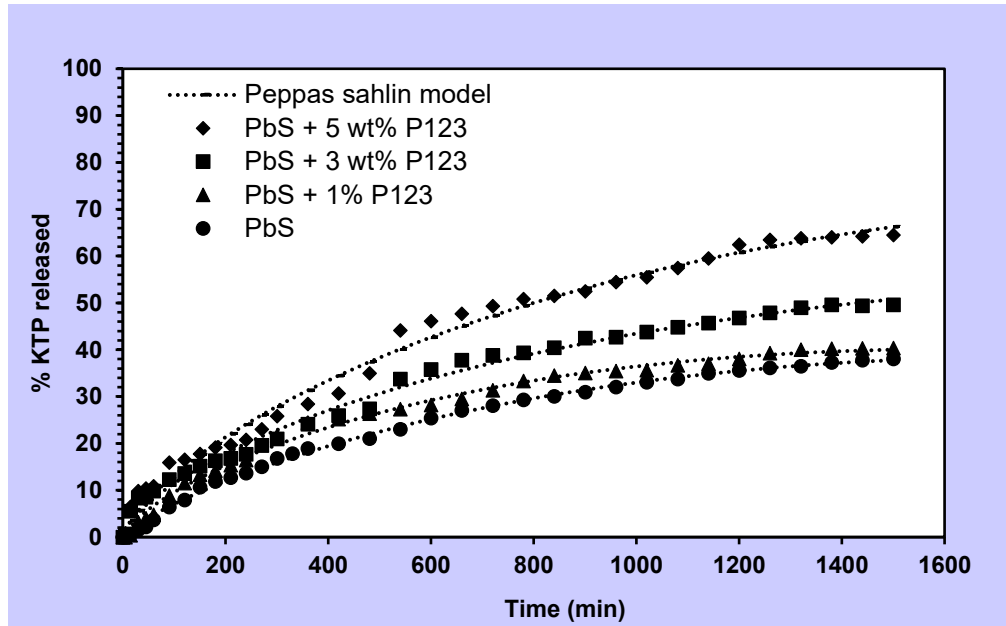


**Figure 5-6.** Experimental KTP release curves from hybrid materials prepared with micellar solutions KEL/W=0.053 under the effect of the addition of P123 in the receptor solution and their corresponding mathematical model adjustment.

**Table 5-4.** Peppas Sahlin parameters for KTP release under the effect of P123 micelles from hybrid materials based on KEL/W micellar solutions

P123 wt%	% KTP released	Parameters				
		$k_1$	$k_2$	$m$	$R^2$	AIC
0	38	0.179	0.01	0.81	0.997	95.8
1	40	0.346	-0.001	0.74	0.996	89.5
3	49	0.521	0.001	0.68	0.992	49.9
5	64	0.477	0.001	0.73	0.989	79.6

In the case of absence of P123 micelles, the maximum value of release reach 38%, this value can be attributed to the slow solubility of KTP. The release in presence of P123 micelles into the receptor solution, the model of Peppas-Shalin is the expression to describe the active principle release that can be written in terms of fickian diffusional combined with a relaxational one phenomena. The general form of this expression is:

$$F = k_1 t^m + k_2 t^{2m} \quad \text{Eq. 5 - 2}$$

Where:

$k_1$  is a constant that describes the controlled release process by diffusion

$k_2$  is a constant which explains the release from the structure

$m$  is the diffusion exponent that determines the release mechanism trough the solvent penetration. When  $m=0.5$ , the drug release mechanism is Fickian diffusion.

When  $m=1$ , transport occurs, leading to zero-order release. When the value of  $m$  is between 0.5 and 1, anomalous transport is observed. (Nikolaos, 1993)

Thanks to this Peppas-Shalin model several complicated systems can be explained due to the particularity that the geometric shape and aspect of the delivery device are independent. This model is an adaptation of the model Peppas-Ritger which was employed to explain the release from polymeric matrixes, so then, after being adapted this allowed to explain the coupled effects of Fickian diffusion and transport. It is observed that the influence of the matrix has a significative effect on the KTP release, as the constants remain at the same value. However, for the experiment with 5% P123, the diffusion constant ( $m$ ) confirm a slower dissolution and the release constant ( $k_1$ ) indicate a less controlled process than those performed in the sample at lower concentrations of P123. This can be attributed to the enclosed pores of the silica matrix, which contains a close relationship between the micropores allowing a very little contact of the receptor solution and the KTP, promoting the molecule diffusion and the solubilization in the P123 micelles. Concerning the pH effect, the releases under acidic conditions (pH 1,2 and 4,6) were evaluated and compared with the solution at neutral pH. The investigation of these pH values allows to simulate the conditions of the drug release experiment though the gastrointestinal tract and stomach reactions. The results are shown in the Figure 9 and the parameters that describe each model in the Table 5.

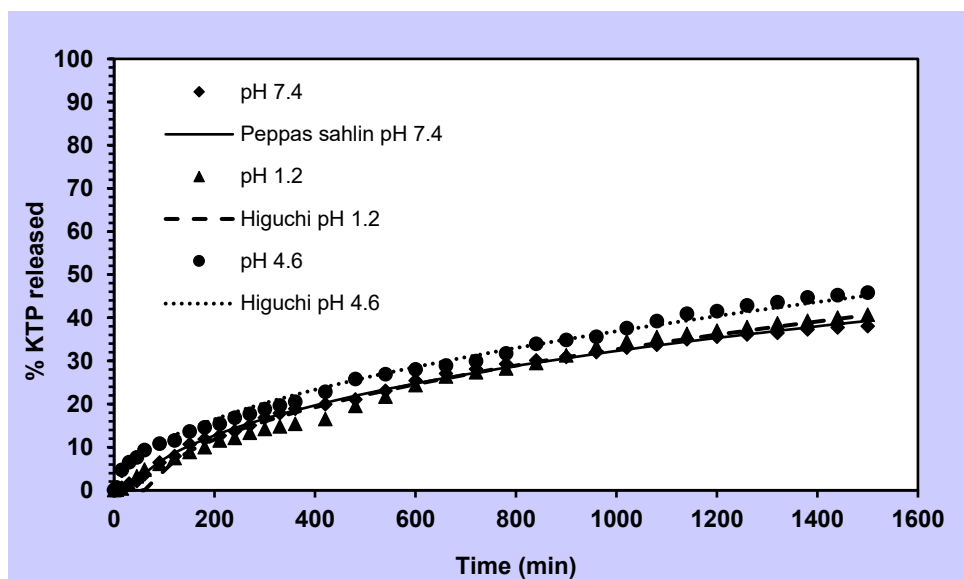


**Figure 5-7.** Effect of the pH in KTP release from hybrid materials  $K/W=0.053$  and adjustment of their mathematical models

**Table 5-5.** Parameters of the fitted models for KTP release under pH effect

pH	Model	% KTP released	Parameters		
			kH	R <sup>2</sup>	AIC
7.4	Peppas Sahlin	38	--	0.99	95.8
1.2	Higuchi	41	1.07	0.98	62.3
4.6	Higuchi	46	1.17	0.99	28.3

The results shown that KTP release is favored under acidic conditions, giving a higher percentage of release compared with the neutral pH. Indeed after 5 hours of release the amount increase from 17 to almost 21% when the pH is decreased from 7.4 to 4.6. The lowest value, 38%, is obtained with a PbS solution. These results are unexpected because considering the KTP pKa which is around 4.4-4.6 (Tsume, 2012), the opposite would be expected. Similar effect was observed previously in other researches with mesostructured nanocarriers (Riachy, 2016). However, considering that the release profile is homogeneous under acidic conditions and regarding to the conditions of the hybrid matrix, the Higuchi model was fitted to explain the evolution. This model explains that the drug release process occurs only through Fickian diffusion and is commonly found in systems with hydrophobic constituents.

This model can explain the matrix system considering that the initial drug concentration in the matrix is much higher than the drug solubility, and considering that the  $C_{KTP}^{mat}$  in this case is around 2.5 wt% could confirm this hypothesis, giving guidelines to explain that the diffusion of the KTP occurs only in one dimension due to the thickness of the KTP that must be much smaller than thickness of the material. (Ramteke, 2014)

This model can confirm also that the swelling of matrix and its dissolution is less or negligible. The most important characteristic attained with this model is that the drug diffusivity constant (kH, Higuchi dissolution constant) is almost similar in both acidic pH which is based on the Fick's law explaining that the perfect sink conditions are always attained in the release environment. This relation is valid during all time of the experiment, except when the saturation of the release medium is achieved (Minhaz, 2010).

Higuchi considers also the porosity of the matrix, explaining that the cargo must be attached to the channels or pores in order to branch them, resulting in small spaces free of active principle from which liquid penetrate inside for the release of KTP from a granular matrix. Since the type of material offers enclosed pores, the water intake is limited inside of the channels and the possible explanation of the release increasing is the ionization of KTP in acidic conditions. This can be assured thanks to the results obtained from the adsorption-desorption nitrogen graphs (Fig.

5-3B) where the organic ligands resulted in the pore blocking giving rise to primary micropores (Shoaib, 2006).

### 5.3 Doped hybrid mesoporous materials characterization prepared from fine emulsions (Em)

In this section we propose the evaluation of the release mechanism of hybrid materials prepared from fine emulsions (Em), containing around 2-3 wt% of KTP in the final preparation as is recommended for commercial formulations. The preparation method about this type of doped hybrid materials is described in Chapter II.

The three mass ratios to prepare the doped emulsions were chosen according with the ternary phase diagram obtained from Mig/KEL/Water system (Chapter III). As for not doped ones, the doped fine emulsions at the end of the preparation are optically transparent having a bluish aspect, previous research indicates that this aspect is related to the size of the drop.

Results are gathered in Table 5-6. The results indicate an increase in size of the non-doped emulsions, with a variation on the surfactant content. Then, compared to doped emulsions, the effect of KTP dissolution increases notably the size.

**Table 5-6.** Hydrodynamic diameter (nm) for drug free and doped fine emulsions (Em) at 25 °C  
*All the emulsions have 80 wt% of water*

Mig/KEL (wt%)	Non-doped Em	Doped Em
0.25	20	38
0.43	28	42
0.66	80	120

Karami, 2019 suggest that the KTP molecule is bound by electrostatic forces to the oil molecule and this in turn, adsorbed in the surfactant to form a film that defines the structure of the nanoemulsion, which is susceptible to deformation due to an increase in its hydrodynamic diameter. This phenomenon makes the diffusion of large amounts of drugs vulnerable to external *stimuli*, which may explain why nano-emulsions are considered one of the most promising fast-absorbing drug delivery systems.

After the size of hydrodynamic diameter was determined, the hybrid materials must be fabricated. To that the synthesis method is explained in the chapter II. To develop these nanocarriers our method consists in incorporating the drug into the

material synthesis. For this purpose, the doped fine emulsions Em were used as a template and the source of silica polymerize around the Miglyol drops and interact with the KTP. This method will allow also to entrap a high amount of KTP. The Table 5-7 shows the KTP amount added into the Em and the KTP determined by HPLC in the hybrid materials. Consult the annex V for the composition of each sample

**Table 5-7.** KTP rate into the fine emulsions (Em) and hybrid materials

Mig/KEL	KTP in fine emulsions (%wt)	$C_{KTP}^{mat}$ (wt%)
0.25	3	2.4
0.43	3.8	3.5
0.66	3.5	2.8

Bergman 2014, highlight the importance of the physicochemical properties of the drug, because they notes that the drug loading inside of the template, specially emulsions, can provide means of sustained release in order to maintain the drug concentrations into an acceptable window which make them suitable for a therapeutic treatments. Following this strategy, the preparation method was done as in the chapter II and the final materials were characterized by SAXS and the results are show in the Figure 3-29 and for adsorption/desorption nitrogen in the Figure 5-5.

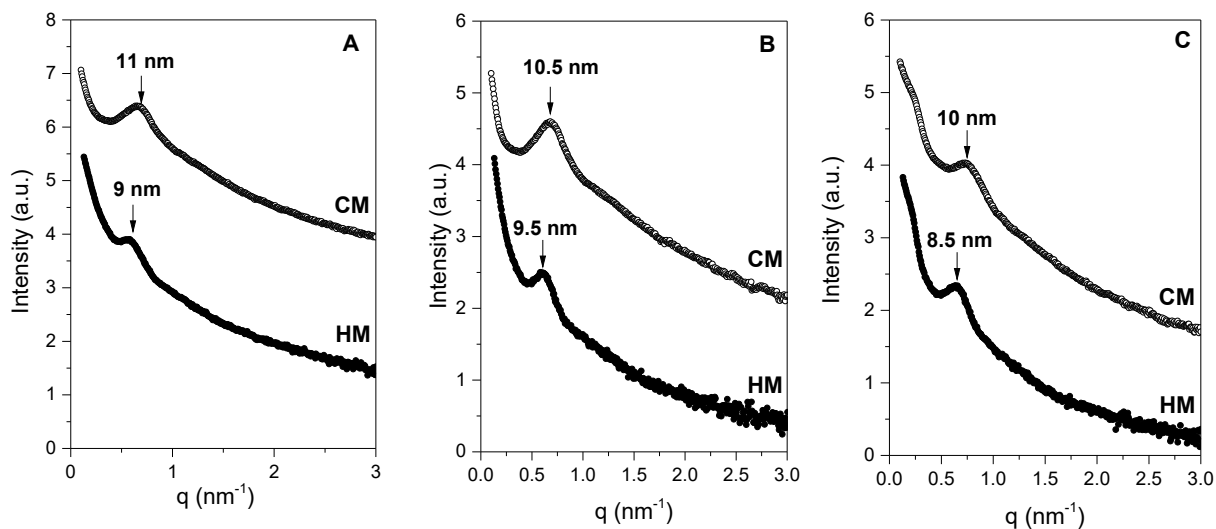


**Figure 5-8.** SAXS spectra of the materials from fine emulsions (Em) in different Mig/KEL ratios and 80 wt% water in all cases

A. 0.25 B. 0.43 C. 0.66

● **HM** = Hybrid Material ○ **CM** = Calcined Material

After mineralization of Em, the SAXS spectra (Figure 5-8) present a smooth peak between 8-9 nm for the hybrid materials. In order to confirm the structure of the bare silica as holders, after their obtention, these were calcined under synthetic air at 150, 350 and 550°C with an increment of 2°C/min and with 1h of plateau in the attained temperature.

The SAXS results spectra in the calcined materials a peak between 10-11 nm. In the case of loaded materials, the results put in spotlight a wormhole-like organization structure, probably due to the perturbation with the micelles of the CTM mechanism caused by the intrusion of KTP.

In the other hand despite of the sharp peak in the SAXS pattern of the drug free materials, the absence of the latter peaks reveals a disordered structure with probably an interconnected channels, which is more evident at higher oil/surfactant ratios where it is possible that the template is not well covered by the hydrolyzed silica precursor and the condensation is not complete, leading a less ordered structure.

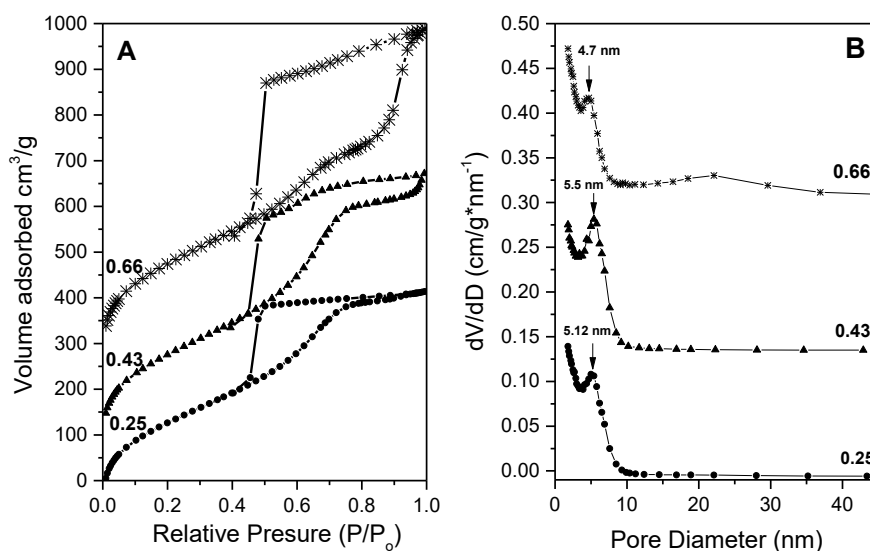


**Figure 5-9.** Nitrogen sorption isotherms (A) and pore size distribution (B) of the calcined materials prepared from fine emulsions (Em) in three Mig/KEL ratios and 80 wt% water in all cases

● Mig/KEL = 0.25, ▲ Mig/KEL = 0.43, \* Mig/KEL = 0.66

Figure 5-9 shows the results of hybrid materials after a calcination process, in these can be observed type IV isotherms where the values of surface area and pore volume are quite large (Table 5-9). Lu et al 1999 suggest that on this type of synthesis the percolation phenomenon is very common, which implies that the template is randomly dispersed generating small pores and after calcination the appearance of macropores is evident, without collapsing. The size of the

macropores may be related to the size of the template, which is influenced by the participation of the KTP, although it may also be due to inter-porosity.

**Table 5-8.** Characteristics of calcined materials prepared from fine emulsions (Em) in different Mig/KEL ratios and 80 wt% of water

Mig/KEL (wt%)	Surface area (m <sup>2</sup> /g)	Pore volume (cm <sup>3</sup> /g)	Pore distribution (nm)
0.25	911	0.72	5
0.43	943	1.13	5.3
0.66	1015	1.33	4.7

#### 5.4 Drug release from loaded hybrid materials prepared with fine emulsions (Em)

In this section we describe the release of the KTP from the hybrid materials synthesized from fine emulsions. After being characterized in the section 5.2, the materials were tested under different conditions: first into a receptor PbS solution at pH 7,4, then in acidic conditions at pH 4.5 and finally into PbS receptor solution with three different concentrations of P123 micelles: 1, 3 and 5 wt% in neutral conditions. The Figure 12 shows the release of KTP in the PbS solution at pH 7.4 as well as the effect of the addition of P123 micelles into the receptor solution.

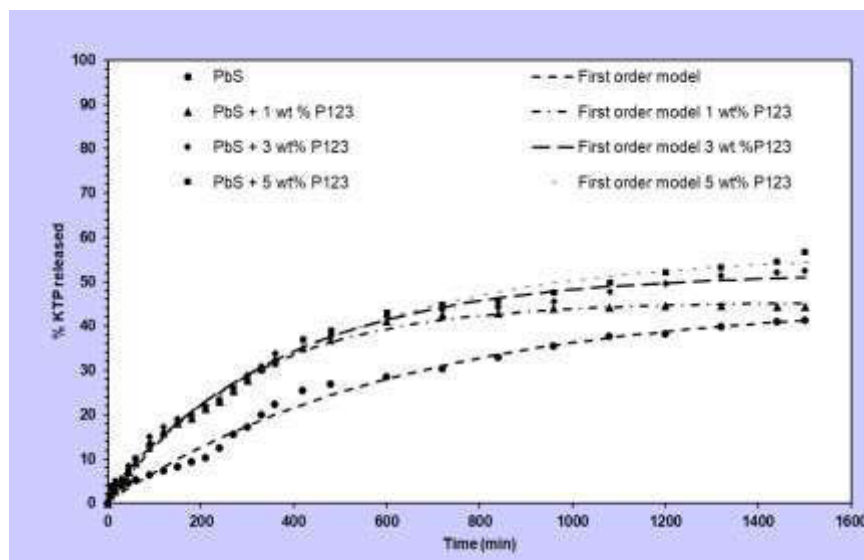


**Figure 5-10.** Experimental curves of KTP release from hybrid materials prepared with doped fine emulsions (Mig/ KEL = 0.43) in function of the P123 amount into the receptor solution and the fitted mathematical models of the release.

The KTP dissolution in the P123 assisted receptor solution can be described by the first order model, which describes well the solubility phenomena for poorly water-soluble drugs at early periods of time. Therefore, many adaptations have been done to this model in order to explain the parameters that can describe better the results.

The dissolution phenomena of a solid particle in liquid media can be described by the first order model, which at short times can work better than Hixon Crowell and zero order model. (Ramteke, 2014) The table 5-9 list the parameters of the fitted model for the KTP released from the hybrid material considered.

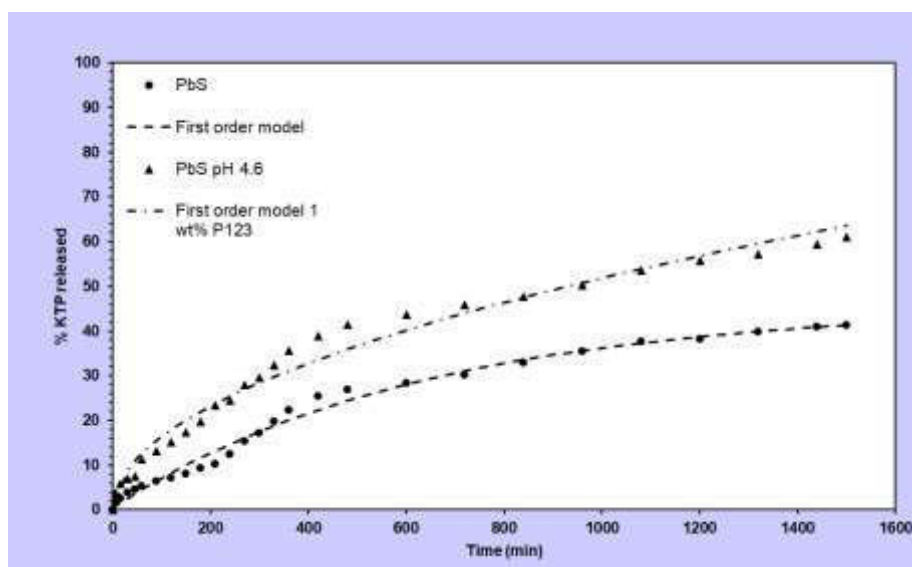


**Figure 5-11.** Experimental curves of KTP release from hybrid materials prepared with doped fine emulsions (Mig/ KEL = 0.43) in function of the pH of the receptor solution and the fitted mathematical models of the release

**Table 5-9.** Parameters of fitted models

Condition	% released	R2	K <sub>1</sub>
PbS pH 7.4	41	0.99	0.002
PbS pH 4.6	61	0.98	0.003
PbS 1% P123	44	0.98	0.002
PbS 3% P123	52	0.99	0.004
PbS 5% P123	57	0.98	0,003

In the Table 5-9 shows the percentage of KTP released under different concentrations of P123, having an amount from 41 % until almost 60% with the maximum concentration of the micelles. It is possible to observe that the curves of

the experimental data show an attained release, where the released concentration is proportionally constant.

This materials could means a good nanocarrier to carry out a sustained release in order to maintain a drug concentration within a therapeutic window. One way to adjust the release profile is using molecular gates attached to the pore entrances or inside the pores themselves, which can be triggered by an external stimulus. Other factor affecting the release profile is the particle pore size. Moreover, the physical state that the incorporated drugs holds amorphous, crystal or a combination has an influence on the drug dissolution rate.

### 5.5 Rheological characterization of the doped concentrated emulsions from the system KEL/Mig/Water

Concentrated and highly concentrated from the system Kolliphor EL (KEL), Miglyol 812N (Mig) and water (W) containing 70 wt% (CE70) and 90 wt% (CE90) of Miglyol were rheological studied (Figure 3-18). The concentrated emulsions present a viscoelastic behavior that depend of the amount of dispersed fraction, considered from 84%. This is due to the tightly packed liquid droplets that form resistant liquid films between themselves (Babak,2002). The doped samples were contrasted with the non-doped ones to determine the viscoelastic and structural characteristics of each for that the rheological process is described in the chapter II. The results from this section will serve as background in the evaluation of this systems as a drug carrier.

The aging time: AFM, 24h and 1week into the analysis was also a crucial point. The doped emulsions with KTP are noted as: CE70\_KTP and CE90\_KTP. The drug free and loaded samples were prepared according to the process described in the Chapter II. The compositions are showed in Table 3-5.

**Table 5-10.** Composition of concentrated emulsions for rheology experiments KEL/water = 0.18 (w/w)

<b>Formulation</b>	<b>Mig<sub>total</sub> (wt %)</b>	<b>KTP<sub>final</sub> (wt %)</b>
CE70	70.6	--
CE70_KTP	68.0	2.1
CE90	90.0	--
CE90_KTP	88.0	2.0

The figure 3-22A, shown the comparison of the viscoelastic behavior of drug free and doped concentrated emulsions with 70 wt% of Mig AFM. When the rheological properties of a viscoelastic material are independent of strain up to a critical strain level the material behavior is linear. Beyond this critical value, the material behavior is non-linear and the storage modulus (G') declines.

The sample free of KTP, keep the storage modulus ( $G'$ ) only in the first decade, that can presume that the sample will flow with minimum efforts, having a critical strain about 0.005-0.007 after that the loose modulus  $G''$  dominates, which can presume the slow resistance of the sample for the ceding efforts, presenting a fluid-like behavior. In the other hand, the sample loaded with KTP has a critical strain of 0.01%, below this value the material behaves solid-like and  $G' > G''$ , indicating that the material has a high resistant to the yielding forces. Increasing the strain above the critical value, the network structure is disrupted.

The figure 3-22B and C presents the images from microscope of the drug free and doped concentrated emulsion respectively. It is possible to note an increase in the apparent diameter for the sample loaded with KTP compared to the drug-free sample.

Considering that oil in water concentrated emulsions require a water-soluble surfactant, the stability of the emulsion is linked also to the structure of the continuous medium which is into the micellar solution, that in the same time depends of the chemical nature components and to the interface created between them and the dispersed phase. (Babak, 2002).

When the material becomes progressively more fluid-like, the module declines and  $G''$  normally exceeds  $G'$ . The strength of the colloidal forces is reflected by:

$$\tan \delta = \frac{G''}{G'} \quad Eq. 5 - 3$$

Where:

$\tan \delta < 1$  suggest that the colloidal forces are strong

$\tan \delta > 1$  suggest that the particles into the system are largely unassociated.

For a stable system an intermediate  $\tan \delta$  is desired. From the reported results in figure 3-22A, the colloidal forces ( $\tan \delta$ ) of the samples were evaluated from their values of the modulus ( $G'$  and  $G''$ ) on their critical strain point. These values are showed in the Table 3-9. The higher value of  $\tan \delta$  can explain the increased stabilization of the loaded concentrated emulsion.

**Table 5-11.** Strength of colloidal forces for drug free and loaded after-making concentrated emulsions

Formulation	$G'$ (Pa)	$G''$ (Pa)	$\tan \delta$
CE70	3.5	3.6	1.03
CE70_KTP	7	3.9	0.56
CE90	21	47	2.24
CE90_KTP	35	71	2.03

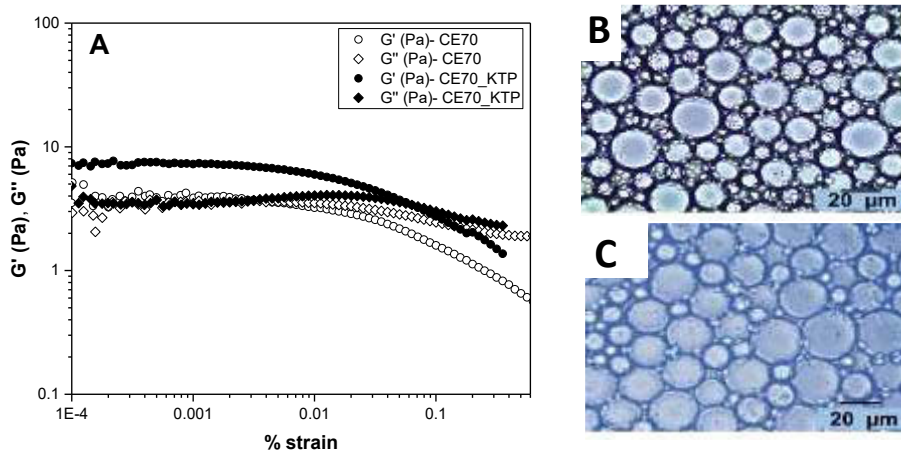


**Figure 5-12.** A) Comparison of experimental data for viscoelastic behavior between drug free and loaded after-making concentrated emulsion with 70 wt% of Mig B, C Microscope Optical image for the samples CE70 and CE70\_KTP, respectively

The fluid's linear viscoelastic region was defined. Its structure can be further characterized at strain values below to the critical one (0.010%) for the doped samples. This provide more information about the effect of the colloidal forces and the interaction among droplets. In the figure 3-23, the data shows that  $G'$  and  $G''$  behavior increase in the window of the low frequencies, while for high ones (from  $100 \text{ rad s}^{-1}$ ) is often nearly independent having always a drop of the elastic profile.

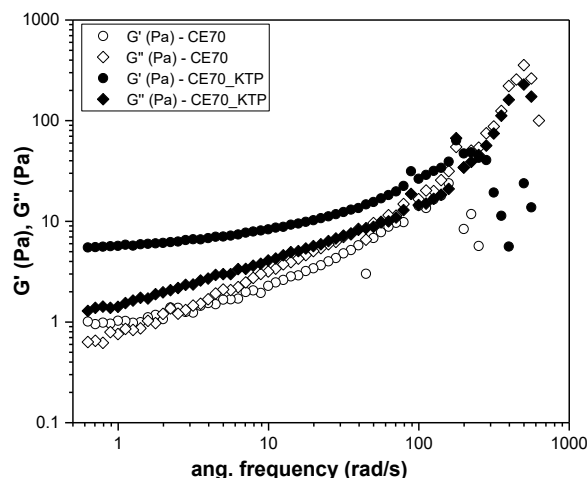


**Figure 5-13** Effect of the drug addition in the structural properties for drug free and loaded after-making emulsions with 70 wt% of Miglyol

For the sample CE70 the storage modulus ( $G'$ ) keeps below to the loss modulus ( $G''$ ) at small and high frequencies probably due to a large separation between drops, therefore is easy to make it flow with less effort. The more frequency dependent the elastic modulus is, the more fluid-like is the material. In contrast, the sample CE70\_KTP which maintains the energy storage module ( $G'$ ) above the viscous module ( $G''$ ), making it necessary to apply high angular frequencies values

to make it flow. Concerning the aging, the Figure 3-24A show the viscoelastic behavior of the drug free CE70 where we can constate that the linear region decreases from 0.003 to 0.002 % strain when the aging time goes from AFM to 1 wk. The  $G''$  overlap  $G'$  in short deformation periods to eventually fall into the elastic profile being surpassed by its viscous part.

This may be attributed to the high polydispersity of the sample regarded to the drop size (Table 3-10) and morphology. As they are very large droplets, it is hypothesized that under certain mechanical conditions: long resting times or high deformation stresses, the sample will end up separating because the inter-droplet forces are not strong enough to maintain the elasticity behavior.

**Table 5-12.** Droplet size ( $\mu\text{m}$ ) of the concentrated emulsion in the aging

Time	CE70	CE70_KTP	CE90	CE90_KTP
t=0	37	20	13	12.4
24h	30	21	12.8	12
1 week	25	24	12.3	10

The figure 3-24 B,C,E,F shows the picture of the sample drug free CE70. The big size of the apparent diameter of the droplets (about 37  $\mu\text{m}$ ) denotes big size droplet that can justify the drop of the elastic profile behavior at the 0.003 %strains (Table 3-11). In all cases, the elastic profile prevails over the viscous one, however the linear region is limited before to the first decade having a viscous predominance at low efforts predicting coalescence. In the case of doped samples, the elastic profile remains constant in time, predicting good stability of the emulsion.

**Table 5-13.** Values of %strain for the elastic modulus in the aging

Sample	AFM	1 week
CE70	0.0025	0.003
CE70_KTP	0.007	0.01
CE90	0.003	0.002
CE90_KTP	0.004	0.0035

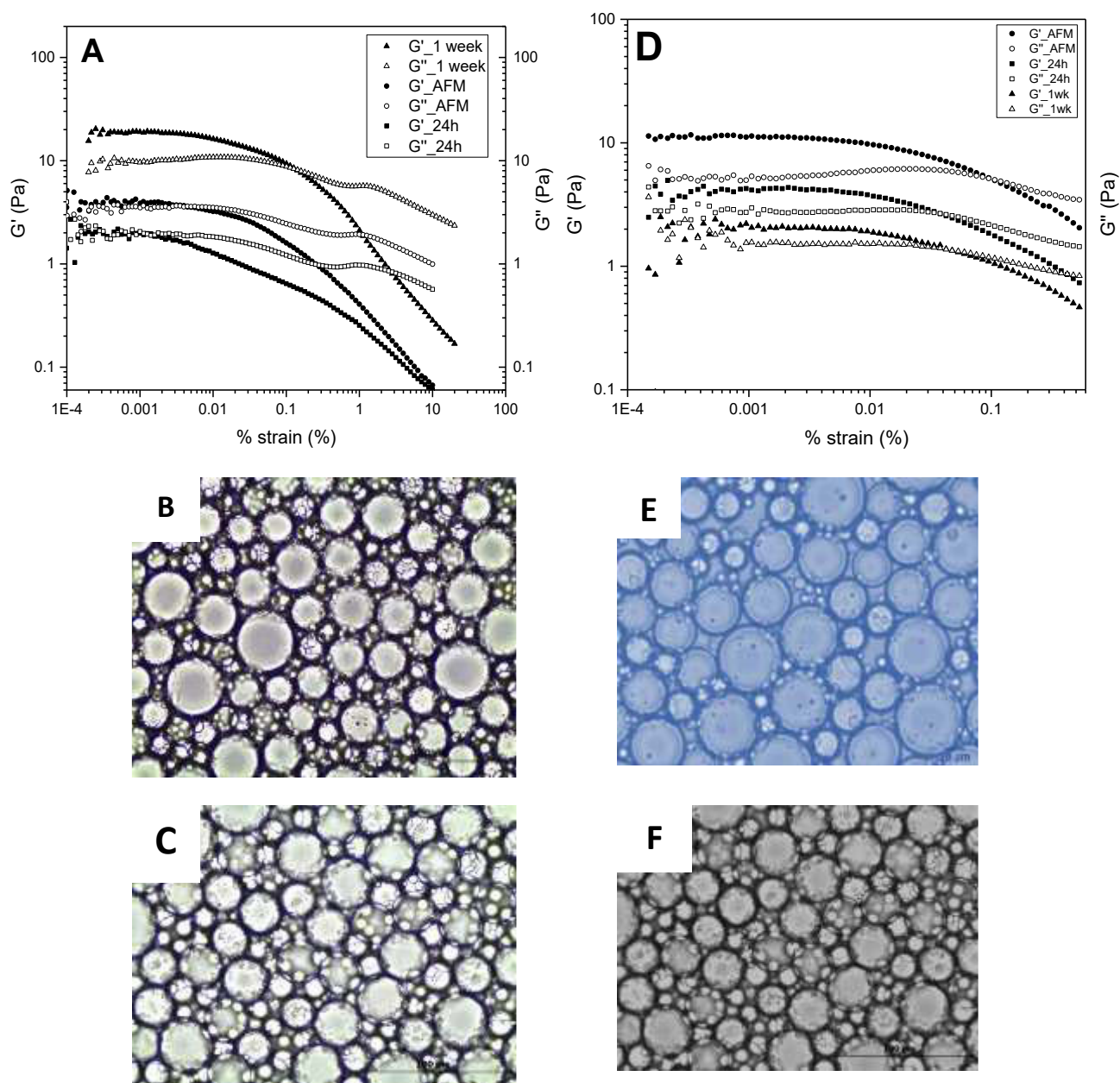


**Figure 5-14.** Effect of the drug addition in the viscoelastic profile for CE70 in function of time

- A.** Viscoelastic profile for CE70 at 24h and 1 week aging
- B, C** Microscope Optical Image for CE70 at 24h and 1 week aging respectively
- D.** Viscoelastic profile for CE70\_KTP at 24h and 1 week aging
- E, F** Microscope Optical Image for CE70\_KTP at 24h and 1 week aging respectively

The Figure 3-24D exhibit the viscoelastic profile for drug loaded CE70 at 24h and 1-week aging. We can constate that the 1-week aged sample shows a drop in its viscoelastic behavior with respect to the sample aged 24h. However, the zone of linear visco-elasticity is maintained for almost three decades, showing more stability to high strain percentage. In both aging times the elastic component remains above

the viscous, presenting an inflection point almost at the same time, about 0.03% of strain. In the Figure 3-24E and F it is also observed that the droplet size is significantly reduced compared with the KTP free samples.

In the figure 18 we can observe that the viscoelastic profile is highly sustained for almost 3 decades in the sample 1week aged, where the elastic component is always over de viscous one. This result notes that this emulsion is stable to the coalescence. Care should be taken in analyzing the rheological results. Coalescence is usually followed by a reduction in the viscosity of this type of emulsion. Ostwald ripening should be considered in the analysis of the rheological data.

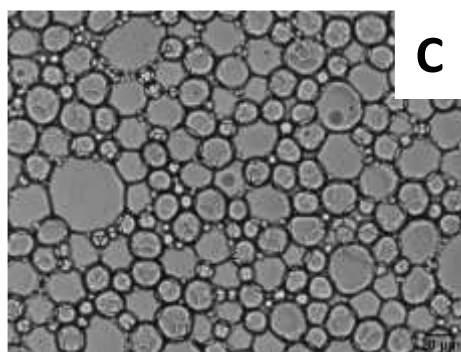
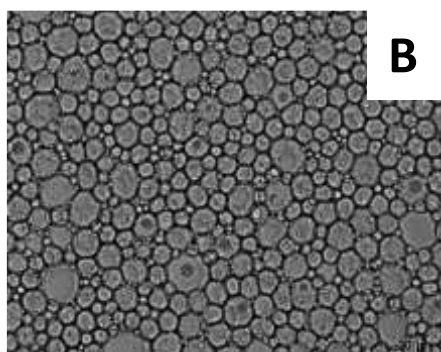
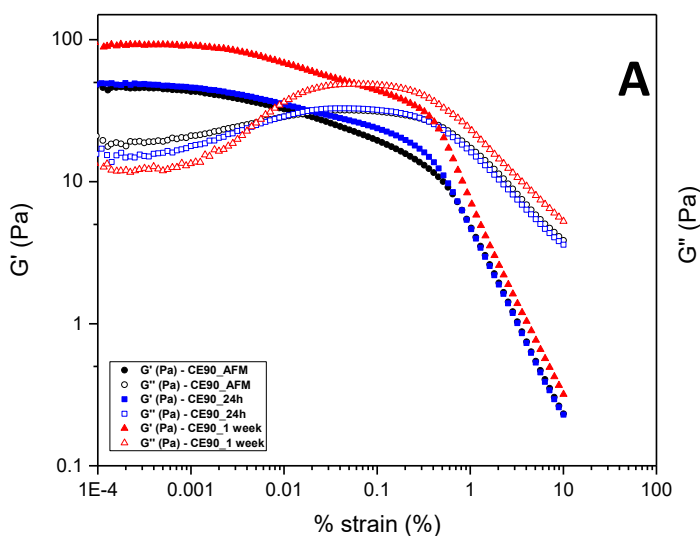


**Figure 5-15** Aging effect for CE90  
 A. Viscoelastic profile for CE90 at through the time  
 B, C Microscope Optical Image for CE90 AFM and 1 week aging respectively

This parameter can be confirmed with the structural properties of the sample, which are showed in the Figure 3-26, where It is possible to see that the elastic modulus is over the viscous one, giving to the sample an elastic characteristics in all the frequency range covering several orders of magnitude. This kind of elastic profile is promoted for those materials that are considered as elastic ones, giving the chances to keep the structure despite the high frequencies. In the Figure3-27A,B the effect of the aging over the viscoelastic profile and structural parameters of the high concentrated emulsion is reported respectively.

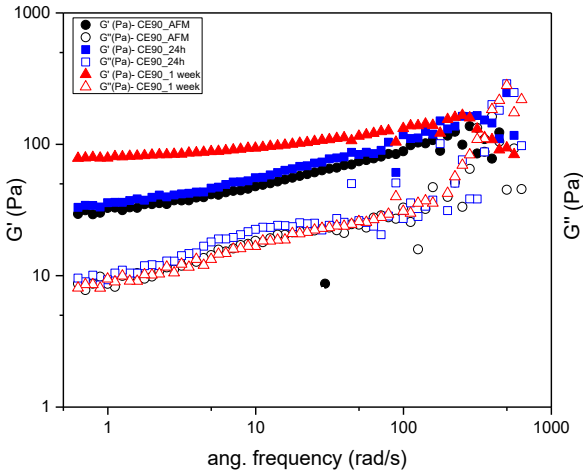


**Figure 5-16** Aging effect for drug free CE90 over its structural properties

In the Figure 3-27B we can constate the elastic modulus is constant in a very wide frequency range covering several orders of magnitude. Such kind of behavior is standard for ideal elastic materials, the elastic modulus of which must be independent of frequency.

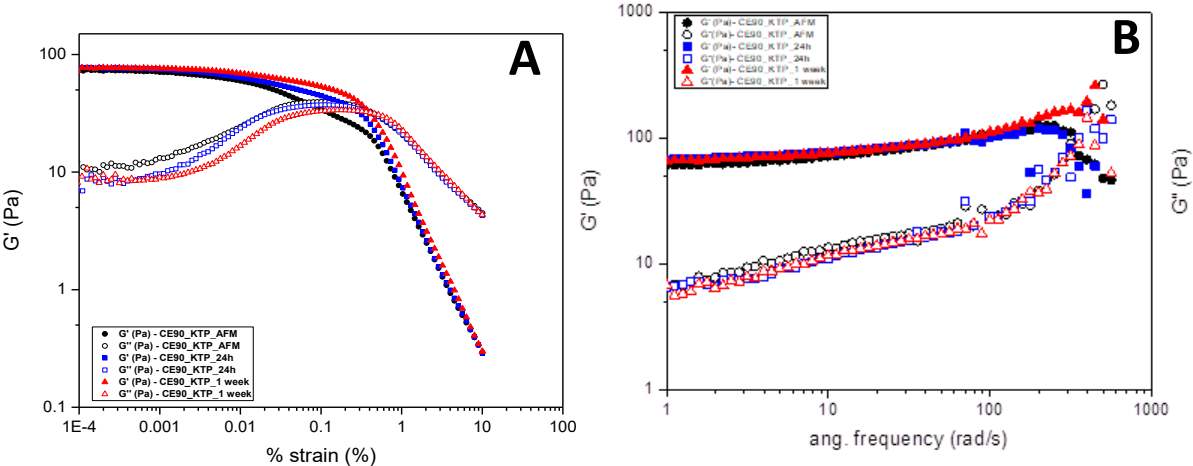


**Figure 5-17** Aging effect for CE90\_KTP over its structural properties  
A) Viscoelastic profile B) Structural properties

**Table 5-14.** Results of the fitted models for concentrated emulsions

Sample	AFM	1 week
CE70	0.0025	0.003
CE70_KTP	0.007	0.01
CE90	0.003	0.002
CE90_KTP	0.004	0.0035

## 5.6 Drug release from loaded concentrated emulsions

In this section, the study of the KTP release from highly concentrated emulsions will be explained. The  $C_{KTP}^{mat}$  determination the protocol was followed under the same conditions as for materials, view chapter II, the difference is the physical form of the material, from solid to cream. In the previous section it was demonstrated that the addition of oil in a surfactant-water system allows a high incorporation of hydrophobic active principles. As much as the amount of oil increase, the capacity to enlarge the concentration of the active ingredient is acquired. A good example of this type of formulations are concentrated emulsions, which have been studied in our group for several years, establishing the characteristics according to the concentrations and types of mixtures. In this section, the highly concentrated emulsions contain around 2.5% of KTP in the final formulation (view chapter II) and the conditions to release were respected as for the previous experiments. Two batches of concentrated emulsions with a dopped oil content of 70 and 90 % were tested, the KTP release from this system attends not just to its solubility, but also to the viscoelastic and structural properties of the carrier. In the figure 5-18, the results of KTP release from concentrated emulsions at two different oils concentrations into PbS receptor solution is observed. The sample CE\_70KTP

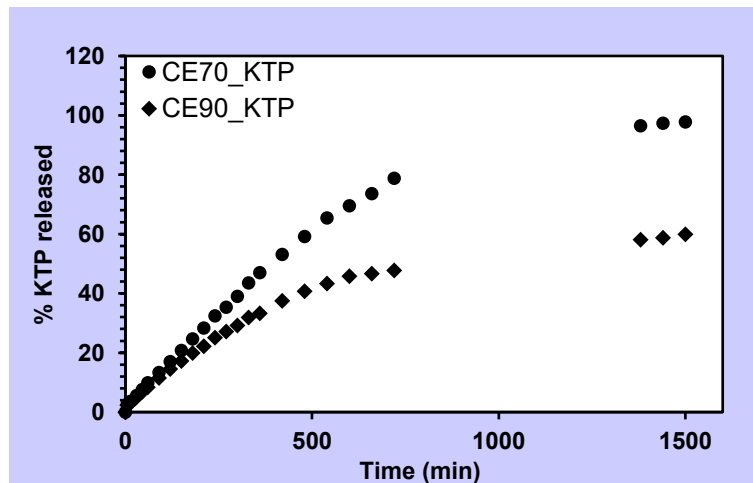


**Figure 5-18.** Experimental curves of KTP release from concentrated emulsions KEL/W= 0.17+ ● 70wt% Mig and ♦ 90wt% Mig in PbS as receptor solution at pH 7.4

The results showed a 97% of released drug from the sample prepared with 70%wt of Mig after 24h of experiment. In contrast with the sample at 90 wt% of Mig showed a release of 60%. The profiles observed were similar in the same cumulated time, assuming that the drug diffusion occurs in one sense. As the diffusion is the main mechanism, the Fickian equation is used to represent the drug amount released in the referred conditions. According to the results presented in the section 5.5, the surface and inter-drop contact is important to describe the release.

In the case of the emulsion containing 70 wt% Miglyol, it has released 80% of the KTP at 12 hours, while the sample containing 90wt% has not even reached 50%. This may be due to disturbance of the emulsion structure and progressive release of KTP. In the experiment the drug flows through the oily phase of the emulsion and the dialysis pouch, as its concentration decreases inside the system the equilibrium appears.

In the case of the emulsion containing 90wt% Miglyol, its resistance to drug release is evident. This can be explained through its structural characteristics where its viscous appearance predominates. The influence of droplet size on viscosity was investigated by Pal 1996 who showed that the viscosity of smaller droplets is greater than that of larger droplets in the same volume fraction. The small droplets are so close between themselves that they do not permit high amounts of KTP diffuse through the boundaries. Other effect that may be causing the retention of KTP inside of the system is that the sample It's piling up in the internal wall of the dialysis bag then the diffusion process is limited. According to the results, the kinetic model that fitted best to the curves was the Peppas-Sahlin model. The Figure 5-19 show the graphs with the fitted model.

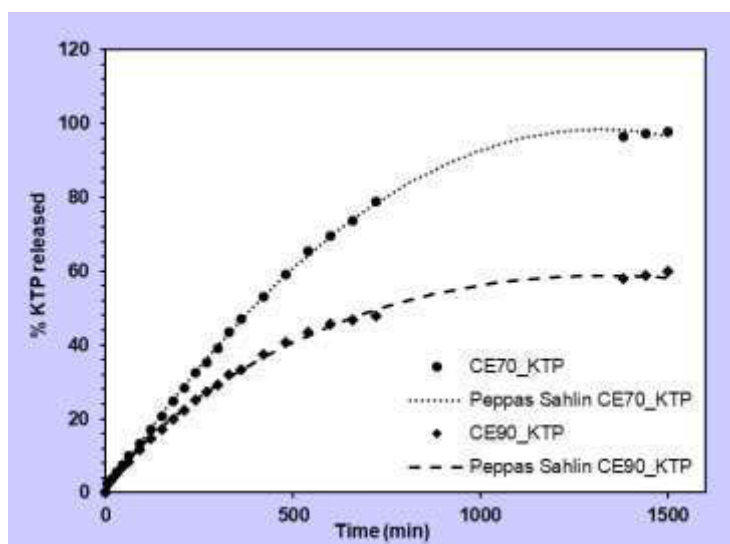


**Figure 5-19.** Experimental curves of KTP release from concentrated emulsions KEL/W= 0.17+ ● 70wt% Mig and ◆ 90wt% Mig in PbS with fitted models

## 5.7 Biological toxicity of hybrid materials towards HeLa cells

A detailed understanding of the particle-cell interaction is essential and of immense interest to create a specific carrier for each application. In this section the toxicity of hybrid material based on a non-ionic surfactant is evaluated in HeLa cells. The toxicity of many non-ionic surfactants generally decreases with the increasing of the alkyl chain length (Hofland, 1992). Despite their null antibacterial activity, the non-ionic surfactants demonstrated not to be harmful to epithelial cells, which make them attractive for cosmetic applications. (Inácio 2011) In this study, was proposed to evaluate different carriers prepared from biocompatible sources. It is important to mention that, each carrier was tested first free of drug, then the results were contrasted with those prepared with the trapped drug. As was already mentioned, the KTP is used as a model active principle.

The samples to test are: micelles containing 5 wt% KEL in water (MS5, MS5\_KTP), concentrated emulsions with the oily phase about 90% of Mig812N (CE90, CE90\_KTP) and hybrid silica material prepared from micelles (HMS5, HMS5\_KTP). The composition of the samples and the protocol for the analysis are described in the chapter II. Under the first route the results revealed that the culture died almost immediately after to place the samples over it, probably by crushing. Derived from this, it was proposed to test only the supernatant (SN) resulting from the mixture of the culture medium and each sample, the procedure to obtain the SN and the technique for cells preparation is described in the chapter II. HeLa cells in sample-free medium approached a confluent monolayer within 48h of growth, were angular in shape and retained their healthy appearance during 72h observation period, the cultures named as non-toxic are those which containing samples in a respective dilution present equal growth as controls ones and achieve at least 80% of viability.

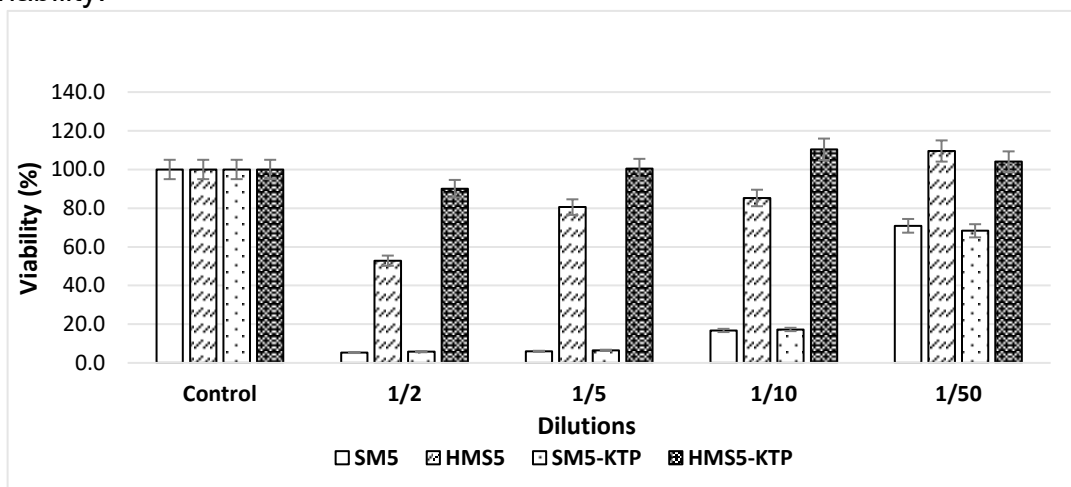


**Figure 5-20.** Graphical results of viability from the studied samples

**Table 5-15.** Viability results of the studied samples

Dilutions (v/v)	SM5		HMS5		SM5-KTP		HMS5-KTP	
	Viability (%)	CV (%)	Viability (%)	CV (%)	Viability (%)	CV (%)	Viability (%)	CV (%)
Control	<b>100.0</b>	<b>13.1</b>	<b>100.0</b>	<b>12.3</b>	<b>100.0</b>	<b>13.9</b>	<b>100.0</b>	<b>13.9</b>
1/2	5.4	9.3	52.8	18.3	<b>5.8</b>	<b>11.5</b>	<b>90.1</b>	14.00
1/5	6.0	7.6	<b>80.5</b>	<b>9.3</b>	<b>6.5</b>	<b>8.7</b>	<b>100.5</b>	11.00
1/10	16.8	19.3	<b>85.3</b>	<b>11.1</b>	<b>17.3</b>	<b>18.3</b>	<b>110.5</b>	19.00
1/50	<b>70.9</b>	<b>5.9</b>	<b>109.5</b>	<b>11.4</b>	<b>68.3</b>	<b>10.1</b>	<b>104.2</b>	18.80
FS	--	--	48.6	19.3	--	--	63.5	17.6
SN	--	--	24.4	26.6	--	--	47	13.7

The results show that the SM sample has a negative impact over the cells presenting a toxicity in the diluted solution except with the most diluted solution 1/50 where is noted that the viability increase considerably reaching almost 71%, then it is possible to presume that is possible to achieve better results above this concentration. The vulnerability of HeLa cells can be explained since they have not well-formed tight junctions and have less ordered membrane configuration. (Inácio 2011). The toxicity of this sample can be explained with the surfactant concentration that can have certain toxicity grade that is dependent upon the ability to its partition between the aqueous phase and the cell membrane and may also depend upon their ability to subsequently cross the membrane and enter the cytoplasm (Arechabala, 1999).

In contrast, the viability of the cell was superior from dilutions of 1/5 (v/v) dilutions, with that permeation of the surfactant molecules is lower than inside of the membrane making them more accessible for the release cargo. This can be also observed for the results for the HMS5-KTP, where the viability percentage is acceptable since the dilution 1/2 (v/v), presuming that the hybrid material can be considered as a carrier of poorly water-soluble drugs. However, the results of the test for the drug free and loaded hybrid material shows that in direct contact, that means the spreading powder over cells culture was not favorable showing a viability around 50-64%, this may be because the cell culture dies by crushing.

This can be explained thanks to the tight junctions between epithelial cell, making them less exposed to the surfactant and the toxic effects may be reduced. Is also important to mention that the long exposures to the hybrid material does not present a toxic effect in HeLa cells, supporting that the material can be used for sustained release into the epithelial culture.

**Conclusions**  
**and**  
**Perspectives**

## Conclusions

In this work the hybrid mesostructured and macro-mesostructured materials were prepared as nanocarriers for the transport of an interest molecules into the pharmaceutical domain, using Ketoprofen (KTP) as a model drug. The aim of this study was to test the drug loading capacity of these materials and their release kinetics under standard conditions. The understanding of the biocompatible system Kolliphor EL (KEL)/water/oil for the formation of hybrid materials with pharmaceutical applications was carried out through 5 chapters.

The first chapter was devoted to the existent molecular structures of biocompatible surfactants with emphasis on non-ionic types. The characteristics of the Organized Molecular Systems (OMS) were also described. The characteristics of materials prepared from non-ionic surfactants as structuring agents were then provided. Finally, the current impact of these meso and macro-meso structured materials as drug carriers on the mechanisms of controlled and sustained release was highlighted. The second chapter of this thesis was devoted in the description of materials and methods used to develop this study.

The third chapter was divided into two parts, the first researched-oriented to the investigation of the KEL/water system for the preparation of mesoporous materials. First the behavior of the KEL was studied and the phase diagram was determined. The KEL forms micelles ( $L_1$ ) in water and in high concentrations the domain of liquid crystals appears, which is constituted by the cubic phase ( $Pm3n$ ) and direct hexagonal phases. SAXS experiments were carried out to study the structure of different Organized Molecular Systems. It was shown that spherical micelles in water are formed having a size of about 12-13 nm. Next the mesoporous materials were synthesized and characterized by experiments of SAXS and nitrogen adsorption-desorption. The results revealed that the organization of the material is affected by the variation of the molar ratio KEL/ TMOS (silica precursor). In the second part of chapter three, the solubilization of biocompatible oils: Isopropyl Myristate (IM) and Miglyol 812N (Mig) on the KEL/water system was studied. Ternary phase diagrams were established with each oil. In the oil-rich field, between 70 and 90%, the concentrated emulsions were highlighted. The stability of these emulsions is remarkably long. Consequently, the preparation of the porous materials was carried out from these two types of emulsions. The materials obtained from IM have a larger pore size (43.2 nm) than those prepared with Miglyol (35.4 nm) for identical concentrations of surfactant (7 wt%).

Chapter four was divided also in two sections. The first section concerns the investigation of the KEL/water system in presence of P123. The compatibility of these 2 surfactants allows the formation of micelles and liquid crystals. The micellar phase exists up to a total surfactant concentration of 25 wt% regardless of the ratio between KEL and P123. Cubic phase limits are imposed for pure cubic phases of KEL (58%) and P123 (38%). The hexagonal phase extends from 55 wt% of KEL rich region to almost 70 wt% P123 rich region. In the second part of the chapter, the characteristics of the porous materials synthesized from the combination of fine emulsions (Em) of the KEL/water/IM system and the micelles of P123 (mic P123) were described. Using different ratios, it is possible to modify the degree of porosity in these materials. In proportions lower than 50/50 mesoporous silica materials with two pore sizes are obtained. This effect is produced due to the methanol released during TMOS hydrolysis, where the presence of P123 micelles destabilizes the fine emulsions and the porosity effect is negative. By increasing the Em/mic P123 ratio, the proportion of P123 micelles and the amount of methanol decreases and the fine emulsions are no longer disturbed, allowing them to better control the final porosity of the material.

Finally, understanding the KEL/water/oils systems allows the preparation of silicated hybrid materials which are described into the fifth chapter of this work. These materials without removing of the organic phase are excellent candidates as drug delivery system (DDS) application. The synthesis conditions were optimized to avoid degradation of the encapsulated active ingredient and to allow it to be released under standard conditions. The release was evaluated under different pH conditions and in the presence of P123 micelles in the receiving solution. In the case of materials prepared from micellar solutions, the release percentage increases from 38 to 64% when the concentration of P123 micelles increase of 0 to 5 wt% in the receptor solution respectively. Materials prepared from fine emulsions, progressively release 41% to 57% in the presence of the same content of P123, where the presence of Miglyol within the formulation is highlighted by promoting a sustained and controlled KTP release profile from 6 hours of kinetics.

The mathematical models corresponding to the release curves explain the functionality of the material as a controlled and/or sustained release system. In recent investigations the models have been adapted for hydrophobic compounds thanks to the cooperation of external agents for the release, as in this case of the presence of P123 micelles. As a final part of the thesis, the toxicity of hybrid materials was evaluated on HeLa cell cultures, where it was possible to prove that the silica matrix protects the cells making them more accessible for the release of the charge.

To conclude, this study made it possible to propose hybrid systems based on silica and organic matter to transport active ingredients. This work should be continuing to improve the control of drug release. In particular, it is necessary to vary in a systematic way to change all the parameters for the experiment: hybrid material characteristics, dosage of active principle and release conditions, among others. In this way we will understand better the mechanisms of the amounts of active principles released. It is necessary also, to test other hydrophobic active principles to extend the application field.

## Perspectives

The results showed that the system based on non-ionic and biocompatible surfactants such as Kolliphor EL is a good candidate for the development of a new and novel type of drug delivery system. However, in order to better understand the influence of the material on the release results, it is necessary to vary the parameters to test increase in the concentration of the active ingredient, vary the conditions of the receptor solution, vary the conditions of experimentation in the dissolving equipment, among others.

An interesting point into this study is to evaluate the performance of mesoporous hybrid materials as carriers of hydrophilic drugs, for example, cephalexin. In this study it was mentioned that the release kinetics of hydrophobic drugs generally have a sustained and controlled profile, however, an important factor to make it happens is the matrix where the drug is located, therefore, the variation in the type of drug is also important. Optimized conditions for the synthesis of hybrid materials containing a hydrophilic drug must then be re-established.

Since KEL demonstrate a good synergy with Pluronic P123 to form biocompatible polymer-surfactant scaffolds and since these structures have played a significant role in wide range of tissue engineering application such as bone healing. It could be interesting to evaluate the capacity of the partnership to increase the bioavailability of the active principle into the tissue engineering.

The ability of Pluronic to provide steric stabilization to lyotropic liquid crystalline particles might also be of particular interest for the design of innovative nanostructured drug delivery systems as Cubosomes that possess an internal ordered structure made of lipid bilayers and water channels (Pitto-Barry, 2014). It is proved that both: efficient drug vectors (*via* controlled release through diffusion) and suitable for intravenous administration (being dispersed and stabilised as sub-micron sized nanostructured particles). Despite this promise, the stabilisation of such Cubosomes remains challenging, and only a few stabilisers have been reported.

# **Bibliography**

## Bibliography

1. Abd-Elrahman A.A., El Nabarawi M.A., Hassan D.H., Taha A.A., (2016) Ketoprofen mesoporous silica nanoparticles SBA-15 hard gelatin capsules: preparation and *in vitro/in vivo* characterization, *Drug Delivery*, 23:9, pages: 3387-3398, DOI: 10.1080/10717544.2016.1186251
2. Ahuja N., Katare O. P., Singh B., (2007). Studies on dissolution enhancement and mathematical modeling of drug release of a poorly water-soluble drug using water-soluble carriers. *European Journal of Pharmaceutics and Biopharmaceutics*, 65(1), 26-38.
3. Akaike, H. (1974). A new look at the statistical model identification. *IEEE Transactions on Automatic Control*, Volume: AC-19, pages: 716–723 DOI:
4. Alibrahim M., Stébé M.J., Dupont G., Ravey J.C., Effect of an ionic surfactant on the phase behavior of a nonionic surfactant-based system, *J. Chim. Phys. Phys. Chim. Biol.* 94 (1997) 1614–1633.
5. Anderson D., Wennerstroem H., Olsson U. (1989). Isotropic bicontinuous solutions in surfactant-solvent systems: the L3 phase. *The Journal of Physical Chemistry*, 93(10), 4243-4253.
6. Anton N., Vandamme T. F. (2011). Nano-emulsions and micro-emulsions: clarifications of the critical differences. *Pharmaceutical research*, 28(5), 978-985.
7. Arruebo M., WIREs, Drug delivery from structured porous inorganic materials, *Nanomed. Nanobiotechnol.* 4 (2012) 16–30.
8. B. Arechabala, C. Coiffard, P. Rivalland, L. J. M. Coiffard and Y. de Roeck-Holtzhauer, Comparison of Cytotoxicity of Various Surfactants Tested on Normal Human Fibroblast Cultures using the Neutral Red Test, MTT Assay and LDH Release, *Journal of Applied Toxicology*, 1999, Volume 19, pages 163-165, DOI: 10.1002/(sici)10991263(199905/06)19:3<163::aid-jat561>3.0.co;2-h
9. Babak V.G. Stébé M.J., Highly Concentrated Emulsions: Physicochemical principles of Formulation, *Journal of Dispersion Science and Technology*, 2002, Volume 23, Issue: 1-3, 1-22, DOI: 10.1080/01932690208984184
10. Baccile N., Babonneau F., Thomas B., Coradin T., Introducing eco-design in silica sol-gel materials, *J. Mater. Chem.* 19 (2009) 8537–8559.
11. Bagshaw S.A., Prouzet E., Pinnavaia T.J., Templating of mesoporous molecular sieves by nonionic polyethylene oxide surfactants, *Science* 269 (1995) 1242–1244
12. Balamuralidhara V., Pramodkumar T.M., Srujana N., Venkatesh M.P., Vishal Gupta N., Krishna K.L. Gangadharappa H.V., pH sensitive Drug Delivery Systems: A review, *American Journal of Drug Discovery and Development*, 2011, Volume 1, pages: 24-48, DOI: 10.3923/ajdd.2011.24.48
13. Banhart, J. (2001). Manufacture, characterisation and application of cellular metals and metal foams. *Progress in materials science*, 46(6), 559-632.

14. Barrett E.P., Joyner L.G., Halenda P.P., The determination of pore volume and area distributions in porous substances. I. Computations from nitrogen isotherms, *J. Am. Chem. Soc.* 73 (1951) 373–380.
15. Beck, J. S., Vartuli, J. C., Roth, W. J., Leonowicz, M. E., Kresge, C. T., Schmitt, K. D., Higgins, J. B. (1992). A new family of mesoporous molecular sieves prepared with liquid crystal templates. *Journal of the American Chemical Society*, 114(27), 10834-10843.
16. Bergman L., Thesis: Influence of surface functionalization on the behaviour of silica nanoparticles in biological systems, 2014, Laboratory of Physical Chemistry Center for Functional Materials, Dept. of Chemical Engineering. Abo Alademi University, Finland.
17. Bidon, B., Iltis, I., Semer, M. *et al.* XPC is an RNA polymerase II cofactor recruiting ATAC to promoters by interacting with E2F1. *Nat Commun* 9, 2610 (2018) doi:10.1038/s41467-018-05010-0
18. Bize, C., Blanzat, M., Rico-Lattes, I. *Journal of Surfactant Detergents* (2010) 13, vol 4. Page 465-473. DOI:10.1007/s11743-010-1181-z
19. Bleta R. 2007, Systèmes fluorés pour la conception de matériaux poreux : Matrices pour la physisorption de biomolécules. Autre. Université Henri Poincaré - Nancy 1, 2007. Français. NNT: 2007NAN10111.
20. Bleta, R., Blin, J. L., Stébé, M. J. (2006). Solubilization of various fluorocarbons in a fluorinated surfactant/water system: relation with the design of porous materials. *The Journal of Physical Chemistry B*, 110(46), 23547-23556.
21. Blin J.L., Du N., Stébé M.J., Alcohols solubilization in a nonionic fluorinated surfactant-based system: effect on the mesoporous silica characteristics, *J. Colloid Interface Sci.* 373 (2012) 34–45.
22. Blin J.L., Impéror-Clerc M., Mechanism of self-assembly in the synthesis of silica mesoporous materials: in situ studies by X-ray and neutron scattering, *Chem. Soc. Rev.* 42 (2013) 4071–4082.
23. Blin J.L., Stébé M.J., Effect of fluorocarbon addition on the structure and pore diameter of mesoporous materials prepared with a fluorinated surfactant, *Microporous Mesoporous Mater.* 87 (2005) 67–76.
24. Botella P., Corma A., Quesada M., Synthesis of ordered mesoporous silica templated with biocompatible surfactants and applications in controlled release of drugs, *J.Mater. Chem.* 22 (2012) 6394–6401.
25. Botella, P., Abasolo, I., Fernández, Y., Muniesa, C., Miranda, S., Quesada, M., Corma, A. (2011). Surface-modified silica nanoparticles for tumor-targeted delivery of camptothecin and its biological evaluation. *Journal of controlled release*, 156(2), 246-257.
26. Braganca L.F., Ojeda M., Fierro J.L.G., Pais da Silva M.I., Bimetallic Co-Fe nanocrystals deposited on SBA-15 and HMS mesoporous silicas as catalysts for Fischer-Tropsch synthesis, *Appl. Catal. A-Gen.* 423–424 (2012) 146–153.

27. Bruinsma, J., Dalvi, C., Lamego, M. (2015). *U.S. Patent No. 9,186,102*. Washington, DC: U.S. Patent and Trademark Office.
28. Charvolin J., Sadoc J.F., Periodic systems of frustrated fluid films and micellar cubic structures in liquid crystals, *J. Phys.* 49 (1988) 521–526.
29. Clifford N.W., Iyer K.S., Raston C.L., Encapsulation and controlled release of nu- traceuticals using mesoporous silica capsules, *J. Mater. Chem.* 18 (2008) 162–165.
30. Coaccioli S. Ketoprofen 2.5% gel: a clinical overview, *European Review Medical Pharmacology Sciences*, 2011, Volume 15, pages: 943-949, DOI: <https://www.ncbi.nlm.nih.gov/pubmed/21845805>
31. Corma, M. Moliner, M.J. Díaz-Cabanas, P. Serna, B. Femenia, J. Primo, H. García, Biomimetic synthesis of microporous and mesoporous materials at room temperature and neutral pH, with application in electronics, controlled release of chemicals, and catalysis, *New J. Chem.* 32 (2008) 1338–1345.
32. Corma, M. Moliner, M.J. Díaz-Cabanas, Serna P., Femenia B., Primo J., García H., Biomimetic synthesis of microporous and mesoporous materials at room tempera- ture and neutral pH, with application in electronics, controlled release of chemicals, and catalysis, *New J. Chem.* 32 (2008) 1338–1345.
33. Costa, S. G., Nitschke, M., Lépine, F., Déziel, E., & Contiero, J. (2010). Structure, properties and applications of rhamnolipids produced by *Pseudomonas aeruginosa* L2-1 from cassava wastewater. *Process Biochemistry*, 45(9), 1511-1516.
34. Davidson I.G., Langner E. J., Steven V.P., Blair J.A., Release mechanism of insulin encapsulated in trehalose ester derivative microparticles delivered via inhalation, *International Journal of Pharmaceutics*, Volume 254, Issue 2, 2003, pages 211-222. doi.org/10.1016/S0378-5173(03)00035-8
35. Davison, G. R., Konig, A., Gibbons, C., Ripley, M. B., Macgilp, N. A., Milich, G. L. C., Pretswell, E. L. (2003). *U.S. Patent No. 6,638,918*. Washington, DC: U.S. Patent and Trademark Office.
36. Diab, R., Canilho, N., Pavel, I. A., Haffner, F. B., Girardon, M., Pasc, A. (2017). Silica-based systems for oral delivery of drugs, macromolecules and cells. *Advances in colloid and interface science*, 249, 346-362.
37. Du, N., Stébé, M. J., Bleta, R., Blin, J. L. (2010). Preparation and characterization of porous silica templated by a nonionic fluorinated systems. *Colloids and Surfaces A: Physicochemical and Engineering Aspects*, 357(1-3), 116-127.
38. Ducret, A., Giroux, A., Trani, M., & Lortie, R. (1996). Characterization of enzymatically prepared biosurfactants. *Journal of the American Oil Chemists' Society*, 73(1), 109-113.
39. Dumitriu, S., Magny, P., Montane, D., Vidal, P. F., Chornet, E. (1994). Polyionic hydrogels obtained by complexation between xanthan and chitosan: their properties

as supports for enzyme immobilization. *Journal of bioactive and compatible polymers*, 9(2), 184-209.

40. El-Safty S.A., Kiyozumi Y., Hanaoka T., Mizukami F., Controlled design of ordered and disordered pore architectures, geometries, and dimensions of HOM-type mesostructured monoliths and their hydrothermal stabilities, *J. Phys. Chem. C* 112 (2008) 5476–5489.

41. El-Shattory Y., Abo-Elwafa GA, Aly SM, Nashy el-SH. Production of Ethoxylated Fatty Acids Derived from jatropha Non Edible Oil as nonionic Fat-liquoring agent. *J Oleo Sci.* 2012;61(5):255-66.

42. Eruke, O. S., & Udoh, A. J. (2015). Potentials for Biosurfactant enhanced bioremediation of hydrocarbon contaminated soil and water—A review. *Advances in Research*, 4(1), 1-14.

43. Espitalier F. Biscns B., Laguérie C., Physicochemical Data on Ketoprofen in Solutions, *Journal of Chemical Engineering Data*, 1995, Volume 40, pages: 1222-1224, DOI: 10.1021/je00022a016

44. Esquena J., Rodriguez C., Solans C., Kunieda H., Formation of mesostructured sílica in nonionic fluorinated surfactant systems, *Microporous Mesoporous Mater.* 92(2006) 212–219.

45. Fan, J., Yu, C., Lei, J., Zhang, Q., Li, T., Tu, B., Zhao, D. (2005). Low-temperature strategy to synthesize highly ordered mesoporous silicas with very large pores. *Journal of the American Chemical Society*, 127(31), 10794-10795.

46. Ferrer, M., Perez, G., Plou, F. J., Castell, J. V., & Ballesteros, A. (2005a). Antitumour activity of fatty acid maltotriose esters obtained by enzymatic synthesis. *Biotechnology and applied biochemistry*, 42(1), 35-39.

47. Folmer B., Svensson M., Holmberg K. Brown W., The Physicochemical Behavior of Phytosterol Ethoxylates, *Journal of Colloid and Interface Science*, Volume 213, Issue 1, 1999, pages 112-120. doi.org/10.1006/jcis.1999.6099.

48. Fontell K., Fox K.K., Hansson E., On the structure of the cubic phase I<sub>1</sub> in some lipid- water systems, *Mol. Cryst. Liq. Cryst.* 1 (1985) 9–17

49. Fritz G., Glatter O., Structure and interaction in dense colloidal systems: evaluation of scattering data by the generalized indirect Fourier transformation method, *J.Phys. Condens. Matter* 18 (2006) S2403–S2419.

50. Fryd M.M., Mason T.G., Advanced Nanoemulsions, *Annual. Review of Physical Chemistry*, Volume: 63, 2012, pages: 493–518, DOI:10.1146/annurev-physchem-032210-103436.

51. Fryd, M. M., Mason, T. G. (2012). Advanced nano-emulsions. *Annual review of physical chemistry*, 63, 493-518.

52. Fulvio P.F., Pikus S., Jaroniec M., Tailoring properties of SBA-15 materials by controlling conditions of hydrothermal synthesis, *J. Mater. Chem.* 15 (2005) 5049–5053.

53. G.S. Attard, J.C. Glyde, C.G. Göltner, Liquid-crystalline phases as templates for the synthesis of mesoporous silica, *Nature* 378 (1995) 366–368.
54. Galarneau A., Nader M., Guenneau F., Di Renzo F., Gedeon A., Understanding the stability in water of mesoporous SBA-15 and MCM-41, *J. Phys. Chem. C* 111 (2007) 8268–8277
55. Galarneau M., Nader F., Guenneau F., Di Renzo A., Understanding the stability in water of mesoporous SBA-15 and MCM-41, *J. Phys. Chem. C* 111 (2007) 8268–8277.
56. Gao, C., Sakamoto, Y., Sakamoto, K., Terasaki, O., Che, S. (2006). Synthesis and Characterization of Mesoporous Silica AMS-10 with Bicontinuous Cubic Pn $\bar{3}$ m Symmetry. *Angewandte Chemie International Edition*, 45(26), 4295-4298.
57. Gelderblom H., Verweij J., Nooter K., Sparreboom A., Chremophor EL: the drawbacks and advantages of vehicle selection for drug formulation, *European Journal of Cancer*, Volume: 37, 2001, pages 1590-1598, DOI: 10.1016/s0959-8049(01)00171-x
58. Gérardin C., Reboul J., Bonne M., Lebeau B., Eco-design of ordered mesoporous silica materials, *Chem. Soc. Rev.* 42 (2013) 4217–4255.
59. Gérardin C., Reboul J., Bonne M., Lebeau B., Eco-design of ordered mesoporous silica materials, *Chem. Soc. Rev.* 42 (2013) 4217–4255.
60. Gibaldi M., Feldman S., Establishment of sink conditions in dissolution rate determinations. Theoretical considerations and application to non-disintegrating dosage forms., *Journal of Pharmaceutical Sciences*, 2006, Volume 56, Issue 10, pages: 1238-1242, DOI: 10.1002/jps.2600561005
61. Gibson, H. W., Hamilton, L. and Yamaguchi, N. (2000), Molecular self-assembly of dendrimers, non-covalent polymers and polypseudorotaxanes. *Polym. Adv. Technol.*, 11: 791-797
62. Glatter O., Kratky O., *Small Angle X-Ray Scattering*, Academic Press, 1982, pp.167–196.
63. Griffin W.C., *Classification of Surface-Active Agents by HLB*, *Journal of the Society of Cosmetic Chemists* 1 (1949), page 311.
64. Guerra-Santos, L. H., Käppeli, O., Fiechter, A. (1986). Dependence of *Pseudomonas aeruginosa* continuous culture biosurfactant production on nutritional and environmental factors. *Applied Microbiology and Biotechnology*, 24(6), 443-448.
65. Haferburg, D., Hommel, R., Claus, R., Kleber, H. P. Extracellular microbial lipids as biosurfactants. In *Bioproducts* (pp. 53-93). Springer, Berlin, Heidelberg, 1986.
66. He Q., Shi J., Chen F., Zhu M., Zhang L., An anticancer drug delivery system based on surfactant-templated mesoporous silica nanoparticles, *Biomaterials* 31 (2010) 3335–3346.
67. Hofland H.E. Bouwstra J.A., Verhoef J.C., Buckton G. Chowdry B.Z., Ponec M., Junginger H.E. Safety Aspects of Non-ionic Surfactant Vesicles: A Toxicity Study

Related to the Physicochemical Characteristics of Non-ionic Surfactants, *Journal of pharmacy and pharmacology*, 1992, Volume 44, Issue 4, pages 287-294. DOI: 10.1111/j.2042-7158.1992.tb03608.x

68. Holmberg Krister. *Natural Surfactants*, *Colloid & Interface Science*, *Current Opinion in colloid & Interface Science* 148-159, 2001.

69. Holmberg, K. *Novel surfactants: preparation applications and biodegradability*. 2<sup>nd</sup> edition revised and expanded (Vol. 114). Marcel Dekker Inc. New York, 2003.

70. Hossain K.Z., Sayari A., Synthesis of onion-like mesoporous silica from sodium silicate in the presence of  $\alpha,\omega$ -diamine surfactant, *Microporous Mesoporous Mater* 114 (2008) 387–394.

71. Huo, Q., Margolese, D., Ciesla, U. et al. Generalized synthesis of periodic surfactant/inorganic composite materials. *Nature* Volume:368, pages: 317–321, 1994, DOI:10.1038/368317a0

72. Inácio A.S., Mesquita KA, Baptista M, Ramalho-Santos J, Vaz WLC, et al. (2011) *In Vitro Surfactant Structure-Toxicity Relationships: Implications for Surfactant Use in Sexually Transmitted Infection Prophylaxis and Contraception*. *PLoS ONE* 6(5): e19850. doi:10.1371/journal.pone.0019850

73. Johansson I., Svensson M., *Surfactants based on fatty acids and other natural hydrophobes*, *Current Opinion in Colloid & Interface Science*; Volume 6, Issue 2, 2001, Pages 178-188. doi.org/10.1016/S1359-0294(01)00076-0.

74. Karami Z, Saghatchi Zanjani MR, Hamidi M, *Nanoemulsions in CNS drug delivery: recent developments, impacts and challenges*, *Drug Discovery Today* (2019). DOI: 10.1016/j.drudis.2019.03.021

75. Kewal J. K., Jain, K. K. (2008). *The handbook of nanomedicine* (Vol. 404). Totowa: Humana Press.

76. Kickeklick, G. (Ed.). (2007). *Hybrid materials: synthesis, characterization, and applications*. John Wiley & Sons.

77. Koh, A., & Gross, R. (2016). Molecular editing of sophorolipids by esterification of lipid moieties: effects on interfacial properties at paraffin and synthetic crude oil-water interfaces. *Colloids and Surfaces A: Physicochemical and Engineering Aspects*, 507, 170-181.

78. Kresge C.T., Leonowicz M.E., Roth W.J., Vartuli J.C., Beck J.S., *Ordered mesoporous molecular sieves synthesized by a liquid-crystal template mechanism*, *Nature* 359 (1992) 710–712.

79. Kresge C.T., Roth W.J., *The discovery of mesoporous molecular sieves from the twenty-year perspective*, *Chem. Soc. Rev.* 42 (2013) 3663–3670. Complementary medicine evaluation committee, 16th Meeting, (n.d.)

80. Landry J.J. Theodor P.P. Rausch T., Zichner T., Tekkedil M.N., Stutz A.M., Jauch A., Aiyar R.S., Pau G., Delhomme N., Gagneur J., Korbel J.O., Huber W., Steinments L., *The genomic and transcriptomic landscape of a HeLa cell line*,

Genes-Genomes-Genetics, 2013, Volume 3, Issue 8, pages 1213-1224, DOI: 10.1534/g3.113.005777

81. Laughlin R., Surfactant phase science, Current Opinion in Colloid & Interface Science, Volume 1, Issue 3, 1996, Pages 384-390, ISSN 1359-0294. doi.org/10.1016/S1359-0294(96)80138-5

82. Léonard A., Blin J.L., Jacobs P.A., Grange P., Su B.L., Chemistry of silica at different concentrations of non-ionic surfactant solutions: effect of pH of the synthesis gel on the preparation of mesoporous silicas, Microporous Mesoporous Mater. 63 (2003) 59–73

83. Léonard A., Blin J.L., Jacobs P.A., Grange P., Su B.L., Chemistry of silica at different concentrations of non-ionic surfactant solutions: effect of pH of the synthesis gel on the preparation of mesoporous silicas, Microporous Mesoporous Mater. 63 (2003)

84. Limnell T., Riikonen J., Salonen J., Kaukonen A.M., Laitinen L., Hirvonen J., Letho V.P., Surface chemistry and pore size affect carrier properties of mesoporous silicon microparticles, International Journal of Pharmacy, 2007, Volume 343 (1-2), pages: 141-7.

85. Limnell, T., Riikonen, J., Salonen, J., Kaukonen, A. M., Laitinen, L., Hirvonen, J., Lehto, V. P. (2007). Surface chemistry and pore size affect carrier properties of mesoporous silicon microparticles. *International journal of pharmaceutics*, 343(1-2), 141-147.

86. Martens J.A., Jammaer J., Bajpe S., Aerts A., Lorgouilloux Y., Kirschhock C.E.A., Simple synthesis recipes of porous materials, Microporous Mesoporous Mater. 140 (2011) 2–8.

87. McClements, D. J. (2012). Nanoemulsions versus microemulsions: terminology, differences, and similarities. *Soft matter*, 8(6), 1719-1729.

88. Michaux F. 2009, Thesis : Contribution des tensioactifs fluorés à la synthèse de matériaux mésoporeux. Application à la conception d'un bioréacteur. Français Equipe Physico-chimie des Colloïdes - UMR 7565 SRSMC CNRS – Nancy Université Faculté des Sciences et Techniques BP 239, 54506 Vandoeuvre-lès-Nancy Cedex.

89. Michaux F., Stébé M.J., Blin J.L., Systematic investigation of the synthesis parameters driving the preparation of mesoporous materials using a nonionic fluorinated surfactant, Microporous Mesoporous Mater. 151 (2012) 201–210.

90. Minhaz A, Islam S, Rahman H, In vitro release study of Ketorolac from extended release capsules filled with semisolid matrix of Glyceryl esters of fatty acids. Bangladesh Pharm J., 2010; 13(2): 25-30. <http://www.bpj-bd.com/index.php/current-issue/category/6-volume-13-no-2-july-2010?download=124:article-05>

91. Mir, S. H., Nagahara, L. A., Thundat, T., Mokarian-Tabari, P., Furukawa, H., Khosla, A. (2018). Organic-inorganic hybrid functional materials: An integrated

platform for applied technologies. *Journal of The Electrochemical Society*, 165(8), B3137-B3156.

92. Mitchell D.J., Tiddy T., Waring L., Bostock T., Mc Donald M.P., Phase behaviour of polyoxyethylene surfactants with water. Mesophase structures and partial miscibility (cloud points), *J. Chem. Soc. Faraday Trans. I* 79 (1983) 975–1000.

93. Mohammad A., Mawgoud A., Lépine F., Déziel E. ; Rhamnolipids: diversity of structures, microbial origins and roles. *Appl Microbiol Biotechnol* (2010) 86:1323–1336. DOI 10.1007/s00253-010-2498-2

94. Moritz M., Geszke-Moritz M., Mesoporous materials as multifunctional tools in biosciences: principles and applications, *Mater. Sci. Eng. C* 49 (2015) 114–151.

95. Mosmann T. Rapid Colorimetric Assay for Cellular Growth and Survival: Application to Proliferation and Cytotoxicity Assays. *Journal of Immunology Methods*, 1983, Volume 65, pages: 55–63.

96. Mulye, N. V., Turco, S. J. (1995). A simple model based on first order kinetics to explain release of highly water soluble drugs from porous dicalcium phosphate dihydrate matrices. *Drug development and industrial pharmacy*, 21(8), 943-953.

97. Murphy, D. B.; Spring, K. R.; Fellers, T. J.; Davidson, M. W. Introduction to Optical Birefringence  
<https://www.microscopyu.com/articles/polarized/birefringenceintro.html>.

98. Nikolaos A.P. Khare A.R., Preparation, structure and diffusional behaviour of hydrogels in controlled release, *Advanced Drug Delivery Reviews*, 2013, Volume 11 Issue 1-2, pages 1-35, DOI: 10.1016/0169-409X(93)90025-Y

99. Parikh K.J., Sawant K.K., Solubilization of vardenafil HCl in lipid-based formulations enhances its oral bioavailability in vivo: A comparative study using Tween - 20 and Cremophor – EL, *Journal of Molecular Liquids*, Volume 277, 2019, pages 189-199, DOI: 10.1016/j.molliq.2018.12.079.

100. Park I., Pinnavaia T.J., Large-pore mesoporous silica with three-dimensional Wormhole framework structures, *Microporous Mesoporous Mater.* 118 (2009) 239–244.

101. Park I., Pinnavaia T.J., Large-pore mesoporous silica with three-dimensional Wormhole framework structures, *Microporous Mesoporous Mater.* 118 (2009) 239–244.

102. Park S.Y., Barton M., Pendleton P., Mesoporous silica as a natural antimicrobial carrier, *Colloid. Surf. Physicochem. Eng. Asp.* 385 (2011) 256–261.

103. Perego P., Millini R., Porous materials in catalysis: challenges for mesoporous materials, *Chem. Soc. Rev.* 42 (2013) 3956–3976.

104. Pérez B. Anankanbil S.; Guo Z., Synthesis of Sugar Fatty Acid Esters and Their Industrial Utilizations. In *Fatty Acids*; Elsevier, 2017; pp 329–354.

105. Pinazo A., Pons R., Pérez L., Infante, M. R. (2011). Amino acids as raw material for biocompatible surfactants. *Industrial & Engineering Chemistry Research*, 50(9), 4805-4817.

106. Porter M.R. Handbook of surfactants, Springer science + business media LLC, Chapter I, page 3, New York 1993. ISBN 978-1-4757-1293-3 (eBook) DOI 10.1007/978-1-4757-1293-3
107. Ramteke K., Dighe H., Kharat P. A., A. R., Patil, S. V. (2014). Mathematical models of drug dissolution: a review. *Scholar Academy Journal of Pharmacy*, Volume: 3, Issue: 5, pages: 388-396.
108. Ravey J.C., Stébé M.J., Properties of fluorinated non-ionic surfactant-based systems and comparison with non-fluorinated systems, *Colloids and Surfaces A: Physicochemical and Engineering Aspects*, Volume 84, Issue 1, 1994, Pages 11-31, doi.org/10.1016/0927-7757(93)02731-S.
109. Ravey J.C., Stébé M.J., Sauvage S., Water in fluorocarbon gel emulsions: Structures and rheology, *Colloids and Surfaces A: Physicochemical and Engineering Aspects*, Volume 91, 1994 bis, pages 237-257, ISSN 0927-7757, DOI:10.1016/0927-7757(94)02942-3.
110. Riachy P., Roig F., García-Celma M.J., Stébé M.J., Pasc A., Esquena J., Solans C., Blin J.L., Hybrid Hierarchical Porous Silica Templated in Nanoemulsions for Drug Release, 2016, *European Journal of Inorganic Chemistry*, volume 2016 Issue 13-14, pages 1989-1997, DOI: 10.1002/ejic.201501127
111. Roig F., Blanzat M., Solans C., Esquena J., García-Celma M.J., Hyaluronan based materials with cationic sugar-derived surfactants as drug delivery systems, *Colloids and Surfaces B: Biointerfaces*, Volume 164, 2018, Pages 218-223, ISSN 0927-7765, DOI: 10.1016/j.colsurfb.2018.01.037.
112. Rurack K., Martínez-Máñez R. (Eds.). (2010). *The supramolecular chemistry of organic-inorganic hybrid materials*. John Wiley & Sons.
113. Salager Jean-Louis, *Surfactants Types and uses*, Universidad de los Andes, chapter I, page 3, Mérida Venezuela 2002.
114. Salonen, J., Laitinen, L., Kaukonen, A. M., Tuura, J., Björkqvist, M., Heikkilä, T., Vähä-Heikkilä, K., Hirvonen, J. and Lehto, V. P. (2005). Mesoporous silicon microparticles for oral drug delivery: Loading and release of five model drugs. *Journal of Controlled Release* 108: 362-374.
115. Schick Martin J. *Nonionic surfactants physical chemistry*, *Surfactant Science* Volume 23; New York, 1966, 1987 and 1970.
116. Schott H., Effect of inorganic additives on solutions of nonionic surfactants, *J. Colloid Interface Sci.* 189 (1997) 117–122.
117. Schueth, F., Schmidt, W. (2002). Microporous and mesoporous materials. *Advanced Engineering Materials*, 4(5), 269-279.
118. Shinoda K., Lagowski J.J. (Ed.), *In Principles of Solution and Solubility*, M. Dekker Inc, New York and Basel, 1978, p. 180.
119. Shinoda, K. (1967). The correlation between the dissolution state of nonionic surfactant and the type of dispersion stabilized with the surfactant. *Journal of Colloid and Interface Science*, 24(1), 4-9.

120. Shoaib HM, Tazeen J, Merchant AH, Yousuf IR; Evaluation of drug release kinetics from ibuprofen matrix tablets using HPMC. *Pak. J. Pharmaceutical Sciences*, 2006; 19: 119-24.
121. Sing K.S.W., Everett D.H., Haul R.A.W., Moscou L., Pierotti R.A., Rouquerol J., Siemieniowska T., Reporting physisorption data for gas/solid systems with special reference to the determination of surface area and porosity (Recommendations 1984) IUPAC, *Pure Appl. Chem.* 57 (1985) 603–619.
122. Sing K.S.W., Everett D.H., Haul R.A.W., Moscou L., Pierotti R.A., Rouquerol J., Siemieniowska T., Reporting physisorption data for gas/solid systems with special reference to the determination of surface area and porosity (Recommendations 1984) IUPAC, *Pure Appl. Chem.* 57 (1985) 603–619
123. Singh A., Van Hamme J.D., Ward O.P., Surfactants in microbiology and biotechnology: Part 2. Application aspects. *Biotechnol Adv.* 2007 Jan-Feb;25(1):99-121. Epub 2006 Oct 28. DOI: 10.1016/j.biotechadv.2006.10.004
124. Singh-Joy S.D., McLain V.C., Safety assessment of poloxamers 101, 105, 108, 122, 123, 124, 181, 182, 183, 184, 185, 188, 212, 215, 217, 231, 234, 235, 237, 238, 282, 284, 288, 331, 333, 334, 335, 338, 401, 402, 403, and 407, poloxamer 105 benzoate, and poloxamer 182 dibenzoate as used in cosmetics, *International Journal of Toxicology*, 2008, Volume 27, Supplement 2, pages 93-128, DOI: 10.1080/10915810802244595
125. Sjöblom J., *Encyclopedic Handbook of Emulsion Technology*; CRC Press book-Taylor & Francis Group; 1<sup>st</sup> edition; USA 2001. ISBN 9780824704544
126. Solans, C., Solé, I. (2012). Nano-emulsions: formation by low-energy methods. *Current opinion in colloid & interface science*, 17(5), 246-254
127. Soussan E., Cassel S., Blanzat M., Rico-Lattes I., Drug Delivery by soft matter: matrix and vesicular carriers, 2009, *Drug Vectors*, *Angew. Chemical International*, Volume 48, pages 274-288. DOI: 10.1002/anie.200802453
128. Stébé M.J., Emo M., Forny-Le Follotec A., Metlas-Komunjer L., Pezron I., Blin J.L., Triblock siloxane copolymer surfactant: template for spherical mesoporous silica with a hexagonal pore ordering, *Langmuir* 29 (2013) 1618–1626.
129. Svensson Martin (2010), *Surfactants Based on Natural Fatty Acids, Surfactants from Renewable Resources* John Wiley Sons. doi.org/10.1002/9780470686607.ch1
130. Svetlana R.D., Rheology of emulsions, *Advances in Colloid and Interface Science*, Volume: 151, 2009, pages: 1-23. DOI: 10.1016/j.cis.2009.07.001
131. T. Benamor, L. Vidal, B. Lebeau, C. Marichal, Influence of synthesis parameters on the physico-chemical characteristics of SBA-15 type ordered mesoporous silica, *Microporous Mesoporous Mater.* 153 (2012) 100–114.
132. Tadros T. Izquierdo P., Esquena J., Solans C.; Formation and stability of nano-emulsions. *Advances in colloid and interface science* Vol. 108-109, 2004 p. 303-318,

133. Tadros T. ; Applied Surfactants:Principles and Applications ; Wiley-VCH Verlag GmbH; Weinheim 2005. ISBN:9783527604814 DOI:10.1002/3527604812.
134. Tan B., Dozier A., Lehmler H.J., Knutson B., Rankin S.E. Elongated silica nanoparticles with a mesh phase mesopore structure by fluorosurfactant templating, *Langmuir* 20 (2004) 6981–6984.
135. Tiddy G.J.T., Surfactant-water liquid crystal phases, *Physics Reports*, Volume 57, Issue1,1980,Pages 1-46, ISSN 0370-1573, doi.org/10.1016/0370-1573(80)90041-1
136. Tiddy, G. J. (1980). Surfactant-water liquid crystal phases. *Physics reports*, 57(1), 1-46.
137. Tiddy, G. J., Mateer, D. L., Ormerod, A. P., Harrison, W. J., & Edwards, D. J. (1995). Highly ordered aggregates in dilute dye-water systems. *Langmuir*, 11(2), 390-393.
138. Tsume, Y., Langguth, P., Garcia-Arieta, A. and Amidon, G.L. (2012), *In silico* prediction of drug dissolution and absorption with variation in intestinal pH for BCS class II weak acid drugs: ibuprofen and ketoprofen. *Biopharm. Drug Dispos.*, 33: 366-377. doi:10.1002/bdd.1800
139. Van Der Plank, P., & Rozendaal, A. (1991). *U.S. Patent No. 5,071,975*. Washington, DC: U.S. Patent and Trademark Office.
140. Wagner J. G., Drug Accumulation, *The Journal of Clinical Pharmacology and The Journal of New Drugs*, 2013, Volume 7, Issue 2, pages 84-88, DOI: 10.1002/j.1552-4604.1967.tb00290.x
141. Wan Y., Zhao D., On the controllable soft-templating approach to mesoporous silicates, *Chem. Rev.* 107 (2007) 2821–2860
142. Xu W., Gao Q., Xu Y., Wu D., Sun Y., Shen W., Deng F., Controllable release of ibuprofen from size-adjustable and surface hydrophobic mesoporous silica spheres, *Powder Technology*, Volume 191, 2009, pages 13-20. DOI: 10.1016/j.powtec.2008.09.001
143. Yanagisawa T., Shimizu T., Kuroda K., Kato C. (1990). The preparation of alkyltriethylammonium–kaneinite complexes and their conversion to microporous materials. *Bulletin of the Chemical Society of Japan*, 63(4), 988-992.
144. Yang X. Y., Li Y., Lemaire A., Yu J. G., Su B. L. (2009). Hierarchically structured functional materials: synthesis strategies for multimodal porous networks. *Pure and Applied Chemistry*, 81(12), 2265-2307.
145. Yu J. N., Zhu Y., Wang L., Peng M., Tong S. S., Cao, X., Xu X.M. (2010). Enhancement of oral bioavailability of the poorly water-soluble drug silybin by sodium cholate/phospholipid-mixed micelles. *Acta pharmacologica sinica*, 31(6), 759
146. Yuan, Z. Y., Su B. L. (2006). Insights into hierarchically meso–macroporous structured materials. *Journal of Materials Chemistry*, 16(7), 663-677.

147. Zana Raoul, Dynamics of surfactant self-assemblies: micelles, microemulsions, vesicles and Lyotropic phases. Surfactant Science Series Volume 125; Santa Barbara California 2005.
148. Zhang H., Dunphy D.R., Jiang X., Meng H., Sun B., Tarn D., Xue M., Wang X., Lin Z., Ji S., Li R., Garcia F.L., Yang J., Yang Kirk M.L., Xia T., Zink J.I., Nel A., Brinker C.J., Processing pathway dependence of amorphous silica nanoparticle toxicity - colloidal versus pyrolytic, *J. Am. Chem. Soc.* 134 (2012) 15790–15804.
149. Zhang Q., Dunphy D.R., Jiang X., Meng H., Sun B., Tarn D., Xue M., Wang X., Lin S., Ji Z., Li R., Garcia F.L., Yang J., Kirk M.L., Xia T., Zink J.I., Nel A., Brinker C.J., Processing pathway dependence of amorphous silica nanoparticle toxicity – colloidal versus pyrolytic, *J. Am. Chem. Soc.* 134 (2012) 15790–15804. Complementary medicine evaluation committee, 16th Meeting, (n.d.)
150. Zhang Q., Ko N. R., Oh J. K. (2012). Recent advances in stimuli-responsive degradable block copolymer micelles: synthesis and controlled drug delivery applications. *Chemical communications*, 48(61), 7542-7552.
151. Zhang Y., Wang J., Bai X., Jiang T., Zhang Q., Wang S. (2012). Mesoporous silica nanoparticles for increasing the oral bioavailability and permeation of poorly water-soluble drugs. *Molecular pharmaceutics*, 9(3), 505-513.
152. Zhao D., Huo Q., Feng J., Chmelka B.F., Stucky G.D., Nonionic triblock and star diblock copolymer and oligomeric surfactant syntheses of highly ordered, hydro- thermally stable mesoporous silica structures, *J. Am. Chem. Soc.* 120 (1998) 6024–6036.
153. Zhao D., Yang P., Huo Q., Chmelka B.F., Stucky G.D., Topological construction of mesoporous materials, *Curr. Opin. Solid State Mater. Sci.* 3 (1998) 111–121.
154. Zimny K., Blin J.L., Stébé M.J., Influence of methanol on the phase behavior of nonionic fluorinated surfactant: relation to the structure of mesoporous silica materials, *J. Colloid Interface Sci.* 330 (2009) 456–462.
155. Zimny K., Blin J.L., Stébé M.J., Ordered mesoporous silica templated by nonionic fluorinated liquid crystals, *J. Phys. Chem. C* 113 (2009) 11285–11293.

# Annexes:

1. "Insights of the kollophor/water system for the design of mesostructured silica materials" Claudia Violeta Cervantes-Martinez, MélanieEmo, BénédicteLebeau, Maria-JoséGarcía-Celma, Marie-JoséStébé, Jean-LucBlin.  
<https://doi.org/10.1016/j.micromeso.2019.05.019>
2. CHERD-D-19-00730R1 "Morphosynthesis of porous silica from biocompatible templates" Claudia VioletaCervantes-Martinez, MélanieEmo, Maria-JoséGarcía-Celma, Marie-JoséStébé, Jean-LucBlin <https://doi.org/10.1016/j.cherd.2019.09.006>
3. Porous silica templated by the combination of fine emulsion and P123 micelles for consideration to Colloids and Surfaces A: Physicochemical and Engineering Aspects. (submitted, under revision process). Claudia Violeta Cervantes-Martinez, MélanieEmo, Marie-JoséStébé, Jean-LucBlin
4. Table 1. Solubility results for KTP in different solutions
5. Table 2. Composition of the hybrid material for the release experiments
6. Table 3. Composition of the doped concentrated emulsions for the release experiments and rheological test



## Insights of the kolliphor/water system for the design of mesostructured silica materials

Claudia Violeta Cervantes-Martinez<sup>a</sup>, Mélanie Emo<sup>a</sup>, Bénédicte Lebeau<sup>b,c</sup>,  
 Maria-José García-Celma<sup>d,e</sup>, Marie-José Stébé<sup>a</sup>, Jean-Luc Blin<sup>a,\*</sup>

<sup>a</sup> Institut Jean Barriol, UMR CNRS 7053 L2CM, Université de Lorraine, Faculté des Sciences et Technologies, BP 70239, 54506, Vandoeuvre Lès Nancy Cedex, France

<sup>b</sup> Université de Haute Alsace (UHA), CNRS, IS2M UMR 7361, F-68100, Mulhouse, France

<sup>c</sup> Université de Strasbourg, 67000, Strasbourg, France

<sup>d</sup> Department of Pharmacy and Pharmaceutical Technology and Institute of Nanoscience and Nanotechnology (IN<sup>2</sup>UB), University of Barcelona, Av/ Joan XXIII S/n, 08028, Barcelona, Spain

<sup>e</sup> CIBER of Bioengineering, Biomaterials and Nanomedicine (CIBER-BBN), Barcelona, Spain

### ARTICLE INFO

#### Keywords:

Biocompatible surfactant  
 Phase diagram  
 Micelles structure  
 Synthesis parameters mesostructured silica

### ABSTRACT

Herein, mesostructured silica materials have been prepared through the Cooperative Templating Mechanism (CTM) using kolliphor EL (KEL) as biocompatible surfactant.

First, the behavior of KEL in water has been studied and the phase diagram has been determined. KEL forms micelles ( $L_1$ ) in water and in higher concentrations a liquid crystal domain appears, which is constituted of a cubic phase (Pm3n) and a direct hexagonal phase. Small Angle X-ray Scattering (SAXS) experiments were performed to study the structure of the Organized Molecular Systems. We show that KEL leads to spherical micelles in water, which have a radius comprised between 6.2 and 6.5 nm, depending on the surfactant concentration.

Then, mesoporous materials were synthesized and characterized by SAXS measurements and nitrogen adsorption-desorption analysis. The structure of the recovered material is affected by the surfactant/silica molar ratio. Indeed, the mesopore ordering is detected only for ratios in the range between 0.017 and 0.031. As long as mesostructures are obtained, the mesopores diameters are in accordance with the dimension of the hydrophobic size of the micelles.

### 1. Introduction

Mesoporous materials are materials with pore size between 2 and 50 nm according to the IUPAC nomenclature. Their main characteristic is their high surface area and their big pore volume [1,2]. They also offer a relatively large pore size compared with the zeolites, and allow the diffusion of larger molecules. Thanks to their properties they have several potential applications in many fields, such as adsorbents, catalysts, host matrixes for electronic and photonic devices and sensors [3–5]. To develop these applications, much efforts have been devoted to favor their ecodesign [6,7] and to simplify the synthesis procedures [8].

Regarding their mechanisms of formation there exist two main mechanisms, the Cooperative Templating Mechanism (CTM) [6–12] and the Liquid Crystal Templating (LCT) [13–15]. Both mechanisms

require the presence of an Organized Molecular System. The LCT pathway consists on the transcription of a liquid crystal already formed, whereas the CTM route produces a material with an ordering resulting from the interactions between the silica precursor and a micellar phase. Indeed, in the initial step, the interactions between small silica oligomers and surfactants drive in a cooperative way the formation of hybrid organic-inorganic micelles or aggregates. Then, the condensation of the inorganic precursor at the external surface of the micelles occurs. The ordered mesophase is obtained after intermicellar condensation. Finally, the hydrothermal treatment at higher temperature completes the assembly of micelles and the polymerization of the silica source. The ordered mesoporous material is recovered after surfactant removal. Numerous hydrogenated or fluorinated surfactant-based systems have been investigated as structure directing agents [1,2,11,16–20]. By this way, different kinds of materials called MCM (Mobil Crystalline

\* Corresponding author. Université de Lorraine, UMR CNRS 7053 L2CM, Faculté des Sciences et Technologies, BP 70239, F-54506, Vandoeuvre-lès-Nancy cedex, France.

E-mail address: [Jean-Luc.Blin@univ-lorraine.fr](mailto:Jean-Luc.Blin@univ-lorraine.fr) (J.-L. Blin).

<https://doi.org/10.1016/j.micromeso.2019.05.019>

Received 2 November 2018; Received in revised form 9 May 2019; Accepted 10 May 2019

Available online 11 May 2019

1387-1811/ © 2019 Elsevier Inc. All rights reserved.

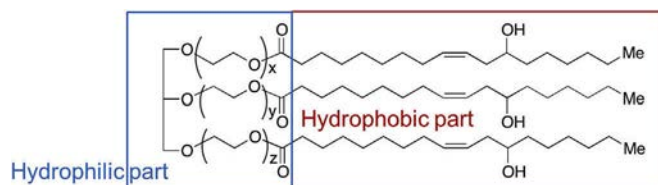
Materials) [1,2], SBA (Santa Barbara Amorphous) [9], MSU (Michigan State University) [10] have been obtained.

Recently more interest of mesoporous materials has been focused on their use in drug delivery. In that case, the organized porosity has been used to achieve a sustained, controlled or pulsed release in drug delivery [21,22]. Their large surface areas together with their large pore volumes have been used to improve the solubility of poorly soluble drugs and their low density allows them to flat into the gastrointestinal tract and prolong the gastric retention of oral drugs. The drug loading into the mesostructured silica is usually performed by physisorption through interactions with the silanol groups. However, the hydrophobic features of most of the drugs limit their diffusion inside the mesopores, resulting in a low drug loading and in a heterogeneous distribution. Much effort has been devoted to overcome this drawback, silica materials can be functionalized with hydrophobic groups. By this way the interactions between the mesostructured material and the drug are enhanced as a consequence a higher loading is achieved and the kinetic of release is facilitated and better controlled.

Another way to improve the drug loading and to control the drug release consists in designing mesostructured hybrid carriers. In that case the surfactant is not eliminated, playing a dual role. First, it allows the solubilization of the drug, then, it acts as a template for the formation of the silica network. For this kind of application, even if silica, especially the one prepared by sol-gel chemistry [23], is known to be safe, not only for the environment, but also for the human body within a certain dose [24], one peculiar attention should be paid to the components used to prepare the silica mesostructure. In literature some studies concern preparation of such hybrid carriers, mainly mesoporous nanoparticles, from cetyltrimethylammonium bromide (CTABr) surfactant [25–27], but applications are rather limited because of the high toxicity of CTABr. The use of biocompatible and nontoxic surfactant is barely reported. For example, Botella et al. [28] have developed the synthesis of ordered mesoporous silica from alkyl maltoside surfactants as organic structure agents under biomimetic conditions. The authors have also demonstrated that the hybrid materials are effective carriers for the delivery of ibuprofen. The drug has been encapsulated in the hydrophobic core of the micelles template prior to the mineralization with TMOS as the silica source. The design of mesostructured silica from biocompatible and nontoxic components is thus still worth to be investigated. In this paper, we have investigated the ability of kolliphor EL, named KEL, to generate ordered mesoporous materials through the Cooperative Templating Mechanism (CTM). The main component of kolliphor EL is glycerol polyethylene glycol ricinoleate. The fatty acid forms the hydrophobic part of the product. The hydrophilic side consists of ethoxylated groups. KEL is widely used as a non-ionic oil-in-water emulsifier and/or solubilizer. This established product demonstrates very good compatibility with other ingredients, and can be used with fat-soluble vitamins and essential oils, or as a purified solubilizer in paclitaxel formulations. To the best of our knowledge, KEL has not been yet considered for the preparation of mesoporous silica. When the CTM pathway is used to synthesize these materials, the characteristics of the recovered materials, such as the structure and the pore diameter, are strongly related to the phase behavior of the structure directing agent in the synthesis solvent. Therefore, in a first part of the present work, we have determined the phase diagram of KEL in water and we have investigated the micellar structure by SAXS. Since the synthesis conditions, such as the quantity of silica source or the surfactant concentration also play an important role in getting a well-defined architecture [29–32], we have studied their influence on the properties of the mesostructure in order to optimize the synthesis parameters.

## 2. Materials and methods

Kolliphor EL (Scheme 1), which is a surfactant synthesized from the reaction of castor oil and ethylene oxide in a molar ratio 1:35 (BASF Corporation, technical literature), was purchased from Sigma Aldrich



**Scheme 1.** Chemical formula of the surfactant Kolliphor EL, with  $x + y + z = 35$ .

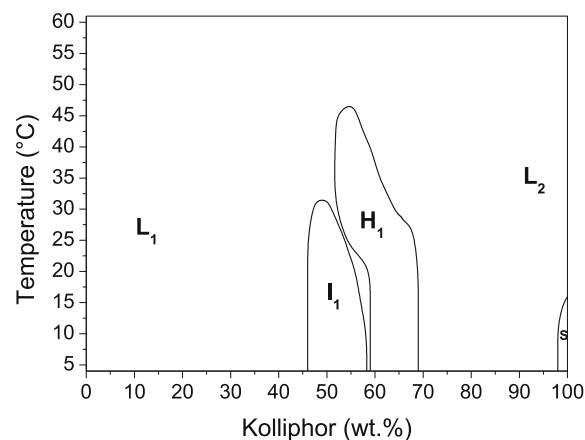


**Fig. 1.** Concentration-temperature phase diagram of the surfactant-water system.  $L_1$  and  $L_2$  correspond to direct and reverse micellar phases, respectively,  $I_1$  corresponds to a direct micellar cubic phase and  $H_1$  corresponds to a direct hexagonal phase. S denotes a solid.

**Table 1**

Lattice parameter (a), hydrophobic radius ( $R_H$ ) and cross-sectional area (S) for the cubic and hexagonal phases at different surfactant/water ratios.

Composition (surfactant/water)	Phase	a (nm)	$R_H$ (nm)	S (nm <sup>2</sup> )
1.0	Pm3n	20.0	3.5	1.2
0.67	$H_1$	10.7	2.6	1.1
0.54	$H_1$	10.4	2.6	1.1

and used as received, without any further purification. Deionized water was obtained using a Milli-Q water purification system. Tetramethoxysilane (TMOS), used as the silica source, was purchased from Sigma Aldrich.

### 2.1. Phase diagram determination

Samples were prepared, by weighting the needed amounts of surfactant and water in hermetically sealed glass tubes. The homogenization of the samples was done by mixing with a vortex stirrer. To improve the homogeneity of the samples, they were also centrifuged several times.

The phase diagram was established by preparing samples over the whole range of surfactant/water concentrations, and placing them in a water bath at the desired temperature until reaching equilibrium (1 week). Visual observations coupled with polarized light optical microscopy (Olympus BX 50) were used to identify the different phases and to determine the mono-, bi- or multiphase domains. Additional Small Angle X-ray Scattering measurements were performed to establish precisely the phase boundaries and to confirm the nature of the different phases.

### 2.2. Silica materials preparation

To synthesize the mesostructured materials, micellar solutions were

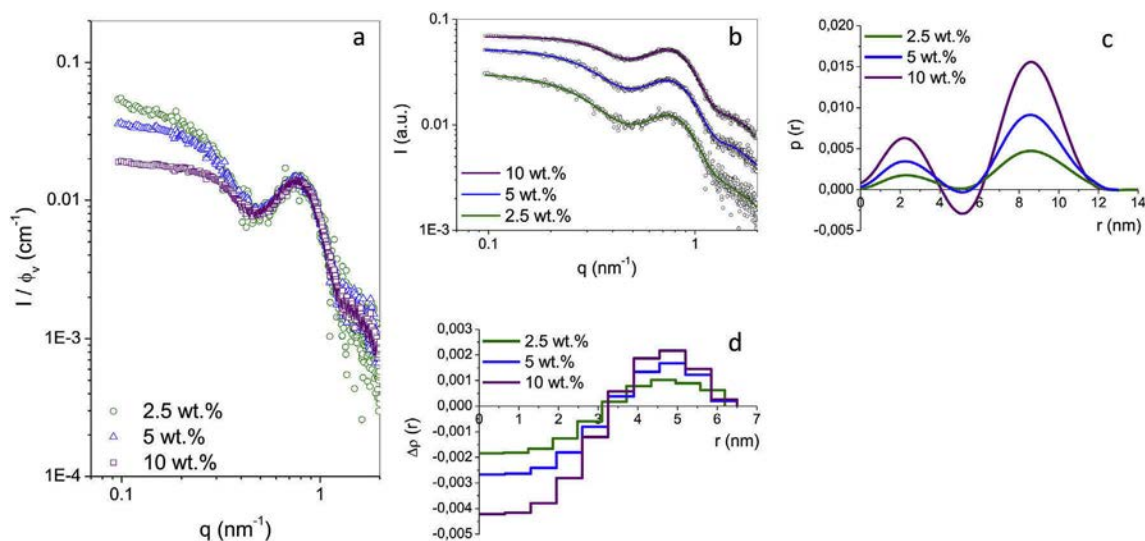


**Fig. 2.** (a) SAXS spectra of the samples at 2.5 wt % (green ○), 5 wt % (blue △) and 10 wt % (purple □) of Kolliphor at 25 °C in log-log representation in absolute units and normalized with regard to the surfactant volume fraction; (b) Experimental (black dotted line) and approximated (GIFT) (solid line) SAXS spectra at 2.5 wt % (green), 5 wt % (blue) and 10 wt % (purple) of Kolliphor at 25 °C; (c) Corresponding pair-distance distribution functions (PDDFs); (d) Corresponding excess-electron density profiles. (For interpretation of the references to colour in this figure legend, the reader is referred to the Web version of this article.)

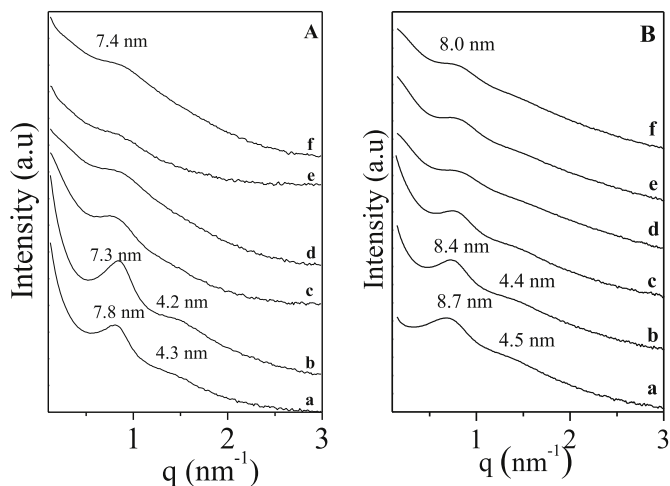


**Fig. 3.** SAXS patterns of the materials synthesized with a surfactant/TMOS molar ratio ( $R'$ ) equal to a: 0.017; b: 0.024; c: 0.031; d: 0.049; e: 0.051 and f: 0.066. The micellar concentration is equal to 2.5 (A) and 10 wt% (B).

first prepared with aqueous solutions at pH = 7.0 and at 25 °C. Six concentrations of surfactant in water were investigated, 2.5, 5, 10, 20, 30 and 40 wt %. Then, TMOS was added dropwise to the solutions and the mixtures were stirred at 300 rpm for 1 h. The surfactant/silica molar ratio ( $R'$ ) was varied from 0.017 to 0.066.

In all cases after preparation the obtained mixtures were placed into sealed Teflon autoclaves at 40 °C for 24 h, then at 100 °C for 24 h. After the hydrothermal treatment, the materials were transferred into cellulose extraction cartridges to remove the template by Soxhlet ethanol extraction for 48 h. After drying at room temperature during 24 h, samples were thermally treated under synthetic air as follow. A first temperature increase was applied at 2 °C/min until 150 °C with a 1 h plateau, followed by a second temperature ramp at 2 °C/min to reach 350 °C. Temperature was held for 1 h, then, a final temperature ramp at 2 °C/min was imposed to reach 550 °C with a 1 h plateau. The cooling process was uncontrolled and directed by the oven inertia.

### 2.3. Characterization

Small angle X-Ray scattering (SAXS) measurements were carried out on a “SAXSess mc<sup>2</sup>” instrument (Anton Paar), using line-collimation system. This instrument is attached to a ID 3003 laboratory X-Ray generator (General Electric) equipped with a sealed X-Ray tube (PANalytical,  $\lambda_{Cu, K\alpha} = 0.1542$  nm) operating at 40 kV and 50 mA. Each sample was introduced in a “Special Glass” capillary, with a diameter equal to 1.5 mm and 2.0 mm for micellar solutions and liquid crystals, respectively, or between two sheets of Kapton® for materials, then placed inside an evacuated sample chamber and exposed to X-Ray beam. Scattering of X-Ray beam was recorded on a CCD detector (Princeton Instruments, 2084 × 2084 pixels array with 24 × 24  $\mu\text{m}^2$  pixel size, sample-detector distance = 309 mm). Using SAXSQuant software (Anton Paar), the two-dimensional image was integrated into one-dimensional scattering intensities  $I(q)$  as a function of the magnitude of the scattering vector  $q = (4\pi/\lambda) \sin(\theta)$ , where  $2\theta$  is the total scattering angle. Thanks to a translucent beamstop allowing the measurement of an attenuated primary beam at  $q = 0$ , all measured intensities can be calibrated by normalizing the attenuated primary intensity. All data were then corrected for the background scattering from the cell and for slit-smearing effects by a desmearing procedure from SAXSQuant software, using Lake method. For micellar solutions, after correction, obtained intensities are scaled into absolute units using water as a reference material. Nitrogen sorption isotherms were determined on a Micromeritics TRISTAR 3000 equipment at -196 °C over a wide relative pressure range from 0.01 to 0.995. The pore diameter and the pore size distribution were determined by applying the BJH (Barret, Joyner, Halenda) method [33] to the adsorption branch of the isotherm.

Transmission electron microscopy (TEM) images were recorded on a JEOL ARM200-CFEG microscope operating at 200 kV. For TEM observation, samples were previously dispersed in chloroform with ultrasounds and few drops of the suspension was spread on Au grid covered by Formvar/amorphous carbon film.

## 3. Results and discussion

### 3.1. The kolliphor EL/water system

The behavior of the surfactant in water was investigated and the

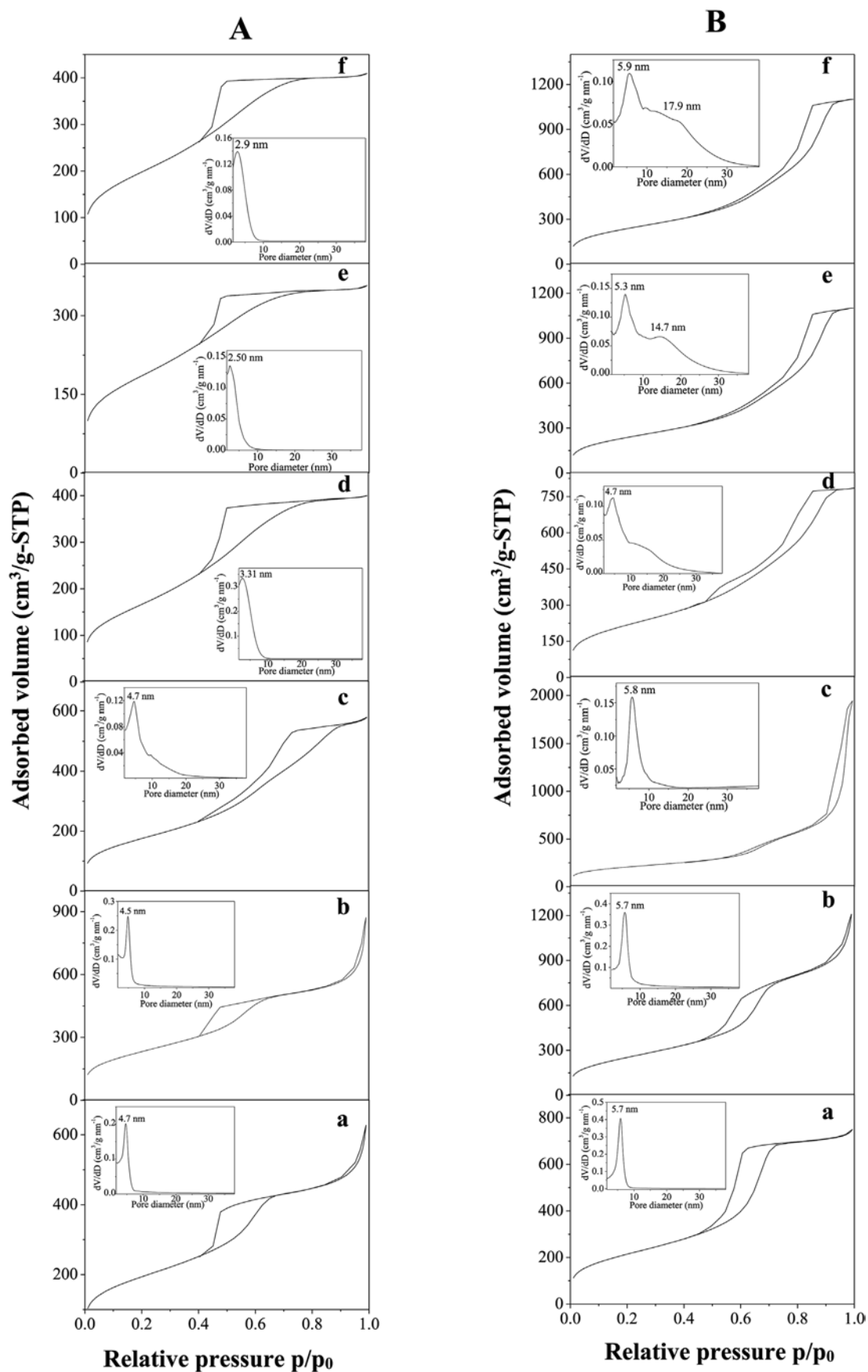
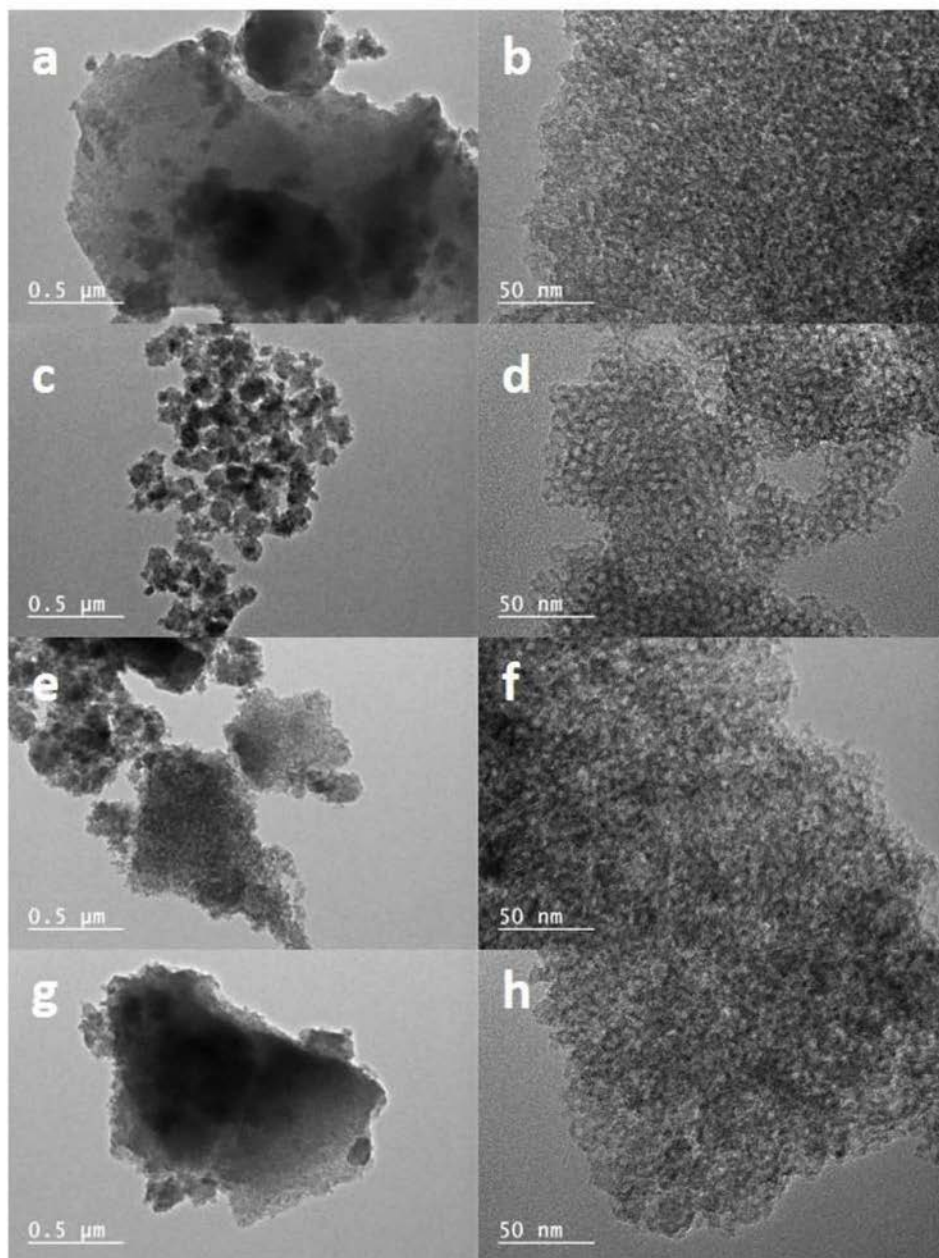


Fig. 4. Nitrogen adsorption-desorption isotherms with the corresponding pore size distribution (insert) of the materials synthesized with a surfactant/TMOS molar ratio ( $R'$ ) equal to a: 0.017; b: 0.024; c: 0.031; d: 0.049; e: 0.051 and f: 0.066. The micellar concentration is equal to 2.5 (A) and 10 wt% (B).



**Fig. 5.** TEM images of the materials synthesized with a surfactant/TMOS molar ratio ( $R'$ ) equal to a,b: 0.017; c,d: 0.024; e,f: 0.031; g,h: 0.049. The micellar concentration is equal to 2.5 wt%.

binary phase diagram is represented on Fig. 1.

For concentrations below 45 wt % of surfactant, micellar solutions stable with temperature are obtained. For higher concentrations of kolliphor EL, liquid crystals phase domain appears. From 46 wt % to 58 wt % of surfactant, a very stiff and isotropic phase which melts at 30 °C is observed; it can be attributed to a cubic phase. The identification of the space group of this cubic phase was determined by SAXS. The relative positions of the reflection lines are  $1: \sqrt{\frac{3}{2}}: \sqrt{2}: \sqrt{\frac{5}{2}}: \sqrt{3}: \sqrt{\frac{29}{4}}$ , which can be assigned to the  $Pm\bar{3}n$  direct micellar cubic phase. From 58 wt % to 68 wt % of surfactant and up to almost 50 °C, an hexagonal phase is obtained. Indeed, the pictures observed by polarized light optical microscopy show a characteristic texture and the relative positions of the reflection lines on the SAXS patterns are  $1: \sqrt{3}: 2$ .

The structural parameters of these liquid crystals phases were determined at several temperatures (10, 20, 25 and 30 °C) by using SAXS. For the cubic phase, the ratio water/Kolliphor ( $R$ ) equal to 1 was

investigated and for the hexagonal phase the studied ratios were 0.67 and 0.54. The structural parameters were determined in accordance with the equations reported in the literature [34]. The lattice parameters  $a$  were obtained from the following equations:  $a = \frac{4\pi}{q_0\sqrt{3}}$  (for the hexagonal phase)  $\frac{q_{hkl}}{2\pi} = \frac{1}{a} \cdot \sqrt{h^2 + k^2 + l^2}$  (for the cubic phase) with  $q_0$ , the position of the first reflection and  $q_{hkl}$  is the position of the peak for the reflection line ( $hkl$ ).

For the hexagonal phase, the hydrophobic radius  $R_H$  is related to the distance  $d$  associated to the first reflection by the following equation [34]:

$$\frac{V_B}{V_S + \alpha V_W} = \frac{\sqrt{3}\pi R_H^2}{2d^2}$$

where  $\alpha$  stands for the number of water molecules per molecule of surfactant,  $V_B$ ,  $V_S$ ,  $V_W$  respectively stand for the molar volumes of the hydrophobic part of the surfactant, the surfactant and water

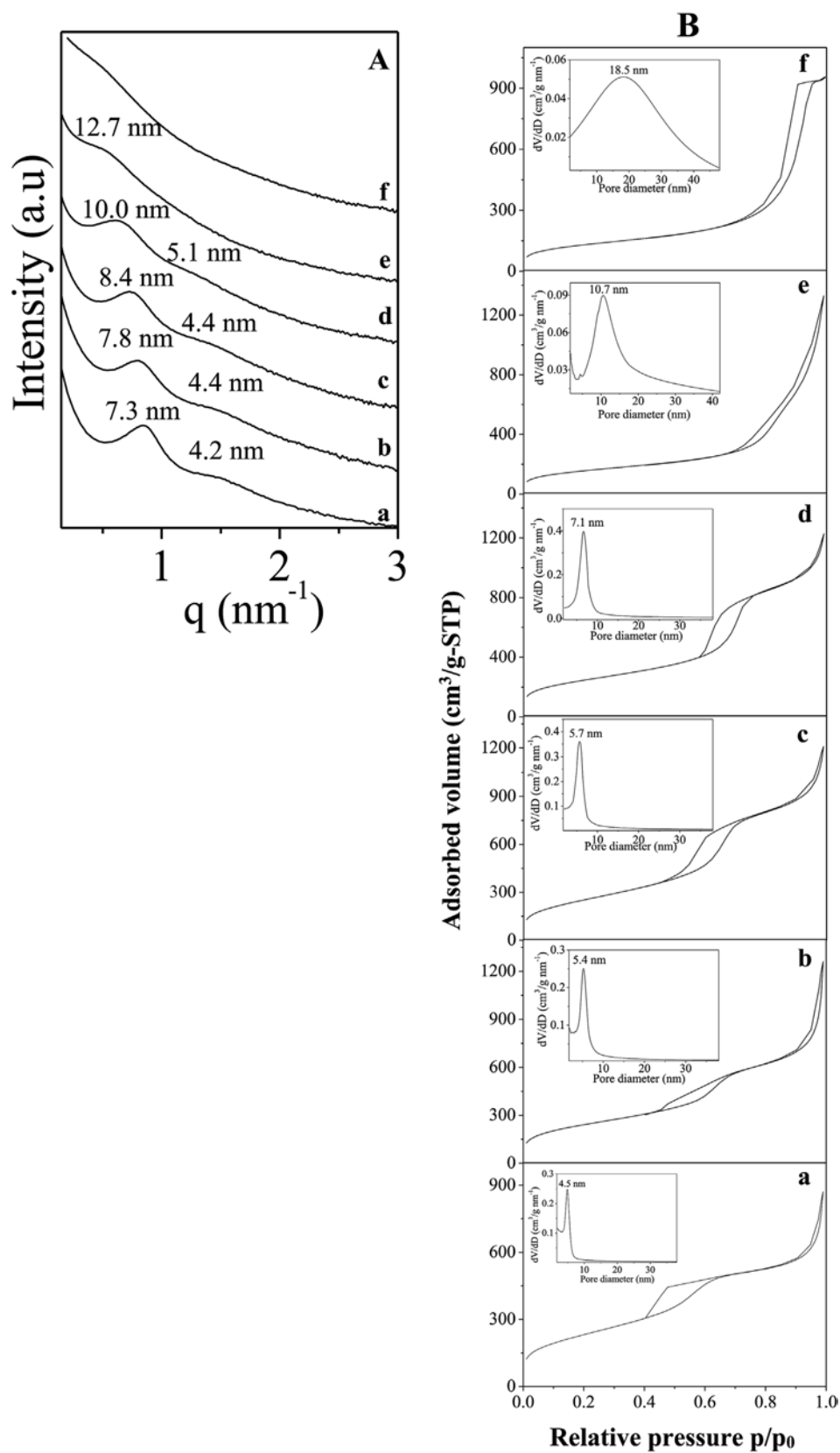


Fig. 6. SAXS patterns (A) and Nitrogen adsorption-desorption isotherms (B) with the corresponding pore size distribution (insert) of the samples synthesized with a KEL concentration (wt.%) of a: 2.5, b: 5, c: 10, d: 20, e: 30 and f: 40. The KEL/TMOS molar ratio is fixed to 0.024.

**Table 2**

Mesoporous materials: cell parameter ( $a_0$ ), specific surface area ( $S_{\text{BET}}$ ), pore volume ( $V_p$ ), pore diameter ( $\varnothing$ ) and pore wall thickness ( $e$ ) concerning the samples obtained at different surfactant concentrations. The KEL/TMOS molar ratio is fixed to 0.024.

[KEL] (wt.%)	$a_0$ (nm)	$S_{\text{BET}}$ (m <sup>2</sup> /g)	$V_p^*$ (cm <sup>3</sup> /g-STP)	$\varnothing^*$ (nm)	$e$ (nm)
2.5	8.4	702	0.7	4.5	3.9
5	9.0	872	0.6	5.4	6.6
10	9.7	928	1.4	5.7	4.0
20	11.5	885	1.5	7.1	4.4
30	–	560	1.4	10.7	–
40	–	466	1.4	18.5	–

\* Values obtained from BJH method applied to the adsorption branch of the isotherm.

- Wormhole like structure.

( $V_W = 18 \text{ cm}^3/\text{mol}$ ,  $V_B = 834 \text{ cm}^3/\text{mol}$  and  $V_S = 2354 \text{ cm}^3/\text{mol}$ ).

Then, the cross sectional area  $S$  can be deduced as:

$$S = \frac{2V_B}{N_A R_H}$$

where  $N_A$  is the Avogadro's number.

For the cubic phase, the hydrophobic radius  $R_H$  is related to the lattice parameter  $a$  by the following equation [34]:

$$\frac{V_B}{V_S + \nu V_W} = \frac{4\nu\pi R_H^3}{3a^3}$$

with  $\nu$  the number of micelles per cubic lattice ( $\nu = 8$  for the  $Pm\bar{3}n$  cubic phase).

Then, the cross sectional area  $S$  can be deduced as:

$$S = \frac{3V_B}{N_A R_H}$$

The results are given in Table 1. For the hexagonal phase, the lattice parameter  $a$  slightly increases with the content of water from 10.4 to 10.7 nm, while the hydrophobic radius and the cross sectional area remain constant, equal to 2.6 nm and  $1.1 \text{ nm}^2$ , respectively. The value of  $R_H$  is higher for the cubic phase (3.5 nm), while the cross sectional area is in the same range ( $1.2 \text{ nm}^2$ ). No significant change of the structural parameters in function of the temperature was observed. Given that, from the length of the bonds, the extended alkyl chains have a dimension of about 2.5 nm and looking at the determined values of the hydrophobic radius for the hexagonal phase, we can deduce that the alkyl chains are completely extended in this phase. For the cubic phase, the hydrophobic radius is bigger than the estimated value. This result can be due to the deviation from the perfect spherical micelles to slightly rods in the  $Pm\bar{3}n$  cubic phase, as suggested by Fontell et al. [35], or to disks as proposed in the Charvolin and Sadoc model [36].

The structure of the micelles of Kolliphor in water were determined by SAXS with the samples at 2.5, 5 and 10 wt % of surfactant. The SAXS spectra are given on Fig. 2a in absolute units.

For all the studied concentrations, the spectra present the same profile. All the curves are overlapped for  $q > 0.45 \text{ nm}^{-1}$  and they exhibit a maximum at  $0.78 \text{ nm}^{-1}$ . For low  $q$  values ( $q < 0.45 \text{ nm}^{-1}$ ), the intensity decreases with the concentration. This feature is characteristic of the existence of interparticle interactions.

To determine the micellar structure, the data were analyzed by using the Generalized Indirect Fourier Transform (GIFT) method [37,38], taking into consideration the interparticle interactions (Fig. 2b). The obtained pair-distance distribution functions (PDDFs) were represented on Fig. 2c. The curves exhibit a pronounced dip, which even goes to negative values for the concentrated solution (10 wt %), indicating that the micelles can be considered as inhomogeneous and so called “core-shell” type particles. All the curves present also a bell-like shape, characteristic of spherical micelles, with a maximum

dimension of about 12.5–13 nm, regardless of the surfactant concentration. These results are in good agreement with the hydrodynamic diameter determined at 25 °C by Dynamic Light Scattering (DLS) measurements (14 nm with diluted micellar solutions (< 2 wt% of surfactant)). Additionally, the excess-electron density profiles have been determined by the deconvolution of the pair-distance distribution functions (PDDFs) (Fig. 2d). The profiles confirm the core-shell type particles for the three micellar solutions. Indeed, the negative density difference corresponds to the hydrophobic part ( $\rho_{\text{phobic}} = 310 \text{ e/nm}^3$ ), whereas the positive density difference can be attributed to the hydrophilic shell ( $\rho_{\text{philic}} = 369 \text{ e/nm}^3$ ). The hydrophobic radius corresponds to the  $r$ -value when the sign of  $\Delta\rho(r)$  changes. It can be estimated at 3.1 and 3.3 nm for 2.5 and 5–10 wt % surfactant concentration, respectively. Then, the micelles radii can be evaluated at 6.2 and 6.5 nm for 2.5 and 5–10 wt % surfactant concentration, respectively. These values are in accordance with the maximum dimension found on the PDDFs. Looking at the excess electron density profile (Fig. 2d), the hydrophobic moieties, corresponding to the lowest values of  $\Delta\rho(r)$ , have a dimension of about 1.9–2.0 nm since the dimension of the hydrophobic chains is estimated at 2.5 nm. We can thus deduce that the alkyl chains are slightly folded. For the hydrophilic chains, considering that one EO group has a dimension of 0.35 nm, their total dimension can be evaluated at 4.5 nm. From Fig. 2d, the hydrophilic part has a length of 4–4.5 nm. Thus, these chains have a rather extended conformation.

### 3.2. Mesoporous silica materials from kolliphor micelles

When the cooperative mechanism is used to prepare the mesoporous silica, the surfactant has to form micelles in solution, but this is not a sufficient condition. Indeed, the other partner, the silica precursor, also plays a crucial role in the formation of the materials [30,31,39]. In particular, the surfactant/silica molar ratio is an important parameter that should be optimized. For two kolliphor concentrations belonging to the micellar domain (2.5 and 10 wt%), the kolliphor/TMOS molar ratio ( $R'$ ) has been varied from 0.017 to 0.066. By this way, from the surfactant point of view, the conditions are gathered for the CTM to occur. The observed variations will thus be due to the effect of the inorganic precursor. Whatever the kolliphor concentration, mesoporous silica materials are recovered until a kolliphor/TMOS ratio of 0.031 (Fig. 3). If the value of  $R'$  is increased the main peak becomes less intense and no secondary reflections are detected any longer. This means that the mesopores arrangement evolves towards a wormhole-like structure. In that case, the quantity of the added TMOS is not enough to cover all the micelles and the interactions between micelles and hydrolyzed precursor are disturbed. As a consequence, the intermicellar condensation leads to a less ordered hybrid mesophase and wormhole-like mesostructures are obtained.

Concerning the nitrogen adsorption-isotherm, regardless the synthesis conditions, all the materials present a type IV isotherm (Fig. 4), characteristic of mesoporous materials. For  $R'$  ratios in the range 0.017–0.031, the mesopore size distribution is quite narrow and the pore diameter remains almost constant for a given kolliphor concentration (insert of Fig. 4). An increase of the mesopore size is noted when the KEL concentration is varied from 2.5 to 10 wt%, for example, for  $R' = 0.017$  the pore diameter increases from 4.7 to 5.7 nm. We can also see that the nitrogen adsorption-desorption isotherm of materials synthesized with a kolliphor/TMOS ratio in this range of values, increases at high relative pressure instead of reaching a plateau as usually observed for type IV isotherms. This behavior has already been reported in literature [31,40] and can be related to the pH conditions which favor the appearance of an interparticle porosity, which is responsible of the ascent of the adsorbed volume at high  $p/p_0$  values. For  $R'$  beyond 0.031, the disorganization of the mesopores network is accompanied by a decrease of the pore diameter (insert of Fig. 4A) or by the appearance of a broad second component in the mesopore size

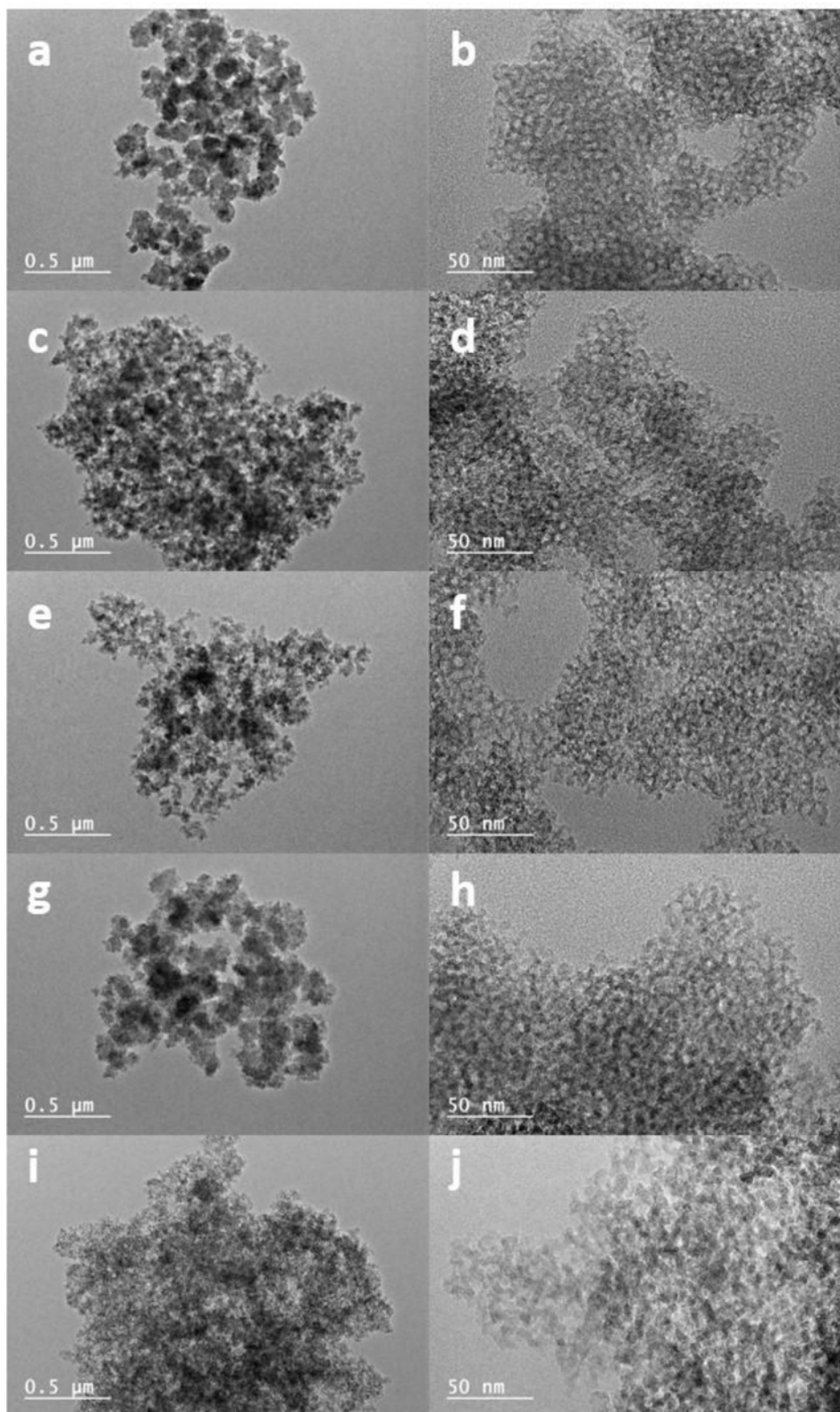


Fig. 7. TEM images of the samples synthesized with a KEL concentration (wt.%) of a,b: 2.5, c,d: 5, e,f: 10, g,h: 20 and i,j: 30. The KEL/TMOS molar ratio is fixed to 0.024.

distribution (insert of Fig. 4B), consequence of the hybrid mesophase reorganization due to the insufficiency of the amount of the inorganic precursor. According to TEM observations at high magnification (Fig. 5) materials with KEL concentration of 2.5% are mesoporous. Mesopores appear larger and more regular in size for  $R' = 0.024$ , that is consistent

with SAXS and nitrogen adsorption/desorption data. It can be clearly observed that pore size increases from  $R' = 0.017$  to 0.024 and then decreases from  $R' = 0.024$  to 0.044. It is interesting to note that particles at  $R' = 0,024$  are smaller and regular in size compared to the others.

From the above results, obtained for a low and high surfactant concentration, it appears that to recover a mesostructured silica with a well-defined pore size distribution the  $R'$  value should be in the range between 0.017 and 0.031. Thus, for the next studies, the kolliphor/TMOS ratio has been fixed to 0.024. Since it also appears that the pore size varies as a function of the kolliphor concentration, the surfactant amount has been varied from 2.5 to 40 wt% to explore the overall micellar domain. The SAXS patterns depicted on Fig. 6A show that mesostructured silica materials are recovered until 20 wt% of kolliphor in water (Fig. 6Aa-d). Increasing the concentration of the micellar solution from 2.5 to 20 wt%, the first peak  $d_{100}$  is shifted from 7.3 to 10 nm, the cell parameter  $a_0$  thus varies from 8.4 to 11.5 nm ( $a_0 = 2d_{100}/\sqrt{3}$ ). Since the cell parameter is the sum of the mesopore diameter ( $\varnothing$ ) and the silica wall thickness ( $e$ ) this suggests that either  $\varnothing$  or  $e$  or both increase as a function of the kolliphor concentration. In this range of KEL concentration, the mesostructured silica presents a type IV isotherm (Fig. 6Ba-d) characteristic of mesoporous materials, according to the IUPAC classification [41]. The relative pressure at which the capillary condensation occurs is progressively shifted to higher  $p/p_0$  values when the surfactant concentration used to prepare the materials is increased. Since this value is related to the mesopore diameter according to the Kelvin equation this means that bigger mesopores are formed. This is confirmed by the pore size distribution, whose maximum is shifted from 4.5 to 7.1 nm as a function of the kolliphor concentration. By contrast it can be seen from Table 2 that the mesopore wall thickness remains almost constant to 4.0 nm. It is also interesting to note that the mesopore diameter is in good accordance with the hydrophobic core size of the micelles determined by SAXS. This observation confirms the templating effect of the KEL micelles. The specific surface area and the pore volume slowly increase from respectively 702 to around 900 m<sup>2</sup>/g and from 0.7 to 1.5 cm<sup>3</sup>g<sup>-1</sup>, when the KEL concentration varies from 2.5 to 20 wt% (Table 2).

The SAXS spectrum of the material synthesized with 30 wt% of kolliphor is characteristic of a wormhole-like structure since it exhibits only a broad peak at 12.7 nm (Fig. 6 Ae). If the KEL concentration is raised to 40 wt% no peak is detected any longer (Fig. 6 Af), meaning that the channel arrangement is completely random. The shape of the isotherm of the samples prepared with a KEL concentration higher than 20 wt% is modified and it becomes intermediate between type IV and type II (Fig. 6 Be,f). Meanwhile the pore size is broader, its maximum is shifted towards higher mesopore diameter and the  $dV/dD$  values decrease. Meantime the specific surface area drops to around 460 m<sup>2</sup>/g, reflecting disorganization of the channel array even if all the conditions are gathered to get an ordered mesostructured silica material. TEM observations confirm the presence of regular mesopores for all samples with  $R' = 0.024$  when KEL concentration increased from 2.5 to 30 wt% (Fig. 7). On the TEM images at high magnification (Fig. 7 b,d,f,h,j) the gradual loss of pore ordering is clearly observed when KEL concentration increased from 10 to 30 wt%. The origin of the loss of the mesopore ordering with the increase of the surfactant concentration can be due to a change of the micelles shape for example from spherical to rods, which disturbs the Cooperative Templating Mechanism. Indeed, when micelles are closed together, due to the limitations on the conformation of oxyethylene groups arising from steric hindrance, repulsive forces occur. This leads to a micelle shape transition like sphere-to-rod [42]. We can also assume that with the increase of the concentration of the micellar solution more and more micelles are formed and the interactions between micelles predominate in the detriment of the ones with the hydrolyzed precursor. Finally, we cannot exclude a shift of the domain of the phase diagram because of the release of the methanol produced during the hydrolysis of the TMOS. Indeed, it is well known that the presence of additives such as salt or alcohol strongly modify the surfactant behavior in water [43,44] and as a consequence affect the formation of the mesostructured silica materials [45,46].

#### 4. Conclusions

Mesoporous materials have been prepared using an aqueous solution of a biocompatible surfactant, the kolliphor EL. In order to determine the phase sequence as a function of the temperature, the phase behavior of KEL in aqueous solution was first investigated. We have delimited the different phase domains and determined the structure of the micelles as well as the structural parameters of the liquid crystals.

Determination of the micellar structure by SAXS provides information about the conformation of the hydrophilic and hydrophobic chains in  $L_1$ . The alkyl chains are slightly folded whereas the hydrophilic chains are rather extended. The micelles are found to be spherical and their radius has been evaluated between 6.2 and 6.5 nm, depending on the kolliphor concentration. In the liquid crystals phases  $H_1$  and  $I_1$ , the hydrophobic chains adopt an extended conformation.

Micellar solutions of kolliphor EL were used as template to prepare the mesoporous materials through the Cooperative Templating Mechanism. The influence of the synthesis conditions on the properties of the mesopore ordering has been investigated. As long as the surfactant concentration is lower than 30 wt% mesostructured silica can be obtained. These materials exhibit a high specific surface area and a narrow pore size distribution, whose maximum varies from 4.5 to 7.1 nm. These values of the mesopores diameters are in accordance with the ones of the size of the hydrophobic core of the micelles determined by SAXS. If the kolliphor concentration is increased, disordered mesoporous silica with broad mesopore size distributions are recovered.

Here, we succeed in preparing bare silica from the biocompatible surfactant Kolliphor EL. KEL has been removed to characterize the porosity. Regarding the interest of hybrid materials for drug delivery we can assume that without removing KEL the hybrid mesostructured silica are excellent candidates for this application. This work is under progress.

#### Acknowledgements

Claudia Violeta Cervantes-Martinez thanks the CONACYT for the financial support of her PhD. Loïc Vidal the person in charge of the "Electronic Microscopy" platform of IS2M is acknowledged for TEM images.

#### References

- [1] C.T. Kresge, W.J. Roth, The discovery of mesoporous molecular sieves from the twenty year perspective, *Chem. Soc. Rev.* 42 (2013) 3663–3670.
- [2] C.T. Kresge, M.E. Leonowicz, W.J. Roth, J.C. Vartuli, J.S. Beck, Ordered mesoporous molecular sieves synthesized by a liquid-crystal template mechanism, *Nature* 359 (1992) 710–712.
- [3] L.F.F.P.G. Braganca, M. Ojeda, J.L.G. Fierro, M.I. Pais da Silva, Bimetallic Co-Pe nanocrystals deposited on SBA-15 and HMS mesoporous silicas as catalysts for Fischer-Tropsch synthesis, *Appl. Catal. A-Gen.* 423–424 (2012) 146–153.
- [4] P. Perego, R. Millini, Porous materials in catalysis: challenges for mesoporous materials, *Chem. Soc. Rev.* 42 (2013) 3956–3976.
- [5] S.Y. Park, M. Barton, P. Pendleton, Mesoporous silica as a natural antimicrobial carrier, *Colloid. Surf. Physicochem. Eng. Asp.* 385 (2011) 256–261.
- [6] N. Baccile, F. Babonneau, B. Thomas, T. Coradin, Introducing ecodeign in silica sol-gel materials, *J. Mater. Chem.* 19 (2009) 8537–8559.
- [7] C. Gérardin, J. Reboul, M. Bonne, B. Lebeau, Ecodeign of ordered mesoporous silica materials, *Chem. Soc. Rev.* 42 (2013) 4217–4255.
- [8] J.A. Martens, J. Jammaer, S. Bajpe, A. Aerts, Y. Lorgouilloux, C.E.A. Kirschhock, Simple synthesis recipes of porous materials, *Microporous Mesoporous Mater.* 140 (2011) 2–8.
- [9] D. Zhao, Q. Huo, J. Feng, B.F. Chmelka, G.D. Stucky, Nonionic triblock and star diblock copolymer and oligomeric surfactant syntheses of highly ordered, hydrothermally stable mesoporous silica structures, *J. Am. Chem. Soc.* 120 (1998) 6024–6036.
- [10] S.A. Bagshaw, E. Prouzet, T.J. Pinnavaia, Templating of mesoporous molecular sieves by nonionic polyethylene oxide surfactants, *Science* 269 (1995) 1242–1244.
- [11] Y. Wan, D. Zhao, On the controllable soft-templating approach to mesoporous silicates, *Chem. Rev.* 107 (2007) 2821–2860.
- [12] J.L. Blin, M. Impéror-Clerc, Mechanism of self-assembly in the synthesis of silica mesoporous materials: in situ studies by X-ray and neutron scattering, *Chem. Soc. Rev.* 42 (2013) 4071–4082.
- [13] G.S. Attard, J.C. Glyde, C.G. Göltner, Liquid-crystalline phases as templates for the

- synthesis of mesoporous silica, *Nature* 378 (1995) 366–368.
- [14] S.A. El-Safty, Y. Kiyozumi, T. Hanaoka, F. Mizukami, Controlled design of ordered and disordered pore architectures, geometries, and dimensions of HOM-type mesostructured monoliths and their hydrothermal stabilities, *J. Phys. Chem. C* 112 (2008) 5476–5489.
- [15] K. Zimny, J.L. Blin, M.J. Stébé, Ordered mesoporous silica templated by nonionic fluorinated liquid crystals, *J. Phys. Chem. C* 113 (2009) 11285–11293.
- [16] I. Park, T.J. Pinnavaia, Large-pore mesoporous silica with three-dimensional Wormhole framework structures, *Microporous Mesoporous Mater.* 118 (2009) 239–244.
- [17] K.Z. Hossain, A. Sayari, Synthesis of onion-like mesoporous silica from sodium silicate in the presence of  $\alpha,\omega$ -diamine surfactant, *Microporous Mesoporous Mater.* 114 (2008) 387–394.
- [18] J.L. Blin, M.J. Stébé, Effect of fluorocarbon addition on the structure and pore diameter of mesoporous materials prepared with a fluorinated surfactant, *Microporous Mesoporous Mater.* 87 (2005) 67–76.
- [19] B. Tan, A. Dozier, H.J. Lehmler, B. Knutson, S.E. Rankin, Elongated silica nanoparticles with a mesh phase mesopore structure by fluorosurfactant templating, *Langmuir* 20 (2004) 6981–6984.
- [20] J. Esquina, C. Rodriguez, C. Solans, H. Kunieda, Formation of mesostructured silica in nonionic fluorinated surfactant systems, *Microporous Mesoporous Mater.* 92 (2006) 212–219.
- [21] M. Arruebo, WIREs, Drug delivery from structured porous inorganic materials, *Nanomed. Nanobiotechnol.* 4 (2012) 16–30.
- [22] M. Moritz, M. Geszke-Moritz, Mesoporous materials as multifunctional tools in biosciences: principles and applications, *Mater. Sci. Eng. C* 49 (2015) 114–151.
- [23] H. Zhang, D.R. Dunphy, X. Jiang, H. Meng, B. Sun, D. Tarn, M. Xue, X. Wang, S. Lin, Z. Ji, R. Li, F.L. Garcia, J. Yang, M.L. Kirk, T. Xia, J.I. Zink, A. Nel, C.J. Brinker, Processing pathway dependence of amorphous silica nanoparticle toxicity - colloidal versus pyrolytic, *J. Am. Chem. Soc.* 134 (2012) 15790–15804.
- [24] **Complementary medicine evaluation committee, 16<sup>th</sup> Meeting, (n.d.).**
- [25] A. Corma, M. Moliner, M.J. Díaz-Cabanas, P. Serna, B. Femenia, J. Primo, H. García, Biomimetic synthesis of microporous and mesoporous materials at room temperature and neutral pH, with application in electronics, controlled release of chemicals, and catalysis, *New J. Chem.* 32 (2008) 1338–1345.
- [26] N.W. Clifford, K.S. Iyer, C.L. Raston, Encapsulation and controlled release of nutraceuticals using mesoporous silica capsules, *J. Mater. Chem.* 18 (2008) 162–165.
- [27] Q. He, J. Shi, F. Chen, M. Zhu, L. Zhang, An anticancer drug delivery system based on surfactant-templated mesoporous silica nanoparticles, *Biomaterials* 31 (2010) 3335–3346.
- [28] P. Botella, A. Corma, M. Quesada, Synthesis of ordered mesoporous silica templated with biocompatible surfactants and applications in controlled release of drugs, *J. Mater. Chem.* 22 (2012) 6394–6401.
- [29] P.F. Fulvio, S. Pikus, M. Jaroniec, Tailoring properties of SBA-15 materials by controlling conditions of hydrothermal synthesis, *J. Mater. Chem.* 15 (2005) 5049–5053.
- [30] T. Benamor, L. Vidal, B. Lebeau, C. Marichal, Influence of synthesis parameters on the physico-chemical characteristics of SBA-15 type ordered mesoporous silica, *Microporous Mesoporous Mater.* 153 (2012) 100–114.
- [31] A. Léonard, J.L. Blin, P.A. Jacobs, P. Grange, B.L. Su, Chemistry of silica at different concentrations of non-ionic surfactant solutions: effect of pH of the synthesis gel on the preparation of mesoporous silicas, *Microporous Mesoporous Mater.* 63 (2003) 59–73.
- [32] A. Galarneau, M. Nader, F. Guenneau, F. Di Renzo, A. Gedeon, Understanding the stability in water of mesoporous SBA-15 and MCM-41, *J. Phys. Chem. C* 111 (2007) 8268–8277.
- [33] E.P. Barrett, L.G. Joyner, P.P. Halenda, The determination of pore volume and area distributions in porous substances. I. Computations from nitrogen isotherms, *J. Am. Chem. Soc.* 73 (1951) 373–380.
- [34] M. Alibrahim, M.J. Stébé, G. Dupont, J.C. Ravey, Effect of an ionic surfactant on the phase behavior of a nonionic surfactant-based system, *J. Chim. Phys. Phys. Chim. Biol.* 94 (1997) 1614–1633.
- [35] K. Fontell, K.K. Fox, E. Hansson, On the structure of the cubic phase I<sub>1</sub> in some lipid-water systems, *Mol. Cryst. Liq. Cryst.* 1 (1985) 9–17.
- [36] J. Charvolin, J.F. Sadoc, Periodic systems of frustated fluid films and micellar cubic structures in liquid crystals, *J. Phys.* 49 (1988) 521–526.
- [37] O. Glatter, O. Kratky, *Small Angle X-Ray Scattering*, Academic Press, 1982, pp. 167–196.
- [38] G. Fritz, O. Glatter, Structure and interaction in dense colloidal systems: evaluation of scattering data by the generalized indirect Fourier transformation method, *J. Phys. Condens. Matter* 18 (2006) S2403–S2419.
- [39] F. Michaux, M.J. Stébé, J.L. Blin, Systematic investigation of the synthesis parameters driving the preparation of mesoporous materials using a nonionic fluorinated surfactant, *Microporous Mesoporous Mater.* 151 (2012) 201–210.
- [40] M.J. Stébé, M. Emo, A. Forný-Le Follot, L. Metlas-Komunjer, I. Pezron, J.L. Blin, Triblock siloxane copolymer surfactant: template for spherical mesoporous silica with a hexagonal pore ordering, *Langmuir* 29 (2013) 1618–1626.
- [41] K.S.W. Sing, D.H. Everett, R.A.W. Haul, L. Moscou, R.A. Pierotti, J. Rouquerol, T. Siemieniowska, Reporting physisorption data for gas/solid systems with special reference to the determination of surface area and porosity (Recommendations 1984) IUPAC, *Pure Appl. Chem.* 57 (1985) 603–619.
- [42] D.J. Mitchell, G.J.T. Tiddy, L. Waring, T. Bostock, M.P. Mc Donald, Phase behaviour of polyoxyethylene surfactants with water. Mesophase structures and partial miscibility (cloud points), *J. Chem. Soc. Faraday Trans. 1* 79 (1983) 975–1000.
- [43] H. Schott, Effect of inorganic additives on solutions of nonionic surfactants, *J. Colloid Interface Sci.* 189 (1997) 117–122.
- [44] K. Shinoda, J.J. Lagowski (Ed.), *In Principles of Solution and Solubility*, M. Dekker Inc, New York and Basel, 1978, p. 180.
- [45] J.L. Blin, N. Du, M.J. Stébé, Alcohols solubilization in a nonionic fluorinated surfactant based system: effect on the mesoporous silica characteristics, *J. Colloid Interface Sci.* 373 (2012) 34–45.
- [46] K. Zimny, J.L. Blin, M.J. Stébé, Influence of methanol on the phase behavior of nonionic fluorinated surfactant: relation to the structure of mesoporous silica materials, *J. Colloid Interface Sci.* 330 (2009) 456–462.

Contents lists available at [ScienceDirect](https://www.sciencedirect.com)

Chemical Engineering Research and Design

journal homepage: [www.elsevier.com/locate/cherd](http://www.elsevier.com/locate/cherd)IChemE  
ADVANCING  
CHEMICAL  
ENGINEERING  
WORLDWIDE

# Morphosynthesis of porous silica from biocompatible templates

Claudia Violeta Cervantes-Martinez<sup>a</sup>, Mélanie Emo<sup>a</sup>,  
Maria-José García-Celma<sup>b,c</sup>, Marie-José Stébé<sup>a</sup>, Jean-Luc Blin<sup>a,\*</sup>

<sup>a</sup> Institut Jean Barriol, UMR CNRS 7053 L2CM, Université de Lorraine, Faculté des Sciences et Technologies, BP 70239, 54506, Vandoeuvre lès Nancy cedex, France

<sup>b</sup> Department of Pharmacy and Pharmaceutical Technology and Institute of Nanoscience and Nanotechnology (IN<sup>2</sup>UB), University of Barcelona, Av/ Joan XXIII s/n, 08028, Barcelona, Spain

<sup>c</sup> CIBER of Bioengineering, Biomaterials and Nanomedicine (CIBER-BBN), Barcelona, Spain

## ARTICLE INFO

### Article history:

Received 10 May 2019

Received in revised form 24 July 2019

Accepted 2 September 2019

Available online 11 September 2019

### Keywords:

Biomimetics

Sol-gel

Silica

Controlled porosity

Emulsions

SAXS

## ABSTRACT

Taking inspiration from morphogenesis, synthetic porous silica materials have been synthesized through rational designs combining the sol-gel process and the surfactant templating method. Materials have been prepared from biocompatible systems using kolliphor as surfactant.

The effect of Miglyol and Myristate solubilization in the Kolliphor/water system was first investigated in detail. The phase diagram proved that only a weak fraction of these oils ( $\approx 1$  wt.%) can be incorporated into the hydrophobic core of the micelles ( $L_1$ ). Results also show that whatever the liquid crystal phases [direct hexagonal ( $H_1$ ) and lamellar ( $L_\alpha$ )] the swelling effect take place upon addition of oil. Moreover, at low oil concentration oil-in-water fine emulsions are formulated, while at high oil concentration, oil-in-water concentrated emulsion are formulated.

Starting from the various systems, porous silica materials were then synthesized. Results obtained by SAXS and nitrogen adsorption-desorption analysis show that Miglyol and Myristate can expand the mesopore size. The variations of the pore diameter have been related to the solubilization properties of the oil in the surfactant. In addition, macroporous silica could be design by using concentrated emulsions as template.

This work demonstrates that synthetic silica materials can be obtained by mimic of natural processes.

© 2019 Institution of Chemical Engineers. Published by Elsevier B.V. All rights reserved.

## 1. Introduction

The interest of designing inorganic materials having a microscopic or nanoscopic size lies on the importance of their shape and their texture compared to the intrinsic properties of the solid, for phenomena such as diffusion, catalytic activity, efficiency in separation and so on. The topology of the surface, as well as the manufacture of hollow or cellular structures are essential factors in new processes for the design of synthetic inorganic materials, with precise and defined architectures. Material design at the mesoporous scale can mimic nat-

ural processes by which, from minerals, microorganisms build their vital elements such as the carapaces of different marine organisms, bones, teeth, etc., and which are also explained on the basis of the concept of template (Mann and Ozin, 1996). The replication phenomena and the specificities observed in the biogenic crystals may provide the means and the molecules that will be used in morphosynthesis. Taking inspiration from Mother Nature, sol-gel chemistry is indeed the perfect chemical tool to generate sophisticated materials. For example, combining the sol-gel process with the surfactant templating mechanism the morphosynthesis can lead to ordered mesostructured silica.

\* Corresponding author at: Université de Lorraine, UMR CNRS 7053 L2CM, Faculté des Sciences et Technologies, BP 70239, F-54506, Vandoeuvre-lès-Nancy cedex, France.

E-mail address: [Jean-Luc.Blin@univ-lorraine.fr](mailto:Jean-Luc.Blin@univ-lorraine.fr) (J.-L. Blin).

<https://doi.org/10.1016/j.cherd.2019.09.006>

0263-8762/© 2019 Institution of Chemical Engineers. Published by Elsevier B.V. All rights reserved.

Thanks to their properties, the emergence of these materials provides not only a series of novel materials that possess large uniform pore sizes (1.5–10 nm), highly ordered nanochannels, large surface areas ( $\sim 1000 \text{ m}^2/\text{g}$ ) (Kresge et al., 1992; Beck et al., 1992), but also an idea of the design of periodic arrangements of inorganic-organic composite nanoarrays. To prepare these compounds two strategies can be adopted following the example of nature: synergistic synthesis also named the cooperative templating mechanism (CTM) (Wan and Zhao, 2007; Martens et al., 2011; Kresge and Roth, 2013; Blin and Imp eror-Clerc, 2013) and the transcriptive synthesis (Attard et al., 1995; El-Safty et al., 2008; Zimny et al., 2009; Veliscek-Carolan 2015). In any case, the characteristics of the resulting materials is strongly related to the physicochemical properties of surfactant, which can be modified by the incorporation of additive. In particular, the introduction of oil into the surfactant-water system can lead to the formation of swollen micelles or microemulsions (Tiddy, 1980), depending on whether or not an oily core can exist. If the concentration of oil is widely increased the oil-rich-corner of the ternary phase diagram is reached and depending on the properties of the system and in particular its phase inversion temperature (PIT), concentrated emulsions can be formulated (Bleta et al., 2006). Indeed, at this temperature the transition from direct systems to reverse ones, where the continuous media is non-polar, occurs. When the value of the PIT is very high, the curvature radius of the surfactant is not changed and the Bancroft rule is then verified. Thus, the aqueous phase is the external one and oil-in-water (o/w) concentrated emulsions, which can contain high quantity of the dispersed phase (oil) can be formulated. Direct emulsions consist of oil droplets dispersed in the aqueous phase, whereas inverse emulsions refer to the dispersion of water droplets in oil. If the internal phase volume is higher than 74%, the emulsion belongs to the high internal phase emulsion (HIPE) family, also called concentrated emulsions or gel emulsions (Princen, 1983; Ravey et al., 1994; Cameron and Sherrington, 1996). As micelles or liquid crystals, these various systems, which appear in the presence of oil, can also be used as templates to design porous materials by morphosynthesis. Depending on the structure of the initial selected surfactant-system either large size mesostructures, macroporous or hierarchical materials are recovered (Imhof and Pine, 1997; Sayari et al., 1999; Lind et al., 2002; Zhang et al., 2003; Carn et al., 2004; Ottaviani et al., 2004; Sen et al., 2005; Kruk and Cao, 2007; Zhang and Chen, 2007; Zhao et al., 2007). Generally, the large pore mesoporous silica are formed from microemulsions and in that case the amount of oil is relatively low. For example, the Meso-Cellular Silica Foams (MCF's) are prepared from oil-in-water microemulsions (Schmidt-Winkel et al., 2000). Their structure is described as a macroporous network consisting of spherical cells interconnected by windows, whose presence has been evidenced by TEM experiments and theoretical calculations. (Lettow et al., 2000) Similar structures were obtained by employing the emulsion method, where the role of oil is to act both as a swelling agent for the mesopore size expansion and as a template for the generation of the MCFs (Imhof and Pine, 1997; Zhang and Chen, 2007; Zhao et al., 2007).

The obtained porous materials have applications in various domains such as electronic, catalysis, adsorption and so on (Park et al., 2011; Braganca et al., 2012; Perego and Millini, 2013). More recently, interest has been paid to these compounds in drug delivery (Arruebo, 2012; Moritz and Geszke-Moritz, 2015). Indeed, they enhance the solubilization of poorly soluble drugs and allow a sustained, controlled or pulsed release (Arruebo, 2012). In that way, much efforts are devoted to the preparation of these porous silica from biocompatible compounds, i.e. surfactant and oil. However, in the literature this kind of studies is barely reported. In this paper, we have investigated in detail the effect of oil solubilization into Kolliphor EL in relation with the design by morphosynthesis of porous silica. Kolliphor EL is a biocompatible surfactant, which is synthesized from the reaction of castor oil with ethylene oxide in a molar ratio of 1:35.

## 2. Materials and methods

Kolliphor EL and isopropyl Myristate (IM) were purchased from Sigma Aldrich and used as received, without any further purifi-

cation. Miglyol<sup>®</sup> 812N (Miglyol), which is a medium-chain triglyceride composed mainly of caprylic and capric fatty acids, was provided by IOI Oleo GmbH- IOI Oleochemical company. Deionized water was obtained using a Milli-Q water purification system. Tetramethoxysilane (TMOS), used as the silica source, was purchased from Sigma Aldrich.

### 2.1. Phase diagrams determination

Samples were prepared, by weighting the needed amounts of surfactant, water and oil in hermetically sealed glass tubes. The homogenization of the samples was done by mixing with a vortex stirrer. To improve the homogeneity of the samples, they were also centrifuged several times.

The phase diagrams were established by preparing samples over the whole range of surfactant/water and oil concentrations, and placing them in a water bath at the desired temperature until reaching equilibrium (1 week). Visual observations allowed to determine the mono-, bi- or multiphasic domains and polarized light optical microscopy (Olympus BX 50) was used to identify the different liquid crystals phases. Additional Small Angle X-ray Scattering measurements were performed to establish precisely the phase boundaries, to confirm the nature of the different phases and to determine the space group of the cubic phase.

### 2.2. Emulsion formation process

The water-rich emulsions were formed either by the Phase Inversion Composition (PIC) or the Phase Inversion Temperature (PIT) (Solans and Sol e, 2012). Those two techniques are based on the capacity of the surfactants to change their curvature, thus modifying the continuous medium. Using the PIT method, emulsions are obtained by increasing the temperature quickly to pass through the PIT. With the PIC method, the mixtures of the oil and surfactant with different oil/surfactant ratios were first prepared. Then, water was added dropwise by using an automatic peristaltic pump which injects the right amount of water in a constant settled rate of  $250 \mu\text{L s}^{-1}$ ; the mixture was constantly magnetically stirred at 1250 rpm at 25 °C.

For the oil-rich emulsions, mixtures of water and surfactant were prepared with ratios water/surfactant (R) between 1.9 to 9. Then, the oil is added dropwise to the mixture under continuous stirring. The emulsions with the ratio R equal to 5.7 containing 70, 80, 90 et 95 wt.% of oil were characterized.

### 2.3. Silica materials preparation

To synthesized the mesostructured materials, first the oil and the surfactant were mixed at 1250 rpm at 25 °C, then water (pH=7) was added at a fixed rate of  $250 \mu\text{L s}^{-1}$ . The surfactant concentration in water was fixed to 10 wt.% and samples containing 1, 3, 5, 7, 10 and 15 wt.% of Miglyol or Myristate were studied. Then, TMOS was added dropwise to the solutions and the mixtures were stirred at 300 rpm for 1 h. The surfactant/silica molar ratio was fixed to 0.024

Macroporous materials were obtained by the emulsions templating mechanism. Before the incorporation of oil, a micellar solution of Kolliphor containing 15 wt.% of surfactant was prepared. The concentration of oil, added to the micellar solution, was made to vary from 70 to 95 wt.%. The pH value of the solutions and the surfactant/silica molar ratio were fixed to 7 and 0.024, respectively.

In all cases after preparation the obtained mixtures were placed into sealed Teflon autoclaves at 40 °C for 24 h, then at 100 °C for 24 h. After the hydrothermal treatment, the materials were transferred into cellulose extraction cartridges to remove the template by Soxhlet ethanol extraction for 48 h. After drying at room temperature during 24 h, samples were thermally treated under synthetic air as follow. A first temperature increase was applied at 2 °C/min until 150 °C with a 1 h plateau, followed by a second temperature ramp at 2 °C/min to reach 350 °C. Temperature was held for 1 h, then, a final temperature ramp at 2 °C/min was imposed to reach 550 °C with a 1 h plateau. The cooling process was uncontrolled and directed by the oven inertia.

## 2.4. Characterization

Small Angle X-Ray Scattering (SAXS) measurements were carried out on a “SAXSess mc<sup>2</sup>” instrument (Anton Paar), using line-collimation system. This instrument is attached to a ID 3003 laboratory X-Ray generator (General Electric) equipped with a sealed X-Ray tube (PANalytical,  $\lambda_{\text{Cu, K}\alpha} = 0.1542 \text{ nm}$ ) operating at 40 kV and 50 mA. Each sample was introduced in a “Special Glass” capillary, with a diameter equal to 1.5 mm and 2.0 mm for micellar solutions and liquid crystals, respectively, or between two sheets of Kapton<sup>®</sup> for materials, then placed inside an evacuated sample chamber and exposed to X-Ray beam. Scattering of X-Ray beam was recorded on a CCD detector (Princeton Instruments, 2084 × 2084 pixels array with 24 × 24  $\mu\text{m}^2$  pixel size, sample-detector distance = 309 mm). Using SAXSQuant software (Anton Paar), the two-dimensional image was integrated into one-dimensional scattering intensities  $I(q)$  as a function of the magnitude of the scattering vector  $q = (4\pi/\lambda) \sin(\theta)$ , where  $2\theta$  is the total scattering angle. Thanks to a translucent beamstop allowing the measurement of an attenuated primary beam at  $q = 0$ , all measured intensities can be calibrated by normalizing the attenuated primary intensity. The data were then corrected for the background scattering from the cell and for slit-smearing effects by a desmearing procedure from SAXSQuant software, using Lake method. For micellar solutions, after correction, obtained intensities are scaled into absolute units using water as a reference material. Nitrogen sorption isotherms were determined on a Micromeritics TRISTAR 3000 equipment at −196 °C over a wide relative pressure range from 0.01 to 0.995. The pore diameter and the pore size distribution were determined by applying the BJH (Barret, Joyner, Halenda) method (Barrett et al., 1951) to the adsorption branch of the isotherm. Samples were prepared for Scanning electron microscopy (SEM) by dispersing some material in ethanol. The experiments were done on HITACHI S-2500 at 15 keV. Intrusion/extrusion mercury porosimetry were measured with a Micromeritics Autopore IV 9500 porosimeter. Dynamic Light Scattering (DLS) experiments were performed with a Malvern 300HSA Zetasizer instrument.

## 3. Results and discussion

### 3.1. Solubilization of Miglyol or Myristate in the Kolliphor/water system

#### 3.1.1. Ternary phase diagrams

The phase diagram of Kolliphor/Miglyol/water and Kolliphor/Myristate/water at 25 °C are reported on Fig. 1. A micellar solution is observed for surfactant concentrations until 45 wt.% but only a few quantities (1 wt.%) of Miglyol

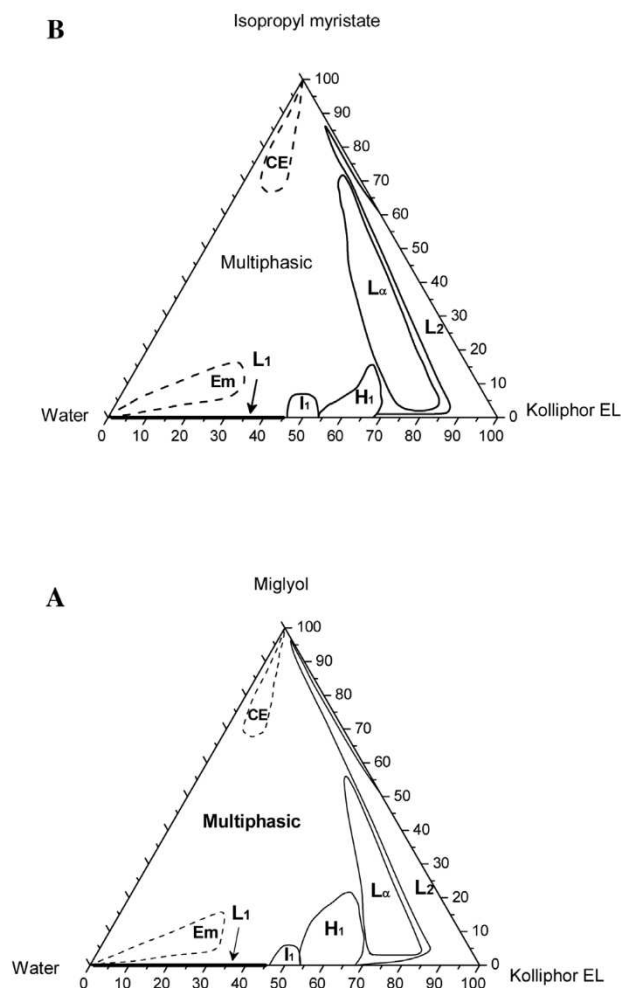


**Fig. 1** – Ternary phase diagram, at 25 °C, of the Kolliphor EL/Miglyol/water (A) and Kolliphor EL/Myristate/water (B) systems.  $L_1$  and  $L_2$  denote direct and reverse micellar phase, respectively.  $I_1$ ,  $H_1$  and  $L_\alpha$  correspond to direct micellar cubic phase, direct hexagonal phase and lamellar phase, respectively.  $Em$  and  $CE$  correspond to fine emulsion and concentrated emulsion, respectively.

(Fig. 1A) or Myristate (Fig. 1B) can be solubilized in the micelles of Kolliphor. The cubic phase can incorporate some amounts of oil, up to around 5 wt.% of Miglyol and 8 wt.% of Myristate. A more significant amount of oil can be accommodated in the hexagonal liquid crystal, up to 20 and 15 wt.% of Miglyol and Myristate, respectively. For water/surfactant ( $R$ ) ratios between 0.18 and 0.33, a lamellar phase ( $L_\alpha$ ) appears, but only after the addition of 5 wt.% of Miglyol (Fig. 1A). This lamellar phase is highly stable and it can incorporate until 55 wt.% of Miglyol. In the Kolliphor Myristate/water system (Fig. 1B) this lamellar phase appears after the addition of 4 wt.% of oil and for  $R$  ratio between 0.14 and 0.4. In that case up to 70 wt.% of oil can be incorporated in  $L_\alpha$ . Two types of direct emulsions can be prepared. On the one hand, by the PIC method, emulsions stable for few days were formed in the water-rich domain ( $Em$ ) and can be incorporated until 15 wt.% of oil (Fig. 1). Depending on the kind of oil and on its quantity the size of the emulsions varies between 20 and 45 nm (Table 1). Thus these emulsions have been labeled as fine emulsions. On the other hand, in the oil-rich domain, high concentrated emulsions (between 70 and 95 wt.% of oil) were highlighted for  $1.9 < R < 9$ . ( $CE$  in Fig. 1). The size of the concentrated emulsions obtained by optical microscopy is around 15  $\mu\text{m}$  and to 12  $\mu\text{m}$  for the emul-

**Table 1 – Size (nm) of the fine emulsions from DLS measurements. The kolliphor concentration in aqueous solution is 10 wt.%.**

Wt.% of oil	Miglyol	Myristate
3	21.4	28.7
5	30.5	39.5
7	35.4	43.2
10	41.5	45.8

sions containing 90 and 95 wt.% of Miglyol, respectively. These systems are stable for several months.

### 3.1.2. Effect of oil solubilization on the liquid crystals

SAXS measurements were performed to determine the evolution of the structural parameters of the liquid crystals in function of the addition of oil.

The structural parameters were determined in accordance with the equations reported in the literature (Sakya et al., 1997; Alibrahim et al., 1997). For the lamellar phase, the cross sectional area  $S$  can be obtained from the the following Equation:

$$S = \frac{2(V_S + \alpha V_W + \beta V_O)}{N_A d}$$

The hydrophobic thickness  $d_B$  and the hydrophilic thickness  $d_A$  can be deduced from the following Equations:

$$d_B = \frac{2(V_B + \beta V_O)}{N_A S} \text{ and } d = d_A + d_B$$

where  $\alpha$  stands for the number of molecules of water per molecule of surfactant,  $\beta$  stands for the number of molecules of oil per molecule of surfactant, and  $V_W$ ,  $V_O$ ,  $V_B$ ,  $V_S$ , respectively stand for the molar volumes of water, oil, the hydrophobic part of the surfactant, and the surfactant, ( $V_W = 18$ ,  $V_O = 524$  (Miglyol® 812N) or 318 (isopropyl myristate),  $V_B = 834$  and  $V_S = 2354$  cm<sup>3</sup>/mol).

Plots of the structural parameters in function of the quantity of incorporated oil for  $L\alpha$  are represented on Figs. 2A and 2B for Miglyol and Myristate, respectively. Whatever the oil used, the spacing parameter  $d$  and the hydrophobic thickness  $d_B$  increase with the addition of oil in the system, while the area of the polar head  $S$  and the hydrophilic thickness  $d_A$  are constant and equal to 1.1 nm<sup>2</sup> and 6.5 nm, respectively. This means that the oil probably does not penetrate between the hydrophobic chains, but rather forms an oily film which becomes thicker with the addition of Miglyol or Myristate. Interestingly, by extrapolating the value of  $d_B$  for  $\beta=0$ , the hydrophobic thickness for the lamellar phase is comprised between 2.5 and 2.0 nm, depending on the oil used. Given that the dimension of a hydrophobic chain is estimated at 2.5 nm, we can deduce that the alkyl chains in the lamellar phase are folded. It is noted that the thickness of the hydrophobic part is much thicker with isopropyl myristate, about 30 nm against 10 nm with miglyol since the incorporation of this latter can reach 75 wt.%, while the incorporation of Miglyol is limited to 55 wt.%.

For the hexagonal phase, the hydrophobic radius  $R_H$  is related to the distance  $d$  associated to the first peak by the following relation:

$$\frac{V_B + \beta V_O}{V_S + \alpha V_W + \beta V_O} = \frac{\sqrt{3}\pi R_H^2}{2d^2}$$

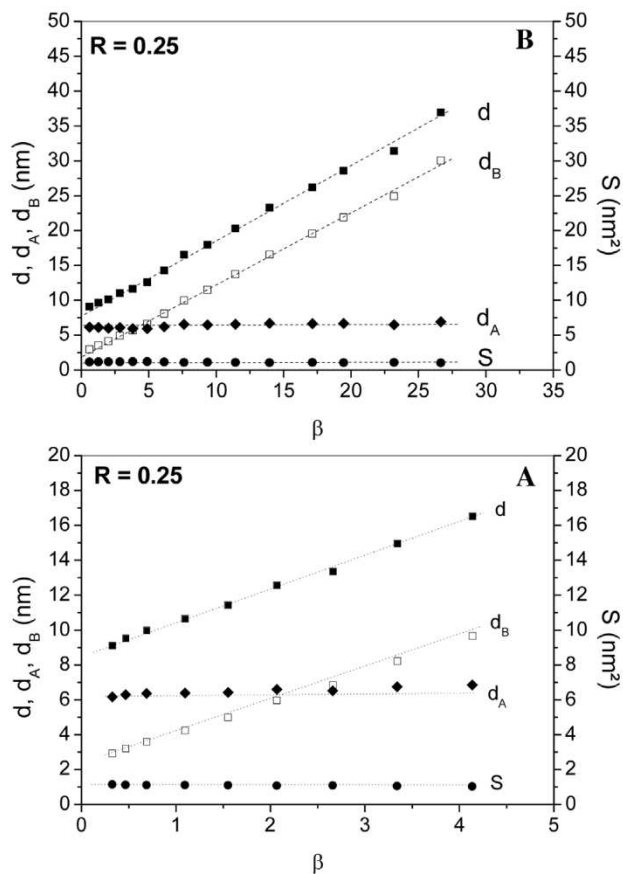


**Fig. 2 – Lamellar liquid crystal: Evolution of the structural parameters in function of  $\beta$  at 25 °C for  $R=0.25$  for the Kolliphor EL/Miglyol/water (A) and Kolliphor EL/Myristate/water (B) systems.  $\beta$  is the number of molecules of oil per molecule of surfactant.**

The cross sectional area  $S$  can be deduced as:

$$S = \frac{2(V_B + \beta V_O)}{N_A R_H}$$

The spacing parameter  $d$  and the hydrophobic radius  $R_H$  increase with the addition of oil in the system (Fig. 3), whereas the area of the polar head  $S$  equal at 1.1 nm<sup>2</sup> (Fig. 3) remains constant. This indicates that the oil is located essentially in the hydrophobic core of the cylinders. The value of  $S$  is the same than the one obtained for the lamellar phase.

### 3.1.3. Micellar structure

The effect of the addition of oil on the micelles structure was examined by comparing the SAXS spectrum of the micelles containing 5 wt.% of Kolliphor in water ( $R=19$ ) with the one of the swollen micelles with 1 wt.% of Miglyol or Myristate (same  $R$ ). The appearance of the spectra shown in Fig. 4 are different. Indeed, while the micellar solution presents a peak at  $q=0.78$  nm<sup>-1</sup>, which is characteristic of the micellar structure, the spectra of the swollen micelles show an interaction peak at  $q=0.50$  (Fig. 4Aa) and 0.53 nm<sup>-1</sup> (Fig. 4Ba) in the presence of Miglyol and Myristate, respectively. The data were analyzed by using the Generalized Indirect Fourier Transform (GIFT) method (Glatter, 1982; Fritz and Glatter, 2006). The obtained pair-distance distribution functions (PDDFs) were represented on Fig. 4Ab and Bb. For all samples, the PDDFs exhibit a pronounced dip which goes to negative values, suggesting that the micelles are inhomogeneous (“core-shell” type particles). The curve presents also a bell-like shape, characteristic of spherical micelles, with a maximum dimension of about

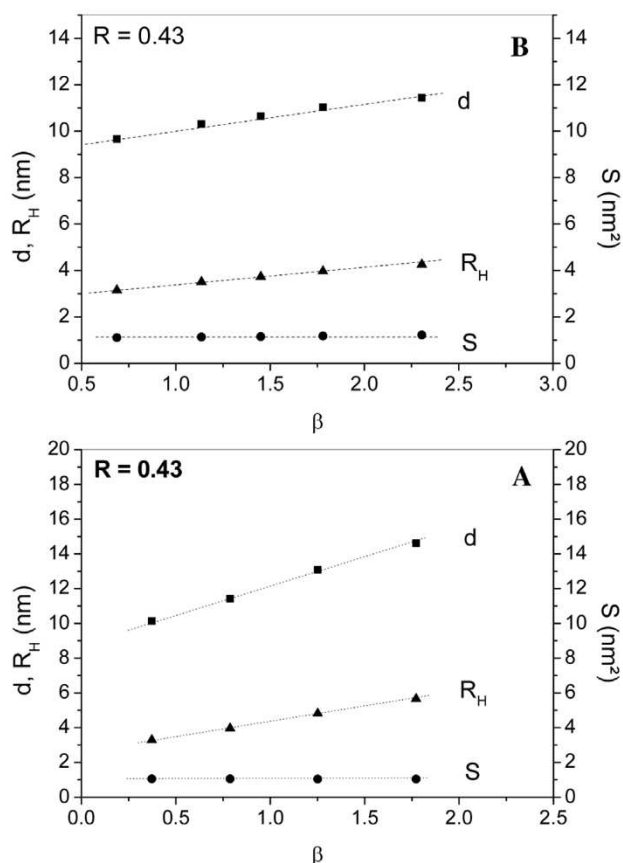


**Fig. 3 – Hexagonal liquid crystal: Evolution of the structural parameters in function of  $\beta$  at 25 °C for  $R = 0.43$  for the Kolliphor EL/Miglyol/water (A) and Kolliphor EL/Myristate/water (B) systems.  $\beta$  is the number of molecules of oil per molecule of surfactant.**

12.5–13 nm for the micelles and 17.5–18 nm for the swollen micelles with Myristate (Fig. 4Bb). For the swollen micelles with Miglyol (Fig. 4Ab), a slightly elongated tail with a size at about 19–20 nm is observed. In any cases the results are in good agreement with the hydrodynamic diameter found by DLS measurements: 12–15 nm for the micelles, depending on the Kolliphor concentration and  $\approx 16$  nm for the swollen micelles with 1 wt.% of oil. Moreover, looking at the excess-electron profile on Fig. 4Ac and Bc, the core-shell type is confirmed for all the samples. The hydrophobic radius  $R_H$  can be determined when  $\Delta\rho(r) = 0$ . It is equal to 3.3 nm for the micelles, and around 5.3 nm for the swollen micelles. The micelle size increases of about 2.5 nm when adding oil. This suggests that with the incorporation of small quantities of Miglyol or Myristate, a core of oil is created. Additionally, the dimension of the alkyl chains in the swollen micelles, corresponding to the lowest value of  $\Delta\rho(r)$ , can be estimated at about 2.6 (Fig. 4Ac) and 2.3 nm (Fig. 4Bc) in the presence of Miglyol and Myristate, respectively. The value of the alkyl chain in the presence of oil slightly increases from the value found for the sample without oil (1.9–2.0 nm). Given that the dimension of the alkyl chains in Kolliphor is 2.5 nm, the hydrophobic chains are folded in the micelles and the addition of oil induces a slight unfolding of the alkyl chains, which characterizes the existence of a real oily environment in the core of the micelles.

#### 3.1.4. Concentrated emulsions

Highly direct concentrated emulsions were prepared for a ratio  $R = 5.7$  and quantities of oil varying from 70 to 95 wt.%. The systems are stable for several months. These emulsions were

**Table 2 – Specific area ( $S_V$ ) and radii of oil droplets ( $r$ ) estimated from SAXS measurements for the direct concentrated emulsions at  $R = 5.7$  at 25 °C.**

	Miglyol		Myristate	
wt.% oil	$S_V$ (cm <sup>-1</sup> )	$r$ (μm)	$S_V$ (cm <sup>-1</sup> )	$r$ (μm)
90	2605	10	6300	4.4
95	3985	7	4300	6.7

observed by optical microscopy and the oil droplets are poly-disperse. SAXS experiments were performed and for all the samples, the SAXS spectra present the same behavior (Fig. 5)

At low  $q$ -values, the intensity is proportional to  $q^{-4}$  and characterizes the presence of big oil droplets. At higher  $q$ -values, a broad peak ( $q \approx 0.7$  nm<sup>-1</sup> for Miglyol and  $q \approx 0.5$  nm<sup>-1</sup> for Myristate) which becomes less visible for higher concentrations of oil is observed. The position of this broad peak corresponds to the one of the micelles. When miglyol is used as oil (Fig. 5A), an additional very broad peak at 3.5 nm<sup>-1</sup> is observed. This peak, which is associated to a repeated distance of 1.8 nm, has the same appearance and the same position than the one on the SAXS spectrum of pure Miglyol. Given that Miglyol is mostly a mixture of triglycerides of capric (C10:0) and caprylic acids (C8:0), the dimension of the backbone of the triglycerides can be estimated around 1.7–1.8 nm, which fits to the position of this peak. Papadimitriou et al. observed the same phenomenon with veiled virgin olive oils, showing a broad peak on SAXS spectra corresponding to the structural organization of triglycerides in the oils (Papadimitriou et al., 2013). Thus, the SAXS spectra of the concentrated emulsions correspond to the sum of the scattering of the big droplets of Miglyol and the scattering of the swollen micelles, completed by the diffraction peak of Miglyol due to the molecular structure of the triglycerides. To summarize, looking at the ternary diagram (Fig. 1A and B), the structure of the concentrated emulsions are thus big droplets of Miglyol or Myristate stabilized by molecules of Kolliphor and the continuous phase is constituted of swollen micelles of Kolliphor in water. The scattered intensity  $I(q)$  of such concentrated emulsions has already been studied before and can be expressed by the following equation (Rocca and Stébé, 2000) :

$$I(q) = \frac{2\pi \cdot S_V \cdot I_s(q)}{q^4} + (1 - \phi_V)I_m(q) \quad (1)$$

where the first term represents the diffusion due to large droplets and is approximated by Porod-Auvray's law, with  $S_V$  the specific surface and  $I_s$  is a function of the scattering length density  $Q$  profile at the water/oil interface and can be noted as:

$$I_s(q) = (Q_{ext} - Q_{int})^2$$

where  $Q_{ext}$  and  $Q_{int}$  represent the scattering length densities of the external and internal phase of the emulsion respectively. The second term  $I_m$  can be defined as the contribution of the continuous phase.

According to Eq. (1), the specific area  $S_V$  can be calculated from the slope of the portion of the curve with a scattering proportional to  $q^{-4}$ . Then, the corresponding radius of oil droplets  $r$  can be estimated as:

$$r = \frac{3\phi_V}{S_V}$$

where  $\phi_V$  is the volume fraction of oil.

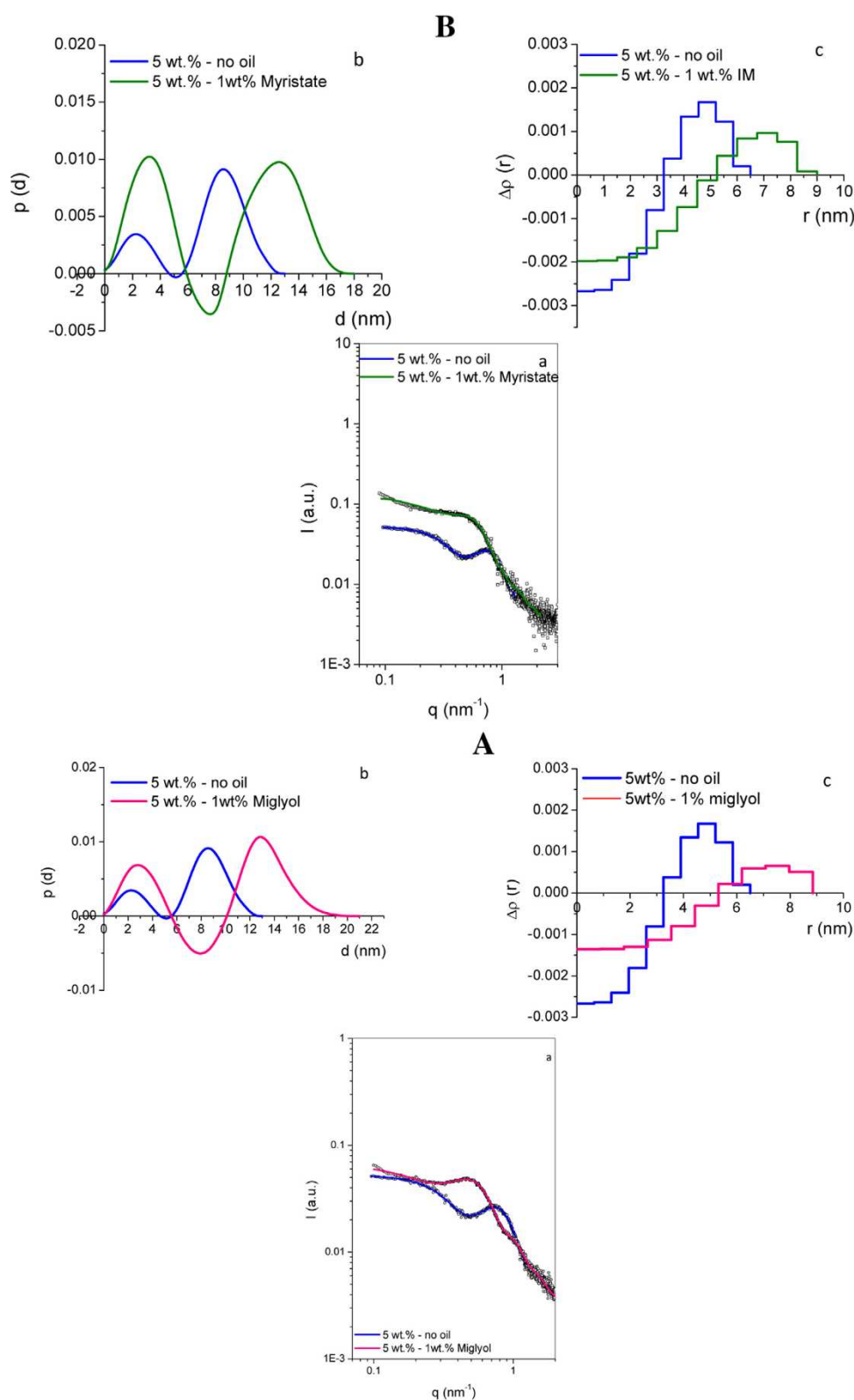


**Fig. 4 – Micellar structure: Experimental (dotted line) and approximated (GIFT) (solid line) SAXS spectra of the samples at  $R=19$  without oil and with 1 wt.% of oil at 25 °C (a); corresponding pair-distance distribution functions (PDDFs) (b) and corresponding excess-electron density profiles (c). Micelles have been obtained from the Kolliphor EL/Miglyol/water (A) and Kolliphor EL/Myristate/water (B) systems. IM corresponds to isopropyl Myristate.**

The results are given in Table 2 for the two higher concentrations of oil. Given that the number of points in the portion of the curve with a scattering proportional to  $q^{-4}$  is limited, the error on the calculation of the radius of the droplets can be important. Consequently, the calculated values given in Table 2 have to be taken as an estimation.

### 3.2. Porous materials

After the determination of the phase behavior, starting from the ternary systems, porous materials have been synthesized. Compounds have been prepared with a 10 wt.% of surfactant in the aqueous mixture, and in the presence of Miglyol and,

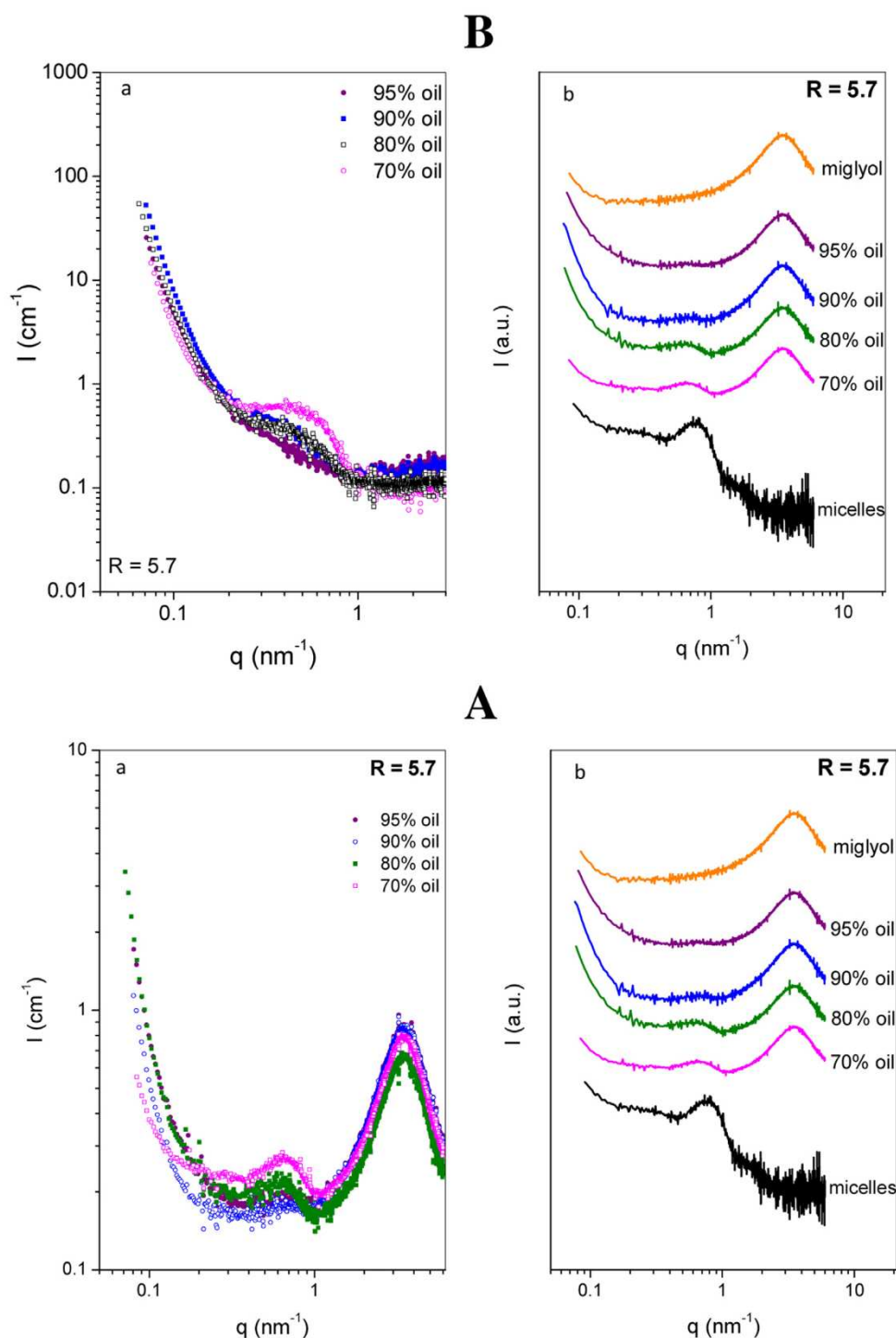


**Fig. 5 – Concentrated emulsions containing various amount of oil: SAXS spectra of the concentrated emulsions at  $R=5.7$  in log–log representation in absolute units (a); SAXS spectra of the concentrated emulsions and the micelles at  $R=5.7$  (b). For clarity reasons, the spectra are shifted towards y-axis. Emulsions have been obtained from the Kolliphor EL/ Miglyol/water (A) and Kolliphor EL/Myristate/water (B) systems.**

we can see that mesostructured silica materials are recovered until the addition of 1 wt.% of oil (Fig. 6A); i.e. using the swollen micelles as template. If the Miglyol concentration is increased, that means using the fine emulsions as template, no secondary reflections are detected any longer. Only a broad peak is observed on the SAXS spectra. The material synthesized with an oil quantity higher than 1% thus adopt a wormhole-like structure. The position of this peak remains around 12.0 nm when the oil concentration is raised from 3 to 7 wt.% (Fig. 6Ac–e). Beyond 7 wt.% of Miglyol no peak is observed, meaning that the channel arrangement is

completely random. Thus, the regular mesopores array is completely lost and in this case, the addition of oil disfavors the formation of mesostructure.

Nitrogen adsorption–desorption isotherms and the corresponding BJH pore size distributions (obtained from an analysis of the adsorption branch of the isotherm) are shown in Fig. 7. According to the IUPAC classification (Sing et al., 1985) a type IV isotherm, characteristic of mesoporous materials is obtained for the material prepared with a concentration of oil lower than 7 wt.% (Fig. 7Aa–d). When the loading of oil is raised the shape of the isotherm changes and it becomes type

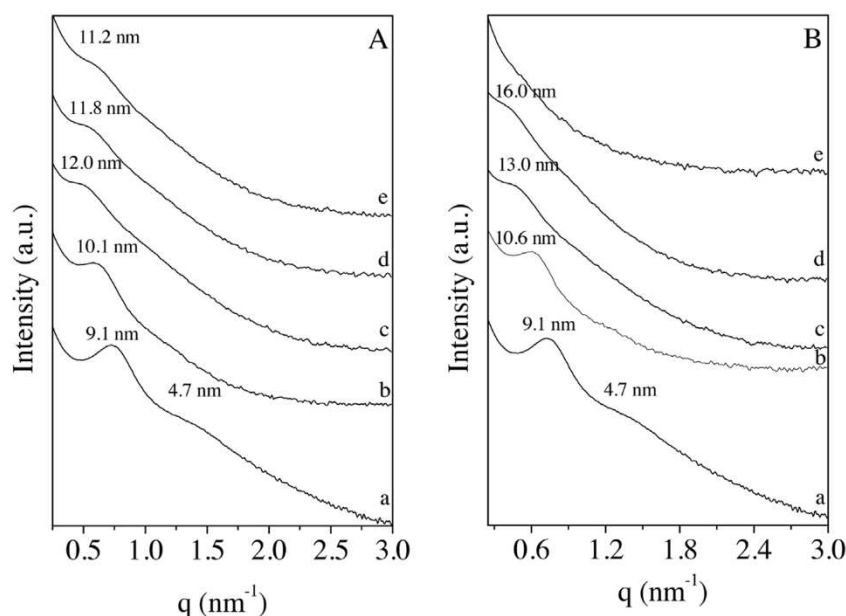


Fig. 6 – Porous materials: SAXS patterns of samples synthesized with a: 0, b: 1, c: 3, d: 5 and e: 7 wt.% of Miglyol (A) or Myristate (B).

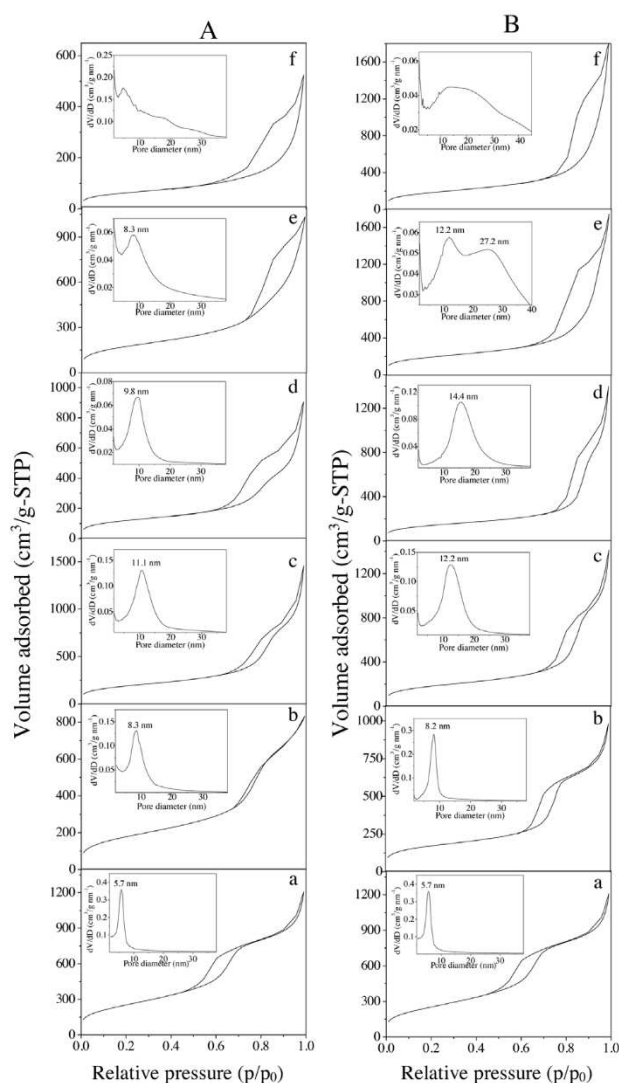


Fig. 7 – Porous materials: adsorption–desorption isotherms and pore size distribution of compounds synthesized with a: 0, b: 1, c: 3, d: 5, e: 7 and f: 10 wt.% of Miglyol (A) or Myristate (B).

II (Fig. 7Ae,f). In addition, with increasing the Miglyol concentration, the relative pressure for which capillary condensation takes place is shifted toward higher values. Since the  $p/p_0$  position of the inflection point is related to the pore diameter, it can be inferred that an enlargement of the mean pore diameter occurs when the loading of oil is raised. This increase in pore diameter is further confirmed by the pore size distribution whose maximum is shifted from 5.7 to 11.1 nm when the content of Miglyol is varied from 0 to 3 wt.% (insert of Fig. 7Ab,c). However, the mesopore size distribution becomes broader. This indicates that the mesopores become less homogeneous. If the Miglyol loading is further increased, the  $dV/dD$  values decrease and no significant pore size distribution in the mesopore range is obtained for oil amount higher than 7 wt.% (insert Fig. 7A d–f)

Materials obtained from the Kolliphor/Myristate/water system exhibit the same characteristics than the ones synthesized from the Kolliphor/Miglyol/water one. (Figs. 6B and 7 B). The main differences between the two systems are that the increase of the d-spacing with the addition of oil is more significant (10.6 to 16.0 nm when the Myristate amount is varied from 1 to 5 wt.% (Fig. 6Bb–d)) and the complete disorganization of the channel array occurs at a lower oil concentration (after 5 wt.% of oil). In addition, beyond the addition of 1 wt.% of oil, materials prepared in the presence of Myristate have a higher pore diameter (insert of Fig. 7) than the ones obtained using Miglyol as oil. For example, in the presence of 5 wt.% of Myristate the mesopore diameter is 14.4 nm against 9.8 nm when the same amount of miglyol is used to prepare the porous silica.

The specific surface area drops from 930 to around 650 and 600  $m^2/g$  when 1 wt.% of Miglyol and Myristate are added, respectively (Fig. 8). Taking into account the error on the measurement, beyond 1 wt.%, higher amount of oil has no effect on the specific surface area, indeed from Fig. 8 it can be seen that for concentration of Miglyol or Myristate in the range of 1–15 wt.%, its value remains almost constant upon addition of oil.

At high concentrations of Miglyol (beyond 70 wt.%) the emulsions can be used as templates to prepare macroporous

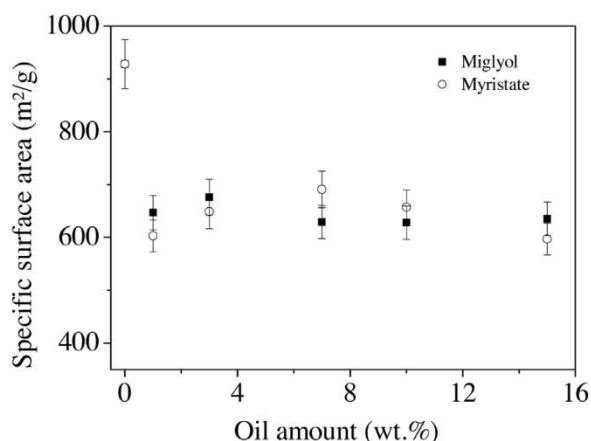


**Fig. 8 – Porous materials: Evolution of the specific surface area as a function of the oil amount (wt.%) from 0 to 15 wt.%.**

materials. Indeed, as evidenced in Fig. 9a–c, macropores having a size in the micrometer range are visible. The presence of macropores in the samples was further confirmed by mercury intrusion experiments (Fig. 9d). The macropore size distribution exhibits two main components at 4.1 and 105  $\mu\text{m}$ . The first component corresponds approximately to the size of the pores observed by SEM. It is compatible with the size of the oil droplets of the emulsions determined by SAXS likely arises from their mineralization. We believe that the second peak at around 105  $\mu\text{m}$  is due to the interparticle porosity induced by the aggregation of particles. Depending on the oil quantity, the percentage of porosity varies from 84 (70 wt.% of Miglyol) to 96% (95 wt.% of Miglyol). Consequently, the skeleton density varies from 0.7 to 3.7  $\text{g}/\text{cm}^3$  when the Miglyol amount used to prepare the concentrated emulsion is changed from

70 to 95 wt.%. By nitrogen adsorption–desorption analysis, the obtained macroporous silica also present type II isotherm characteristic of macroporous materials, according to the IUPAC classification. Their specific surface area is around 300  $\text{m}^2/\text{g}$  and no pore size distribution is detected in the mesopore range.

### 3.3. Discussion

To explain the variation of pore diameter with the incorporation of oil, we should have a look at the phase diagrams. From Fig. 1A and B, it can be seen that very low amount of oil, about 1 wt.% of Miglyol or Myristate can be solubilized in the micelles involving an increase of their size. As a consequence of the swelling of the micelles core, when the porous silica are prepared from the micelles, according to the cooperative templating mechanism (CTM) the mesopore size is enlarged from 5.7 to about 8.5 nm. This mechanism is usually considered in order to explain the pore size expansion of mesoporous materials by adding organic auxiliaries as swelling agents (Boissière et al., 2003; Jana et al., 2004; Ottaviani et al., 2004; Cao et al., 2009). The determination of the micellar structure has shown that the size of the micelles is not affected by the type of oil and remains around 17.5–20 nm. This can explain why similar mesopore size is obtained in the presence of Miglyol and Myristate. Spherical micelles are formed with Myristate whereas the latter are slightly elongated when Miglyol is used as oil. As a consequence, the mesopore pore size distribution is slightly broader when this oil is used as expander.

If the oil amount incorporated in the Kolliphor/water system is increased, in the water rich part of the diagram, the fine emulsions are formed until around 10 wt.% of oil for the

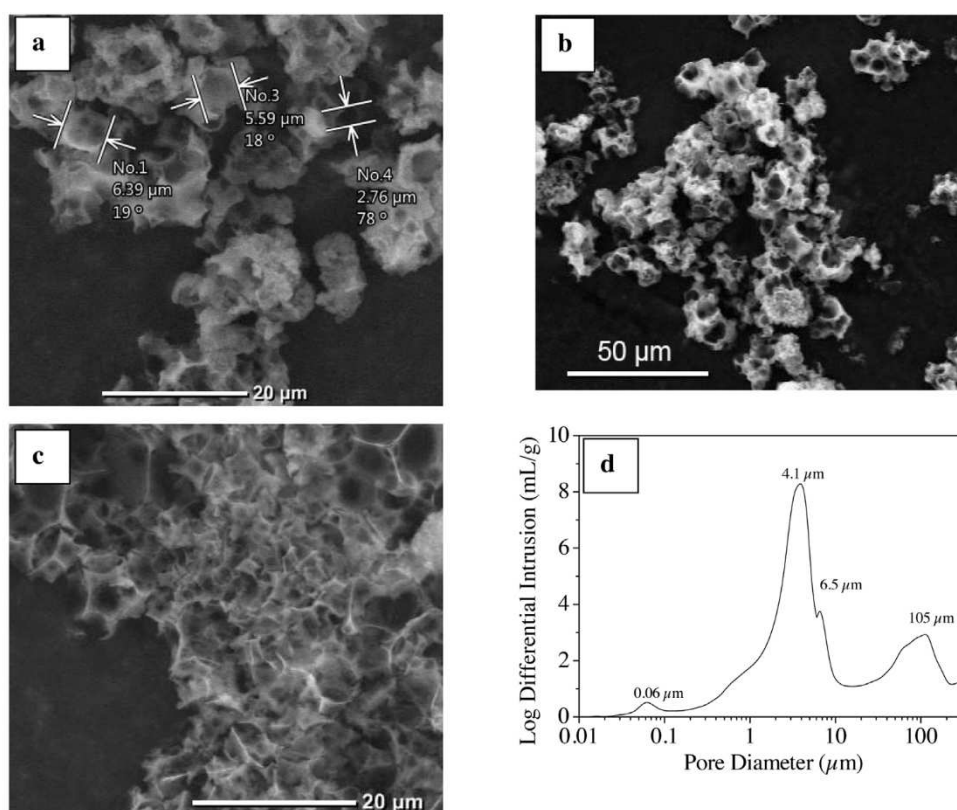


**Fig. 9 – Porous materials: SEM images of the macroporous materials prepared with concentrated emulsions containing 80 (a, b) and 95 wt.% (c) of Miglyol with the corresponding macropore size distribution (d) obtained by mercury porosity.**

considered Kolliphor quantity. The oil droplets are stabilized by the surfactant molecules and when the silica precursor is added, hydrogen-bonds between hydrogen atoms of hydrolyzed TMOS and the oxygen atoms of the oxyethylene group of the surfactant are formed, leading to the formation of a hybrid-silica. After the hydrothermal treatment and surfactant removal the large mesopore silica materials are recovered. Since the size, obtained from DLS measurements, of the oil droplets formed with Myristate (43.2 nm for a solution containing 7 wt.% of Kolliphor) are larger than the ones obtained with Miglyol (35.4 nm for a solution containing 7 wt.% of Kolliphor), the mesoporous materials recovered in the presence of Myristate have a higher diameter than the silica synthesized in the presence of Miglyol.

If more and more oil is added, the oil-rich part of the diagram is reached and the concentrated emulsions with oil droplets having a size in the micrometer range are obtained. The oil droplets stabilized by the surfactant are dispersed in the continuous medium. The mineralization of the concentrated emulsions gives rise to the macroporous silicas where the oil droplet is the imprint of the macropore.

#### 4. Conclusion

In the present paper silica materials with well-defined porosity have been prepared by biomimetics by combining the sol-gel process, which is a powerful chemical tool to design complex materials taking inspiration from Mother Nature, and the surfactant templating method.

First, we have investigated the ability of the Kolliphor/Miglyol/water and Kolliphor/Myristate/water surfactant-based systems to be used for the preparation of porous silica by morphosynthesis. For each system, we have delimited the domains of the various phases and determined the structural parameters of the liquid crystals. We have shown that only a low quantity of oil can be incorporated in micelles ( $L_1$ ). Fine emulsions particularly stable which may contain up to 15% of oil have been formulated. Highly direct concentrated emulsions stable for several months were also prepared with a water/Kolliphor ratio = 5.7 and for oil concentrations between 70 and 95 wt.%.

As regards the porous materials syntheses, the incorporation of low fraction of Miglyol or of Myristate leads to the formation of large mesoporous silica templated by swollen micelles or fine emulsions. Results also show that macropores templated by the oil droplets appear if the amount of oil concentration is increased (>70 wt.%), these macropores are the imprint of the oil droplets of the concentrated emulsions.

This study shows that synthetic mesoporous or macroporous silicas can be prepared from biocompatible compounds by mimic of natural processes. The approach described herein will open a new way to prepare hierarchical meso-macroporous silica or hybrid organic-inorganic materials and straightforward applications toward catalysis, particularly as support where molecular hindrance of big active confined entities as enzymes can be minimized. In addition, regarding the interest of hybrid materials for drug delivery we can assume that without removing organic the hybrid porous silica are excellent candidates for this application. This work is under progress.

#### Acknowledgements

Authors would like to thank the IOI Oleo GmbH- IOI Oleochemical company which kindly provides Miglyol® 812 N. Claudia Violeta Cervantes-Martinez also thanks the CONACYT for the financial support of her PhD.

#### References

- Alibrahim, M., Stébé, M.J., Dupont, G., Ravey, J.C., 1997. *Effect of an ionic surfactant on the phase behavior of a nonionic surfactant-based system*. *J. Chim. Phys. Phys.-Chim. Biol.* **94**, 1614–1633.
- Arruebo, M., 2012. *Drug delivery from structured porous inorganic materials* *WIREs. Nanomed. Nanobiotechnol.* **4**, 16–30.
- Attard, G.S., Glyde, J.C., Göltner, C.G., 1995. *Liquid-crystalline phases as templates for the synthesis of mesoporous silica*. *Nature* **378**, 366–368.
- Barrett, E.P., Joyner, L.G., Halenda, P.P., 1951. *The determination of pore volume and area distributions in porous substances. I. Computations from nitrogen isotherms*. *J. Am. Chem. Soc.* **73**, 373–380.
- Beck, J.S., Vartuli, J.C., Roth, W.J., Leonowicz, M.E., Kresge, C.T., Schmitt, K.D., Chu, C.T.W., Olson, D.H., Sheppard, E.W., McCulle, S.B., Higgins, J.B., Schlenker, J.L., 1992. *A new family of mesoporous molecular sieves prepared with liquid crystal templates*. *J. Am. Chem. Soc.* **114**, 10834–10843.
- Cameron, N.R., Sherrington, D.C., 1996. *High internal phase emulsions (HIPEs) structure, properties and use in polymer preparation*. *Adv. Polym. Sci.* **126**, 163–214.
- Bleta, R., Blin, J.L., Stébé, M.J., 2006. *Solubilization of various fluorocarbons in a fluorinated surfactant/water system: relation with the design of porous materials*. *J. Phys. Chem. B* **110**, 23547–23556.
- Blin, J.L., Impéror-Clerc, M., 2013. *Mechanism of self-assembly in the synthesis of silica mesoporous materials: in situ studies by X-ray and neutron scattering*. *Chem. Soc. Rev.* **42**, 4071–4082.
- Boissière, C., Marines, M.A.U., Tokumoto, M., Larbot, A., Prouzet, E., 2003. *Mechanisms of Pore Size Control in MSU-X Mesoporous Silica*. *Chem. Mater.* **15**, 509–515.
- Braganca, L.F.F.P.G., Ojeda, M., Fierro, J.L.G., Pais da Silva, M.I., 2012. *Bimetallic Co-Fe nanocrystals deposited on SBA-15 and HMS mesoporous silicas as catalysts for Fischer-Tropsch synthesis*. *Appl. Catal. A-Gen* **423–424**, 146–153.
- Cao, L., Man, T., Kruk, M., 2009. *Synthesis of ultra-large-pore SBA-15 silica with two-dimensional hexagonal structure using Triisopropylbenzene as micelle expander*. *Chem. Mater.* **21**, 1144–1153.
- Carn, F., Colin, A., Achard, M.F., Deleuze, H., Sellier, E., Birot, M., Backov, R., 2004. *Inorganic monoliths hierarchically textured via concentrated direct emulsion and micellar templates*. *J. Mater. Chem.* **14**, 1370–1376.
- El-Safty, S.A., Kiyozumi, Y., Hanaoka, T., Mizukami, F., 2008. *Controlled design of ordered and disordered pore architectures, geometries, and dimensions of HOM-type mesostructured monoliths and their hydrothermal stabilities*. *J. Phys. Chem. C* **112**, 5476–5489.
- Fritz, G., Glatter, O., 2006. *Structure and interactions in dense colloidal systems: evaluation of scattering data by the generalized indirect Fourier transformation method*. *J. Phys. Condens. Matter* **18**, S2403–S2419.
- Glatter, O., 1982. *Small Angle X-Ray Scattering*. Academic Press Inc. ed., London.
- Imhof, A., Pine, D.J., 1997. *Ordered macroporous materials by emulsion templating*. *Nature* **389**, 948–951.
- Jana, S.K., Nishida, R., Shindo, K., Kugita, T., Namba, S., 2004. *Pore size control of mesoporous molecular sieves using different organic auxiliary chemicals*. *Microporous Mesoporous Mater.* **68**, 133–142.

- Kresge, C.T., Leonowicz, M.E., Roth, W.J., Vartuli, J.C., Beck, J.S., 1992. Ordered mesoporous molecular sieves synthesized by a liquid-crystal template mechanism. *Nature* 359, 710–712.
- Kresge, C.T., Roth, W.J., 2013. The discovery of mesoporous molecular sieves from the twenty year perspective. *Chem. Soc. Rev.* 42, 3663–3670.
- Kruk, M., Cao, L., 2007. Pore size tailoring in large-pore SBA-15 silica synthesized in the presence of hexane. *Langmuir* 23, 7247–7254.
- Lettow, J.S., Han, Y.J., Schmidt-Winkel, P., Yang, P.D., Zhao, D.Y., Stucky, G.D., Ying, J.Y., 2000. Hexagonal to mesocellular foam phase transition in polymer-templated mesoporous silicas. *Langmuir* 16, 8291–8295.
- Lind, A., Andersson, J., Karlsson, S., Ågren, P., Bussian, P., Amenitsch, H., Lindén, M., 2002. Controlled solubilization of toluene by silicate-catanionic surfactant mesophases as studied by in situ and ex situ XRD. *Langmuir* 18, 1380–1385.
- Mann, S., Ozin, G.A., 1996. Synthesis of inorganic materials with complex form. *Nature* 382, 313–318.
- Martens, J.A., Jammaer, J., Bajpe, S., Aerts, A., Lorgouilloux, Y., Kirschhock, C.E.A., 2011. Simple synthesis recipes of porous materials. *Microporous Mesoporous Mater.* 140, 2–8.
- Moritz, M., Geszke-Moritz, M., 2015. Mesoporous materials as multifunctional tools in biosciences: principles and applications. *Mater. Sci. Eng. C* 49, 114–151.
- Ottaviani, M.F., Moscatelli, A., Desplandier-Giscard, D., Di Renzo, F., Kooyman, P., Galarnau, A., 2004. Synthesis of micelle-templated silicas from cetyltrimethylammonium bromide/1,3,5-trimethylbenzene micelles. *J. Phys. Chem. B* 108, 12123–12129.
- Papadimitriou, V., Dulle, M., Wachter, W., Sotiroidis, T.G., Glatter, O., Xenakis, A., 2013. Structure and dynamics of veiled virgin olive oil: influence of production conditions and relation to its antioxidant capacity. *Food Biophys.* 8, 112–121.
- Park, S.Y., Barton, M., Pendleton, P., 2011. Mesoporous silica as a natural antimicrobial carrier. *Colloids Surfaces A: Physicochem. Eng. Aspects* 385, 256–261.
- Perego, P., Millini, R., 2013. Porous materials in catalysis: challenges for mesoporous materials. *Chem. Soc. Rev.* 42, 3956–3976.
- Princen, H.M., 1983. Rheology of foams and highly concentrated emulsions. IV. An experimental study of the shear viscosity and yield stress of concentrated emulsions. *J. Colloids Interface Sci* 91, 160–175.
- Ravey, J.C., Stébé, M.J., Sauvage, S., 1994. Water in fluorocarbon gel emulsions: structures and rheology. *Colloids and surfaces A: physicochem. Eng. Aspects* 91, 237–257.
- Sakya, P., Seddon, J.M., Templar, R.H., Mirkin, R.J., Tidley, G.J.T., 1997. Micellar cubic phases and their structural relationships: the nonionic surfactant system C<sub>12</sub>EO<sub>12</sub>/water. *Langmuir* 13, 3706–3714.
- Rocca, S., Stébé, M.J., 2000. Mixed concentrated Water/Oil emulsions (Fluorinated/Hydrogenated): formulation, properties, and structural studies. *J. Phys. Chem. B* 104, 10490–10497.
- Sayari, A., Yang, Y., Kruk, M., Jaroniec, M., 1999. Expanding the pore size of MCM-41 silicas: use of amines as expanders in direct and postsynthesis procedures. *J. Phys. Chem. B* 103, 3651–3658.
- Schmidt-Winkel, P., Lukens, W.W., Yang, P.D., Margolese, D.I., Lettow, J.S., Ying, J.Y., Stucky, G.D., 2000. Microemulsion templating of siliceous mesostructured cellular foams with well-defined ultralarge mesopores. *Chem. Mater.* 12, 686–696.
- Sen, T., Tidley, G.J.T., Casci, J.L., Anderson, M.W., 2005. Meso-cellular silica foams, macro-cellular silica foams and mesoporous solids: a study of emulsion-mediated synthesis. *Microporous Mesoporous Mater.* 78, 255–263.
- Sing, K.S.W., Everett, D.H., Haul, R.A.W., Moscou, L., Pierotti, R.A., Rouquerol, J., Siemieniowska, T., 1985. Reporting physisorption data for gas/solid systems with special reference to the determination of surface area and porosity (Recommendations 1984). *IUPAC, Pure and Appl. Chem.* 57, 603–619.
- Solans, C., Solé, I., 2012. Nano-emulsions: formation by low-energy methods. *Curr. Opin. Colloid Interface Sci.* 17, 246–254.
- Tidley, G.J.T., 1980. Surfactant-water liquid crystal phases. *Phys. Rep.* 57, 1–46.
- Veliscek-Carolan, J., Knott, R., Hanley, T., 2015. Effects of precursor solution aging and other parameters on synthesis of ordered mesoporous Titania powders. *J. Phys. Chem. C* 119, 7172–7183.
- Wan, Y., Zhao, D., 2007. On the controllable soft-templating approach to mesoporous silicates. *Chem. Rev.* 107, 2821–2860.
- Zhang, H., Hardy, G.C., Rosseinsky, M.J., Copper, A.I., 2003. Uniform emulsion-templated silica beads with high pore volume and hierarchical porosity. *Adv. Mater.* 15, 78–81.
- Zhao, C., Danish, E., Cameron, N.R., Katakura, R., 2007. Emulsion-templated porous materials (polyHIPEs) for selective ion and molecular recognition and transport: applications in electrochemical sensing. *J. Mater. Chem.* 17, 2446–2453.
- Zhang, S., Chen, J., 2007. Synthesis of open porous emulsion-templated monoliths using cetyltrimethylammonium bromide. *Polymer* 48, 3021–3025.
- Zimny, K., Blin, J.L., Stébé, M.J., 2009. Ordered mesoporous silica templated by nonionic fluorinated liquid crystals. *J. Phys. Chem. C* 113, 11285–11293.

## **Porous silica templated by the combination of fine emulsion and P123 micelles**

Claudia Violeta Cervantes-Martinez<sup>1</sup>, Marie-José Stébé<sup>1</sup>, Mélanie Emo<sup>1</sup>, Bénédicte Lebeau<sup>2,3</sup>,

Jean-Luc Blin <sup>1,\*</sup>

<sup>1</sup> Institut Jean Barriol, UMR CNRS 7053 L2CM, Université de Lorraine, Faculté des Sciences et Technologies, BP 70239, 54506 Vandoeuvre lès Nancy cedex, FRANCE

<sup>2</sup> : Université de Haute Alsace (UHA), CNRS, IS2M UMR 7361, F-68100 Mulhouse, France

<sup>3</sup> : Université de Strasbourg, 67000 Strasbourg, France

\*Corresponding authors

Pr. Jean-Luc Blin

Université de Lorraine

UMR CNRS 7053 L2CM

Faculté des Sciences et Technologies

BP 70239

F-54506 Vandoeuvre-lès-Nancy cedex, France

Tel. +33 3 83 68 43 70

E-mail: Jean-Luc.Blin@univ-lorraine.fr

## **ABSTRACT**

Here, porous silica have been prepared by combining fine emulsion, which is formulated from the Kolliphor/Myristate/Water system and Pluronic P123 micellar solution. The materials have been characterized by SAXS, nitrogen adsorption-desorption analysis and Scanning Electron Microscopy. Results show that the porosity can be tuned by varying the weight ratio between the fine emulsion and the P123 micelles.

To get informations concerning the degree of compatibility between the two surfactants, which can affect the formation of the porous materials, the Kolliphor/P123/water system has been first investigated in detail. The phase diagram suggests that, when they are mixed P123 and Kolliphor surfactants form mixed organized molecular systems. The structural parameters of the mixed liquid crystal phases have been determined and the mixed micellar structure has been investigated by SAXS.

Then porous silica have been synthesized. When the weight proportion of the fine emulsion in the mixture used to prepare the silica is lower than 50%, the P123 micelles and the methanol released during the hydrolysis of the silica precursor involves a destabilization of the fine emulsion, which leads to the formation of P123/Kolliphor mixed micelles and Myristate droplets, which have coalesced. Thanks to the presence of the mixed micelles a dual mesoporosity is obtained. A macroporosity is also detected by SEM. The macropores of few microns in diameter are formed by the interaction of the hydrolyzed silica precursor with the Myristate droplets stabilized by surfactant molecules either P123 or Kolliphor or both. Beyond 50%, the fine emulsion is more stable and it governs the porosity.

**KEYWORDS:** Fine emulsion; Mixed-system; Micellar structure; Silica materials; Hierarchical porosity

## 1. Introduction

Hierarchical porous materials, which present a porosity at multiple length scales such as micro-mesoporosity, meso-macroporosity or meso-mesoporosity have applications in various domains such as photonics, bioengineering and nanotechnology [1-4]. Their importance comes from their properties such as a large surface area (around 1000 m<sup>2</sup>/g for silica), their large pore volume, and the presence of pores that allows the control of the diffusion [5-6]. For example, micro-macro or meso-macroporous materials are particular interesting and useful for catalysis and drug delivery systems. From an application viewpoint, drugs or catalysts can be loaded in the mesopores and in the micropores, while the macropores enhance the mass transfer and reduce the transport limitations [7,8]. This is particularly beneficial in the case of large molecules or in viscous systems where diffusion rates are low. The development of hierarchical porous materials at multiple scales was thus the subject of interest over the last few years. Different strategies have been developed to design these compounds [9-15]. One of them consists of combining the sol-gel chemistry and the use of surfactant molecules assemblies as framework templates. The chemically induced liquid-liquid phase separation [16] has been applied to synthesize mesoporous silica material with interconnected macropores. This technique is based on the hydrolysis and condensation of inorganic precursors in the aqueous domain, derived from the self-assembly phase of the template used. The earlier the phase separation takes place in the sol-gel transition, the larger the characteristic size of pores and gel skeletons become. A wide variety of water soluble block copolymers, such as polyoxyethylene surfactants, has been used to control the phase separation/gelation kinetics in the preparation of monolithic silica exhibiting both interconnected macropores and textual mesopores. With the use of various silica precursors such as tetramethoxysilane, tetraethoxysilane and bis(trimethoxysilyl)-ethane, amorphous or disordered mesopores can be integrated in gel networks which constitute a co-continuous

macroporous structure [10, 17]. Using this approach, Nakanishi et al. synthesized monolithic silica gels with a hierarchical meso-macroporous structure via a spontaneous sol-gel process and yielded materials with highly ordered hexagonal arrays of mesopores [18]. The authors explain that the monolithic body with well-defined interconnected macropores is a result of concurrent phase separation and sol-gel transition induced by the polymerization reaction, whereas the mesopores are templated by the cooperative self-assembly of inorganic species and the assembly directing agent polyethylene oxide-block-poly-polypropylene oxide-block-polyethylene oxide. A versatile method widely used to get the macro-mesoporous materials consists in combining the emulsion templating method and the surfactant templating one [19-24]. In that case the main role of oil is to act as a template for the generation of the macropore network. For example, using concentrated emulsions and micellar templates, Carn and co-workers [25] prepared hierarchical inorganic porous monoliths. These materials show interconnected macroporosity with disordered structures. The mesopore size varies from 1.2 to 4.0 nm. Tiddy and co-workers [9,26] also use this approach to achieve the room-temperature synthesis of a macro-mesoporous silica material during the natural creaming of oil-in-water emulsion. This synthesis was carried out using cetyltrimethylammonium bromide as surfactant and trimethylbenzene as oil. The obtained material has a high surface area (800 m<sup>2</sup>/g) with a narrow pore size distribution centered at around 4.0 nm. Monolithic silica foams bearing a cubic organization of the mesopores, obtained under alkaline condition with non-ionic surfactant have also been proposed by Esquena et al. [14,15]. Other imprints such as latex spheres [27] or solid lipid nanoparticles [28] can serve as mold to generate the macropores. If as mentioned above concentrated emulsions have been widely considered to design the macro-mesoporous materials, in contrary fine emulsions have been barely investigated for this purpose. Usually they are employed for practical applications, such as the preparation of polymeric nanoparticles, agrochemical applications, food technology,

pharmaceutical and cosmetic fields [29-32]. Recently we have reported that fine emulsions, stable for few days, can be formulated in the water rich part of the Kolliphor/Myristate/water system [33]. In this paper, in combination with the cooperative templating mechanism (CTM), we have used these fine emulsions as imprints to prepare porous silica materials. Before the synthesis of the materials, we have investigated in detail the Kolliphor/P123/water system to have informations concerning the possible interactions between the two surfactants, which can affect the formation of the porous materials.

## **2. Materials and methods**

Kolliphor EL (denoted as KEL), a surfactant synthesized from the reaction of castor oil and ethylene oxide in a molar ratio 1:35 (BASF Corporation, technical literature), was purchased from Sigma Aldrich and used as received, without any further purification. The selected triblock copolymer is the Pluronic P123 (EO)<sub>20</sub>(PO)<sub>70</sub>(EO)<sub>20</sub>, it was also purchased from Aldrich as well as the tetramethoxysilane (TMOS), used as the silica source and Myristate. Deionized water was obtained using a Milli-Q water purification system.

### **2.1. Phase diagram determination**

Samples were prepared, by weighting the required amounts of surfactants and water in sealed glass tubes. The homogenization of the samples was induced by mixing with a vortex stirrer or by mechanical milling. To favor homogenization, the samples were also centrifuged several times. The Kolliphor/P123/water phase diagram has been established by preparing samples over the whole range of surfactants concentrations, keeping them in a water bath at 23 °C until reaching thermodynamic equilibrium (after few days). Observations with the eyes combined with optical microscope equipped with cross polarizers (Olympus BX 50) were used to identify the different phases and to determine the phase boundaries. Small angle X-ray

scattering measurements were additionally performed to establish the phase boundaries accurately, to confirm the nature of the different phases and to determine the space group of the cubic structures.

## **2.2. Porous materials preparation**

*Preparation of the fine emulsion* : Fine emulsion has been formulated from the Kolliphor/Myristate/water system system using the PIC method, according to a procedure previously reported [33]. Here the oil to surfactant ratio and the weight fraction of water have been fixed to 0.43 and 0.90, respectively. These conditions lead to formation of fine emulsion with a size, determined by DLS, of around 30 nm in diameter.

*Preparation of the porous silica* : First a solution of fine emulsion (noted Em) at pH = 7 and a micellar solution of Pluronic P123 (5 wt.% at pH =0.3) are separately prepared. Then both solutions are mixed in different proportions to get 10g of the final mixture. The fine emulsion/P123 micellar solution weight ratio (labelled as Em/P123) has been varied from 0/10 to 9/1. After that tetramethoxysilane (TMOS), used as the silica source was added. The quantity of silica, expressed as the P123/TMOS molar ratio, has been fixed to 0.005. The mixture was stirred at ambient temperature for 1 hour using a magnetic stirrer. Then, it was transferred and sealed in a Teflon autoclave. The autoclave was heated at 40°C for 24 hours, afterwards at 100°C for 24 hours. The final products were recovered after ethanol extraction with a Soxhlet apparatus for 48 hours. After drying at room temperature during 24 h, samples were thermally treated under synthetic air as follow. A first temperature increase was applied at 2 °C/min until 150 °C with a 1 h plateau, followed by a second temperature ramp at 2 °C/min to reach 350 °C. Temperature was held for 1 h, then, a final temperature ramp at 2 °C/min was imposed to reach 550 °C with a 1 h plateau. The cooling process was uncontrolled and directed by the oven inertia.

### 2.3. Characterization

Small angle X-Ray scattering (SAXS) data were collected on a “SAXSess mc<sup>2</sup>” instrument (Anton Paar), using line-collimation system. This instrument is attached to a ID 3003 laboratory X-Ray generator (General Electric) equipped with a sealed X-Ray tube (PANalytical,  $\lambda_{\text{Cu, K}\alpha} = 0.1542$  nm) operating at 40 kV and 50 mA. Each sample was introduced in a “Special Glass” capillary for liquids and liquid crystals ( $\Phi = 1.5$  mm and 2.0 mm for micellar solutions and liquid crystals, respectively), or between two sheets of Kapton® for materials, then placed inside an evacuated sample chamber, and exposed to X-Ray beam. Scattering of X-Ray beam was registered by a CCD detector (Princeton Instruments, 2084 x 2084 pixels array with 24 x 24  $\mu\text{m}^2$  pixel size) at 309 mm distance from the sample. Using SAXSQuant software (Anton Paar), the 2D image was integrated into one-dimensional scattering intensities  $I(q)$  as a function of the magnitude of the scattering vector  $q = (4\pi/\lambda) \sin(\theta)$ , where  $2\theta$  is the total scattering angle. Thanks to a translucent beamstop allowing the measurement of an attenuated primary beam at  $q = 0$ , all measured intensities can therefore be calibrated by normalizing the attenuated primary intensity. Data were then corrected for the background scattering from the cell and for slit-smearing effects by a desmearing procedure from SAXSQuant software, using Lake method. For micellar solutions, after treatment, obtained intensities were scaled into absolute units using water as a reference material.

Nitrogen adsorption and desorption isotherms were determined on a Micromeritics TRISTAR 3000 sorptometer at - 196 °C over a wide relative pressure range from 0.01 to 0.995. The pore diameter and the pore size distribution were determined by the BJH (Barret, Joyner, Halenda) method [34] applied to the adsorption branch of the isotherm.

The morphology of the samples was observed by Scanning Electron Microscopy (SEM) using a Philips FEI XL30 FEG microscope with an accelerating voltage = 7 kV). The samples were first metallised by a thin gold layer (< 10 nm).

### 3. RESULTS AND DISCUSSION

#### 3.1. The Kolliphor/P123/water ternary diagram

The investigation of the Kolliphor/P123/water phase diagram shows that in the water rich part of the diagram (Fig. 1), at least up to a total surfactant concentration equal to 25 wt.%, a micellar solution ( $L_1$ ) is obtained, whatever the ratio between Kolliphor and P123. The  $L_1$  domain is extended up 46 wt.% of surfactant for solutions rich in Kolliphor. The cubic ( $I_1$ ), the hexagonal ( $H_1$ ) and the lamellar ( $L_\alpha$ ) liquid crystal domains appear as the total surfactant concentration increases. The limits of  $I_1$  are unbroken and almost continuous between the pure cubic phase of Kolliphor and that of P123; i.e. from 46 to 58 wt. % of KEL and from 22 to 37 wt.% of P123 (Fig. 1). In the same way, except for the Kolliphor-rich domain, which gives way to a reverse micellar phase, a hexagonal phase whose water quantity corresponds approximately to the one present in the pure liquid crystals of Kolliphor and P123 appears. This observation suggests the existence of mixed liquid crystals [35,36]. For the pure KEL system this phase is detected between 58 and 68 wt.% of Kolliphor in water, whereas it is located between 40 and 65 wt.% of Pluronic in the P123/water system. If the total surfactant concentration is further increased the lamellar phase ( $L_\alpha$ ), which is not detected in the Kolliphor/water binary system appears. However,  $L_\alpha$  can incorporate up to 71.5% of Kolliphor. For the richer part in Kolliphor a reverse micellar phase ( $L_2$ ) can be formed for total surfactant concentrations higher than 87%. This  $L_2$  phase extends into a tongue shape when it is enriched in P123. Finally, a solid phase is observed for total surfactant concentrations higher than 97 wt.% if the P123 loading in the mixture is higher than 21%.

Whatever the organized molecular system, the compatibility between the head groups, composed of oxyethylene units and of the alkyl chains of Kolliphor and P123 allows the formation of mixed entities in all proportion. No gap of miscibility is observed.

### **3.2 Micellar structure and determination of the structural parameters**

To go further in the micelles characterization, SAXS experiments have been performed. Figure 2A presents, the experimental SAXS spectra of mixed micellar solutions with a total surfactant concentration of 5 wt.% in water for various ratios between Kolliphor and P123. All the spectra present only one broad peak, characteristic of the form factor. It is shifted from 0.78 to 0.59 nm<sup>-1</sup> when the quantity of P123 in the surfactants mixture varies from 0 to 100%. To determine the micellar structure, the data were analyzed by using the Generalized Indirect Fourier Transform (GIFT) method [37,38], taking into consideration the interparticle interactions (Fig. 2A solid line). The obtained pair-distance distribution functions (PDDFs) are depicted in Figure 2B. All the curves present a bell-like shape, characteristic of spherical micelles, with a dimension which depends on the P123 content in the surfactants mixture. Its value progressively varies from 13.9 for the pure Kolliphor micelles to 24.3 nm for the pure P123 micelles (Table 1). It should be also noted that like for the P123 micelles, the PDDF of the curve corresponding to the solution prepared with a Kolliphor/P123 ratio of 0.33 presents a shoulder on the left side of the maximum of the  $\rho(r)$  functions at around 4 nm, featuring a lower inhomogeneity of the particles compared with the ones of the pure Kolliphor solution and with the other mixed solutions. The excess-electron density profiles have been determined by the deconvolution of the pair-distance distribution functions (PDDFs) (Fig. 2C). The profiles confirm the core-shell type particles for the different micellar solutions. Indeed, the negative density difference corresponds to the hydrophobic part, whereas the positive density difference can be attributed to the hydrophilic shell. The micelles diameter

increases from 14.0 to 25.0 nm when the amount of P123 in the surfactants mixtures is changed from 0 to 100% (Table 1). These values are in accordance with the micelle size found on the PDDFs. When the P123/Kolliphor ratio is increased more and more P123 molecules are accommodated in the micelles leading to micelles with bigger size. The hydrophobic radius corresponds to the  $r$ -value when the sign of  $\Delta\rho(r)$  changes. It can be estimated at 3.5 and 3.9 nm for the Kolliphor and P123 micelles, respectively. For the mixed systems its value varies between 4.0 and 4.5 nm, depending on the P123 content (Table 1). The dimension of the alkyl chains in the micelles, corresponding to the lowest value of  $\Delta\rho(r)$ , can be estimated at about 2.5 and 3.8 nm respectively for the Kolliphor and P123 micelles. Given that, from the length of the bonds, the extended alkyl chains of Kolliphor have a dimension of about 2.5 nm, we can conclude that the alkyl chains, in the pure Kolliphor micelles, are rather extended. In the same way, estimating that the length of the PPO-part of the P123 is equal to 24.5 nm (1 PPO = 0.35 nm), we can deduce that the PPO chain, in the pure P123 micelles, can only be self-folded and it rather adopts a meandering conformation as previously reported [39]. Looking at the dimension of the hydrophobic moieties in the mixed-micelles, around 3 nm, we can assume that the alkyl chains of Kolliphor and PPO chain of P123 likely adopt the same conformation than in the pure micelles.

All the observations reported above support the existence of mixed micelles regardless the proportion between the two surfactants in the solutions.

Assuming that the mixture of surfactant forms a mixed entity, the structural parameters of the liquid crystal phases have also been determined. The water amount has been kept constant and the weight fraction of Kolliphor in the surfactant mixture, noted  $x_{KEL}$ , has been varied from 0 to 1.

For a given composition the average molar weight ( $M$ ) of the mixed entity is

$$M = \frac{N^P M^P + n^{KEL} M^{KEL}}{N^P + n^{KEL}}$$

where  $n^P$  and  $n^{KEL}$  respectively stand for the mole number of Pluronic and Kolliphor surfactant;  $M^P$  and  $M^{KEL}$  are the corresponding molar weight.

*Cubic liquid crystal phase* : For the cubic phase, the hydrophobic radius  $R_H$  is related to the lattice parameter  $a$  by the following equation [40] :

$$\frac{V_B}{V_s + \alpha V_w} = \frac{4 \nu \pi R_H^3}{3a^3}$$

with  $\nu$  the number of micelles per cubic lattice ( $\nu = 8$  or  $4$  for the Pm3n and Fm3m space group, respectively)

where  $\alpha$  stands for the number of water molecules per surfactant molecule and  $V_s, V_B, V_w$  respectively stand for the molar volumes of the mixed surfactant, the hydrophobic part of the mixed surfactant and water ( $V_w = 18 \text{ cm}^3/\text{mol}$ ).  $V_s$  and  $V_B$  depend on the molar ratio between the two amphiphiles. For example, for a mixture containing 30 wt.% of Kolliphor, these values are  $V_s = 4016 \text{ cm}^3/\text{mol}$  and  $V_B = 2656$ . The values of  $V_s$  and  $V_B$  for the pure surfactant were calculated from densities and are  $V_s = 2354$ ,  $V_B = 834 \text{ cm}^3/\text{mol}$  for Kolliphor and  $V_s = 5577$  and  $V_B = 4030 \text{ cm}^3/\text{mol}$  for P123.

Then, the cross sectional area  $S$  can be deduced as [40]:

$$S = \frac{3 V_B}{N R_H}$$

$N$  is the number of Avogadro.

Scattering spectra of samples belonging to the cubic domain are reported in Figure 3A. Until

$x_{KEL} = 0.8$ , The relative positions of the Bragg reflections are ,  $\sqrt{\frac{4}{3}}$ ,  $\sqrt{\frac{8}{3}}$ ,  $\sqrt{\frac{11}{3}}$ ,  $\sqrt{\frac{12}{3}}$ ,  $\sqrt{\frac{16}{3}}$

and  $\sqrt{\frac{20}{3}}$ . According to results published by Tiddy et al. [41], they can be indexed in the

Fm3m space group. For  $x_{KEL} = 0.9$  the ratios between the reflection lines change and they become  $1 : \sqrt{\frac{3}{2}}, \sqrt{2}, \sqrt{\frac{5}{2}}, \sqrt{3}, \sqrt{\frac{29}{4}}$ , which can be assigned to the Pm3n direct micellar cubic phase [41]. The cell parameter is related to the space spacing by the relations :  $a = d_{111} \sqrt{3}$  and  $a = 2 d_{200}$  for the Fm3m and Pm3n space group, respectively.

*Hexagonal liquid crystal phase:* The hexagonal phase is composed of infinite cylinders packed in a hexagonal array. In case of direct systems, cylinders are filled by the hydrophobic chains and are covered by both head groups and water. The hexagonal phase is characterized by its typical SAXS profile with the relative peak positions, 1,  $\sqrt{3}$ , 2 (Fig 4A). The distance  $d_{100}$  associated to the first peak is related to the hydrophobic core radius  $R_H$  by the relation [40]:

$$\frac{V_B}{V_S + \alpha V_W} = \frac{\sqrt{3}\pi R_H^2}{2d_{100}^2}$$

The cross-sectional area  $S$  can then be deduced from the following relation [40]:

$$S = \frac{2 V_B}{N R_H}$$

*Lamellar liquid crystal phase :* The lamellar phase can be described as an infinite bi-layer of surfactants stacked in a parallel manner. The diffraction pattern exhibits two reflections with the relative peak positions 1, 2 (Fig. 5A). The repetition distance corresponds to the layer spacing, which comprises the water separated by the surfactant bi-layer. The cross-sectional area can be calculated from the following formula [40] :

$$S = \frac{2(V_S + \alpha V_W)}{N d_{001}}$$

where  $d_{001}$  stands for the repetition distance.

The hydrophobic thickness  $d_B$  and the hydrophilic thickness  $d_A$  can be deduced from the following equations [40] :

$$d_B = \frac{2V_B}{S} \text{ and } d_A = d_{001} - d_B$$

Figures 3B, 4B and 5B display the variation of structural parameter as a function of  $x_{KEL}$  for the cubic, the hexagonal and the lamellar liquid crystal phases, respectively. From these figures it can be noted that with the increase of  $x_{KEL}$ , whatever the liquid crystal, all the structural parameters vary in a linear manner between the values corresponding to the two binary systems. As an example for the cubic phase  $R_H$  and  $S$  decrease from 5.9 to 4.6 nm and from 2.3 to 1.3 nm<sup>2</sup> when  $x_{KEL}$  is changed from 0.30 to 0.80 (Fig. 3B). The linear relationship between the structural parameters and the weight fraction of Kolliphor ( $x_{KEL}$ ) in the surfactants mixture is in a good agreement with the formation of a mixed liquid crystal phases in which both the Kolliphor and P123 molecules are present without segregation of the surfactants. The formation of mixed entities is possible thanks to the compatibility of the hydrophilic and the hydrophobic parts of the two surfactants.

Figure 3C, 4C and 5C describe the evolution of the structural parameters as a function of  $\alpha$ , the number of water molecules per surfactant molecule. We can note an increase in the d-spacing due to the hydration of the head group and the water surrounding the surfactant. As it could be expected for mixed liquid crystal phases, the variation of the structural parameters as a function of  $\alpha$  follows the same trend than as a function of  $x_{KEL}$ . Indeed, in that case, even if the water content and the total surfactant concentration are constant, since the proportion between Kolliphor and P123 varies in the surfactant mixture, the average molar weight ( $M$ ) of the mixed entity is changed for each content of Kolliphor present in the mixture. The number of surfactant molecules is thus modified and consequently,  $\alpha$  which is the number of water molecules per surfactant molecules also varies when  $x_{KEL}$  is increased from 0 to 1.

It has been reported that in the pure P123  $H_1$  and  $I_1$  domains, the values of  $R_H$  are around 4.8 and 4.5 nm, respectively [39,42]. Taking into account the different bonds, the length of the extended PPO block is 24.5 nm and comparing this value to the hydrophobic radius, it was

concluded that the hydrophobic chains of the P123 hexagonal and cubic phases are completely self-folded. In the pure Kolliphor/water system, from the length of the bonds the dimension of the extended alkyl chains it was concluded that in H<sub>1</sub> and I<sub>1</sub> the alkyl chains adopt an extended conformation. Looking at the R<sub>H</sub> values reported in Figure 3 and 4, we can therefore assume that, in the mixed hexagonal and cubic phases, the alkyl chains are also completely extended, whereas the PPO blocks are self-folded.

In the L<sub>α</sub> phase, d<sub>B</sub> varies from 7.8 to 3.8 nm when x<sub>KEL</sub> is increases from 0 to 0.8 (Fig.5), considering the dimensions of the alkyl chains and of the PPO units in an extended conformation the variation of d<sub>B</sub> suggests that the hydrophobic parts in the mixed lamellar phase are rather extended.

### 3.3. Silica porous materials

Porous materials are prepared by combining the fine emulsion and the P123 micelles. From Figure 6, which presents the variation of the SAXS pattern as a function of Em/P123 weight ratio, it can be noted that under the synthetic conditions reported in this study, no mesopore ordering is recovered when P123 micelles are used alone as templates. Indeed, in that case no peak is detected on the SAXS pattern. For Em/P123 ratios comprised between 2/8 and 4/6, two peaks around 12 and 7 nm are observed on the SAXS patterns (Fig. 6). Their relative position 1,  $\sqrt{3}$  shows that in this range of Em/P123 ratios, ordered mesostructured silica materials are recovered. The unit cell a<sub>0</sub>, which is the sum of the pore diameter and of the thickness of the pore wall, can be deduced from the following relation :  $a_0 = 2d_{100}/(3)^{1/2}$ , and its value is found around to 13.9 nm. Increasing Em/P123 from 5/5 to 8/2, no secondary reflections are detected any longer. Only a broad peak characteristic of a wormhole-like mesostructure, as observed for MSU, is detected at 13.0 nm for Em/P123 = 5/5 (Fig. 6). This peak gives an indication of the average pore-to-pore distance in the disordered wormhole

framework, which presents a lack of long-range crystallographic order. It is shifted toward smaller  $q$  values, when the Em/P123 ratio is raised until 8/2 (Fig. 6). Beyond Em/P123 = 8/2, no reflection is detected anymore on the SAXS pattern, meaning that the channel arrangement is completely random.

The sample prepared from the pure P123 micellar solutions exhibits a type IV isotherm (Fig. 7), characteristic of mesoporous materials according to the IUPAC classification [43]. The pore size distribution presents a maximum at around 2.8 nm (insert of fig. 7). The values of the specific surface area and of the pore volume are 818 m<sup>2</sup>/g and 0.52 cm<sup>3</sup>/g, respectively (Fig. 8). Preparing the silica materials from the P123 micelles and fine emulsion mixture, the isotherm remains type IV until a Em/P123 weight ratio of 5/5. It should be noted that with the addition of Em, the capillary condensation step is more pronounced and is shifted towards higher relative pressure for example it occurs at  $p/p_0 = 0.45$  for the material prepared from the pure P123 micelles and at  $p/p_0 = 0.75$  for the sample synthesized with a Em/P123 ratio higher from 1/9 to 5/5 (Fig. 7). Since the  $p/p_0$  position of the inflection point is related to the pore diameter according to the Kelvin's equation, it can be inferred that bigger mesopores appear when the porous silica are prepared from the Em/P123 mixture. Nevertheless, on the mesopore size distribution the component at 2.8 nm is observed until a Em/P123 weight ratio of 3/7. A second maximum at 9.3 and 8.7 nm is observed for materials prepared in the presence of 10 and 20% of Em, respectively. The materials synthesized under these conditions thus present at least a dual mesoporosity. Increasing the Em/P123 from 2/8 to 5/5, the component at 2.8 disappears in favor of a doubling of the one at 8.7 nm, which is split into two maxima one around 10.0 nm and the other one at around 8.5 nm (Insert of Fig. 7). The intensity of the two peaks gradually reversed when the Em/P1213 ratio is increased. Beyond Em/P123 = 5/5, the mesopore size distribution becomes broader and only one large component with a maximum between 15.0 and 23 nm (insert Fig.7). It should be noted that

whatever the Em/P123 ratio both the mesopore size distribution and the shape of the isotherms at very low relative pressure suggest also the presence of micropores.

The specific surface area is quite high (Fig. 8) and it slightly increases when the proportion of Em is raised. For example, its value varies from 890 to 970 m<sup>2</sup>/g when the Em/P123 ratio is changed from 1/9 to 8/2. From Figure 8 it can also be seen that the pore volume gradually increases from 0.52 to 1.40 cm<sup>3</sup>/g as a function of the Em/P123 weight ratio.

Figure 9 shows SEM pictures of the samples synthesized at different Em/P123 weight ratios. The morphology of the materials can be mainly described as an agglomerate of small spheres having a diameter less than 10 μm. Higher the Em/P123 ratio is, more agglomerated the spheres are (Fig. 9). Besides the spheres, macropores of a few microns looking like the imprints of droplets can also be detected, in particular for silica prepared with a Em/P123 ratio of 3/7 and 4/6.

### **3.4. Discussion**

When pure P123 micelles are used as template, the mesostructured silica is obtained through the Cooperative Templating Mechanism (CTM). In the initial step, when the silica is added to the micellar solution, hydrogen-bonding interactions between the oxygen atoms of the oxyethylene groups of the surfactant and OH groups of the hydrolyzed TMOS are formed. Then, the condensation of the inorganic precursor at the external surface of the micelles occurs. The mesophase is obtained after intermicellar condensation. Finally, the hydrothermal treatment at higher temperature completes the assembly of micelles and the polymerization of the silica source. The mesostructured material is recovered after surfactant removal by solvent extraction or/and by calcination. Under the conditions reported here, no mesopore ordering is obtained and the mesopore size distribution is centered at around 2.8 nm. Consequently, preparing the porous silica from the P123 micelles and fine emulsion mixtures, the

component at 2.8 nm observed until a Em/P123 weight ratio of 3/7 can be attributed to mesopores templated by the pure P123 micelles.

To explain the evolution of the pore size distributions as a function of the Em/P123 ratio, we have also to consider the potential effect of methanol, released during the hydrolysis on both the micellar solution and the fine emulsion. In previous studies we have shown that while the methanol does not significantly disturb the CTM mechanism for the preparation of mesostructured silica [44], it has a negative effect on the stability of the fine emulsion [45]. Indeed, in the case of nano-emulsions formulated from the Remcopal/decane/water system we have reported that the methanol addition leads to an increase of the oil drop and to a destabilization of the nano-emulsion. Moreover, the existence of the nano-emulsions is not favored in the presence of the Pluronic micelles since the system becomes more hydrophilic [45]. Here, up to a Em/P123 ratio of 5/5, since P123 micelles predominate and since there is a huge amount of methanol released, from 17 to 10 wt. % (Fig. 10), we can assume that the negative effects of both methanol and P123 micelles involve a destabilization of the fine emulsion. With the low amount of Em, this can explain why no pore size due to the mineralization of the fine emulsion is observed until a Em/P123 ratio of 5/5. The Kolliphor molecules arising from the destabilization of the fine emulsion can associate with P123 to form mixed-micelles, which can eventually be swollen by Myristate. Indeed, the investigation of the Kolliphor/P123/water phase diagram has shown that the mixture of these two surfactants leads to the formation of mixed organized molecular systems and in particular mixed micelles. The formation of the mixed micelles is supported by the disappearance of the component at 2.7 nm in the mesopore size distribution when the quantity of P123 micelles decreases. This strongly suggests that the P123 micelles accommodate the Kolliphor molecules. The mixed micelles are likely responsible for the mesopore diameter at around 8.7 nm. As a matter of fact, this size at 8.7 nm is in accordance with the hydrophobic diameter

(between 8.0 and 9.6 nm, depending on the Kolliphor/P123 ratio). The swollen mixed micelles by Myristate give the peak at around 10.0 nm. As observed by the SEM the oil droplets arising from the fine emulsion can also coalesce to lead to the formation of macropores having a size of few microns in diameter.

With the increase of the Em/P123 weight ratio beyond 5/5, the proportion of Pluronic micelles is lowered and less and less of methanol is released (Fig. 10). Indeed, it should be reminded that the TMOS amount has been fixed to get a P123/TMOS molar ratio of 0.005. Due to the lower amount of methanol and P123 micelles, the fine emulsion is less destabilized and we can assume that the porosity mainly arises from the fine emulsion, which proportion increases with the Em/P123 ratio. In that case the hydrolyzed TMOS interacts with the Kolliphor molecules at the surface of the Myristate droplets.

Finally, for all samples the microporosity can arise from the penetration of the oxyethylene units in the silica framework. After surfactant removal this leads to the formation of micropores. This phenomenon is well reported in the literature for the synthesis of SBA-15 [46,47].

#### **4. Conclusion**

Using a mixture of fine emulsion (Em) and Pluronic P123 micelles, hierarchical porous silica materials can be prepared. The porosity features of the materials is strongly depend on the Em/P123 weight ratio. Indeed, if this ratio is lower than 5/5 dual mesoporous silica are obtained. In that case, methanol released during the hydrolysis of TMOS and the presence of P123 micelles have a negative effect on the fine emulsion, which is destabilized. The Kolliphor molecules likely associate with the P123 micelles to form mixed micelles. Indeed, the investigation of the Kolliphor/P123/water systems have shown that when both surfactants are mixed they formed mixed micelles and liquid crystal phases (cubic, hexagonal and

lamellar). A part of Myristate released by the fine emulsion can swell the mixed micelles and the oil droplets of the fine emulsion can also give macropores.

Increasing the Em/P123 weight ratio both the proportion of P123 micelles and methanol decrease and the fine emulsion is not completely destabilized any longer. The porosity is then controlled by the fine emulsion. Whatever the Em/P123 ratio micropores are also formed likely by the penetration of the EO groups in the silica framework.

### **Acknowledgements**

Claudia Violeta Cervantes-Martinez also thanks the CONACYT for the financial support of her PhD.

## References

- [1] L. F. F. P. G. Braganca, M. Ojeda, J.L.G. Fierro, M.I. Pais da Silva, Bimetallic Co-Fe nanocrystals deposited on SBA-15 and HMS mesoporous silicas as catalysts for Fischer-Tropsch synthesis, *Appl. Catal. A-Gen.* 423-424 (2012) 146-153.
- [2] P. Botella, A. Corma, M. Quesada, Synthesis of ordered mesoporous silica templated with biocompatible surfactants and applications in controlled release of drugs, *J. Mater. Chem.* 22 (2012) 6394-6401.
- [3] P. Perego, R. Millini, Porous materials in catalysis: challenges for mesoporous materials, *Chem. Soc. Rev.* 42 (2013) 3956-3976.
- [4] S.Y. Park, M. Barton, P. Pendleton, Mesoporous silica as a natural antimicrobial carrier, *Colloids and Surfaces A: Physicochem. Eng. Aspects* 385 (2011) 256-261.
- [5] F. Schüth, Endo- and exotemplating to create high-surface-area inorganic materials, *Angew. Chem. Int. Ed.* 42 (2003) 3604-3622.
- [6] B.T. Holland, C.F. Blanford, T. Do, A. Stein, Synthesis of highly ordered, three-dimensional, macroporous structures of amorphous or crystalline inorganic oxides, phosphates, and hybrid composites, *Chem. Mater.* 11 (1999) 795-805.
- [7] M.O. Coppens, G.F. Froment, The effectiveness of mass fractal catalysts, *Fractals* 5 (1997) 493-505.
- [8] M.A. Parlett, K. Wilson, A.F. Lee, Hierarchical porous materials: catalytic applications, *Chem. Soc. Rev.* 42 (2013) 3876-3893.
- [9] T. Sen, GJT. Tiddy, J.L. Casci, M.W Anderson, Macro-cellular silica foams: synthesis during the natural creaming process of an Oil-in-Water Emulsion, *Chem. Commun.* 17 (2003) 2182-2183.

- [10] K. Nakanishi, Y. Kobayashi, T. Amatani, K. Hirato, T. Kodaira, Spontaneous formation of hierarchical macro-mesoporous ethane-silica monolith *Chem. Mater.* 16 (2004) 3652-3658.
- [11] J.L. Blin, B. Bleta, J. Ghanbaja, M.J. Stébé, Fluorinated emulsions: Templates for the direct preparation of macroporous–mesoporous silica with a highly ordered array of large mesopores *Microporous and Mesoporous Mater.* 94 (2006) 74-80.
- [12] H. Mori, M. Uota, D. Fujikawa, T. Yoshimura, T. Kuwahara, G. Sakai, T. Kijima, Synthesis of micro-mesoporous bimodal silica nanoparticles using lyotropic mixed surfactant liquid-crystal templates, *Microporous and Mesoporous Mater.* 91 (2006) 172-180.
- [13] O. Sel, D. Kuang, M. Thommes, B. Smarsly, Principles of hierarchical meso-macropore architectures by liquid crystalline and polymer colloid templating *Langmuir* 22 (2006) 2311-2322.
- [14] J. Nestor, A. Vichez, C. Solans, J. Esquena, Facile Synthesis of meso/macroporous dual materials with ordered mesopores using highly concentrated emulsions based on a cubic liquid crystal, *Langmuir* 29 (2013) 432-440.
- [15] J. Esquena, J. Nestor, A. Vílchez, K. Aramaki, C. Solans, Preparation of mesoporous/macroporous materials in highly concentrated emulsions based on cubic phases by a single-step method, *Langmuir* 28 (2012) 12334-12340.
- [16] K. Nakanishi, Pore Structure Control of Silica Gels Based on Phase Separation, *J. Porous Mater.* 4 (1997) 67-112.
- [17] Y. Sato, K. Nakanishi, K. Hirao, H. Jinnai, M. Shibayama, Y.B. Melnichenko, G.D. Wignall, Formation of Ordered Macropores and Templated Nanopores in Silica Sol-

- Gel System Incorporated with EO-PO-EO Triblock Copolymer,. Colloids Surfaces A Physicochem. Eng. Asp. 187-188 (2001) 117-122.
- [18] K. Nakanishi, Y. Sato, Y. Ruyat, K. Hirao, Supramolecular Templating of Mesopores in Phase-Separating Silica Sol-Gels Incorporated with Cationic Surfactant, *J. Sol-Gel Sci. Technol.* 26 (2003) 567-570.
- [19] A. Imhof, D.J. Pine, Ordered macroporous materials by emulsion templating, *Nature* 389 (1997) 948-951.
- [20] H. Zhang, G.C. Hardy, M.J. Rosseinsky, A.I. Copper, Uniform emulsion-templated silica beads with high pore volume and hierarchical porosity, *Adv. Mater.* 15 (2003) 78-81.
- [21] B.P. Binks, Macroporous silica from solids-stabilized emulsion templates, *Adv. Mater.* 14 (2002) 1824-1827.
- [22] C. Oh, S.C. Chung, S.I. Shin, Y.C. Kim, S.S. Im, S.G. Oh, Distribution of macropores in silica particles prepared by using multiple emulsions, *J. Colloids Interface Sci* 254 (2002) 79-86.
- [23] C. Zhao, E. Danish, N.R. Cameron, R. Katak, Emulsion-templated porous materials (polyHIPEs) for selective ion and molecular recognition and transport : applications in electrochemical sensing, *J. Mater. Chem.* 17 (2007) 2446-2453.
- [24] S. Zhang, J. Chen, Synthesis of open porous emulsion-templated monoliths using cetyltrimethylammonium bromide, *Polymer* 48 (2007) 3021-3025.
- [25] F. Carn, A. Colin, M.F. Achard, H. Deleuze, E. Sellier, M. Birot, R. Backov, Inorganic monoliths hierarchically textured via concentrated direct emulsion and micellar templates, *J. Mater. Chem.* 14 (2004) 1370.

- [26] T. Sen, G.J.T. Tiddy, J.L. Casci, M.W. Anderson, Meso-cellular silica foams, macro-cellular silica foams and mesoporous solids : a study of emulsion-mediated synthesis, *Microporous and Mesoporous Mater.* 78 (2005) 255.
- [27] B.T. Holland, C.F. Blanford, A. Stein, Synthesis of macroporous minerals with highly ordered three-dimensional arrays of spheroidal voids, *Science* 281 (1998) 538-540.
- [28] R. Ravetti-Duran, J.L. Blin, M.J. Stébé, C. Castel, A. Pasc, Tuning the morphology and the structure of hierarchical meso–macroporous silica by dual templating with micelles and solid lipid nanoparticles (SLN), *J. Mater. Chem.* 22 (2012) 21540-21548.
- [29] L. Wang, X. Li, G. Zhang, J. Dong, J. Eastoe, Oil-in-Water Nanoemulsions for Pesticide Formulations, *J. Colloid Interface Sci.* 314 (2007) 230-235.
- [30] N. Sadurní, C. Solans, N. Azemara, M.J. García-Celma, Studies on the Formation of O/W Nano-Emulsions, by Low-Energy Emulsification Methods, Suitable for Pharmaceutical Applications, *Eur. J. Pharm. Sci.* 26 (2005) 438-445.
- [31] M. Jaworska, E. Sikora, M. Zielina, J. Ogonowski, Studies on the Formation of O/W Nano-Emulsions, by Low-Energy Emulsification Method, Suitable for Cosmeceutical Applications, *Acta Biochim. Pol.* 60 (2013) 779-782.
- [32] N. Anton, J.P. Benoit, P. Saulnier, Design and Production of Nanoparticles Formulated from Nano-Emulsion Templates—A Review, *J. Controlled Release* 128 (2008) 185-199.
- [33] C.V. Cervantes-Martinez, M. Emo, M.J. García-Celma, M.J. Stébé, J.L. Blin, Morphosynthesis of porous silica from biocompatible templates
- [34] E.P. Barrett, L.G. Joyner, P.P. Halenda, The determination of pore volume and area distributions in porous substances. I. Computations from nitrogen isotherms, *J. Am. Chem. Soc.* 73 (1951) 373-380.

- [35] J.C. Ravey, A. Gherbi, M.J. Stéb , Fluorinated and hydrogenated nonionics in aqueous mixed systems, *Prog. Colloid Polym. Sci.* 79 (1989) 272-278.
- [36] K. Tamori, K. Esumi, K. Meguro, Phase behavior in the mixed surfactant system: Lithium dodecyl sulfate/lithium perfluorooctanesulfonate/water, *J. Colloid Interface Sci.* 142 (1991) 236-243.
- [37] O. Glatter, O. Kratky, in: *Small Angle X-Ray Scattering*, Academic Press, (1982) 167-196.
- [38] G. Fritz, O. Glatter, Structure and interaction in dense colloidal systems: evaluation of scattering data by the generalized indirect Fourier transformation method, *J. Phys.: Condens. Matter* 18 (2006) S2403-S2419.
- [39] A. Roucher, M. Emo, F. Vibert, M.J. St b , V. Schmitt, F. Jonas, R. Backov, J.L. Blin, Investigation of mixed ionic/nonionic building blocks for the dual templating of macro-mesoporous silica, *J. Colloid Interface Sci.* 533 (2019) 385-400.
- [40] M. Alibrahim, M.J. St b , G. Dupont, J.C. Ravey, Effect of an Ionic Surfactant on the Phase Behavior of a Nonionic Surfactant-Based System, *J. Chim. Phys. Phys. - Chim. Biol.* 94 (1997) 1614-1633.
- [41] P. Sakya, J.M. Seddon, R.H. Templer, R.J. Mirkin, G.J.T. Tiddy, Micellar cubic phases and their structural relationships: The nonionic surfactant system C<sub>12</sub>EO<sub>12</sub>/water, *Langmuir* 13 (1997) 3706-3714.
- [42] K. Assaker, I. Naboulsi, M.J. St b , M. Emo, J.L. Blin, Investigation of mixed fluorinated and triblock copolymer liquid crystals: Imprint for mesostructured bimodal silica, *J. Colloid Interface Sci.* 446 (2015) 170-176.
- [43] K. S. W. Sing, D. H. Everett, R. A. W. Haul, L. Moscou, R. A. Pierotti, J. Rouquerol, T. Siemieniowska, Reporting physisorption data for gas/solid systems with special

- reference to the determination of surface area and porosity (Recommendations 1984)  
IUPAC, Pure and Appl. Chem. 57 (1985) 603-619.
- [44] K. Zimny, J.L. Blin, M.J. Stébé, Influence of methanol on the phase behavior of nonionic fluorinated surfactant: Relation to the structure of mesoporous silica materials, *J. Colloid Interface Sci.* 330 (2009) 456-462.
- [45] P. Riachy, M.J. Stébé, B. Lebeau, A. Pasc, L. Vidal, J.L. Blin, Nano-emulsions as imprints for the design of hierarchical porous silica through a dual templating mechanism, *Microporous and Mesoporous Mater.* 221 (2016) 228-237.
- [46] A. Galarneau, M. Nader, F. Guenneau, F. Di Renzo, A. Gedeon, Understanding the stability in water of mesoporous SBA-15 and MCM-41, *J. Phys. Chem. C* 111 (2007) 8268-8277.
- [47] T. Benamor, L. Vidal, B. Lebeau, C. Marichal, Influence of synthesis parameters on the physico-chemical characteristics of the SBA-15 type ordered mesoporous silica, *Microporous and Mesoporous Mater.* 153 (2012) 100-114.

## Figures caption

- Figure 1 : Composition phase diagram (wt.%) at 25°C of the Kolliphor/P123/water system.
- Figure 2 : Experimental (dotted line) and approximated (GIFT) (solid line) SAXS spectra of mixed micellar solutions of Kolliphor and P123 with a total concentration of surfactant in water equal to 5 wt% at 23 °C. The Kolliphor/P123 ratios are indicated on the right (A); Corresponding pair-distance distribution functions (PDDFs) (B); Corresponding excess-electron density profiles (C).
- Figure 3 : Cubic liquid crystal phase : Evolution of the SAXS pattern of the cubic with the Kolliphor (KEL) content in the surfactants mixture (A) and structural parameter of  $I_1$  as a function of  $x_{KEL}$  (B) and  $\alpha$  (C); ■ : d, ○ :  $R_H$  and ▲ : S. The total surfactant concentration is 40 wt.%.
- Figure 4 : Hexagonal liquid crystal phase : Evolution of the SAXS pattern of the hexagonal with the Kolliphor (KEL) content in the surfactants mixture (A) and structural parameter of  $H_1$  as a function of  $x_{KEL}$  (B) and  $\alpha$  (C); ■ :  $d_{100}$ , ○ :  $R_H$  and ▲ : S. The total surfactant concentration is 70 wt.%.
- Figure 5 : Lamellar liquid crystal phase : Evolution of the SAXS pattern of the hexagonal with the Kolliphor (KEL) content in the surfactants mixture (A) and structural parameter of  $L_\alpha$  as a function of  $x_{KEL}$  (B) and  $\alpha$  (C); ■ :  $d_{100}$ , ○ :  $d_B$ , ★ :  $d_A$  and ▲ : S. The total surfactant concentration is 85 wt.%.
- Figure 6 : Porous materials : Variation of the SAXS pattern as a function of the fine emulsion/P123 micellar solution weight ratio.

- Figure 7 : Porous materials : Nitrogen adsorption-desorption isotherms with the corresponding pore size distribution (insert) as a function of the fine emulsion/P123 micellar solution weight ratio.
- Figure 8 : Porous materials : Variation of the specific surface area and of the pore volume as a function of the proportion (%) of Em in the starting solution used to prepare the silica materials; ■ : specific surface area ○ : pore volume.
- Figure 9 : Porous materials : SEM images of the samples prepared with different Em/P123 weight ratios.
- Figure 10 : Porous materials : Variation of the weight percentage of released methanol as a function of the proportion (%) of Em in the starting solution used to prepare the silica materials.

**Table 1** : Micelles diameter and hydrophobic radius of Kolliphor/P123 mixed micelles. The total concentration of surfactant in water is equal to 5 wt%.

Sample	Micelles diameter (nm)*	Micelles diameter (nm)**	Hydrophobic radius $R_H$ (nm)
Kolliphor	13.9	14.0	3.5
Kolliphor/P123 = 3	16.6	17.0	4.3
Kolliphor/P123 = 1	17.8	18.0	4.5
Kolliphor/P123 = 0.33	19.6	20.0	4.0
P123	24.3	25.0	3.9

\* Values obtained from GIFT analysis

\*\* Values obtained from the excess electron density profiles

Figure 1

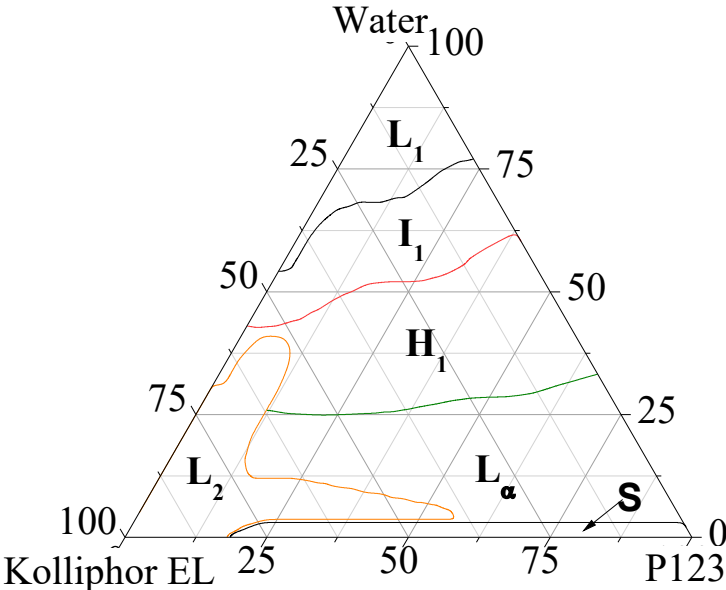


Figure 2

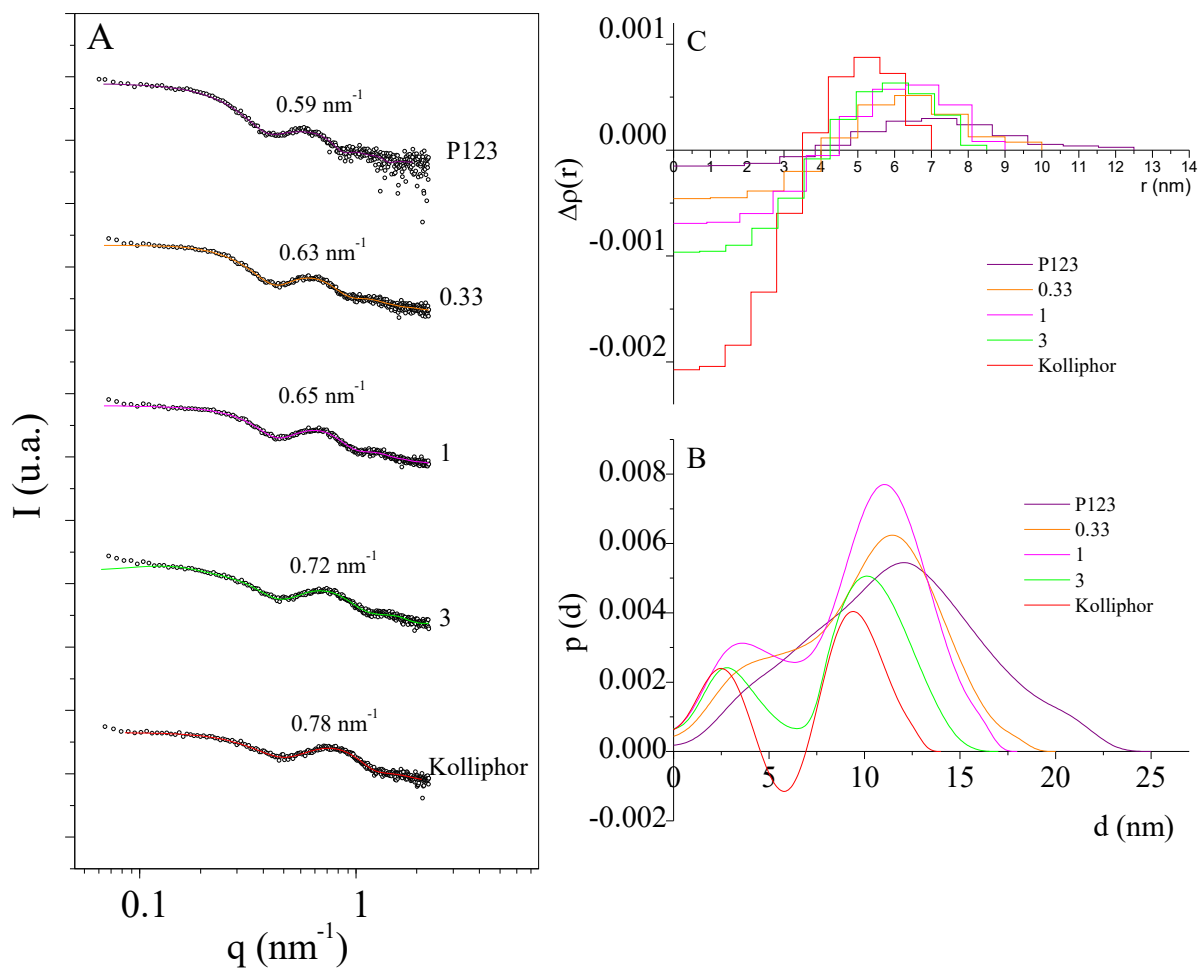


Figure 3

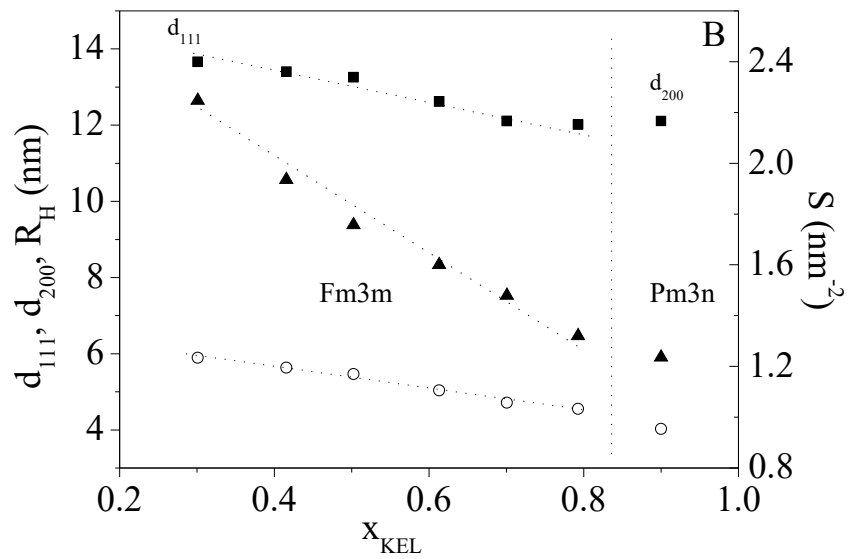
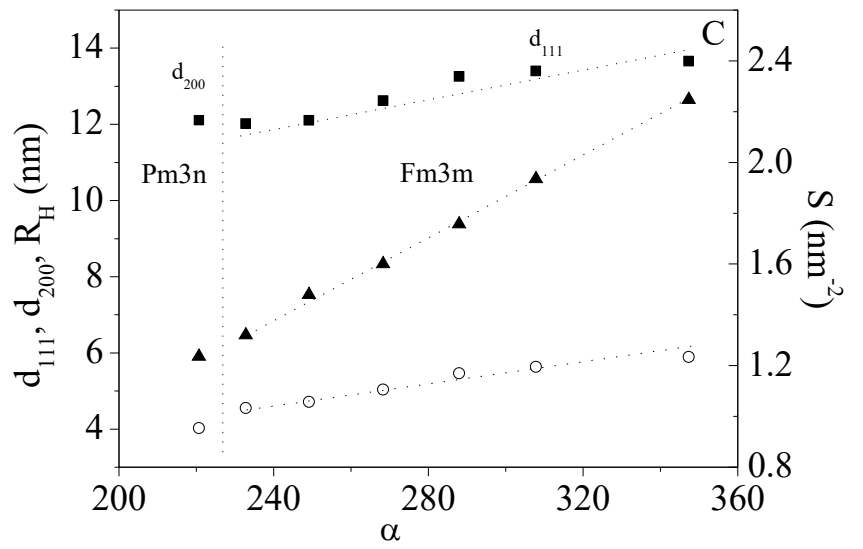
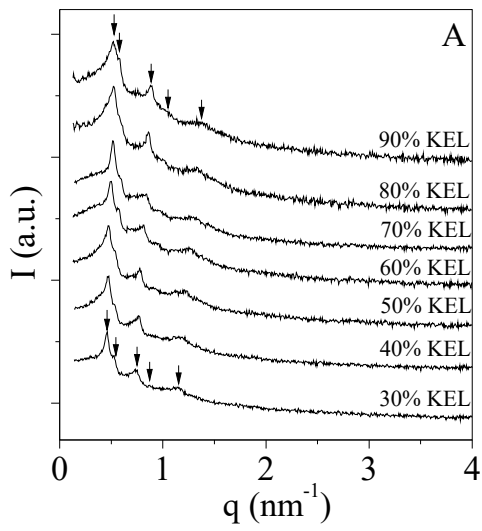


Figure 4

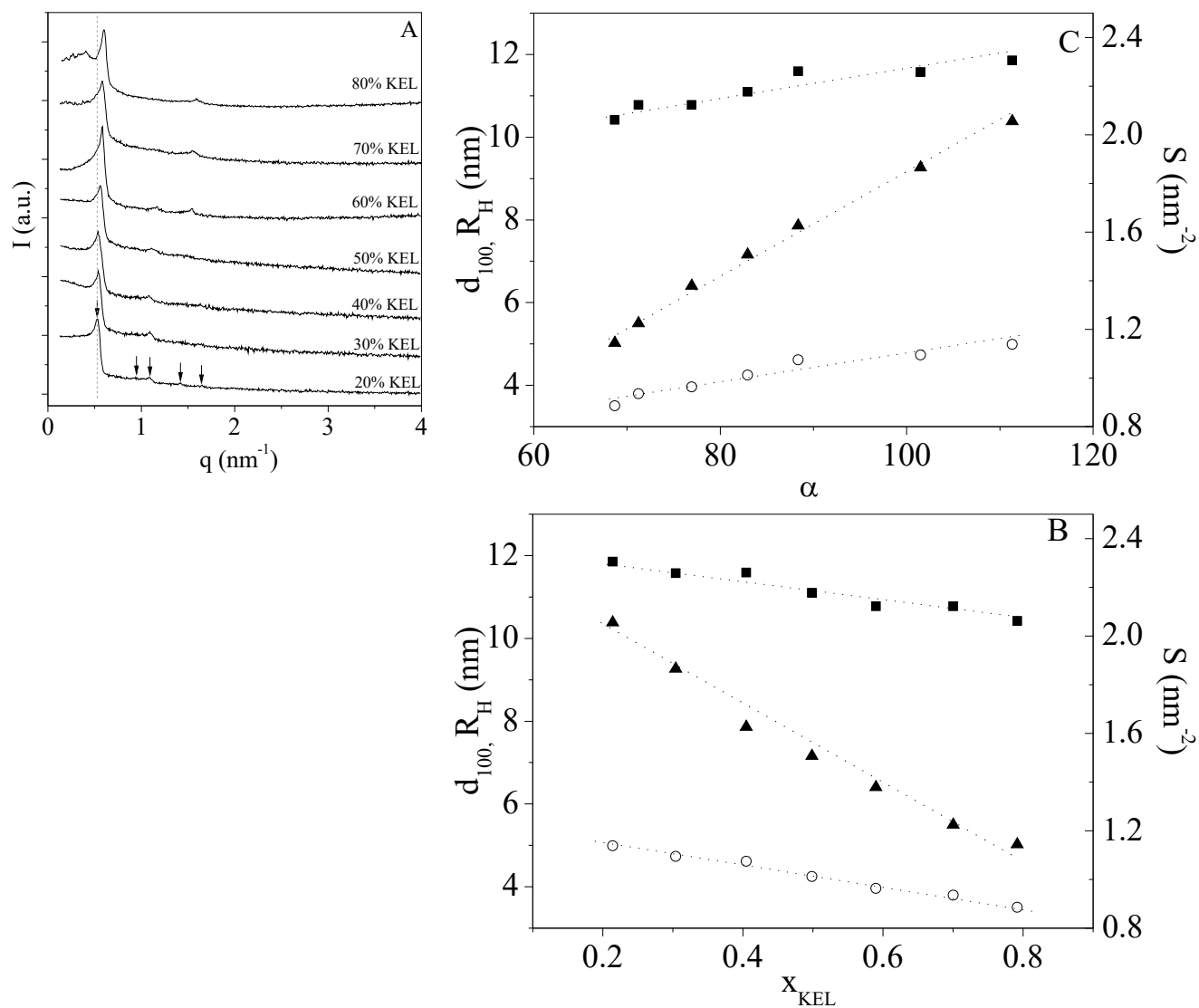


Figure 5

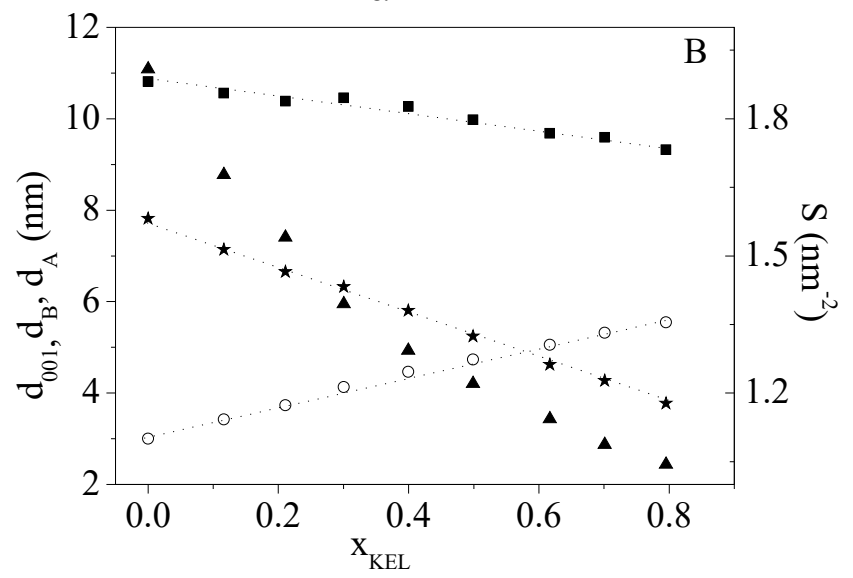
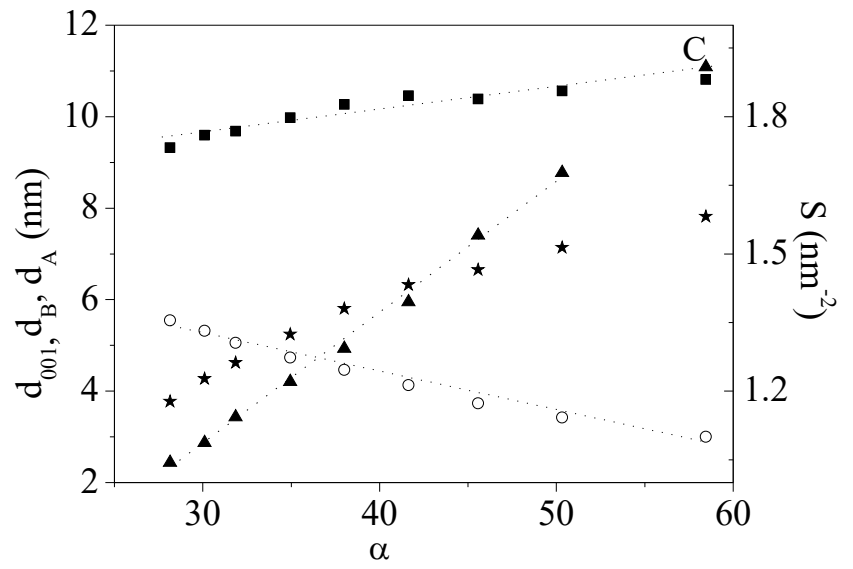
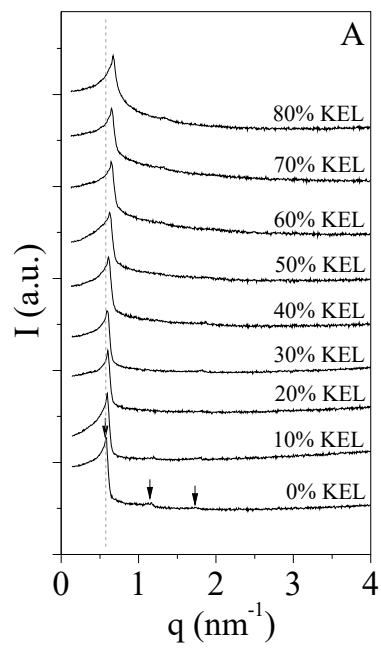


Figure 6

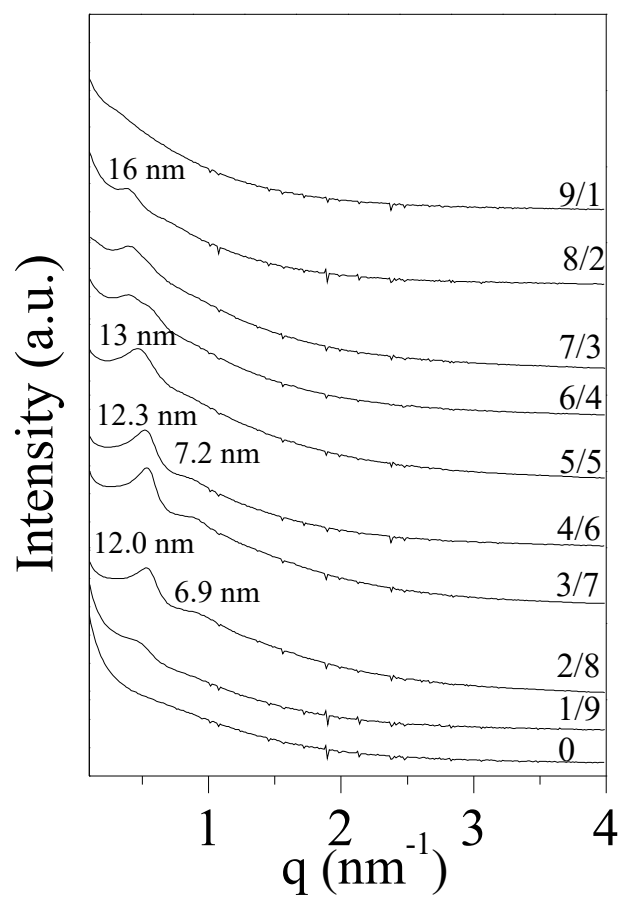
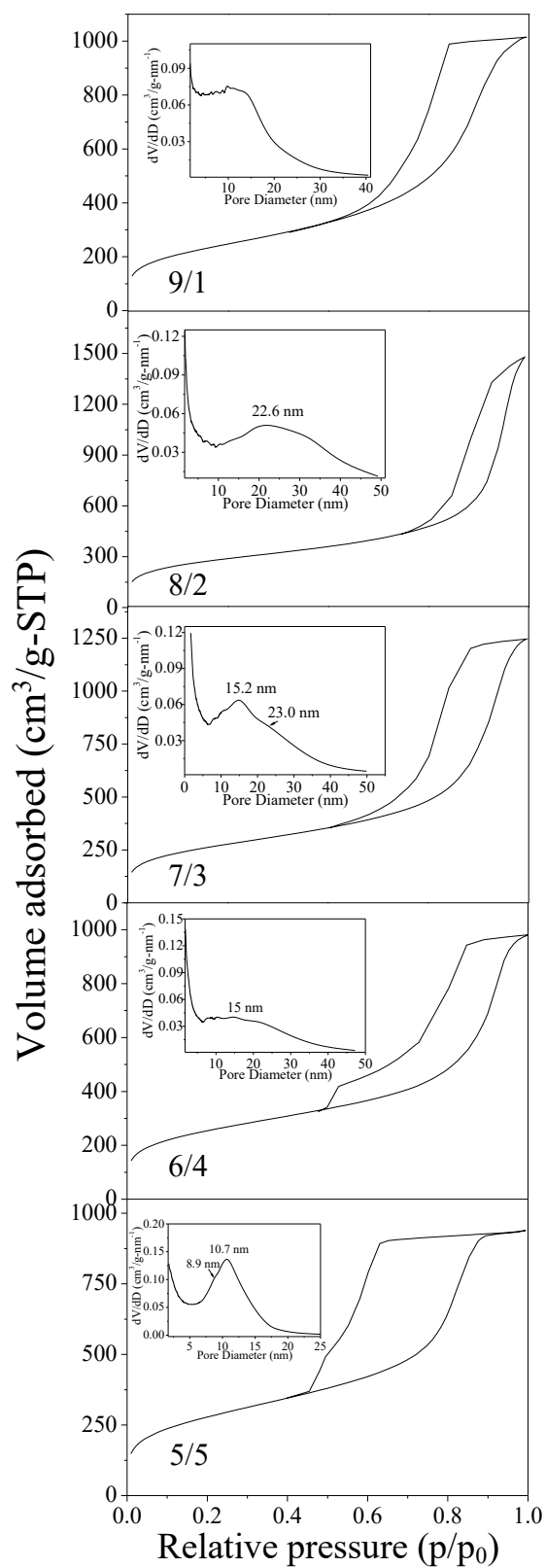
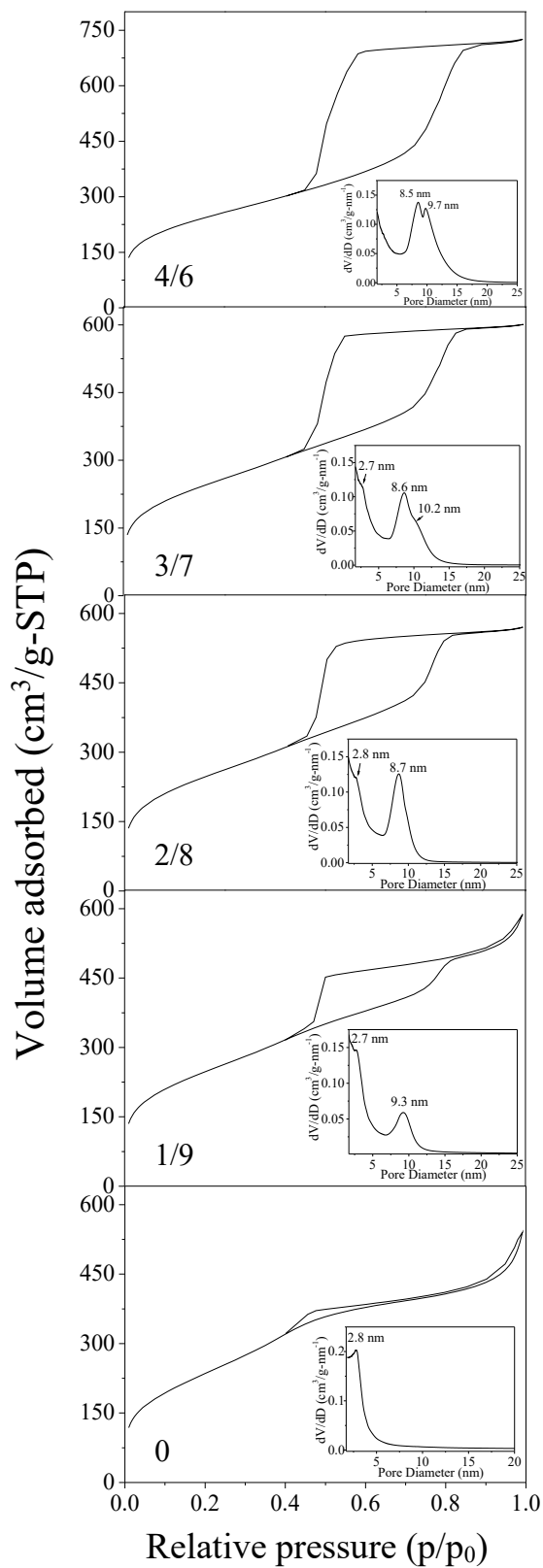


Figure 7



**Figure 8**

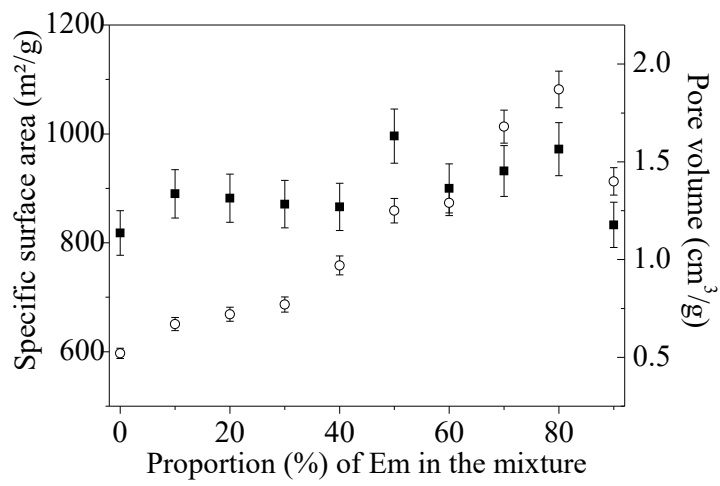
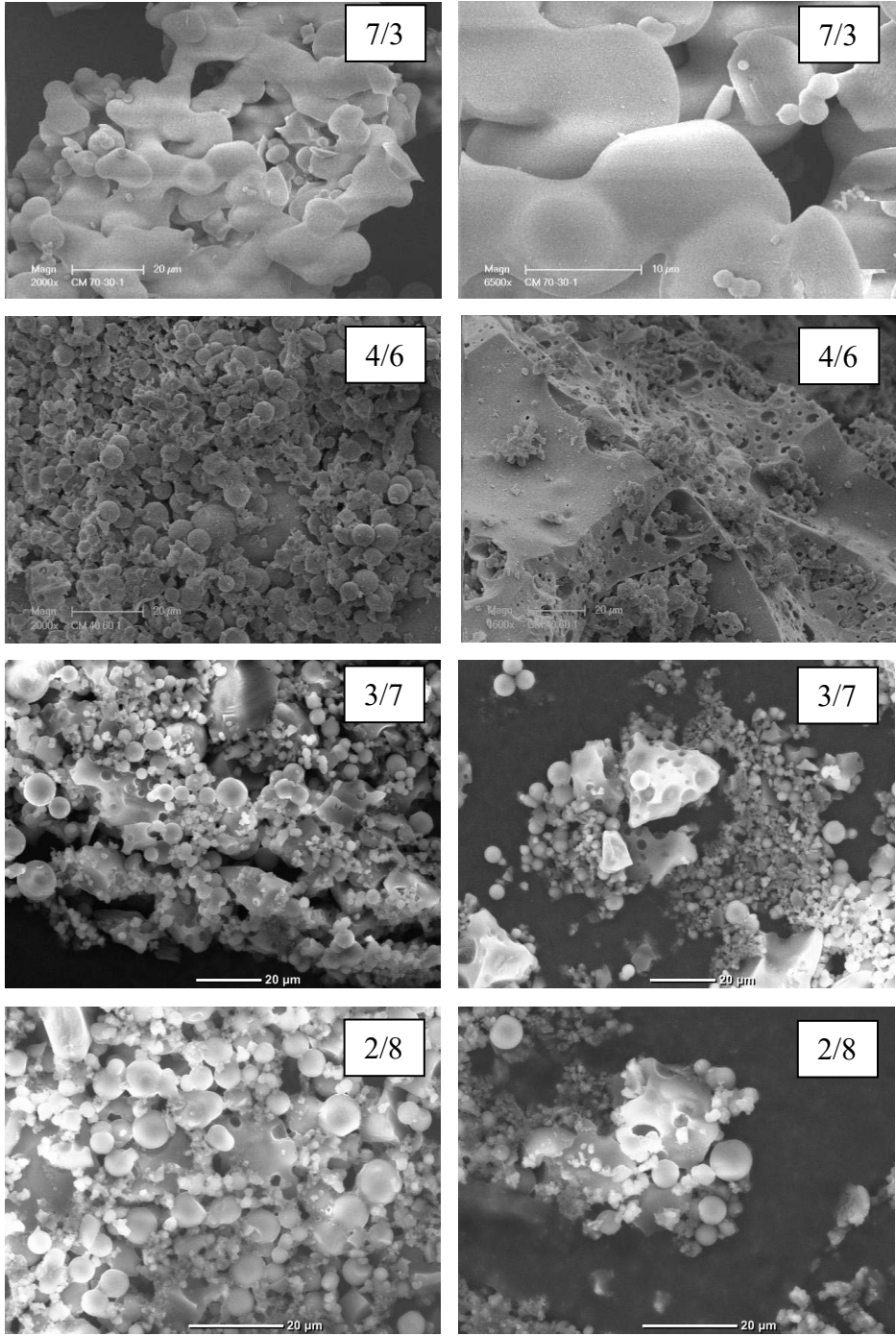
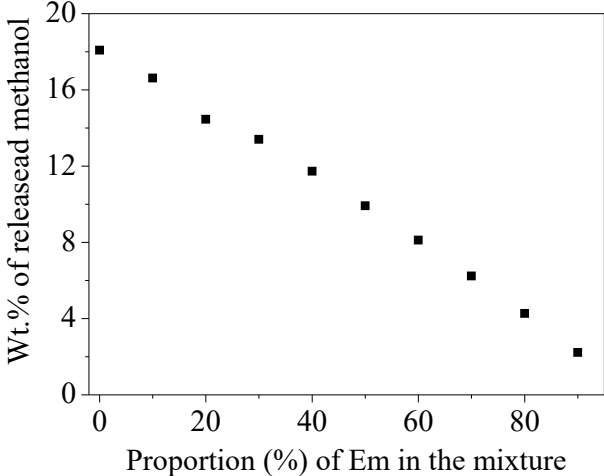


Figure 9



**Figure 10**



## Annex

**Table 1. Solubility results of KTP in different solutions**

<b>Solvent medium</b>	<b>Solubility (%)</b>
Distilled water	0.20
Miglyol	<b>2.55</b>
KEL	<b>28.42</b>
PbS pH= 7.4	0.32
PbS pH= 4.6	0.28
PbS pH= 1.2	0.26
PbS + 1%P123	3.51
PbS + 3%P123	4.15
PbS + 5%P123	6.60
3% KEL in water	0.58
5% KEL in water	0.75
10% KEL in water	1.33
15% KEL in water	2.51
3% Mig in water	25.95
5% Mig in water	30.44
10% Mig in water	35.32
15% Mig in water	47.98

**Table2. Composition of the hybrid material for the release experiments**

Formulation	wt %	KEL (wt %)	Mig (wt %)	KTP (wt %)	TMOS (wt %)
SM: 2.5% KEL	100	47.3	0.00	3.7	48.8
SM: 5% KEL	100	47.7	0.00	3.8	48.3
SM: 10% KEL	100	47.6	0.00	3.6	48.7
Em:20/80 (O/KEL)	100	32.9	8.3	2.4	56.5
Em:30/70 (O/KEL)	100	43.9	19	3.6	33.5
Em:40/60 (O/KEL)	100	36	23.9	2.8	37.9

**Table 3. Composition of the doped concentrated emulsions for the release experiments**

**And rheological tests**

Formulation	wt %	KEL (wt %)	Water (wt %)	Mig (wt %)	KTP (wt %)
CE70_KTP	100	4.5	25.4	68	2.1
CE80_KTP	100	3	17	77.5	2.6
CE90_KTP	100	1.5	8.5	88	2

**Table 2**

Mesoporous materials: cell parameter ( $a_0$ ), specific surface area ( $S_{\text{BET}}$ ), pore volume ( $V_p$ ), pore diameter ( $\varnothing$ ) and pore wall thickness ( $e$ ) concerning the samples obtained at different surfactant concentrations. The KEL/TMOS molar ratio is fixed to 0.024.

[KEL] (wt.%)	$a_0$ (nm)	$S_{\text{BET}}$ (m <sup>2</sup> /g)	$V_p^*$ (cm <sup>3</sup> /g-STP)	$\varnothing^*$ (nm)	$e$ (nm)
2.5	8.4	702	0.7	4.5	3.9
5	9.0	872	0.6	5.4	6.6
10	9.7	928	1.4	5.7	4.0
20	11.5	885	1.5	7.1	4.4
30	–	560	1.4	10.7	–
40	–	466	1.4	18.5	–

\* Values obtained from BJH method applied to the adsorption branch of the isotherm.

- Wormhole like structure.

( $V_W = 18 \text{ cm}^3/\text{mol}$ ,  $V_B = 834 \text{ cm}^3/\text{mol}$  and  $V_S = 2354 \text{ cm}^3/\text{mol}$ ).

Then, the cross sectional area  $S$  can be deduced as:

$$S = \frac{2V_B}{N_A R_H}$$

where  $N_A$  is the Avogadro's number.

For the cubic phase, the hydrophobic radius  $R_H$  is related to the lattice parameter  $a$  by the following equation [34]:

$$\frac{V_B}{V_S + \alpha V_W} = \frac{4\nu\pi R_H^3}{3a^3}$$

with  $\nu$  the number of micelles per cubic lattice ( $\nu = 8$  for the  $Pm3n$  cubic phase).

Then, the cross sectional area  $S$  can be deduced as:

$$S = \frac{3V_B}{N_A R_H}$$

The results are given in Table 1. For the hexagonal phase, the lattice parameter  $a$  slightly increases with the content of water from 10.4 to 10.7 nm, while the hydrophobic radius and the cross sectional area remain constant, equal to 2.6 nm and  $1.1 \text{ nm}^2$ , respectively. The value of  $R_H$  is higher for the cubic phase (3.5 nm), while the cross sectional area is in the same range ( $1.2 \text{ nm}^2$ ). No significant change of the structural parameters in function of the temperature was observed. Given that, from the length of the bonds, the extended alkyl chains have a dimension of about 2.5 nm and looking at the determined values of the hydrophobic radius for the hexagonal phase, we can deduce that the alkyl chains are completely extended in this phase. For the cubic phase, the hydrophobic radius is bigger than the estimated value. This result can be due to the deviation from the perfect spherical micelles to slightly rods in the  $Pm3n$  cubic phase, as suggested by Fontell et al. [35], or to disks as proposed in the Charvolin and Sadoc model [36].

The structure of the micelles of Kolliphor in water were determined by SAXS with the samples at 2.5, 5 and 10 wt % of surfactant. The SAXS spectra are given on Fig. 2a in absolute units.

For all the studied concentrations, the spectra present the same profile. All the curves are overlapped for  $q > 0.45 \text{ nm}^{-1}$  and they exhibit a maximum at  $0.78 \text{ nm}^{-1}$ . For low  $q$  values ( $q < 0.45 \text{ nm}^{-1}$ ), the intensity decreases with the concentration. This feature is characteristic of the existence of interparticle interactions.

To determine the micellar structure, the data were analyzed by using the Generalized Indirect Fourier Transform (GIFT) method [37,38], taking into consideration the interparticle interactions (Fig. 2b). The obtained pair-distance distribution functions (PDDFs) were represented on Fig. 2c. The curves exhibit a pronounced dip, which even goes to negative values for the concentrated solution (10 wt %), indicating that the micelles can be considered as inhomogeneous and so called "core-shell" type particles. All the curves present also a bell-like shape, characteristic of spherical micelles, with a maximum

dimension of about 12.5–13 nm, regardless of the surfactant concentration. These results are in good agreement with the hydrodynamic diameter determined at 25 °C by Dynamic Light Scattering (DLS) measurements (14 nm with diluted micellar solutions (< 2 wt% of surfactant)). Additionally, the excess-electron density profiles have been determined by the deconvolution of the pair-distance distribution functions (PDDFs) (Fig. 2d). The profiles confirm the core-shell type particles for the three micellar solutions. Indeed, the negative density difference corresponds to the hydrophobic part ( $\rho_{\text{phobic}} = 310 \text{ e/nm}^3$ ), whereas the positive density difference can be attributed to the hydrophilic shell ( $\rho_{\text{philic}} = 369 \text{ e/nm}^3$ ). The hydrophobic radius corresponds to the  $r$ -value when the sign of  $\Delta\rho(r)$  changes. It can be estimated at 3.1 and 3.3 nm for 2.5 and 5–10 wt % surfactant concentration, respectively. Then, the micelles radii can be evaluated at 6.2 and 6.5 nm for 2.5 and 5–10 wt % surfactant concentration, respectively. These values are in accordance with the maximum dimension found on the PDDFs. Looking at the excess electron density profile (Fig. 2d), the hydrophobic moieties, corresponding to the lowest values of  $\Delta\rho(r)$ , have a dimension of about 1.9–2.0 nm since the dimension of the hydrophobic chains is estimated at 2.5 nm. We can thus deduce that the alkyl chains are slightly folded. For the hydrophilic chains, considering that one EO group has a dimension of 0.35 nm, their total dimension can be evaluated at 4.5 nm. From Fig. 2d, the hydrophilic part has a length of 4–4.5 nm. Thus, these chains have a rather extended conformation.

### 3.2. Mesoporous silica materials from kolliphor micelles

When the cooperative mechanism is used to prepare the mesoporous silica, the surfactant has to form micelles in solution, but this is not a sufficient condition. Indeed, the other partner, the silica precursor, also plays a crucial role in the formation of the materials [30,31,39]. In particular, the surfactant/silica molar ratio is an important parameter that should be optimized. For two kolliphor concentrations belonging to the micellar domain (2.5 and 10 wt%), the kolliphor/TMOS molar ratio ( $R'$ ) has been varied from 0.017 to 0.066. By this way, from the surfactant point of view, the conditions are gathered for the CTM to occur. The observed variations will thus be due to the effect of the inorganic precursor. Whatever the kolliphor concentration, mesoporous silica materials are recovered until a kolliphor/TMOS ratio of 0.031 (Fig. 3). If the value of  $R'$  is increased the main peak becomes less intense and no secondary reflections are detected any longer. This means that the mesopores arrangement evolves towards a wormhole-like structure. In that case, the quantity of the added TMOS is not enough to cover all the micelles and the interactions between micelles and hydrolyzed precursor are disturbed. As a consequence, the intermicellar condensation leads to a less ordered hybrid mesophase and wormhole-like mesostructures are obtained.

Concerning the nitrogen adsorption-isotherm, regardless the synthesis conditions, all the materials present a type IV isotherm (Fig. 4), characteristic of mesoporous materials. For  $R'$  ratios in the range 0.017–0.031, the mesopore size distribution is quite narrow and the pore diameter remains almost constant for a given kolliphor concentration (insert of Fig. 4). An increase of the mesopore size is noted when the KEL concentration is varied from 2.5 to 10 wt%, for example, for  $R' = 0.017$  the pore diameter increases from 4.7 to 5.7 nm. We can also see that the nitrogen adsorption-desorption isotherm of materials synthesized with a kolliphor/TMOS ratio in this range of values, increases at high relative pressure instead of reaching a plateau as usually observed for type IV isotherms. This behavior has already been reported in literature [31,40] and can be related to the pH conditions which favor the appearance of an interparticle porosity, which is responsible of the ascent of the adsorbed volume at high  $p/p_0$  values. For  $R'$  beyond 0.031, the disorganization of the mesopores network is accompanied by a decrease of the pore diameter (insert of Fig. 4A) or by the appearance of a broad second component in the mesopore size

From the above results, obtained for a low and high surfactant concentration, it appears that to recover a mesostructured silica with a well-defined pore size distribution the  $R'$  value should be in the range between 0.017 and 0.031. Thus, for the next studies, the kolliphor/TMOS ratio has been fixed to 0.024. Since it also appears that the pore size varies as a function of the kolliphor concentration, the surfactant amount has been varied from 2.5 to 40 wt% to explore the overall micellar domain. The SAXS patterns depicted on Fig. 6A show that mesostructured silica materials are recovered until 20 wt% of kolliphor in water (Fig. 6Aa-d). Increasing the concentration of the micellar solution from 2.5 to 20 wt%, the first peak  $d_{100}$  is shifted from 7.3 to 10 nm, the cell parameter  $a_0$  thus varies from 8.4 to 11.5 nm ( $a_0 = 2d_{100}/\sqrt{3}$ ). Since the cell parameter is the sum of the mesopore diameter ( $\varnothing$ ) and the silica wall thickness ( $e$ ) this suggests that either  $\varnothing$  or  $e$  or both increase as a function of the kolliphor concentration. In this range of KEL concentration, the mesostructured silica presents a type IV isotherm (Fig. 6Ba-d) characteristic of mesoporous materials, according to the IUPAC classification [41]. The relative pressure at which the capillary condensation occurs is progressively shifted to higher  $p/p_0$  values when the surfactant concentration used to prepare the materials is increased. Since this value is related to the mesopore diameter according to the Kelvin equation this means that bigger mesopores are formed. This is confirmed by the pore size distribution, whose maximum is shifted from 4.5 to 7.1 nm as a function of the kolliphor concentration. By contrast it can be seen from Table 2 that the mesopore wall thickness remains almost constant to 4.0 nm. It is also interesting to note that the mesopore diameter is in good accordance with the hydrophobic core size of the micelles determined by SAXS. This observation confirms the templating effect of the KEL micelles. The specific surface area and the pore volume slowly increase from respectively 702 to around 900 m<sup>2</sup>/g and from 0.7 to 1.5 cm<sup>3</sup>g<sup>-1</sup>, when the KEL concentration varies from 2.5 to 20 wt% (Table 2).

The SAXS spectrum of the material synthesized with 30 wt% of kolliphor is characteristic of a wormhole-like structure since it exhibits only a broad peak at 12.7 nm (Fig. 6 Ae). If the KEL concentration is raised to 40 wt% no peak is detected any longer (Fig. 6 Af), meaning that the channel arrangement is completely random. The shape of the isotherm of the samples prepared with a KEL concentration higher than 20 wt% is modified and it becomes intermediate between type IV and type II (Fig. 6 Be,f). Meanwhile the pore size is broader, its maximum is shifted towards higher mesopore diameter and the  $dV/dD$  values decrease. Meantime the specific surface area drops to around 460 m<sup>2</sup>/g, reflecting disorganization of the channel array even if all the conditions are gathered to get an ordered mesostructured silica material. TEM observations confirm the presence of regular mesopores for all samples with  $R' = 0.024$  when KEL concentration increased from 2.5 to 30 wt% (Fig. 7). On the TEM images at high magnification (Fig. 7 b,d,f,h,j) the gradual loss of pore ordering is clearly observed when KEL concentration increased from 10 to 30 wt%. The origin of the loss of the mesopore ordering with the increase of the surfactant concentration can be due to a change of the micelles shape for example from spherical to rods, which disturbs the Cooperative Templating Mechanism. Indeed, when micelles are closed together, due to the limitations on the conformation of oxyethylene groups arising from steric hindrance, repulsive forces occur. This leads to a micelle shape transition like sphere-to-rod [42]. We can also assume that with the increase of the concentration of the micellar solution more and more micelles are formed and the interactions between micelles predominate in the detriment of the ones with the hydrolyzed precursor. Finally, we cannot exclude a shift of the domain of the phase diagram because of the release of the methanol produced during the hydrolysis of the TMOS. Indeed, it is well known that the presence of additives such as salt or alcohol strongly modify the surfactant behavior in water [43,44] and as a consequence affect the formation of the mesostructured silica materials [45,46].

#### 4. Conclusions

Mesoporous materials have been prepared using an aqueous solution of a biocompatible surfactant, the kolliphor EL. In order to determine the phase sequence as a function of the temperature, the phase behavior of KEL in aqueous solution was first investigated. We have delimited the different phase domains and determined the structure of the micelles as well as the structural parameters of the liquid crystals.

Determination of the micellar structure by SAXS provides information about the conformation of the hydrophilic and hydrophobic chains in  $L_1$ . The alkyl chains are slightly folded whereas the hydrophilic chains are rather extended. The micelles are found to be spherical and their radius has been evaluated between 6.2 and 6.5 nm, depending on the kolliphor concentration. In the liquid crystals phases  $H_1$  and  $I_1$ , the hydrophobic chains adopt an extended conformation.

Micellar solutions of kolliphor EL were used as template to prepare the mesoporous materials through the Cooperative Templating Mechanism. The influence of the synthesis conditions on the properties of the mesopore ordering has been investigated. As long as the surfactant concentration is lower than 30 wt% mesostructured silica can be obtained. These materials exhibit a high specific surface area and a narrow pore size distribution, whose maximum varies from 4.5 to 7.1 nm. These values of the mesopores diameters are in accordance with the ones of the size of the hydrophobic core of the micelles determined by SAXS. If the kolliphor concentration is increased, disordered mesoporous silica with broad mesopore size distributions are recovered.

Here, we succeed in preparing bare silica from the biocompatible surfactant Kolliphor EL. KEL has been removed to characterize the porosity. Regarding the interest of hybrid materials for drug delivery we can assume that without removing KEL the hybrid mesostructured silica are excellent candidates for this application. This work is under progress.

#### Acknowledgements

Claudia Violeta Cervantes-Martinez thanks the CONACYT for the financial support of her PhD. Loïc Vidal the person in charge of the "Electronic Microscopy" platform of IS2M is acknowledged for TEM images.

#### References

- [1] C.T. Kresge, W.J. Roth, The discovery of mesoporous molecular sieves from the twenty year perspective, *Chem. Soc. Rev.* 42 (2013) 3663–3670.
- [2] C.T. Kresge, M.E. Leonowicz, W.J. Roth, J.C. Vartuli, J.S. Beck, Ordered mesoporous molecular sieves synthesized by a liquid-crystal template mechanism, *Nature* 359 (1992) 710–712.
- [3] L.F.F.P.G. Braganca, M. Ojeda, J.L.G. Fierro, M.I. Pais da Silva, Bimetallic Co-Fe nanocrystals deposited on SBA-15 and HMS mesoporous silicas as catalysts for Fischer-Tropsch synthesis, *Appl. Catal. A-Gen.* 423–424 (2012) 146–153.
- [4] P. Perego, R. Millini, Porous materials in catalysis: challenges for mesoporous materials, *Chem. Soc. Rev.* 42 (2013) 3956–3976.
- [5] S.Y. Park, M. Barton, P. Pendleton, Mesoporous silica as a natural antimicrobial carrier, *Colloid. Surf. Physicochem. Eng. Asp.* 385 (2011) 256–261.
- [6] N. Baccile, F. Babonneau, B. Thomas, T. Coradin, Introducing ecodesign in silica sol-gel materials, *J. Mater. Chem.* 19 (2009) 8537–8559.
- [7] C. Gérardin, J. Reboul, M. Bonne, B. Lebeau, Ecodesign of ordered mesoporous silica materials, *Chem. Soc. Rev.* 42 (2013) 4217–4255.
- [8] J.A. Martens, J. Jammaer, S. Bajpe, A. Aerts, Y. Lorguilloux, C.E.A. Kirschhock, Simple synthesis recipes of porous materials, *Microporous Mesoporous Mater.* 140 (2011) 2–8.
- [9] D. Zhao, Q. Huo, J. Feng, B.F. Chmelka, G.D. Stucky, Nonionic triblock and star diblock copolymer and oligomeric surfactant syntheses of highly ordered, hydrothermally stable mesoporous silica structures, *J. Am. Chem. Soc.* 120 (1998) 6024–6036.
- [10] S.A. Bagshaw, E. Prouzet, T.J. Pinnavaia, Templating of mesoporous molecular sieves by nonionic polyethylene oxide surfactants, *Science* 269 (1995) 1242–1244.
- [11] Y. Wan, D. Zhao, On the controllable soft-templating approach to mesoporous silicates, *Chem. Rev.* 107 (2007) 2821–2860.
- [12] J.L. Blin, M. Impérator-Clerc, Mechanism of self-assembly in the synthesis of silica mesoporous materials: in situ studies by X-ray and neutron scattering, *Chem. Soc. Rev.* 42 (2013) 4071–4082.
- [13] G.S. Attard, J.C. Glyde, C.G. Göltnér, Liquid-crystalline phases as templates for the